BIOPHYSICAL REMOTE SENSING OF SALT MARSHES IN SOUTH-EAST UNITED STATES

by

SHUVANKAR GHOSH

(Under the Direction of Deepak Mishra)

ABSTRACT

Study of salt marsh biophysical properties is imperative to understand its response to environmental change. We developed protocols for mapping biophysical properties of salt marshes such as Green Leaf Area Index (GLAI), Canopy Chlorophyll (CHL_c), Vegetation Fraction (VF), and aboveground Green Biomass (GBM) using moderate resolution satellite images and *in-situ* data for the salt marshes in south-eastern United States. The time-series products derived using the biophysical models have been able to capture the spatio-temporal effects of the environmental events affecting the salt marshes of the region. We also tested the performance of different smoothing functions to derive noise-free phenology for Louisiana (LA) and Georgia (GA) salt marshes from the time-series GBM composites, and selected the best smoothing function to derive and analyze phenological parameters for salt marsh habitats. Long-term trend analysis of phenological parameters indicate positive changes in the base GBM values, and mostly negative changes in the GBM amplitude and small seasonal integral, which

indicate overall progressive decline in the rates of photosynthesis and biomass allocation in the salt marsh ecosystem. This observed decline in photosynthesis and biomass allocation may be attributed to elevated atmospheric carbon dioxide (CO_2) levels and sea level rise. Finally we attempted to map Gross Primary Productivity (GPP) for a salt marsh habitat in the Gulf Coast, using the GBM composites and *in-situ* GPP estimates from eddy covariance CO_2 flux towers. The time-series composites and phenological charts developed using the biophysical GPP model was able to capture the effect of different environmental events such as dieback and hurricane landfall. The results illustrate the relative efficiency of MODIS in analyzing salt marsh biophysical properties. This is the first study to employ MODIS images to study the long-term trends in biophysical characteristics of salt marshes in south-east United States. The methods described in this study as well as the biophysical products derived using the methods has the potential to improve our ability to predict their productivity and carbon sequestration potential. These techniques could also be used to assess the success of previous and ongoing salt marsh restoration projects, and evaluate the productivity of marshes under threat from both natural and anthropogenic drivers.

Index terms: Salt marsh, MODIS, Phenology, Green Leaf Area Index, Canopy Chlorophyll, Vegetation Fraction, Green Biomass, Gross Primary Productivity, Trend Analysis, Eddy Covariance, Carbon Dioxide, Carbon Sequestration.

BIOPHYSICAL REMOTE SENSING OF SALT MARSHES IN SOUTH-EAST UNITED STATES

by

SHUVANKAR GHOSH

B.Sc., UNIVERSITY OF CALCUTTA, INDIA, 2005

M.Sc., FOREST RESEARCH INSTITUTE (DEEMED UNIVERSITY), 2007

A Dissertation Submitted to the Graduate Faculty of the University of Georgia in Partial Fulfillment of the Requirements for the Degree

DOCTOR OF PHILOSOPHY

ATHENS, GEORGIA

2017

© 2017

Shuvankar Ghosh

All Rights Reserved

BIOPHYSICAL REMOTE SENSING OF SALT MARSHES IN SOUTH-EAST UNITED STATES

by

SHUVANKAR GHOSH

Major Professor:	Deepak R. Mishra
Committee:	Marguerite Madden
	Thomas B. Jordan
	Christopher J. Anderson

Electronic Version Approved:

Suzanne Barbour
Dean of the Graduate School
The University of Georgia
December 2017

DEDICATION

To

Late Shri Nirmal Kanti Ghosh

Late Shri Amal Chandra Basu

Late Smt. Rekha Ghosh

Late Smt. Nilima Basu

Late Smt. Dipali Ghosh

ACKNOWLEDGEMENT

This dissertation would not have been possible without collective effort of multiple individuals and institutions. The following paragraphs are too short to acknowledge their impact on this dissertation.

My parents have made innumerable sacrifices to bring me up, and make sure that making sure I never face any obstacles toward achieving my dreams. They gave me the best education and the best childhood, and taught me the value of honesty, discipline and hard work. A thank you would be an understatement for all their support and love…I am proud of them. I extend my gratitude to my parents-in-law as well for being understanding and supportive throughout.

What do I say about my wife Dipanwita? I am indebted to her for doing everything she could to support me in my life, and she continues to do so; whether it is taking care of me, cooking me delicacies, keeping me stress free by entertaining me through her funny gestures, or breaking into a sudden song and dance, or greeting me with a smile when I came home from work. With her around, I never really had to worry about anything else other than my work. I consider myself extremely fortunate to have her as my wife.

I would like to thank my supervisor Dr. Deepak Mishra, for providing me the opportunity to work under his supervision, first at Mississippi State University and then at University of Georgia. No words can describe his invaluable contribution towards this study. His patience, compassion and critical inputs, had not only a tremendous impact on the quality of my research,

but also helped me grow as a researcher, and an instructor. I sincerely hope that I met his expectations during my tenure as a PhD student.

I would like to thank my committee members Dr. Marguerite Madden, Dr. Thomas Jordan, and Dr. Christopher Anderson for their constructive feedback on my research, and their support and encouragement without which this dissertation would never have been possible. I would like to mention Dr. Anatoly Gitelson, Dr. Hyun J. Cho, Dr. Jianbin Tao, Dr. David Cotton and Dr. Jessica O'Connell for their inputs to this research. I would like to thank Dr. Patrick Biber, Dr. Dennis Reed and Dr. John Rodgers for supporting our field and lab work. I would like to thank Dr. Thomas Mote, Dr. Steven Holloway, Dr. Angela Yao, and other departmental faculties for smooth functioning one of the most brilliant Geography Graduate programs in the country. I thank the staff at the department of Geography for their assistance and friendship: Audrey Hawkins, Amy Bellamy, Kayla Timmons, Loretta Scott, Emily Duggar, Jane Worley, Dylan Tracy, Xiaonan Xie, Emily Coffee, Robert Phares and Margaret Bolton. In addition, I would like to thank the faculty and administrative staff of Mississippi State University, where I initiated my research. In addition, I would like to thank my students at Geography, whose support and feedbacks have helped me become a better teacher.

I would like to thank my ex-colleague Sachidananda Mishra at Mississippi State University and my colleagues at University of Georgia…Ike Astuti, Steve Padgett-Vasquez, Igor Ogashawara, Benjamin Page, Abhishek Kumar, Sam Weber, Caroline Narron, Peter Hawman, Lishen Mao, Joy Ganguly, Dina Rasquinha, Caren Remillard, Nancy O'Hare, Jiaying He, Alessandro Pasqua, Andrea Presotto and Sergio Bernardes, for their support and encouragement. I would like to thank Steve and Caren for giving me the opportunity to be a part of NASA Develop National Program at UGA. I would like to thank Mike Bryant, Christopher Downs and Alon Blakeney

(Mississippi State University), Paul Merani (University of Nebraska-Lincoln), Philemon Kirui (Jackson State University), Sarah Moore, Ross Del Rio and Lindsay Dunaj (University of New Orleans), Christina Mohrman (Grand Bay National Estuarine Research Reserve), and Charles Jordan (University of Georgia), for helping me with my fieldwork.

I am deeply thankful to my ex-roommates Tanmay, Soumya and Tushar at Starkville and my friends in Athens…Dipesh(da), Abhinav, Arnab, Arunava, Somenath, Anandi, Biswajit, Nabaneeta, Arka, Thiya, Sumit, Joshita, Srijita, Utsav, Shubham, Saptarshi, Ritapa, Debkanta and Akul, who never let me feel lonely, dull or away from home. I have cherished their company, conversations, banter, as well as their food. I would like to thank my school friends Sanjit, Satyaki, Sourav, Sudip, Debashish, Prosenjit, Paranjoy, Subhodeep, Srimoti, Arunabha, Aritra, Subhankar, Shoumadeep, Sayan, Shantanu, Saikat, and Aniruddha, for their moral support and above all, their friendship. Also, thanks to my friends from Dinabandhu Andrews College, my seniors and friends from Forest Research Institute and Wildlife Institute of India, and my colleagues from Ashoka Trust for Research in Ecology and the Environment. I would also like to thank my previous mentors Dr. Y. V. Jhala, Mr. Qamar Qureshi and Dr. R. Prabhakar.

Lastly, I would like to thank the National Aeronautics and Space Administration, National Science Foundation, Gulf of Mexico Research Initiative, and Northern Gulf Institute for providing the funding for this research. I am thankful to the Graduate School at University of Georgia, for providing me crucial funding in the form of Dean's Award for Social Science, Summer Doctoral Research Fellowship, as well as travel awards for attending conferences. I am also thankful to the Department of Geography for providing departmental teaching assistantship.

TABLE OF CONTENTS

Page

LIST OF TABLES

LIST OF FIGURES

Figure 3.3. a. Relationship between SPAD readings acquired at each sub–plot calibrated against analytical chlorophyll content values from laboratory analysis; b. validation of the SPAD model showing % NRMSE and 1:1 line.

Figure 3.4. a. Reflectance (%) spectra of 69 sub–plots covering multiple species acquired using Ocean Optics sensor.; b. Reflectance (%) spectra derived from MODIS 8–day 500m surface reflectance images for 33 pixels containing the study plots from 2010–2011. c. Sample spectra for individual species as acquired by the *in situ* sensor with highlighted MODIS bandwidths. Differences in the species level spectral response pattern were mainly due to the variability in canopy structure and chlorophyll content; d. Sample spectra acquired using Ocean Optics sensor for individual species averaged to MODIS bandwidths. Differences in species specific spectral response were clearly visible similar to the *in situ* reflectance profile.

Figure 3.5. Coefficient of determination values of species specific and species invariant linear, quadratic, and exponential relationships between VIs and (a, e, i): GBM, (b, f, j): VF, (c, g, k): CHL and (d, h, i): GLAI, respectively developed from *in situ* sensor derived VIs.

Figure 3.6. Calibration of MODIS (250m) derived WDRVI with a: GLAI, b: VF, c: CHL and d: GBM, with co–efficient of determination and 95% confidence intervals and limits. Error bars represent standard deviations. Coefficient of Determination (R), Sample size (N) and Percent Normalized Root Mean Square Error (%NRMSE) for respective models are also shown. Points with no error bars represent highly homogenous pixels with single study plots.

Figure 3.7. Calibration of MODIS (500m) derived VARI with a: GLAI, b: VF, c: CHL and d: GBM, with co–efficient of determination and 95% confidence intervals and limits. Error bars represent standard deviations. Coefficient of Determination (R), Sample size (N) and Percent

Normalized Root Mean Square Error (%NRMSE) for respective models are also shown. Points with no error bars represent highly homogenous pixels with single study plots.

Figure 3.8. Residual plots for MODIS (250m) based biophysical models for a: GLAI, b: CHL, c: VF and d: GBM. WDRVI ($\alpha = 0.1$) was chosen as the best–fit model. e: Slope ratio between linear trends of validation and calibration data. Models with minimum bias have ratios close to 1.

Figure 3.9. Residual plots for MODIS (500m) based best fit biophysical models (using VARI) for a: GLAI, b: CHL, c: VF and d: GBM.

Figure 3.10. Comparison between reflectance (%) between Ocean Optics and MODIS derived spectral response for *Spartina* and *Juncus* from a: 250m and b: 500m spatial resolution. The plots show how species information is lost with progressive decrease in spatial resolution. MODIS 250m dataset does not have blue and green bands; as such spectral information for those bands are missing in Figure 10a.

Figure 3.11. Sample composites (top image) showing spatial distribution of biophysical characteristics (in this case GBM) for four Gulf States using MODIS 250-m data. Expanded maps showing the magnitude and distribution of CHL, GBM, GLAI, and VF pre-and post-Hurricane Gustav.

Figure 3.12. Sample composites (top image) showing spatial distribution of biophysical characteristics (in this case GBM) for four Gulf States using MODIS 500-m data. Expanded maps showing the magnitude and distribution of CHL, GBM, GLAI, and VF pre-and post-Hurricane Katrina.

CHAPTER 1

INTRODUCTION

Salt marshes are one of the most ecologically and economically productive as well as vulnerable ecosystem of the world (Mitsch and Gosselink, 2001; Tiner 2013), performing various ecological functions such as water quality renovation through nutrient retention (White et al. 2004; Valiela et al. 2002), shoreline stabilization (Gedan et al. 2011), sediment trapping (Morgan et al. 2009), ground water recharge (Ganju et al. 2005), providing habitats for numerous species (Seabrook, 2006) , and storm surge protection (Barbier et al. 2008; Langlois et al. 2003). Salt marshes are also crucial in sustaining local and regional fisheries (Kritzer and Hughes, 2010), and supporting hunting of waterfowl and other game animals (United States Fish and Wildlife Service and United States Census Bureau, 2006). Further, the high carbon sequestration potential of salt marshes make them critical habitats especially considering the exponential increment of greenhouse gases in the atmosphere since last few decades (Connor et al. 2001; Chmura et al. 2003). However, these critical habitats are severely threatened by natural and anthropogenic activities such as global warming induced sea-level rise (Fitzgerald et al. 2008; Nicholls et al. 1999), diebacks (Ogburn and Alber, 2006), land use/land cover change (Kennish, 2001; Silliman et al. 2009), soil erosion (Sugumaran et al. 2004; Ravens et al. 2009), natural and man-made disasters and associated clean-up efforts (Hester and Mendelssohn 2000; Mishra et al. 2012; Moller et al. 2014; Mishra and Ghosh, 2015; Khanna et al. 2017), and ecological succession (Chambers et al. 2003; Artigas and Pechmann, 2010).

Majority of the research efforts for monitoring salt marshes using remote sensing have been focused on delineating its spatial extent and change detection, and classifying plant communities using both active and passive satellite sensors and numerous image processing techniques (Wang et al. 2010; Marani et al. 2006; Sadro et al. 2007; Gilmore et al. 2008; Lucas and Carter 2008; Artigas and Pechmann, 2010; Collin et al. 2010; Davranche et al. 2010; Zuo et al. 2012; Goudie, 2013). These techniques provide crucial information regarding the presence/absence of salt marsh patches, with previous and current spatial extents, along with the dynamics of wetland cover change. However, remote sensing studies on monitoring and analyzing the biophysical characteristics of salt marshes such as Canopy Chlorophyll content (CHL_c), Green Leaf Area Index (GLAI), Vegetation Fraction (VF), Green Biomass (GBM), and ultimately Gross Primary Productivity (GPP) is critical as they are the primary indicators of the overall health and productivity of the vegetation specifically the physiological status, photosynthetic capacity, and nitrogen content (Blackburn, 1998; Pierce et al. 1994; Pinar and Curran, 1996). Unfortunately, such studies attempting to understand and analyze long-term trends in biophysical characteristics are very limited and intermittent (Kearney et al. 2009, Mishra et al. 2012; Ghosh et al. 2016; O'Connell and Schalles, 2016). A robust mapping protocol for biophysical characteristics for salt marshes is critical in assessing not only the health of the salt marsh habitats, but also the success/failure of previous restoration efforts (Hinkle and Mitsch, 2005; Friess et al. 2012).

A crucial outcome of mapping biophysical characteristics of any vegetation ecosystem using remote sensing is vegetation phenology. Vegetation phenology affects terrestrial carbon cycling across a wide range of ecosystem and climate regimes (Baldocchi et al. 2001; Churkina et al. 2005; Richardson et al. 2009), and as such, accurate information related to phenology is important to studies of regional-to-global carbon budgets. Therefore, phenological properties or

seasonality parameters, such as the timing of the start and end of season, rate of green–up and brown–down, amplitude, and maximum growth level influences land surface albedo (Moore et al. 1996; Ollinger et al. 2008) and exerts strong control on surface radiation budgets and the partitioning of net radiation between latent and sensible heat fluxes (Chen and Dudhia, 2001; Yang et al. 2001). Therefore, the phenological dynamics influence a host of eco-physiological processes that affect hydrologic processes (Hogg et al. 2000), nutrient-cycling (Cooke and Weih, 2005), and land–atmosphere interactions (Heimann et al. 1998), and hence have become emerging indicators of global environmental changes (Kunkel et al. 2004; Scheifinger et al. 2002). Satellite derived biophysical properties have been frequently utilized to understand vegetation phenology (Soudani et al. 2008; Zhang and Goldberg, 2011). Over the years, remote sensing-based phenology have been intensively studied with fine temporal satellite sensors such as the Advanced Very High Resolution Radiometer or AVHRR (Reed et al. 1994) and Moderate Resolution Imaging Spectroradiometer or MODIS onboard Terra and Aqua satellites (Zhang et al. 2003). Studies have utilized such fine temporal resolution images for monitoring ecosystem phenology at both site-specific and landscape scales (Ahl et al. 2006; Fisher and Mustard, 2007; Zhang et al. 2006; de Beurs and Henebry, 2005; White et al. 1997).

Although development of methods and techniques to automatically retrieve land surface phenology metrics from satellite data has been a popular research topic (de Beurs and Henebry, 2010; White et al. 2009; Walker et al. 2012), nature of satellite data makes it difficult to extract phenological metrics from it directly (de Beurs and Henebry, 2005; Verbesselt et al. 2010). Satellite derived time-series data inevitably contain disturbances caused by cloud presence (Gutman, 1991), atmospheric variability (Huete and Liu, 1994), and aerosol scattering (Xiao et al. 2003), that degrades the data quality and hinders analysis. Therefore, satellite derived time-

series data are commonly quality-screened and/or smoothed to minimize noise and compensate for the absence of data before phenological metrics can be estimated (Atkinson et al. 2012). Several methods such as usage of various smoothing functions and statistical filters data have been proposed to remove such noise and to reconstruct high-quality time-series product (Viovy et al. 1992; Jonsson and Eklundh, 2002; Chen et al. 2005; Moody et al. 2005; Sellers et al. 1994; Roerink et al. 2000). Once the signal-to-noise ratio has been improved in the satellite derived time-series, basic phenological parameters can be derived using different methods (Zhang et al. 2003; Heumann et al. 2007). Phenological parameters have been studied in details in a variety of different terrestrial such as tropical rainforests, deciduous habitats, grasslands, and aquatic ecosystems such as phytoplankton (Asner and Alencar, 2010; Hufkens et al. 2012; Shen et al. 2011; Palmer et al. 2015). However, no such attempt has been made so far to study phenological parameters of salt marsh ecosystem.

Further, while numerous studies have explored the use of satellite remote sensing data for monitoring terrestrial phenology at landscape to regional scales (Fisher et al. 2006; Myneni et al. 1997; Soudani et al. 2008; White et al. 2009), assessing the relationship between satellite-based measurements of phenology, and *in-situ* phenological observations remains a challenge. Since imagery from remote sensing platforms such as MODIS is often collected at a very coarse spatial resolution, it encompasses considerable pixel level landscape heterogeneity. Therefore, comparison of phenological dates derived from satellite images with *in-situ* observations of phenological dates is necessary for evaluation of errors uncertainties in phenological measurements (Graham et al. 2010, Hufkens et al. 2012, Elmore et al. 2012, Klosterman et al. 2014). Again, visual observations are labor intensive to collect and the spatial extent of observations collected by an individual is inherently limited. Hence, digital repeat photography,

a form of near-surface continuous remote sensing, provides data at higher temporal frequency and finer spatial scale than satellite remote sensing (Richardson et al. 2009; Sonnentag et al. 2012). Color indices derived from digital repeat photography have been used to characterize the phenology of diverse plant communities and functional types (PFT) including deciduous broadleaf forest (Richardson et al. 2007: Ahrends et al. 2008: Ide and Oguma, 2010: Sonnentag et al. 2012: Hufkens et al. 2012: Dragoni et al. 2011), evergreen broadleaf forest (Zhao et al. 2012), evergreen needle-leaf forest (Richardson et al. 2009: Ide and Oguma, 2010: Bater et al. 2011), desert shrublands (Kurc and Benton, 2010), bryophyte communities (Graham et al. 2006) and invasive plants (Sonnentag et al. 2011). Phenological events derived from using digital repeat photography has been matched with satellite derived phenology to evaluate the performance of satellite images in phenology estimation (Brown et al. 2016; Melaas et al. 2016; Liu et al. 2016). Using the methods described, phenology has been studied in details in a variety of different terrestrial such as tropical rainforests, deciduous habitats, grasslands, and aquatic ecosystems such as phytoplankton (Asner and Alencar, 2010; Hufkens et al. 2012; Shen et al. 2011; Palmer et al. 2015). However, studying long-term trends of salt marsh phenological parameters have not been performed or reported.

As mentioned before, the potential of salt marshes as significant carbon sinks is well recognized (Connor et al. 2001; Chmura et al. 2003; McLeod et al. 2011). Carbon sequestration rates of salt marshes have been reported to be higher than that of terrestrial forests, but uncertainties exist in the global area of salt marsh and the rates of carbon dioxide sequestration throughout each marsh (McLeod et al. 2011). The carbon sequestration rates reported for salt marshes range from 18 to 1713 g C m^{-2} yr^{-1}; and considering the global extent of salt marshes between 22,000 to 400,000 km^2, these habitats could be storing 4.8 - 87.2 Tg C yr^{-1} (Mcleod et al. 2011). In addition, salt

marshes can store carbon for millennia (Macreadie et al. 2012); the carbon stock often termed as 'blue carbon' (Nelleman and Corcoran, 2009). However, despite their value as carbon sinks, salt marsh habitats have experienced significant global reduction (~25% since the 1800s; Bridgham et al. 2006; Duarte et al. 2006), mostly due to developmental activities, conversion of marsh habitats to agriculture, sea-level rise and environmental hazards (Coverdale et al. 2013; Kennish, 2001; Mishra et al. 2012). Due to such natural and anthropogenic drivers, the environment is losing a crucial carbon sink; significant amounts of carbon is being released in the form of carbon dioxide (CO_2) to the atmosphere due to disturbances, which, in turn, is enhancing global warming (Macreadie et al. 2013). In order to protect such invaluable resources, implementation of effective conservation and restoration of such habitats is crucial, which requires both periodic and long-term monitoring of physiological health and productive status of salt marsh habitats (Ghosh et al. 2016; O'Connell and Schalles, 2016).

GPP is defined as the total amount of energy produced by vegetation and a key component of ecosystem carbon fluxes, and is one of the most important biophysical characteristics and a key indicator of vegetation productivity (Monteith 1972: Beer et al. 2010). GPP can be calculated as the sum of vegetation assimilated carbon flux, partitioned from net carbon exchange measured at eddy covariance (EC) tower sites (Baldocchi et al. 2001; Reichsteinet al. 2007). Long-term readings from the flux towers may provide estimates of GPP within the tower footprint that may range from a hundred meters to several kilometers at the ecosystem level (Gockede et al. 2008; Osmond et al. 2004). However, such observations are limited, both temporally and spatially. Satellite remote sensing can provide consistent observation of vegetation productivity over large areas, and has been reported to be widely used for characterization of canopy structure and GPP estimation that can overcome the lack of extensive EC flux tower measurements (Running et al.

2000; Wu et al. 2010). Various diagnostic models taking advantage of spatially extensive remote sensing and meteorological data have been developed to estimate GPP across stand-to-global scales for a relatively long period (Jung et al. 2008; Running et al. 2004; Sims et al. 2008; Xiao et al. 2005). A lot of research efforts have concentrated on estimation of CO_2 fluxes for terrestrial vegetation such as boreal forest (Goulden et al. 1998; Baldocchi 2003), peatlands (Lafleur et al. 2005; Wille et al. 2008), grasslands (Ponton et al. 2006), and crops (Baker and Griffis 2005; Li et al. 2008). However, similar methods for studying GPP of salt marsh ecosystem has been lacking; the earliest eddy covariance flux tower in salt marsh habitats was set up very recently in 2013 (Georgia Coastal Ecosystem Long Term Ecological Network; http://gce-lter.marsci.uga.edu/). In the last century, invasive methods proposed and used for GPP estimation in salt marshes have yielded discrepant results, with estimates of GPP ranging from 750 – 2600 g C m^{-2} yr^{-1}, depending on the methods followed and integration of measurements (Kaswadji et al. 1990). For effective conservation and restoration of salt marsh ecosystem precise information regarding their actual productivity is required, especially rising atmospheric carbon dioxide and sea-levels pose a significant threat to the long-term health and productive productivity of these habitats (Ainsworth and Long, 2005; Erickson et al. 2007; White et al. 2012).

Research Objectives

The aim of this research was to develop remote sensing based methods to understand the long-term biophysical health and productive status of salt marsh ecosystem in the southeast United States, as well demonstrating the utility of the methods developed to identify salt marsh areas that requires immediate implementation of conservation and restoration measures.

The first chapter provides the background for this research. The pilot study presented the first quantitative assessment on the ecological impact of the Deepwater Horizon oil-spill on the salt marsh habitats along the southeastern Louisiana (LA) coast. The objective of this study was to combine LANDSAT images and *in-situ* observations of Canopy Level Chlorophyll (CHL_c) and aboveground Green Biomass (GBM) to quantify the magnitude and the extent of the impact of the oil-spill and clean-up efforts on the salt marsh habitat. The specific objectives included, (1) application of a suite of algorithms combining Landsat 30-m datasets with field data to map CHL and GBM across southeastern LA salt marshes; and (2) compare and quantify the changes observed in CHL and GBM distribution during the salt marsh growing season between 2009 (pre-spill) and 2010 (post-spill) to isolate the spill impact.

The second chapter developed a new methodological approach for mapping biophysical health of coastal salt marsh habitats in terms of green leaf area index (GLAI), canopy level chlorophyll content (CHL_c), vegetation fraction (VF), and above ground green biomass (GBM). We measured these biophysical characteristics in tidal wetlands of the northern Gulf of Mexico using a combination of ground data collected from field surveys during the growing seasons of 2010 and 2011 and NASA's Moderate Resolution Imaging Spectroradiometer (MODIS) 250 m and 500 m images. The specific objectives of this research were to (1) calibrate and validate MODIS based VIs for estimating the tidal wetland biophysical characteristics (GLAI, CHLc, VF, GBM) in the northern Gulf of Mexico (GoM), (2) develop time-series composites of tidal wetland biophysical characteristics for long-term productivity trend analysis, and (3) analyze broader phenological patterns of the biophysical characteristics to assess the impact of various natural and anthropogenic disasters.

The third chapter examined the phenology of salt marsh ecosystem across coastal Louisiana (LA) for a sixteen-year time-period (2000-2015) using the products developed/described in the second chapter. We utilized GBM composites derived using NASA's Moderate Resolution Imaging Spectroradiometer's (MODIS) 8-day average surface reflectance images (500m), and biophysical models described in the second chapter. The specific objectives of this study were to (1) describe and test methods for deriving noise-free phenology and seasonality parameters for salt marshes in LA, (2) validate the methods through analyzing the annual phenological variations, and (3) analyze the long-term change trends in the seasonality parameters using statistical trend analysis techniques.

The fourth chapter attempts to test the models and methods developed in chapter 2 and 3 in a different geographical salt marsh setting. In this study, we examined the phenology of salt marsh ecosystem across coastal Georgia for a sixteen-year time-period (2000-2015) using NASA's Moderate Resolution Imaging Spectroradiometer's (MODIS) 8-day average surface reflectance images (500m). The specific objectives of this study were to (1) test the performance of an existing MODIS based GBM mapping algorithm, for mapping GBM of salt marshes across coastal Georgia (GA), (2) describe and test methods for deriving noise-free phenology and seasonality parameters for salt marshes in GA, using time-series GBM composites generated using MODIS and *in-situ* phenological observations, and (3) analyze the long-term change trends in the seasonality parameters using statistical trend analysis techniques.

The fifth chapter attempts to develop a Gross Primary Productivity (GPP) mapping algorithm combining *in-situ* estimations of GPP from flux towers and MODIS derived GBM (Ghosh et al. 2016), to develop a GPP mapping algorithm for the Grand Bay National Estuarine Research Reserve (GBNERR) salt marsh habitats. The specific objectives of this study were to (1)

establish a statistical relationship between GBM and GPP, through calibration and validation, (2) generate time-series GPP composites using the statistical relationship for qualitative analysis of inter and intra-annual GPP variations, and (3) derive phenology from the GPP composites to study temporal trends in GPP of GBNERR, for a seventeen year time period (2000 – 2016).

The potential broader impact of the research goes beyond the salt marshes of the northern Gulf or Georgia. The MODIS based models developed through this study can potentially be applied to study salt marsh ecosystems elsewhere in United States, such as coastal Carolina, New England or California, particularly along the San Francisco Bay. Since the salt marsh habitats along those coastal habitats have a similar species assemblage and geomorphology, the models will not require re-calibration to be applied. Since this may be the first study of its kind to use MODIS derived biophysical products to develop salt marsh GPP products, it can be assumed that there will be a lot of interests among coastal resource managers in states with salt marsh habitats to use the tools and products developed in this study.

References:

Ahl, D. E., Gower, S. T., Burrows, S. N., Shabanov, N. V., Myneni, R. B., and Knyazikhin, Y. 2006. Monitoring spring canopy phenology of a deciduous broadleaf forest using MODIS. *Remote Sensing of Environment*, 104, 88-95.

Ahrends, H. E., Brügger, R., Stöckli, R., Schenk, J., Michna, P., Jeanneret, F., Wanner, H. and Eugster, W. 2008. Quantitative phenological observations of a mixed beech forest in northern Switzerland with digital photography. *Journal of Geophysical Research-Biogeosciences*, 113, DOI: 10.1029/2007JG000650.

Ainsworth, E. A., and Long, S. P. 2005. What have we learned from 15 years of free-air CO2 enrichment (FACE)? A meta-analytic review of the responses of photosynthesis, canopy properties and plant production to rising CO_2. *New Phytologist*, 165, 351-372.

Artigas, F. and Pechmann, I. C. 2010. Balloon imagery verification of remotely sensed Phragmites australis expansion in an urban estuary of New Jersey, USA, *Landscape and Urban Planning*, 95, 105–112.

Asner, G. P., and Alencar, A. 2010. Drought impacts on the Amazon forest, the remote sensing perspective. *New Phytologist*, 187, 569–578.

Atkinson, P. M., Jeganathan, C., Dash, J., and Atzberger, C. 2012. Inter–comparison of four models for smoothing satellite sensor time–series data to estimate vegetation phenology. *Remote Sensing of Environment*, 123, 400–417.

Baker, J. M., and Griffis, T. J. 2005. Examining strategies to improve the carbon balance of corn/soybean agriculture using eddy covariance and mass balance techniques. *Agricultural and Forest Meteorology*, 128, 163-177.

Baldocchi, D. D. 2003. Assessing the eddy covariance technique for evaluating carbon dioxide exchange rates of ecosystems: past, present and future. *Global Change Biology*, 9, 479-492.

Baldocchi, D., Falge, E., Gu, L., Olson, R., Hollinger, D., Running, S., Anthoni, P., Bernhofer, C., Davis, K., Evans, R., and Fuentes, J. 2001. FLUXNET: A new tool to study the temporal and spatial variability of ecosystem–scale carbon dioxide, water vapor, and energy flux densities. *Bulletin of the American Meteorological Society*, 82, 2415-2434.

Barbier, E. B., Georgiou, I. Y., Enchelmeyer, B., and Reed, D. J. 2013. The value of wetlands in protecting southeast Louisiana from hurricane storm surges. *PloS One*, 8, e58715.

Barbier, E. B., Koch, E. W., Silliman, B. R., Hacker, S. D., Wolanski, E., Primavera, J., Granek, E.F., Polasky, S., Aswani, S., Cramer, L. A., Stoms, D. M., Kennedy, C., J., Bael, D., Kappel, C. V., Perillo, G. M. E., and Reed, D. J.2008. Coastal ecosystem–based management with nonlinear ecological functions and values, *Science*, 319, 321–323.

Bater, C. W., Coops, N. C., Wulder, M. A., Hilker, T., Nielsen, S. E., McDermid, G., and Stenhouse, G. B. 2011. Using digital time-lapse cameras to monitor species-specific understorey and overstorey phenology in support of wildlife habitat assessment. *Environmental Monitoring Assessment*, 180, 1-13.

Beer, C., Reichstein, M., Tomelleri, E., Ciais, P., Jung, M., Carvalhais, N., Rödenbeck, C., Arain, M.A., Baldocchi, D., Bonan, G.B., and Bondeau, A. 2010. Terrestrial gross carbon dioxide uptake: global distribution and covariation with climate. *Science*, 329, 834-838.

Blackburn, G. A. 1998. Quantifying chlorophyll and carotenoids at leaf and canopy scales: an evaluation of some hyperspectral approaches, *Remote Sensing of Environment*, 66, 273–285

Bridgham, S. D., Patrick Megonigal, J., Keller, J. K., Bliss, N. B., and Trettin, C. 2006. The carbon balance of North American wetlands. *Wetlands*, 26, 889-916.

Brown, C. J., O'connor, M. I., Poloczanska, E. S., Schoeman, D. S., Buckley, L. B., Burrows, M. T., Duarte, C. M., Halpern, B. S., Pandolfi, J. M., Parmesan, C. and Richardson, A. J. 2016. Ecological and methodological drivers of species' distribution and phenology responses to climate change. *Global Change Biology*, 22, 1548-1560.

Chambers, R. M., Osgood, D. T., Bart, D. J., and Montalto, F. 2003. Phragmites australis invasion and expansion in tidal wetlands, interactions among salinity, sulfide, and hydrology. *Estuaries and Coasts*, 26, 398–406.

Chen, F., and Dudhia, J. 2001. Coupling an advanced land surface–hydrology model with the Penn State–NCAR MM5 modeling system. Part I: Model implementation and sensitivity. *Monthly Weather Review*, 129, 569-585.

Chen, X., Hu, B., and Yu, R. 2005. Spatial and temporal variation of phenological growing season and climate change impacts in temperate eastern China. *Global Change Biology*, 11, 1118–1130.

Chmura, G. L., Anisfeld, S. C., Cahoon, D. R., and Lynch, J. C. 2003. Global carbon sequestration in tidal, saline wetland soils. *Global Biogeochemical Cycles,* 17, DOI: 10.1029/2002GB001917.

Churkina, G., Schimel, D., Braswell, B. H., and Xiao, X. M. 2005. Spatial analysis of growing season length control over net ecosystem exchange, *Global Change Biology*, 11, 1777–1787.

Collin, A., Long, B., and Archambault, P.2010. Salt–marsh characterization, zonation assessment and mapping through a dual–wavelength LiDAR. *Remote Sensing of Environment*, 114, 520–530.

Connor, R. F., Chmura, G. L., and Beecher, C. B. 2001. Carbon accumulation in Bay of Fundy salt marshes: Implications for restoration of reclaimed marshes. *Global Biogeochemical Cycles*, 15, 943–954.

Cooke, J. E., and Weih, M. 2005. Nitrogen storage and seasonal nitrogen cycling in Populus: bridging molecular physiology and ecophysiology. *New Phytologist*, 167, 19-30.

Coverdale, T. C., Herrmann, N. C., Altieri, A. H., and Bertness, M. D. 2013. Latent impacts: the role of historical human activity in coastal habitat loss. *Frontiers in Ecology and the Environment*, 11, 69-74.

Davranche, A., Lefebvre, G., and Poulin, B. 2010. Wetland monitoring using classification trees and SPOT–5 seasonal time series, *Remote Sensing of Environment*, 114, 552–562.

De Beurs, K. M., and Henebry, G. M. 2005. A statistical framework for the analysis of long image time series. *International Journal of Remote Sensing*, 26, 1551–1573.

De Beurs, K. M., and Henebry, G. M. 2010. Spatio-temporal statistical methods for modelling land surface phenology. In: Hudson , I . L. and Keatley, M. R. (Eds.) *Phenological research*, pp. 177-208, Springer Netherlands, Dordrecht, South Holland, The Netherlands

Dragoni, D., Schmid, H. P., Wayson, C. A., Potter, H., Grimmond, C. S. B., and Randolph, J. C. (2011). Evidence of increased net ecosystem productivity associated with a longer vegetated season in a deciduous forest in south-central Indiana, USA. *Global Change Biology*, 17, 886-897.

Duarte, C. M., Dennison, W. C., Orth, R. J., and Carruthers, T. J. 2008. The charisma of coastal ecosystems: addressing the imbalance. *Estuaries and Coasts*, 31, 233-238.

Elmore, A. J., Guinn, S. M., Minsley, B. J., and Richardson, A. D. 2012. Landscape controls on the timing of spring, autumn, and growing season length in mid-Atlantic forests. *Global Change Biology*, 18, 656-674.

Erickson, J. E., Megonigal, J. P., Peresta, G., and Drake, B. G. 2007. Salinity and sea level mediate elevated CO_2 effects on C_3–C_4 plant interactions and tissue nitrogen in a Chesapeake Bay tidal wetland. *Global Change Biology*, 13, 202–215.

Fisher, J. I., and Mustard, J. F. 2007. Cross–scalar satellite phenology from ground, Landsat, and MODIS data. *Remote Sensing of Environment*, 109, 261–273.

Fisher, J. I., Mustard, J. F., and Vadeboncoeur, M. A. 2006. Green leaf phenology at Landsat resolution: scaling from the field to the satellite. *Remote Sensing of Environment*, 100, 265-279

Fitzgerald, D. M., Fenster, M. S., Argow, B. A., and Buynevich, I. V. 2008. Coastal impacts due to sea–level rise, *Annual Review of Earth and Planetary Science*, 36, 601–647.

Friess, D. A., Spencer, T., Smith, G. M., Möller, I., Brooks, S. M., and Thomson, A. G. 2012. Remote sensing of geomorphological and ecological change in response to saltmarsh managed realignment, The Wash, UK, *International Journal of Applied Earth Observation and Geoinformation*, 18, 57–68.

Ganju, N. K., Schoellhamer, D. H., and Bergamaschi, B. A. 2005. Suspended sediment fluxes in a tidal wetland: Measurement, controlling factors, and error analysis. *Estuaries and Coasts*, 28, 812-822.

Gedan, K. B., Kirwan, M. L., Wolanski, E., Barbier, E. B., and Silliman, B. R. 2011. The present and future role of coastal wetland vegetation in protecting shorelines: answering recent challenges to the paradigm. *Climatic Change*, 106, 7-29.

Georgia Coastal Ecosystem Long-Term Ecological Research Network; http://gce-lter.marsci.uga.edu

Ghosh, S., Mishra, D. R., and Gitelson, A. A. 2016. Long-term monitoring of biophysical characteristics of tidal wetlands in the northern Gulf of Mexico—A methodological approach using MODIS. *Remote Sensing of Environment*, 173, 39-58.

Gilmore, M. S., Civco, D. L., Wilson, E. H., Barrett, N., Prisloe, S., Hurd, J. D., and Chadwick, C. 2010. Remote sensing and in situ measurements for delineation and assessment of coastal marshes and their constituent species, In: Wang, Y. (Ed.) Remote Sensing of Coastal Environment, pp. 261–280, CRC Press, Boca Raton, Florida, USA.

Gilmore, M. S., Wilson, E. H., Barrett, N., Civco, D. L., Prisloe, S., Hurd, J. D., and Chadwick, C. 2008. Integrating multi-temporal spectral and structural information to map wetland

vegetation in a lower Connecticut River tidal marsh. *Remote Sensing of Environment*, 112, 4048-4060.

Göckede, M., Foken, T., Aubinet, M., Aurela, M., Banza, J., Bernhofer, C., Bonnefond, J. M., Brunet, Y., Carrara, A., Clement, R., and Dellwik, E. 2008. Quality control of CarboEurope flux data–Part 1: Coupling footprint analyses with flux data quality assessment to evaluate sites in forest ecosystems. *Biogeosciences*, 5, 433-450.

Goudie, A. 2013. Characterising the distribution and morphology of creeks and pans on salt marshes in England and Wales using Google Earth, *Estuaries, Coastal and Shelf Science*, 129; 112–123.

Goulden, M. L., Wofsy, S. C., Harden, J. W., Trumbore, S. E., Crill, P. M., Gower, S. T., Fries, T., Daube, B. C., Fan, S. M., Sutton, D. J. and Bazzaz, A. 1998. Sensitivity of boreal forest carbon balance to soil thaw. *Science*, 279, 214-217.

Graham, E. A., Hamilton, M. P., Mishler, B. D., Rundel, P. W., and Hansen, M. H. 2006. Use of a networked digital camera to estimate net CO_2 uptake of a desiccation-tolerant moss. *International Journal of Plant Science*, 167, 751-758.

Graham, E. A., Riordan, E. C., Yuen, E. M., Estrin, D., and Rundel, P. W. 2010. Public internet-connected cameras used as a cross-continental ground-based plant phenology monitoring system. *Global Change Biology*, 16, 3014-3023.

Gutman, G. G. 1991. Vegetation indices from AVHRR, An update and future prospects. *Remote Sensing of Environment*, 35, 121–136.

Heimann, M., Esser, G., Haxeltine, A., Kaduk, J., Kicklighter, D. W., Knorr, W., Kohlmaier, G. H., McGuire, A. D., Melillo, J., Moore, B. and Otto, R. D. 1998. Evaluation of terrestrial carbon cycle models through simulations of the seasonal cycle of atmospheric CO_2: First results of a model intercomparison study. *Global Biogeochemical Cycles*, 121, 1-24.

Hester, M. W. and I. A. Mendelssohn. 2000. Long-term recovery of a Louisiana brackish marsh plant community from oil-spill impact: Vegetation response and mitigating effects of marsh surface elevation. *Marine Environmental Research,* 49, 233–254.

Heumann, B. W., Seaquist, J. W., Eklundh, L., and Jönsson, P. 2007. AVHRR derived phenological change in the Sahel and Soudan, Africa, 1982–2005. *Remote Sensing of Environment*, 108, 385–392.

Hinkle, R. L., and Mitsch, W. J. 2005 Salt marsh vegetation recovery at salt hay farm wetland restoration sites on Delaware Bay. *Ecological Engineering*, 25, 240–251.

Hogg, E. H., Price, D. T., and Black, T. A. 2000. Postulated feedbacks of deciduous forest phenology on seasonal climate patterns in the western Canadian interior. *Journal of Climate*, 13, 4229-4243.

Huete, A. R., and Liu, H. Q. 1994. An error and sensitivity analysis of the atmospheric–and soil–correcting variants of the NDVI for the MODIS–EOS. *IEEE Transactions on Geoscience and Remote Sensing*, 32, 897–905.

Hufkens, K., Friedl, M., Sonnentag, O., Braswell, B. H., Milliman, T., and Richardson, A. D. 2012. Linking near-surface and satellite remote sensing measurements of deciduous broadleaf forest phenology. *Remote Sensing of Environment*, 117, 307-321.

Ide, R., and Oguma, H. 2010. Use of digital cameras for phenological observations. *Ecological Informatics*, 5, 339-347.

Jonsson, P., Eklundh, L. 2002. Seasonality extraction by function fitting to time–series of satellite sensor data. *IEEE Transactions on Geoscience and Remote Sensing*, 40, 1824–1832.

Jung, M., Verstraete, M., Gobron, N., Reichstein, M., Papale, D., Bondeau, A., Robustelli, M., and Pinty, B. 2008. Diagnostic assessment of European gross primary production. *Global Change Biology*, 14, 2349-2364.

Kaswadji, R. F., Gosselink, J. G., and Turner, R. E. 1990. Estimation of primary production using five different methods in a *Spartina alterniflora* salt marsh. *Wetlands Ecology and Management*, 1, 57-64.

Kearney, M. S., Stutzer, D., Turpie, K., and Stevenson, J. C. 2009. The effects of tidal inundation on the reflectance characteristics of coastal marsh vegetation, *Journal of Coastal Research*, 25, 1177–1186.

Kennish, M. J. 2001. Coastal Salt Marsh Systems in the US: a Review of Anthropogenic Impacts. *Journal of Coastal Research*, 17, 731–748.

Khanna, S., Santos, M. J., Koltunov, A., Shapiro, K. D., Lay, M., and Ustin, S. L. 2017. Marsh Loss due to cumulative impacts of Hurricane Isaac and the Deepwater Horizon Oil Spill in Louisiana. *Remote Sensing*, 9, 169.

Klosterman, S. T., Hufkens, K., Gray, J. M., Melaas, E., Sonnentag, O., Lavine, I., Mitchell, L., Norman, R., Friedl, M.A. and Richardson, A. D. 2014. Evaluating remote sensing of deciduous

forest phenology at multiple spatial scales using PhenoCam imagery. *Biogeosciences* , 4305 - 4320.

Kritzer, J., and Hughes, A. 2010. The Role of Salt Marshes in Sustaining Long Island Fisheries. *Memoirs of the Torrey Botanical Society*, 26, 34-41.

Kunkel, K. E., Easterling, D. R., Hubbard, K., and Redmond, K. 2004. Temporal variations in frost-free season in the United States, 1895–2000. *Geophysical Research Letters*, 31, DOI: 10.1029/2003GL018624

Kurc, S. A., and Benton, L. M. 2010. Digital image-derived greenness links deep soil moisture to carbon uptake in a creosote bush-dominated shrubland. *J. Arid. Environ.*, 74, 585-594.

Lafleur, P. M., Moore, T. R., Roulet, N. T., and Frolking, S. 2005. Ecosystem respiration in a cool temperate bog depends on peat temperature but not water table. *Ecosystems,* 8, 619-629.

Langlois, E., Bonis, A., and Bouzille, J. B. 2003. Sediment and plant dynamics in saltmarshes pioneer zone: Puccinellia maritima as a key species?. *Estuarine, Coastal and Shelf Science*, 56, 239-249.

Li, Z., Yu, G., Xiao, X., Li, Y., Zhao, X., Ren, C., Ren, C., Zhang, L., and Fu, Y. 2007. Modeling gross primary production of alpine ecosystems in the Tibetan Plateau using MODIS images and climate data. *Remote Sensing of Environment*, 107, 510-519.

Liu, Q., Fu, Y. H., Zeng, Z., Huang, M., Li, X., and Piao, S. 2016. Temperature, precipitation, and insolation effects on autumn vegetation phenology in temperate China. *Global Change Biology*, 22, 644-655.

Lucas, K. L. and Carter. G. A. 2008. The use of hyperspectral remote sensing to assess vascular plant species richness on Horn Island, Mississippi. *Remote Sensing of the Environment*, 112, 3908–3915.

Macreadie, P. I., Hughes, A. R., and Kimbro, D. L. 2013. Loss of 'blue carbon'from coastal salt marshes following habitat disturbance. *PloS one*, 8, e69244.

Marani, M., Silvestri, S., Belluco, E., Ursino, N., Comerlati, A., Tosatto, O., and Putti. M. 2006. Spatial organization and ecohydrological interactions in oxygen-limited vegetation ecosystems. *Water Resources Research*, 42, W06D06.

Mcleod, E., Chmura, G. L., Bouillon, S., Salm, R., Björk, M., Duarte, C. M., Lovelock, C.E., Schlesinger, W.H. and Silliman, B. R. 2011. A blueprint for blue carbon: toward an improved understanding of the role of vegetated coastal habitats in sequestering CO_2. *Frontiers in Ecology and the Environment*, 9, 552-560.

Melaas, E. K., Friedl, M. A., and Richardson, A. D. 2016. Multiscale modeling of spring phenology across Deciduous Forests in the Eastern United States. *Global Change Biology*, 22, 792-805.

Mishra, D. R. and Ghosh, S. 2015. Using moderate resolution satellite sensors for monitoring the biophysical parameters and phenology of tidal wetlands. In: Tiner, R., Land, M. and Klemas, V. (Eds.) *Remote Sensing of Wetlands, Applications and Advances*, pp. 283 – 314, CRC Press, Boca Raton, Florida, USA.

Mishra, D. R., Cho, H. J., Ghosh, S., Fox, A., Downs, C., Merani, P. B. T., Kirui, P., Jackson, N. and Mishra, S. 2012. Post–spill state of the marsh: Remote estimation of the ecological impact of

the Gulf of Mexico oil spill on Louisiana Salt Marshes, *Remote Sensing of Environment*, 118, 176–185.

Mitsch, W. J. and J. G. Gosselink. 2007. Wetlands. John Wiley and Sons, Hoboken, NJ.

Möller, I., Spencer, T., French, J. R., Leggett, D. J., and Dixon, M. 1999. Wave transformation over salt marshes: a field and numerical modelling study from North Norfolk, England. *Estuarine, Coastal and Shelf Science*, 49, 411–426.

Monteith, J. L. 1972. Solar radiation and productivity in tropical ecosystems. *Journal of Applied Ecology*, 9, 747-766.

Moore, K. E., Fitzjarrald, D. R., Sakai, R. K., Goulden, M. L., Munger, J. W., and Wofsy, S. C. 1996. Seasonal variation in radiative and turbulent exchange at a deciduous forest in central Massachusetts. *Journal of Applied Meteorology*, 35, 122-134.

Morgan, P. A., Burdick, D. M., and Short, F. T. 2009. The functions and values of fringing salt marshes in northern New England, USA. *Estuaries and Coasts*, 32, 483-495.

Myneni, R. B., Keeling, C. D., Tucker, C. J., Asrar, G., and Nemani, R. R. 1997. Increased plant growth in the northern high latitudes from 1981 to 1991, *Nature*, 386, 698–702.

Nellemann, C., and Corcoran, E. (Eds.) 2009. Blue carbon: the role of healthy oceans in binding carbon: a rapid response assessment, UNEP/Earthprint.

Nicholls, R. J., Hoozemans, F. M., and Marchand, M. 1999. Increasing flood risk and wetland losses due to global sea–level rise: regional and global analyses, *Global Environmental Change*, 9, S69–S87.

O'Donnell, J. P., and Schalles, J. F. 2016. Examination of abiotic drivers and their influence on *Spartina alterniflora* biomass over a twenty-eight year period using Landsat 5 TM satellite imagery of the Central Georgia Coast. *Remote Sensing*, 8, 477.

Ogburn, M. B., and Alber, M. 2006. An investigation of salt marsh dieback in Georgia using field transplants. *Estuaries and Coasts*, 29, 54-62.

Ollinger, S. V., Richardson, A. D., Martin, M. E., Hollinger, D. Y., Frolking, S. E., Reich, P. B., Plourde, L. C., Katul, G. G., Munger, J. W., Oren, R. and Smith, M. L. 2008. Canopy nitrogen, carbon assimilation, and albedo in temperate and boreal forests: Functional relations and potential climate feedbacks. *Proceedings of the National Academy of Sciences*, 105, 19336-19341.

Osmond, B., Ananyev, G., Berry, J., Langdon, C., Kolber, Z., Lin, G., Monson, R., Nichol, C., Rascher, U., Schurr, U. and Smith, S. 2004. Changing the way we think about global change research: scaling up in experimental ecosystem science. *Global Change Biology*, 10, 393-407.

Pierce, L. L., Running, S.W., and Walker, J. 1994. Regional-scale relationships of leaf area index to specific leaf area and leaf nitrogen, *Ecological Applications*, 4, 313–321

Pinar, A. and Curran, P. J. 1996. Grass chlorophyll and the reflectance red edge, *International Journal of Remote Sensing*, 17, 135–357

Ponton, S., Flanagan, L. B., Alstad, K. P., Johnson, B. G., Morgenstern, K. A. I., Kljun, N., Black, T. A. and Barr, A. G. 2006. Comparison of ecosystem water-use efficiency among Douglas-fir forest, aspen forest and grassland using eddy covariance and carbon isotope techniques. *Global Change Biology*, 12, 294-310.

Ravens, T. M., Thomas, R. C., Roberts, K. A., and Santschi, P. H. 2009. Causes of salt marsh erosion in Galveston Bay, Texas, *Journal of Coastal Research*, 25, 265–272.

Reed, B. C., Brown, J. F., VanderZee, D., Loveland, T. R., Merchant, J. W., and Ohlen, D. O. 1994. Measuring phenological variability from satellite imagery. *Journal of Vegetation Science*, 5, 703–714.

Reichstein, M., Ciais, P., Papale, D., Valentini, R., Running, S., Viovy, N., Cramer, W., Granier, A., Ogee, J., Allard, V. and Aubinet, M. 2007. Reduction of ecosystem productivity and respiration during the European summer 2003 climate anomaly: a joint flux tower, remote sensing and modelling analysis. *Global Change Biology*, 13, 634-651.

Richardson, A. D., Braswell, B. H., Hollinger, D. Y., Jenkins, J. P., and Ollinger, S. V. 2009. Near–surface remote sensing of spatial and temporal variation in canopy phenology, *Ecological Applications*, 19, 1417–1428.

Richardson, A. D., Jenkins, J. P., Braswell, B. H., Hollinger, D. Y., Ollinger, S. V., and Smith, M. L. 2007. Use of digital webcam images to track spring green-up in a deciduous broadleaf forest. *Oecologia*, 152, 323-334.

Roerink, G. J., Menenti, M., Verhoef, W. 2000. Reconstructing cloudfree NDVI composites using Fourier analysis of time series. *International Journal of Remote Sensing*, 21, 1911–1917.

Running, S. W., Nemani, R. R., Heinsch, F. A., Zhao, M., Reeves, M., and Hashimoto, H. 2004. A continuous satellite-derived measure of global terrestrial primary production. *American Institute of Biological Science Bulletin*, 54, 547-560.

Running, S. W., Thornton, P. E., Nemani, R., and Glassy, J. M. 2000. Global terrestrial gross and net primary productivity from the Earth Observing System. *Methods in Ecosystem Science*, 3, 44-45.

Sadro, S., Gastil-Buhl, M., and Melack, J. 2007. Characterizing patterns of plant distribution in a southern California salt marsh using remotely sensed topographic and hyperspectral data and local tidal fluctuations. *Remote Sensing of the Environment*, 110:226–239.

Scheifinger, H., Menzel, A., Koch, E., Peter, C., and Ahas, R. 2002. Atmospheric mechanisms governing the spatial and temporal variability of phenological phases in central Europe. *International Journal of Climatology*, 22, 1739–1755.

Seabrook, C. (Ed.) 2012. The world of the salt marsh: appreciating and protecting the tidal marshes of the southeastern Atlantic coast. University of Georgia Press, Athens, Georgia, USA.

Sellers, P. J., Tucker, C. J., Collatz, G. J., Los, S. O., Justice, C. O., Dazlich, D. A., Randall, D. A. 1994. A global 1° by 1° NDVI data set for climate studies, Part II. The generation of global fields of terrestrial biophysical parameters from the NDVI. *International Journal of Remote Sensing*, 15, 3519 – 3545.

Shen, M., Tang, Y., Chen, J., Zhu, X., and Zheng, Y. 2011. Influences of temperature and precipitation before the growing season on spring phenology in grasslands of the central and eastern Qinghai–Tibetan Plateau. *Agricultural and Forest Meteorology*, 151, 1711–1722.

Silliman, B. R., Grosholz, E. D., and Bertness, M. D. (Eds.) 2009. Human Impacts on Salt Marshes: A Global Perspective, University of California Press, Berkeley, California, USA.

Sims, D. A., Rahman, A. F., Cordova, V. D., El-Masri, B. Z., Baldocchi, D. D., Bolstad, P. V., Flanagan, L. B., Goldstein, A. H., Hollinger, D. Y., Misson, L., and Monson, R. K. 2008. A new model of gross primary productivity for North American ecosystems based solely on the enhanced vegetation index and land surface temperature from MODIS. *Remote Sensing of Environment*, 112, 1633-1646.

Sonnentag, O., Detto, M., Vargas, R., Ryu, Y., Runkle, B. R. K., Kelly, M., and Baldocchi, D. D. 2011. Tracking the structural and functional development of a perennial pepperweed (*Lepidium latifolium* L.) infestation using a multi-year archive of webcam imagery and eddy covariance measurements. *Agricultural and Forest Meteorology*, 151, 916-926.

Sonnentag, O., Hufkens, K., Teshera-Sterne, C., Young, A. M., Friedl, M., Braswell, B. H., Milliman, T., O'Keefe, J. and Richardson, A. D. 2012. Digital repeat photography for phenological research in forest ecosystems. *Agricultural and Forest Meteorology*, 152, 159-177.

Soudani, K., Le Maire, G., Dufrêne, E., François, C., Delpierre, N., Ulrich, E., and Cecchini, S. 2008. Evaluation of the onset of green–up in temperate deciduous broadleaf forests derived from Moderate Resolution Imaging Spectroradiometer (MODIS) data. *Remote Sensing of Environment*, 112, 2643–2655.

Sugumaran, R., Meyer, J. C., and Davis, J. 2004. A web–based environmental decision support system (WEDSS) for environmental planning and watershed management, *Journal of Geographical Systems*, 6, 307–322.

Tiner, R. W. (Eds.) 2013. Tidal Wetlands Primer: An Introduction to their Ecology, Natural History, Status, and Conservation. The University of Massachusetts Press, Amherst, MA.

U.S. Department of the Interior, Fish and Wildlife Service, and U.S. Department of Commerce, U.S. Census Bureau. 2006. National Survey of Fishing, Hunting, and Wildlife-Associated Recreation.

Valiela, I., Cole, M. L., Mcclelland, J., Hauxwell, J., Cebrian, J., and Joye, S. B. 2002. Role of salt marshes as part of coastal landscapes. In: Winston, M. P. and Kreeger, D. A. (Eds.) *Concepts and controversies in tidal marsh ecology*, pp. 23-36, Springer Netherlands, Dordrecht, South Holland, The Netherlands.

Verbesselt, J., Hyndman, R., Zeileis, A., Culvenor, D. 2010. Phenological change detection while accounting for abrupt and gradual trends in satellite image time series. *Remote Sensing of Environment*, 114, 2970–2980.

Viovy, N., Arino, O., Belward, A. S. 1992. The Best Index Slope Extraction (BISE), A method for reducing noise in NDVI time–series. *International Journal of Remote Sensing*, 13, 1585–1590.

Walker, J. J., De Beurs, K. M., Wynne, R. H., and Gao, F. 2012. Evaluation of Landsat and MODIS data fusion products for analysis of dryland forest phenology. *Remote Sensing of Environment*, 117, 381-393.

Wang, Y., Christiano, M., Traber, M., and Wang, J. 2010. Mapping salt marshes in Jamaica Bay and terrestrial vegetation in Fire Island National Seashore using QuickBird satellite data. In: Wang, Y. (Ed.) Remote Sensing of Coastal Environments, pp. 191-208, CRC Press, Boca Raton, Florida, USA.

White, D. L., Porter, D. E., and Lewitus, A. J. 2004. Spatial and temporal analyses of water quality and phytoplankton biomass in an urbanized versus a relatively pristine salt marsh estuary. *Journal of Experimental Marine Biology and Ecology*, 298, 255-273.

White, K. P., Langley, J. A., Cahoon, D. R., Megonigal, J. P. 2012. C_3 and C_4 biomass allocation responses to elevated CO_2 and nitrogen, contrasting resource capture strategies. *Estuaries and Coasts*, 35, 1028–1035.

White, M. A., Beurs, D., Kirsten, M., Didan, K., Inouye, D. W., Richardson, A. D., Jensen, O. P., O'keefe, J. O., Zhang, G., Nemani, R. R. and Leeuwen, V. 2009. Intercomparison, interpretation, and assessment of spring phenology in North America estimated from remote sensing for 1982–2006. *Global Change Biology*, 15, 2335-2359.

White, M. A., Thornton, P. E., and Running, S. W. 1997. A continental phenology model for monitoring vegetation responses to interannual climatic variability. *Global Biogeochemical Cycles*, 11, 217–234.

Wille, C., Kutzbach, L., Sachs, T., Wagner, D., and Pfeiffer, E. V. A. 2008. Methane emission from Siberian arctic polygonal tundra: eddy covariance measurements and modeling. *Global Change Biology*, 14, 1395-1408.

Wu, C., Munger, J. W., Niu, Z., and Kuang, D. 2010. Comparison of multiple models for estimating gross primary production using MODIS and eddy covariance data in Harvard Forest. *Remote Sensing of Environment*, 114, 2925-2939.

Xiao, X., Braswell, B., Zhang, Q., Boles, S., Frolking, S., Moore, B. 2003. Sensitivity of vegetation indices to atmospheric aerosols, continental–scale observations in Northern Asia. *Remote Sensing of Environment*, 84, 385–392.

Xiao, X., Zhang, Q., Saleska, S., Hutyra, L., De Camargo, P., Wofsy, S., Frolking, S., Boles, S., Keller, M., and Moore, B. 2005a. Satellite-based modeling of gross primary production in a seasonally moist tropical evergreen forest. *Remote Sensing of Environment*, 94, 105-122.

Yan, G., Mas, J. F., Maathuis, B. H. P., Xiangmin, Z., and Van Dijk, P. M. 2006. Comparison of pixel-based and object-oriented image classification approaches—A case study in a coal fire area, Wuda, Inner Mongolia, China. *International Journal of Remote Sensing*, 27, 4039–4055.

Zhang, X. and Goldberg, M. D. 2011. Monitoring fall foliage coloration dynamics using time–series satellite data. *Remote Sensing of Environment*, 115, 382–391.

Zhang, X., Friedl, M. A., and Schaaf, C. B. 2006. Global vegetation phenology from Moderate Resolution Imaging Spectroradiometer (MODIS), Evaluation of global patterns and comparison with *in situ* measurements. *Journal of Geophysical Research: Biogeosciences*, 111, DOI: 10.1029/2006JG000217

Zhang, X., Friedl, M. A., Schaaf, C. B., Strahler, A. H., Hodges, J. C., Gao, F., Reed, B. and Huete, A. 2003. Monitoring vegetation phenology using MODIS. *Remote Sensing of Environment*, 84, 471–475.

Zhao, J., Zhang, Y., Tan, Z., Song, Q., Liang, N., Yu, L., and Zhao, J. 2012. Using digital cameras for comparative phenological monitoring in an evergreen broad-leaved forest and a seasonal rain forest. *Ecol. Inf.*, 10, 65-72.

Zuo, P., Zhao, S., Liu, C. A., Wang, C., and Liang, Y. 2012. Distribution of Spartina spp. along China's coast. *Ecological Engineering*, 40, 160-166.

CHAPTER 2

POST-SPILL STATE OF THE MARSH: REMOTE ESTIMATION OF THE ECOLOGICAL IMPACT OF THE GULF OF MEXICO OIL SPILL ON LOUISIANA SALT MARSHES[†]

[†]Mishra, D. R., Cho, H. J., Ghosh, S., Fox, A., Downs, C., Merani, P. B., Kirui, P., Jackson, N. and Mishra, S. 2012. Post-spill state of the marsh: Remote estimation of the ecological impact of the Gulf of Mexico oil spill on Louisiana Salt Marshes. *Remote Sensing of Environment*, 118, 176-185. Reprinted here with permission of Elsevier.

Abstract

One and a half years after the worst oil spill in U.S. history, we present the first quantitative assessment on the ecological impact of the spill on the salt marsh habitats along the southeastern Louisiana (LA) coast. This research combined satellite and ground data to quantify the impact of the oil and dispersant on the salt marshes in terms of their photosynthetic capacity and physiological status over a large spatial scale. Two of the most important marsh biophysical characteristics, including distribution of canopy chlorophyll content and above ground green biomass, were monitored across the southeastern LA coast during the salt marsh growing season (May-October) of 2009 (pre-spill) and 2010 (post-spill) in order to compare and isolate the spill impacted areas. The initial assessment showed that there was a significant post-spill increase in areas with reduced biomass and canopy chlorophyll (> 400 km^2) during the 2010 growing season compared to 50-65 km^2 during the 2009 growing season. Phenological analysis of the post oil-spill data revealed a significant decrease in the magnitude of biomass and canopy chlorophyll during the peak of the 2010 growing season. June was consistently found to be the worst month in terms of salt marsh health across LA over the 2010 phenological cycle followed by the initial signs of recovery along the fringing marsh areas proximal to the shoreline that were first impacted by oil. Interior marsh patches exhibited persistent signs of stress towards the end of the growing season. Extensive reduction in photosynthetic activity was observed during the peak of the growing season, particularly in Plaquemines Parish and St. Bernard Parish. The products generated through this study successfully delineate the critical hotspots of marsh stress so that prioritization of areas needing immediate restoration can be performed.

Keywords: Gulf of Mexico; LA; Deepwater Horizon Oil Spill; Ecological Impact; Salt Marsh; Canopy Chlorophyll; Above Ground Biomass; Field Spectroscopy; Landsat TM

Introduction

Salt marshes are considered to be the most vulnerable coastal environment (vulnerability index of 10 from a 1-10 scale) that can be adversely affected by an oil spill, with the predicted residence times of over 10 years (Gundlach and Hayes, 1978; Pezeshki et al. 2000). Salt marshes generally have more oil-sensitive vegetation than freshwater marshes and the oil impact on vegetation is most significant in highly organic soils of salt marshes (Lin and Mendelssohn, 1996; Pezeshki et al. 2000). The direct and immediate physical impact of an oil spill on wetland vegetation includes the coating of the plant and soil surfaces causing temperature stress, and reduced photosynthesis due to blockage of stomata and transpiration pathways. Petroleum hydrocarbons also adversely affect the ability of salt marsh vegetation to tolerate salinity, which increases the potential of dieback and hampers recovery (Gilfillan et al. 1989). Additional damage can be caused by the resulting cleanup activities such as skimming, oil collection, burning, flushing, use of dispersants, and plant cutting (Allen and Freck, 1993; Kiesling, 1990; Mendelssohn et al. 1990; Owens et al. 1993a and 1993b). To complicate matters further, the effects of oil spills vary with vegetation types and season. For example, previous research shows that, of the more common Gulf Coast vegetation species, *Spartina alterniflora* is more sensitive to oiling than *Juncus roemerianus* (Pezeshki and DeLaune, 1993), while recent research findings suggest otherwise (Lin and Mendelssohn, 2012). Furthermore, flora is more sensitive to oiling during the growing season than during the pre-dormancy or dormant season (Pezeshki et al. 2000). It is advised that summer burns of contaminated marsh patches be avoided if possible (Lindau et al. 1999), because flooding following burning also adversely affects plant growth in many species (Pezeshki et al. 2000). The Deep Water Horizon Macondo MC252 oil spill beginning on April 20, 2010 poured more than 200 million gallons of crude oil in the Gulf waters

off southeastern Louisiana (LA), and an additional 1.8 million gallons of dispersant were added to countervail the effects of the contamination (US DOI, 2010). Since the oil spill and cleanup efforts occurred mainly in the early summer, the critical growing season for *Spartina* and other marsh species, it was expected that a severe, short-term impact of the spill would occur on salt marshes causing changes in plant community composition associated with species' sensitivity to fouling and physical disturbance.

Canopy chlorophyll content (CHL) is one of the most important foliar biochemicals that is related closely to both the productivity and health of vegetation (Curran et al. 1990). Above ground green biomass (GBM) is a direct result of vegetation productivity and another key variable required for analyzing coastal salt marsh status (Curran, 1982; Hardisky et al. 1984). Due to the synoptic view provided by airborne and space-borne sensors, remote sensing has the potential for estimating both CHL and GBM at a regional level. Remote estimations of these characteristics can be performed using transforms of spectral reflectance, referred to as vegetation indices (VIs) (Rouse et al. 1974). Several VIs for estimating CHL and GBM using remotely sensed data have been developed and are proven to provide accurate predictions in different vegetation types (Gitelson and Merzlyak, 1997; Gitelson and Merzlyak, 1998; Gitelson et al. 2003a; Gitelson et al. 2003b; Kogan et al. 2004). The US Geological Survey's (USGS) Landsat satellite holds considerable potential for advancing our capabilities to estimate and monitor the biophysical characteristics of salt marshes across large geographic areas. Landsat provides 16-day coverage of moderate resolution data that are well calibrated, and have relatively high geolocational accuracy (Tucker et al. 2004). The value of Landsat surface reflectance and VI data for various vegetation-related land use/land cover characterization activities such as forest mapping (Pax-Lenney et al. 2001), marsh biomass mapping (Hardisky et

al. 1984), phenological monitoring (Fisher et al. 2006), and sub-pixel fractional estimation of vegetation area (Chen et al. 2004) has been well demonstrated.

The overall objective of this study was to quantify the short-term impact of the oil spill on the photosynthetic activity and physiological status of the coastal salt marshes over the large area by combining satellite data with ground experiments. This objective was achieved by analyzing two biophysical characteristics of marsh vegetation including CHL and GBM generated through a remote sensing mapping protocol. The specific objectives included, (1) application of a suite of algorithms combining Landsat 30-m datasets with field data to map CHL and GBM across southeastern LA salt marshes; and (2) compare and quantify the changes observed in CHL and GBM distribution during the salt marsh growing season between 2009 (pre-spill) and 2010 (post-spill) to isolate the spill impact. The products generated through this research will provide restoration decision makers across LA with a practical tool to inform the prioritization of marsh restoration effort to the areas, most affected by the spill.

Study Area

Salt Marshes cover almost the entire coast of LA (> 4500 km^2) (Figure 2.1). The habitat is dominated by smooth cord-grass (*Spartina alterniflora*), salt meadow cord-grass (*Spartina patens*), black needle-rush (*Juncus roemarianus*), with occasional presence of *Salicornia virginica, Batis maritima* and *Distichlis spicata*. Highly saline and anaerobic nature of the soil allows only selected species to survive, and as such, floral diversity is remarkably low (Weis, 2010) However, salt marshes act as buffers to strong winds and tidal waves in the Gulf of Mexico. In addition, the marshes serve as a nursery to commercially important species like shrimps, crabs, fishes and birds. Apart from their commercial significance, the salt marshes are

one of the most biologically productive habitats (White et al. 1978). The region experiences a tropical to sub-tropical climate characterized by hot summers, with occasional tropical storms and moderately cold winters. However, the time-period considered for this study observed no major tropical storms (2009 - 2010). Average annual temperature varies between 15 - 25 degrees Celcius while annual precipitation ranges between 80 - 100 centimeters (Weather Underground, http://www.wunderground.com/).

Materials and Methods

a. Field Data Collection

Sixty-nine salt marsh plots across an oil gradient (heavy, moderate, light, and no oil) were sampled in southeastern LA, during the post-spill growing season (May – October, 2010), which were used for model calibration. Another independent dataset containing an additional twenty-six study plots were sampled from a different geographic location on different dates for model validation. The locations of heavy oil contaminated regions were identified based on an airborne survey of the region prior to the field visit. Resident oil and signs of marsh damage were observed in highly contaminated regions across southeastern LA salt marsh habitats (Figures 2.2a - e). Numerous areas of marsh browning, blankets of light oil coating on marsh canopy, evidence of infiltration of the oil to the young marsh root system, and damage due to clean up efforts were observed and photographed for record. The *in situ* data collection included: 1) top of Canopy (TOC) reflectance (R_{rs}), 2) leaf level chlorophyll content, 3) Leaf Area Index (LAI), 4) canopy level chlorophyll (CHL), and 5) above ground green biomass (GBM).

1) Top of Canopy Reflectance (R_{rs}):

Close range reflectance data were acquired using OceanOptics USB 4000 hyperspectral radiometer (OceanOptic Inc., Dunedin, FL, USA). A dual-fiber system, with two inter-calibrated OceanOptics USB4000 radiometers, mounted on an platform (Rundquist et al. 2004) was used to acquire the TOC reflectance data in the range of 200-1100 nm with a sampling interval of 0.3 nm (Rundquist et al. 2004). The radiometer #1 with a field-of-view (FOV) of 25° was mounted on a 5m (16 ft) solid aluminum frame and pointed downward to acquire upwelling radiance (*L*; Wm^2sr^{-1}) and the radiometer #2 equipped with a cosine corrector pointed upward to acquire downwelling irradiance (*E*; Wm^{-2}) simultaneously (Figure 2.2i and Figure 2.3a). Four scans of radiance and irradiance were acquired and converted to five R_{rs} (sr^{-1}) readings by dividing *L* over *E*. The four R_{rs} spectra were averaged out to obtain composite spectra of that study plot. Based on the FOV and the height of the frame, the spatial resolution (IFOV) of the sensor was calculated to be 2.2 meter (Figure 2.3b and c).

$$d = 2\{h \times (tan\frac{\alpha}{2})\} \quad (1)$$

where, *d* = diameter of the IFOV, *h* = height of the sensor from the target, α = FOV of the sensor

Inter-calibration of the radiometers was accomplished by measuring the upwelling radiance of a 99% white Spectralon reflectance standard (Labsphere, Inc., North Sutton, NH) simultaneously with incident irradiance (Figure 2.2h). In case of changing sky conditions, the sensor was recalibrated at regular intervals.

2) Leaf Level Chlorophyll Content:

Minolta 502 SPAD Chlorophyll meter (Spectrum Technologies Inc., East - Plainfield, IL, USA) was used to measure *in situ* leaf level chlorophyll content. A total of twenty stratified random SPAD readings were acquired from the marsh leaves inside the IFOV of the sensor (Figure 2.2f). The readings were averaged and converted to absolute chlorophyll values (mg/m^2) based on a calibration procedure. The calibration procedure was performed to develop a relationship between SPAD readings and the corresponding laboratory extracted leaf chlorophyll concentration as described in Gitelson et al. 2005. In order to account for maximum variability in chlorophyll content, leaves with varying degree of chlorophyll levels (green, greenish yellow, yellow, yellowish brown, brown) were sampled.

3) Leaf Area Index (LAI):

Leaf Area Index (LAI) was measured using LAI Plant Canopy Analyzer 2000 (LICOR Biosciences Inc., Lincoln, NE, USA) (Gitelson et al. 2002). As many as four LAI readings in each study plot were obtained; each measurement involving one above-canopy and four below-canopy readings (Figure 2.2g). The median of the four readings was considered to be the final LAI value for the study plot.

4) Canopy Level Chlorophyll (CHL):

Canopy level chlorophyll (mg/m^2) was calculated as the product of LAI and Leaf Level Chlorophyll as described in Gitelson et al. 2002:

$$CHL = Leaf\ Level\ Chlorophyll \times LAI \quad (2)$$

5) Above ground green biomass (GBM):

Above ground green biomass data were collected from a 0.09 m^2 (1 ft^2) sub-plot within each study plot using a PVC frame and clippers. The biomass was sorted in order to separate the standing dead from the live biomass; oven dried at 50° Celsius overnight (~12 hours), and the dry weight was recorded using a standard measuring balance. Precautions were taken to avoid moisture absorption by the dried biomass during dry weight measurement as much as possible.

The study plots were chosen sufficiently far apart from each other in order to account for as much variability within a single Landsat pixel as possible. In case of multiple study plots located within a single Landsat pixel, ground data were averaged out to accurately establish the relationship between satellite-derived VIs and the field data. The sixty-nine study plots were reduced to fifty-three Landsat pixels which were subsequently used in model calibration. The validation dataset containing twenty-six study plots were reduced to twenty-one Landsat pixels.

b. Landsat Analysis

Multi-temporal Landsat (TM5) 30m datasets for the region were procured from the United States Geological Survey, for the growing seasons of 2009 and 2010 (Table 2.1). The TM5 recorded digital number (DN) were converted to ground reflectance (ρ) using the COS(TZ) or COST atmospheric correction model (Chavez, 1996). COST atmospheric correction is based on a revised dark-object model where the function of the cosine of zenith angle estimates atmospheric transmittance. The method is employed to derive the multiplicative transmittance correction coefficient without *in situ* field measurements for bands 1-5 and band 7 (ARSC, 2002). In order to convert each minimum DN to an at-satellite minimum spectral radiance value, $L_{\lambda min}$ was calculated:

$$L_{\lambda min} = LMIN_{\lambda} + QCAL \times \frac{(LMAX_{\lambda} - LMIN_{\lambda})}{QCAL_{MAX}} \quad (3)$$

where, *QCAL* is the minimum DN, $QCAL_{MAX}$ is 255 (8-bit radiometric resolution), $LMIN_{\lambda}$ and $LMAX_{\lambda}$ are constants given in Markham and Barker (1986). The theoretical radiance of a dark object for each band (assumed 1% reflectance in Chavez, 1996 and Moran et al. 1992) is computed as:

$$L_{\lambda 1\%} = 0.01 \times d^2 \times \frac{cos^2\theta}{(\pi \times E_{SUN\lambda})} \quad (4)$$

where, $E_{SUN\lambda}$ = mean solar exoatmospheric spectral irradiance (Markham and Barker, 1986), *d* = sun-earth distance, and θ *(theta)* = solar zenith angle.

The dark object values are used to compute haze correction as:

$$L_{\lambda haze} = L_{\lambda min} - L_{\lambda 1\%} \quad (5)$$

where, $L_{\lambda haze}$ = Value derived from the image using the dark object criteria ($Wm^{-2}sr^{-1}$), and $L_{\lambda 1\%}$= Theoretical radiance of the dark object ($Wm^{-2}sr^{-1}$)

The output model reflectance units are calculated from radiance DN as:

$$\rho = \pi \times d^2 \times \frac{(L_{\lambda sat} - L_{\lambda haze})}{E_{SUN\lambda}} \times cos^2\theta \quad (6)$$

where, $L_{\lambda sat}$= At-satellite radiance ($Wm^{-2}sr^{-1}$)

The shape of the Landsat derived R_{rs} spectra showed a strong similarity with the corresponding close range R_{rs} spectra acquired using the dual-headed OceanOptics radiometers (Figure 2.4).

Cloud cover in the datasets were eliminated using a threshold NDVI mask, following which several well established VIs were tested during the Landsat model calibration (using Landsat R_{rs}). The correlation coefficients (R^2) and root mean squared error (RMSE) were compared between VIs (Tables 2.2 and 2.3). The Wide Dynamic Range Vegetation Index (WDRVI) (Gitelson, 2004) showed the highest R^2 and was selected for estimating CHL (WDRVI α = 0.1) and GBM (WDRVI α = 0.05) (Figures 2.5a and b). WDRVI (range from -1 to +1) linearizes the relationship between vegetation biophysical parameters and reflectance and reduces the saturation exhibited by NDVI.

$$WDRVI = \frac{\alpha R_{NIR} - R_{red}}{\alpha R_{NIR} + R_{red}} \quad (7)$$

where, α = coefficient used to linearize the index, R_{NIR} and R_{red} are the NIR and red reflectance respectively

The two linear models (Equations 8 and 9) established during calibration were validated using the ground dataset of twenty-six plots (twenty-one Landsat pixels), and the percent normalized RMSE was calculated (Figure 2.5c). The percent normalized RMSE were considered reasonable with a $\pm$12% error for CHL and $\pm$7% for GBM estimation. The residuals for GBM and CHL did not reveal any trend (Figure 2.5d).

$$GBM = 298.943 \times WDRVI\ (\alpha = 0.05) + 264.494 \quad (8)$$

$$CHL = 251.955 \times WDRVI\ (\alpha = 0.1) + 182.327 \quad (9)$$

The above models were applied on the atmospherically corrected Landsat datasets to create monthly composites of CHL and GBM for the LA salt marsh habitats. The variations observed in the spatial distribution of GBM and CHL were analyzed across the area during the marsh

growing season (Apr-Oct) of 2009 and 2010, which were very similar years with no hurricane and/or other local/regional natural/anthropogenic perturbations that directly affected the area except the oil spill. Monthly average temperature and precipitation records acquired from four nearby weather stations (Figure 6a and 6b; Source: Weather Underground) were compared between 2009 and 2010 in order to correlate any changes observed during the 2010 growing season to the spill impact. Further flexibility was allowed in the models to offset the calibration error by considering a decrease of over 200g/m^2 for GBM and 20mg/m^2 for CHL as significant and ignoring any change below that level. These cutoff values (200 g/m^2 for GBM and 20 mg/m^2 for CHL) represent approximately 20% of the maximum biomass and chlorophyll contents observed in *Spartina* marshes in LA (Kirby and Gosselink, 1976).

Results and Discussion

Reflectance spectra of the study plots were grouped into three levels of oil contamination and examined (Figure 2.7). The characteristic 675 nm red absorption feature in healthy vegetation was less prominent in highly contaminated plots when compared to the non-contaminated plots (Li et al. 2005). The overall visible reflectance (400-700 nm) was found higher in contaminated vegetation, which implied reduced effect of the photosynthetic pigments such as chlorophyll a and b. Near Infrared (NIR) reflectance did not fluctuate greatly with the varying degree of contamination, which suggested that the cell structure of the marsh plants was still intact during the time of this particular data collection on Sep 30, 2010. However, with time and further reduction in photosynthetic pigments and increase in physiological stress, the salt marsh vegetation developed discoloration (chlorosis) accompanied by progressive defoliation. In general, it was observed that with oiling, marsh plants first went through the visual sign (oil

coating), followed by reduced photosynthetic pigments/activity (yellowing/browning up), and finally cell structural damage (dead biomass).

The monthly CHL and GBM composites prepared by applying the respective WDRVI models also substantiate the close range reflectance data. Comparison of the corresponding monthly composites pre- and post-oil spill growing season showed a considerable loss of productivity in salt marsh habitat during the 2010 growing season when compared to the 2009 data (Figures 2.8a and b and 9a). Roughly, 400 km^2 of the salt marsh habitat experienced a GBM reduction of 200 gm/m^2 or more in 2010. Similarly, 435 km^2 of the salt marsh habitat experienced a decrease in CHL by 20 mg/m^2 or more in 2010 (Figure 2.9b). These area estimates are a significant increase compared to the pre-spill (52 km^2 for GBM and 59 km^2 for CHL) growing season. It is well known that LA loses 50-65 km^2 (20-25 mi^2) of marshland every year due to numerous reasons including urbanization, leveeing of Mississippi River that result in reduced sedimentation and nutrient input, hurricanes, drought, and marsh fire etc (Egan, 2005; McKee et al. 2004; Michener et al. 1997; Nyman et al. 1994; Nyman and Chabreck, 1995). Coincidentally, the 2009 estimates for loss in GBM and CHL produced similar numbers of approximately 52 and 59 km^2 (18 and 22 mi^2) respectively (Figure 2.9b).

Although losses in GBM and CHL are not directly related to the land loss, they play an important role in triggering land loss. Most of these wetland losses are restricted to the fringing marsh habitats (marsh patches bordering any open water), where the process begins with the vegetation going through physiological stress or chlorosis (browning up) because of the loss in photosynthetic pigments and ultimately the root system loses strength and caves in to the open water. However, the change from 52-59 km^2 in 2009 to 400-435 km^2 in 2010 is considerably large (Figure 2.9b). This change cannot be attributed to inter-annual temperature fluctuations, as

temperature levels were consistent for both pre and post oil-spill growing seasons (Figure 2.6a). On the other hand, precipitation levels showed some inter-annual variations except in April 2009 and 2010. However, significant differences were observed between GBM and CHL levels of April 2009 and 2010, at 95% confidence limit (*p value* = 0.00000744 and 0.00000695 respectively), which clearly corroborates the negligible effect of precipitation on the biophysical parameters. In addition, no major tropical storms were witnessed in the Gulf of Mexico, during 2010 and 2011. Therefore, the loss of marshland can be attributed to the oil spill and associated cleanup efforts including the effect of the toxic dispersant. Results also showed that the salt marsh habitats located in Plaquemines parish and St. Bernard parish were the hardest hit by oiling, which is consistent with the contemporary media reporting (Nungesser, 2010).

Phenological analysis in the fringing marsh habitats across the LA coast consistently showed a decrease in the levels of CHL and GBM in June, the middle of the growing season as well as the peak of the cleanup effort, followed by a steady recovery towards the end of the growing season (Figure 2.10a). Most of the fringing marsh areas of LA, mainly near the Mississippi river delta, close to the source of the oil spill, are dominated by *Spartina alterniflora*, which achieves peak growth and produce flowers in late September and early October in this region. This can be attributed to the recovery in CHL and GBM level in October, 2010, observed in the phenological analysis (Figure 2.10a). In addition, the cleanup efforts mainly restricted to the fringing marsh area in the beginning of the spill may have been successful in keeping the damage under control, which resulted in a recovery in late October. In contrast, the interior marshes, dominated by *Spartina alterniflora*, *Spartina patens*, and *Distichlis spicata*, in Plaquemines parish and St. Bernard Parish, showed peak growth in June followed by a reduction in GBM and CHL in October (Figure 2.10b). This indicates oil reaching the interior marshes much later in the

growing season than the fringing marsh, outer coastal waters, and shorelines. This is also the reason that the interior marshes actually showed greater signs of damage than the fringing marshes towards the end of the growing season.

As previously stated, the effect of the oil spill and cleanup vary with vegetation types, season, water levels, and other physicochemical/ meteorological conditions. Taking into account the close relationship between CHL and GBM with gross primary production (GPP) in salt marshes (Pickney and Zingmark, 1993), the chlorophyll and biomass centered study framework is conceptually well grounded in basic plant physiology. After Hurricane Gustav made landfall on September 1, 2008, Landsat data provided strong evidence that the wetlands and barrier islands off the LA coast were lost from hurricane-related flooding (NASA News Report on 1/12/09). Fortunately, 2009 and 2010 were relatively quiet storm seasons, and LA wetland habitats were on a recovery stage after the Gustav related damage. Theoretically, therefore, 2010, with no hurricanes reported, should have been a better year in term of marsh physiological growth. However, the Deep Water Horizon (DWH) oil spill dramatically reversed the recovery trend by exerting a massive negative short-term impact to the salt marsh habitats during the middle of the growing season. We believe the short-term damage due to oil spill will probably be less in magnitude than that of a major hurricane, but the lingering residual oil will have a sustained long-term impact on the overall health and productivity of the Gulf Coast salt marsh. The results from this study shows that Landsat data can be used to assess the impact of natural (e.g., hurricanes) and anthropogenic disturbances (e.g., oil spill) on the Gulf Coast wetland habitats.

Conclusion

The estimated time-series CHL and GBM maps produced from Landsat imagery possess great potential to quantify the ecological impacts of the oil spill on salt marsh structure and function. These products can be used in conjunction with biogeochemical data to analyze the changes in one of the most important wetland functions i.e., carbon sequestration reduction related to the oil spill effects. Recently, BP has committed $1 billion to repair the environmental damage caused by the oil spill, which will initiate an unprecedented restoration effort across the Gulf wetland (Robertson, 2011). For the first time, managers can have access to the large-scale maps of southeastern LA coastal wetland productivity generated through this research allowing identification of problem areas (areas impacted by the spill), which should be a high priority for restoration and the relative success of prior restoration efforts.

Acknowledgements

We would like to acknowledge Phil McCarty and Mike Brown (Earth and Environmental Sciences-University of New Orleans) for their help in field data collection. This project was funded by National Science Foundation RAPID program (Award # 1050500) and Northern Gulf Institute- Mississippi State University (Award # 306896)

References

Allen, A. A., and Ferek, R. 1993. Advantage and disadvantages of burning oil. In: *Proceedings of the 1993 International Oil Spill Conference.* American Petroleum Institute, Washington, D.C, 765-772.

Arizona Remote Sensing Center (ARSC). 2002. Landsat 5 atmospheric and radiometric correction. Arizona Remote Sensing Center, University of Arizona. Adaptation by S.M. Skirvin, 1996. http://arsc.arid.arizona.edu/resources/image_processing/Landsat/ls5-atmo.html

Chavez, P. S. 1996. Image-based atmospheric corrections – Revisited and improved. *Photogrammetric Engineering and Remote Sensing*, 62, 1025-1036.

Chen, X., Vierling, L., Rowell, E., and DeFelice, T. 2004. Using lidar and effective LAI data to evaluate IKONOS and Landsat 7 ETM+ vegetation cover estimates in a ponderosa pine forest. *Remote Sensing of Environment*, 91, 14-26..

Curran, P. J. 1982. Multispectral photographic remote sensing of green vegetation biomass and productivity. *Photogrammetric Engineering and Remote Sensing*, 48, 243-250.

Curran, P. J., Dungan, J. L., and Gholz, H. L. 1990. Exploring the relationship between reflectance red edge and chlorophyll content in slash pine. *Tree Physiology*, 7, 33-48..

Egan, D. 2005. Taking on the storm. *Ecological Restoration*, 23, 225-226.

Fisher, J. I., Mustard, J. F., and Vadeboncoeur, M. A. 2006. Green leaf phenology at Landsat resolution: scaling from the field to the satellite. *Remote Sensing of Environment*, 100, 265-279.

Gilfillan, E. S., Page, D. S., Bass, A. E., Foster, J. C., Fickett, P. M., Ellis, W. G. H., Rusk, S., and Brown, C. 1989. Use of Na/K ratios in leaf tissues to determine effects of petroleum on salt exclusion in marine halophytes. *Marine Pollution Bulletin*, 20, 272-276.

Gitelson, A. A., Vina, A., Ciganda, V., and Rundquist, D. C. 2005. Remote estimation of canopy chlorophyll content in crops. *Geophysical Research Letters*, 32, L08403

Gitelson, A. A. 2004. Wide dynamic range vegetation index for remote quantification of crop biophysical characteristics. *Journal of Plant Physiology*, 161, 165-173.

Gitelson, A. A., Gritz, U., and Merzlyak, M. N. 2003a. Relationships between leaf chlorophyll content and spectral reflectance and algorithms for non-destructive chlorophyll assessment in higher plant leaves. *Journal of Plant Physiology*, 160, 271-282.

Gitelson, A. A., Stark, R., Grits, U., Rundquist, D., Kaufman, Y., and Derry, D. 2002. Vegetation and soil lines in visible spectral space: a concept and technique for remote estimation of vegetation fraction. *International Journal of Remote Sensing*, 23, 2537-2562.

Gitelson, A. A., Vina, A., Arkebauer, T. J., Rundquist, D. C., Keydan, G., and Leavitt, B. 2003b. Remote estimation of leaf area index and green leaf biomass in maize canopies. *Geophysical Research Letters*, 30, 1148, DOI: 10.1029/2002GL016450

Gitelson, A., and Merzlyak, M. 1997. Remote estimation of chlorophyll content in higher plant leaves. *International Journal of Remote Sensing*, 18, 291-298.

Gitelson, A., and Merzlyak, M. 1998. Remote sensing of chlorophyll concentration in higher plant leaves. *Advances in Space Research*, 22, 689-692.

Gundlach, E. R., and Hayes, M. 1978. Classification of coastal environments in terms of potential vulnerability to oil spill damage. *Marine Technology Society Journal*, 12, 18-27.

Gutro, R. 2009. Landsat Sees LA Wetland and Barrier Island Loss from Hurricane Gustav, NASA News Report, January 12, 2009, at http://www.nasa.gov/mission_pages/hurricanes/archives/2009/wetlandloss_LA.html

Hardisky, M. A., Daiber, F. C., Roman, Charles T., and Klemas, V. 1984. Remote sensing of biomass and annual net aerial primary productivity of a salt marsh. *Remote Sensing of Environment*, 16, 91-106.

Kiesling, R. W., Alexander, S. K., and Webb, J. W. 1988. Evaluation of alternative oil spill cleanup techniques in a *Spartina alterniflora* salt marsh. *Environmental Pollution*, 55, 221-238

Kirby, C., and Gosselink, J. 1976. Primary production in a LA gulf coast Spartina alterniflora marsh. *Ecology*. 57, 1052-1059.

Kogan, F., Stark, R., Gitelson, A., Jargalsaikhan, L., Dugrajav, C., and Tsooj, S. 2004. Derivation of pasture biomass in Mongolia from AVHRR-based vegetation health indices. *International Journal of Remote Sensing*, 25, 2889-2896.

Li, L., Ustin, Susan L., and Lay, M. 2005. Application of AVIRIS data in detection of oil-induced vegetation stress and cover change at Jornada, New Mexico. *Remote Sensing of Environment*, 94, 1-16.

Lin, Q., and Mendelssohn, I. A. 1996. A comparative investigation of the effects of South LA crude oil on the vegetation of fresh, brackish, and salt marshes. *Marine Pollution Bulletin*, 32, 202-209.

Lin, Q., and Mendelssohn, I. A. 2012. Impacts and recovery of the Deepwater Horizon oil spill on vegetation structure and function of coastal salt marshes in the northern Gulf of Mexico. *Environmental Science and Technology*, 46, 3737-3743.

Lindau, C. W., DeLaune, R. D., Jugsujinda, A., and Sajo, E. 1999. Response of Spartina alterniflora vegetation to oiling and burning of applied oil. *Marine Pollution Bulletin*, 38, 1216-1220.

Markham, B. L. 1986. Landsat MSS and TM post-calibration dynamic ranges, exoatmospheric reflectances and at-satellite temperatures. *Landsat Technical Notes*, 1, 3-8.

McKee, K. L., Mendelssohn, I. A., and Materne, M. D. 2004. Acute salt marsh dieback in the Mississippi River deltaic plain: a drought induced phenomenon?, *Global Ecology and Biogeography*, 13, 65-73.

Mendelssohn, I. A., Hester, M. W., Sasser, C., and Fischel, M. 1990. The effect of LA crude oil discharge from a pipeline break on the vegetation of a southeast LA brackish marsh. *Oil and Chemical Pollution*, 7, 1-15.

Michener, W. K., Blood, E. R., Bildstein, K. L., Brinson M. M., and Gardner L. R. 1997. Climate change, hurricanes and tropical storms, and rising sea level in coastal wetlands. *Ecological Applications*, 7, 770-801.

Moran, M. S., Jackson, R. D., Slater, P. N., and Teillet, P. M. 1992. Evaluation of simplified procedures for retrieval of land surface reflectance factors from satellite sensor output. *Remote Sensing of Environment*, 41, 169-184.

Nungesser, B. 2010. Oil spill impact on Plaquemines Parish, LA. Testimony before the Subcommittee on State, Local, and Private Sector Preparedness and Integration. June 10, 2010, at http://hsgac.senate.gov/public/index.cfm?FuseAction=Files.ViewandFileStore_id=8ad1c6e4-dba9-4d76-a071-a01f4a442a97

Nyman, J. A., and Chabreck, R. H. 1995. Fire in coastal marshes: history and recent concerns. In: S.I. Cerulean and R. T. Engstrom (Eds.), *Fire in Wetlands: a Management Perspective. Proceedings of the Tall Timbers Fire Ecology Conference*, 19, Tall Timbers Research Station, Tallahassee, Florida, USA.

Nyman, J. A., Carloss, M., DeLaune, R. D., and Patrick, W. H. Jr. 1994. Erosion rather than plant dieback as the mechanism of marsh loss in an estuarine marsh. *Earth Surface Processes and Landforms*, 19, 69-84.

Owens, E. H., Gould, J. R., and Lindstedt-Siva, J. 1993a. Field studies to determine the ecological effects of cleanup methods on oiled shoreline. In: *Proceedings of the 1993 International Oil Spill Conference*. American Petroleum Institute, Washington, D.C, 401-406.

Owens, E. H., Taylor, E., Marty, R., and Little, D. I. 1993b. An inland oil spill response manual to minimize adverse environmental impacts. In: *Proceedings of the 1993 International Oil Spill Conference*. American Petroleum Institute, Washington, D.C, 105-109.

Pax-Lenney, M., Woodcock, C. E, Macomber, S. A., Gopal, S., and Song, C. 2001. Forest mapping with a generalized classifier and Landsat TM data. *Remote Sensing of Environment*, 77, 241-250.

Pezeshki, S. R., and DeLaune, R. D. 1993. Effect of crude oil on gas exchange functions of Juncus roemerianus and Spartina alterniflora. *Water Air and Soil Pollution*, 68, 461-468.

Pezeshki, S. R., Hester, M. W., Lin, Q., and Nyman, J. A. 2000. The effects of oil spill and clean-up on dominant US Gulf coast marsh macrophytes: a review. *Environmental Pollution*, 108, 129-139.

Pinckney, J., and Zingmark, R. G. 1993. Biomass and production of benthic microalgal communities in estuarine habitats. *Estuaries and Coasts*, 16, 887-897.

Robertson, C. 2011. Beyond the oil spill, the tragedy of an ailing gulf. *The New York Times*. April 20

Rouse, J. W., Haas Jr., R. H., Schell, J. A., and Deering, D. W. 1974. Monitoring vegetation systems in the Great Plains with ERTS, *Third ERTS-1 Symposium*, NASA Special Publication, NASA SP-351, 1, 309-317.

Rundquist, D. C., Perk, R., Leavitt, B., Keydan, G. P., and Gitelson, A. A. 2004. Collecting spectral data over cropland vegetation using machine-positioning versus hand positioning of the sensor. *Computers and Electronics in Agriculture*, 43, 173-178.

Tucker, C. J., Grant D. M., and Dykstra, J. D. 2004. NASA's global orthorectified Landsat data set. *Photogrammetric Engineering and Remote Sensing*, 70, 313-322.

U.S. Department of the Interior, Press Release, U.S. Scientific Teams Refine Estimates of Oil Flow from BP's Well Prior to Capping. State News Service, August 2, 2010, at http://app.restorethegulf.gov/release/2010/08/02/us-scientific-teams-refineestimates-oil-flow-bps-well-prior-capping

Weather Underground, http://www.wunderground.com/ (last accessed: 09/17/2011)

Weis, J. S. 2010. Salt marsh, In: Cleveland, C. J. (Eds.) *Encyclopedia of Earth*. Washington, D.C.: Environmental Information Coalition, National Council for Science and the Environment.

Table 2.1: Dates for which Landsat imageries were acquired.

Months	2009	2010
April	4, 11	7
May	6, 13	9
June	7, 14	3, 10
July	9, 16	5, 12
August	3, 10	6, 13
September	4, 11	7, 14
October	13	9, 16

Table 2.2: Linear Regression coefficients of VIs used in GBM and CHL model calibration.

[*] *Similar to $CI_{red\text{-}edge}$ Index based on Gitelson et al. 2003a but band-3 used instead of a red-edge band*; [**] *Indices with the highest R^2*

Index	Green Biomass (g/m^2)	Canopy Chlorophyll (mg/m^2)
NDVI $(R_{NIR}-R_{red})/(R_{NIR}-R_{red})$	0.469	0.489
WDRVI $(\alpha \times R_{NIR}-R_{red})/(\alpha \times R_{NIR}-R_{red})$ *($\alpha = 0.05$)*	**0.522**[**]	0.515
WDRVI $(\alpha \times R_{NIR}-R_{red})/(\alpha \times R_{NIR}-R_{red})$ *($\alpha = 0.1$)*	0.52	**0.516**[**]
WDRVI $(\alpha \times R_{NIR}-R_{red})/(\alpha \times R_{NIR}-R_{red})$ *($\alpha = 0.2$)*	0.511	0.513
EVI2 $\{2.5\times(R_{NIR}-R_{Red})/(R_{NIR}+2.4\times R_{Red}+1)\}$	0.353	0.067
CI Red [*] $(R_{NIR}-R_{red})/R_{red}$	0.521	0.513
SAVI $\{(R_{NIR}-R_{Red})\times(1+L)\}/(R_{NIR}+R_{Red}+L)$ $(L = 0.5)$	0.364	0.424
TVI $\sqrt{\{(R_{NIR}-R_{red})/(R_{NIR}-R_{red})\}}$	0.398	0.497

Table 2.3: Root mean square errors (RMSE) for different VIs in predicting GBM and CHL during model validation

Index	Green Biomass (g/m^2)	Canopy Chlorophyll (mg/m^2)
NDVI	10.281	79.170
EVI2	33.402	45.767
WDRVI (α = 0.1)	24.284	**11.649**
WDRVI (α = 0.2)	24.871	25.092
WDRVI (α = 0.05)	**6.927**	52.606
CI_{Red}	28.429	34.288
SAVI	40.631	84.891
TVI	67.820	80.989

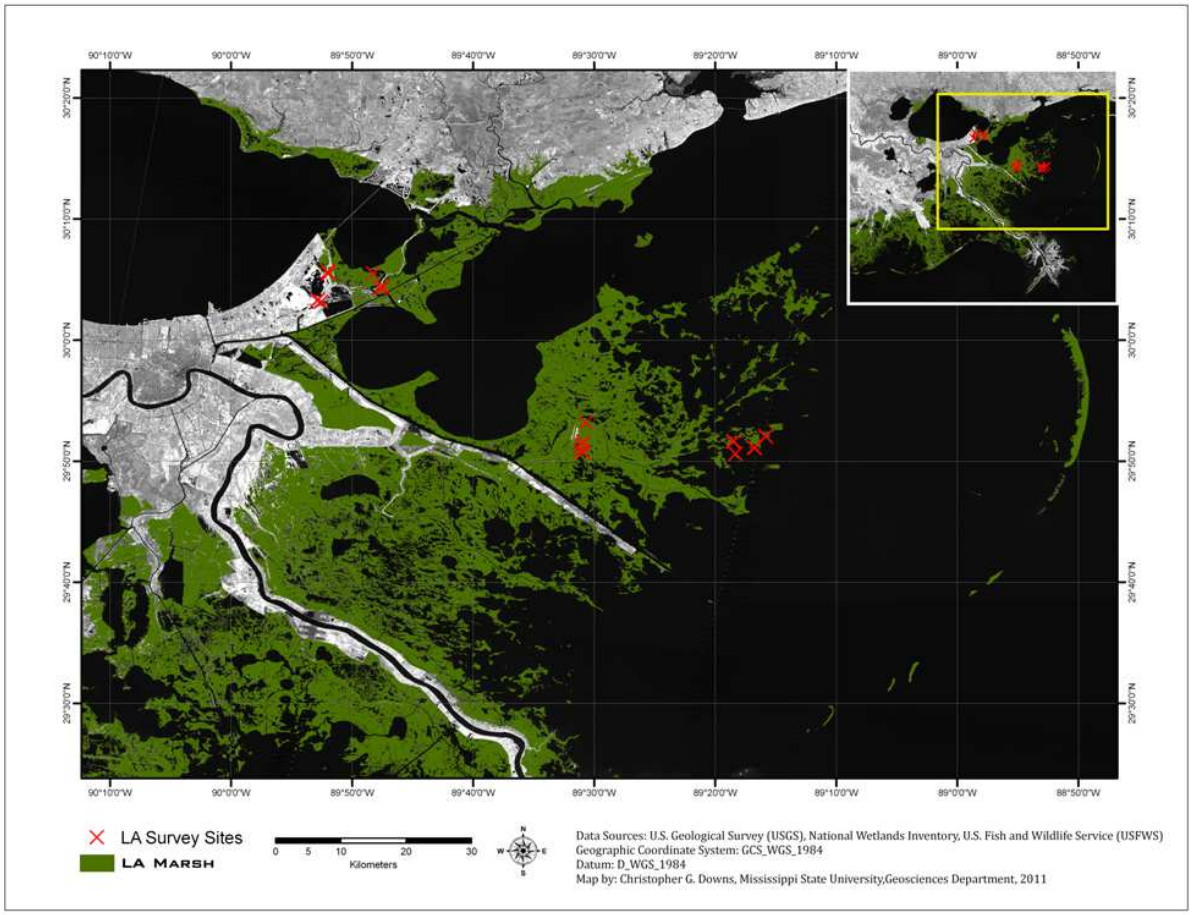

Figure 2.1. Map showing study plots in the salt marshes of St. Bernard Parish and Plaquemines Parish, LA.

Figure 2.2. 2010 Field Research Photographs: (a) Resident oil observed through airplane survey; (b, c, d, and e) Oil observed in vegetation canopy and root system, and soil; (f) Leaf chlorophyll reading using SPAD; (g) LAI reading using LICOR's LAI-2000 meter; (h) *In situ* sensor calibration; (i) *In situ* remote sensing data acquisition

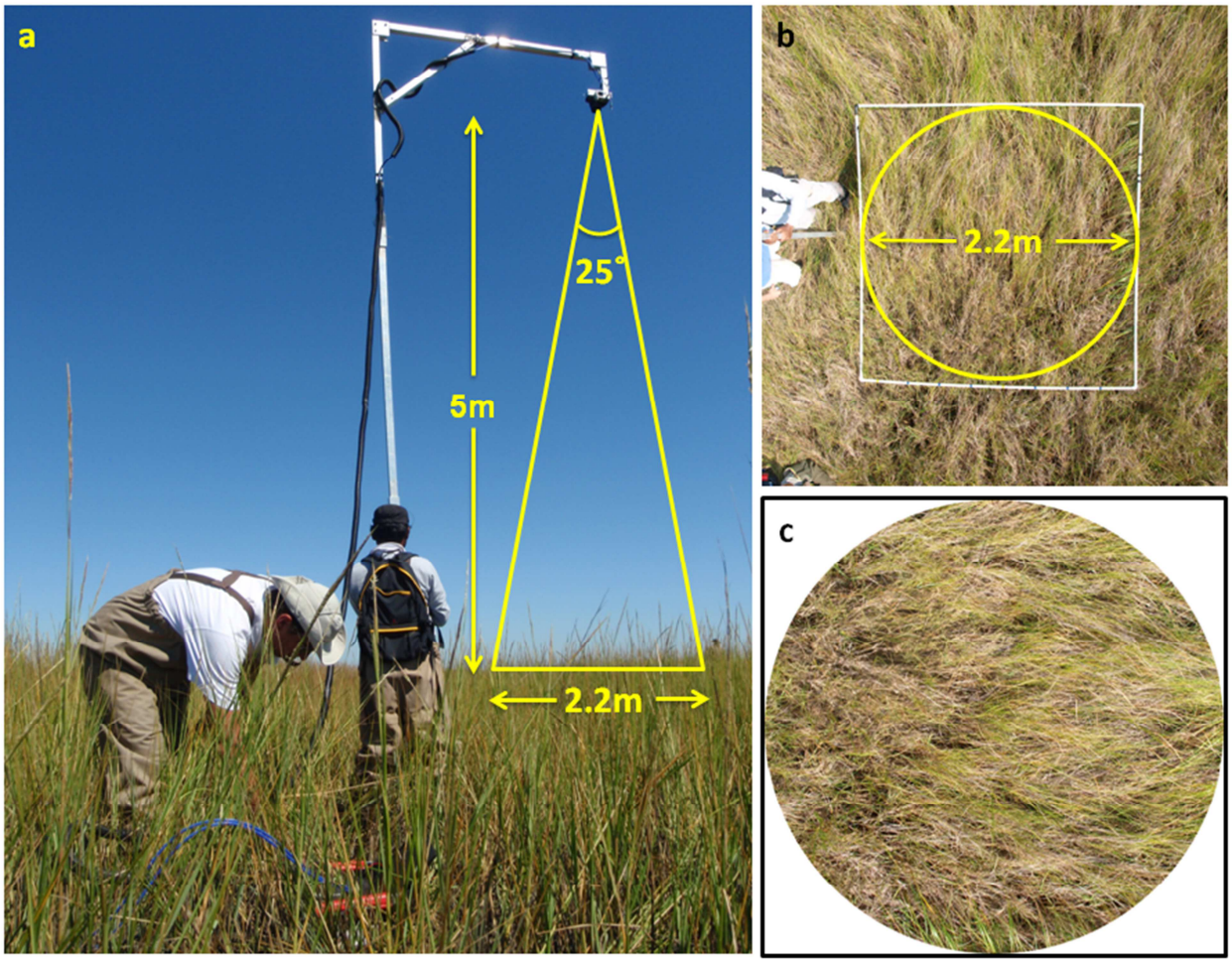

Figure 2.3. Photograph displaying the dual-headed OceanOptics sensor setup during field data collection: (a) Sensor mounted on 5 meter (~16 ft) high frame; (b and c) IFOV of the sensor (diameter: 2.2 m).

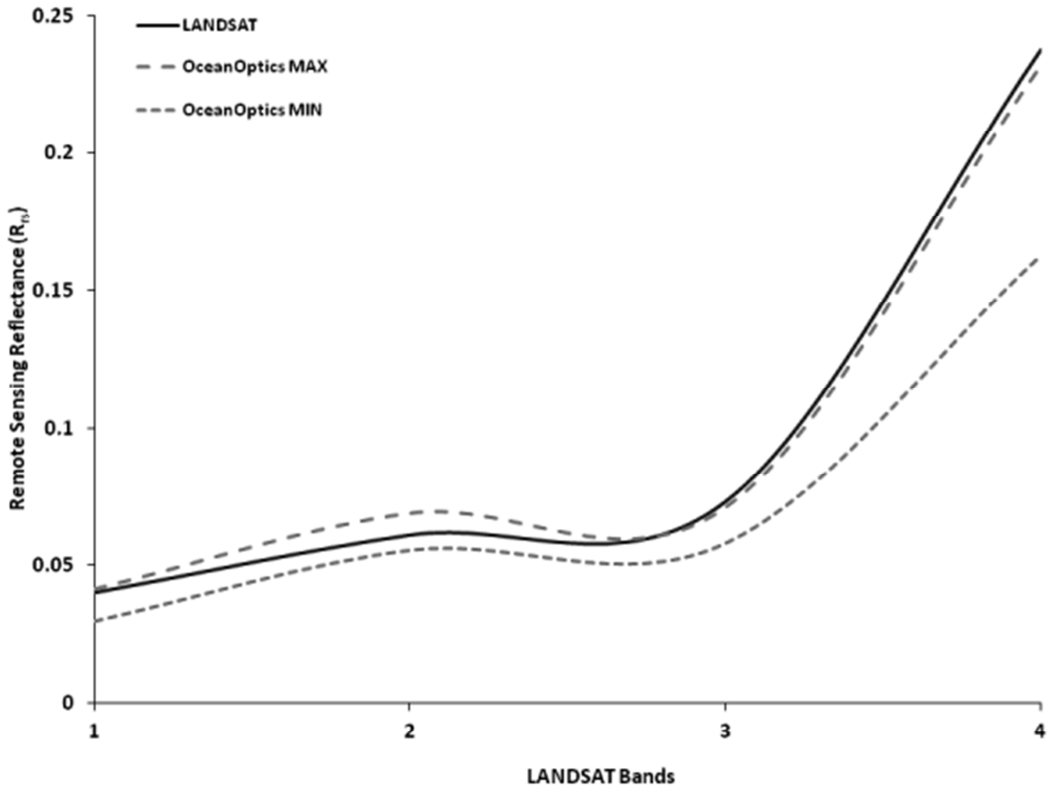

Figure 2.4. Comparison between atmospherically corrected Landsat reflectance and close range reflectance acquired by OceanOptics spectroradiometers. OceanOptics min and max indicate minimum and maximum mean reflectance readings acquired from multiple study plots within a single Landsat pixel.

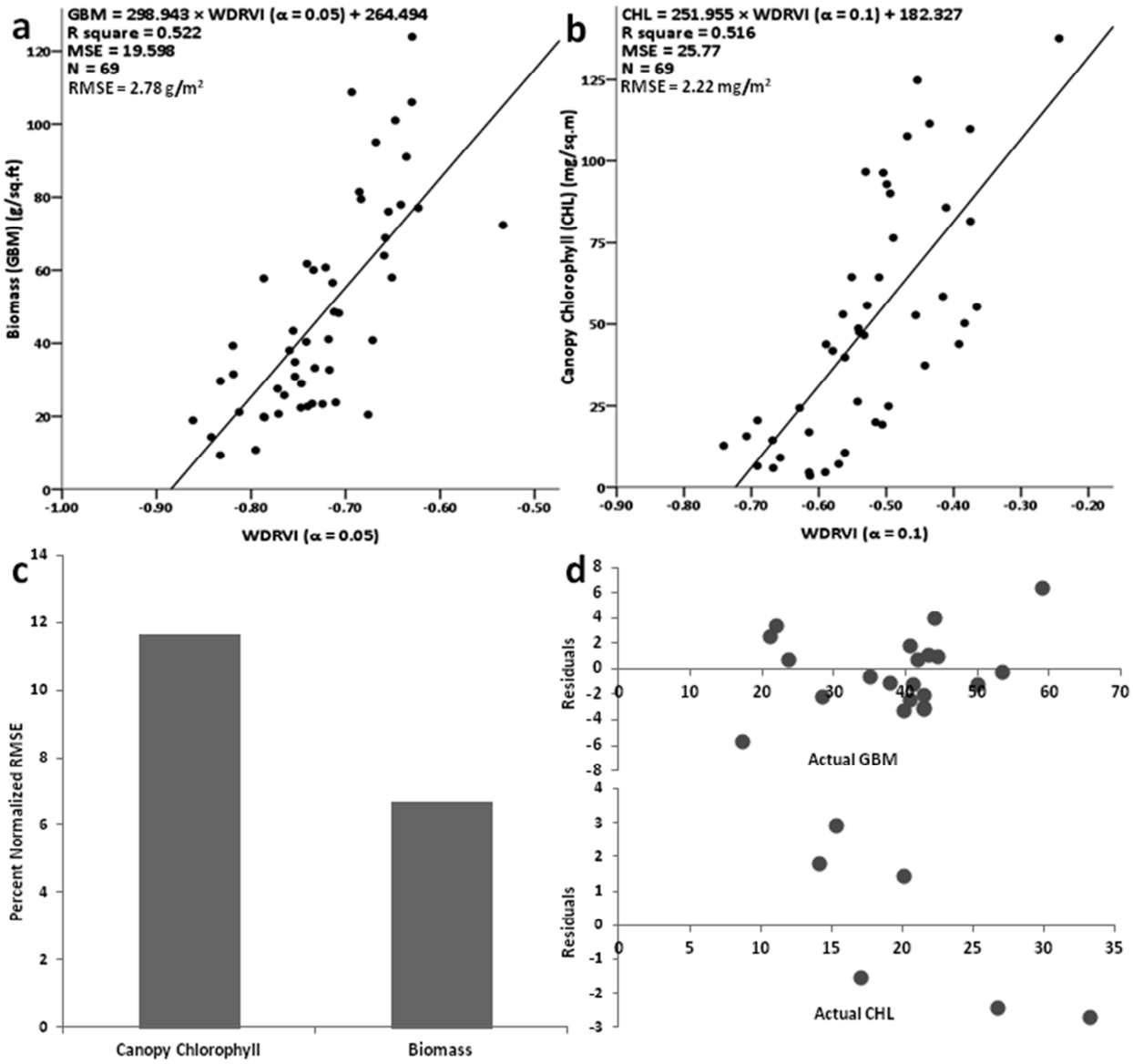

Figure 2.5. Quantitative Results. Model calibration plots (a) GBM and (b) CHL using satellite image derived VIs and biophysical parameters; (c) Model validation result showing percent Normalized RMSE for CHL and GBM; (d) Residual plots for GBM and CHL models.

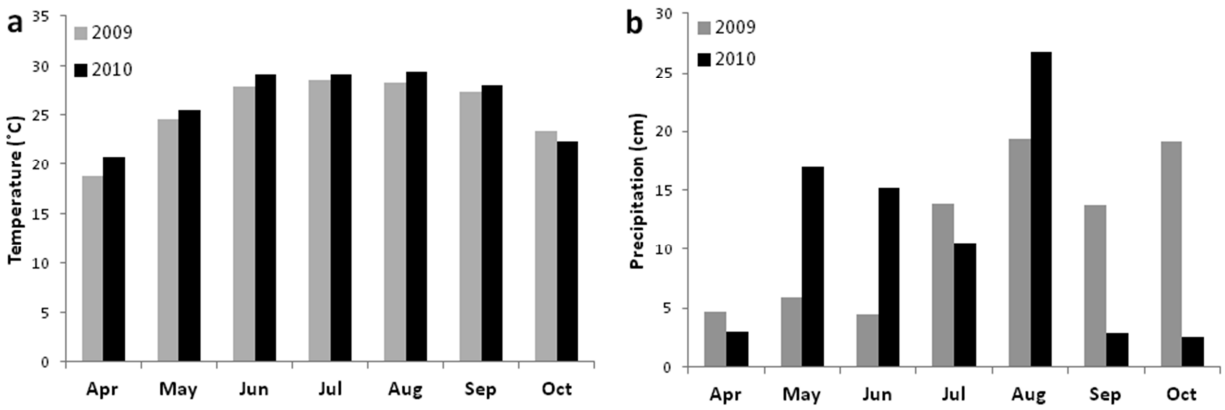

Figure 2.6. Environmental Factors Influencing Biophysical Parameters: (a) Mean monthly temperature and (b) precipitation in salt marsh across pre and post spill growing season (source: http://www.wunderground.com/)

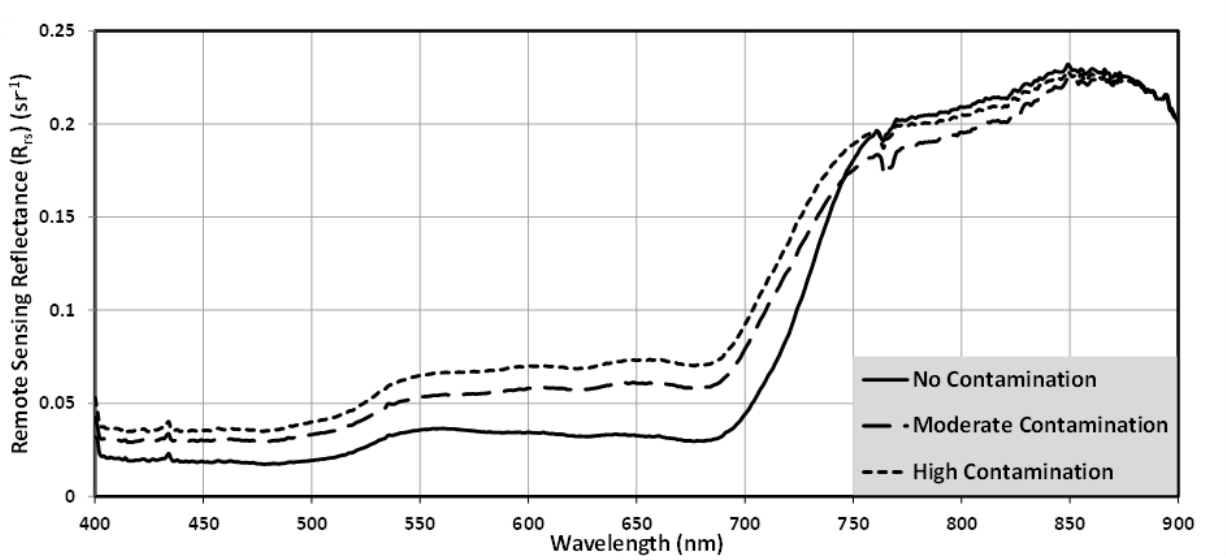

Figure 2.7. Spectral reflectance from selected singular plots containing *Spartina alterniflora*, with varying biophysical parameters, across different levels of oil contamination.

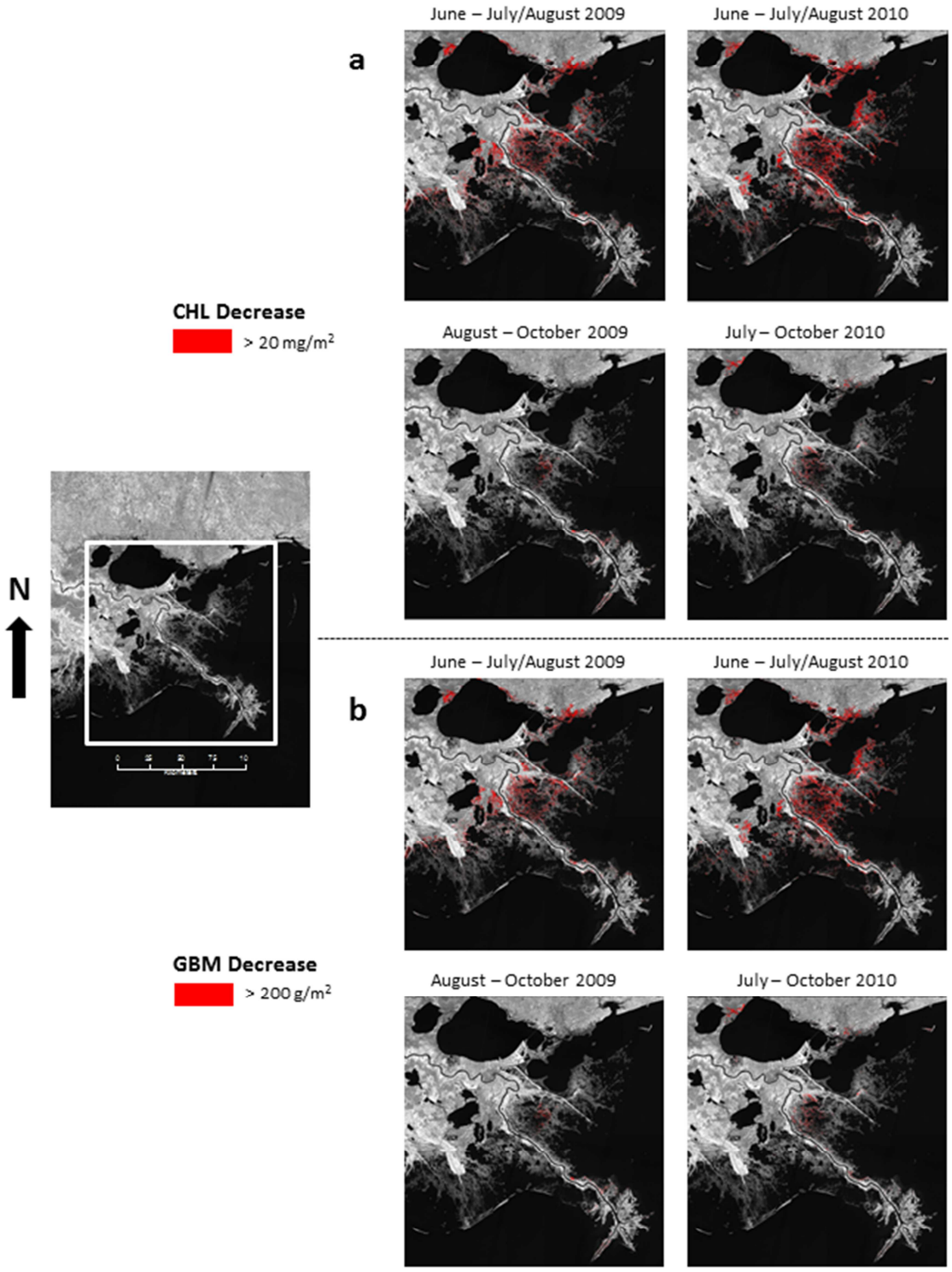

Figure 2.8. Decreases in Biophysical Parameters, 2010. Comparison of areas experiencing reduction in (a) CHL and (b) GBM respectively, pre- and post-spill growing season.

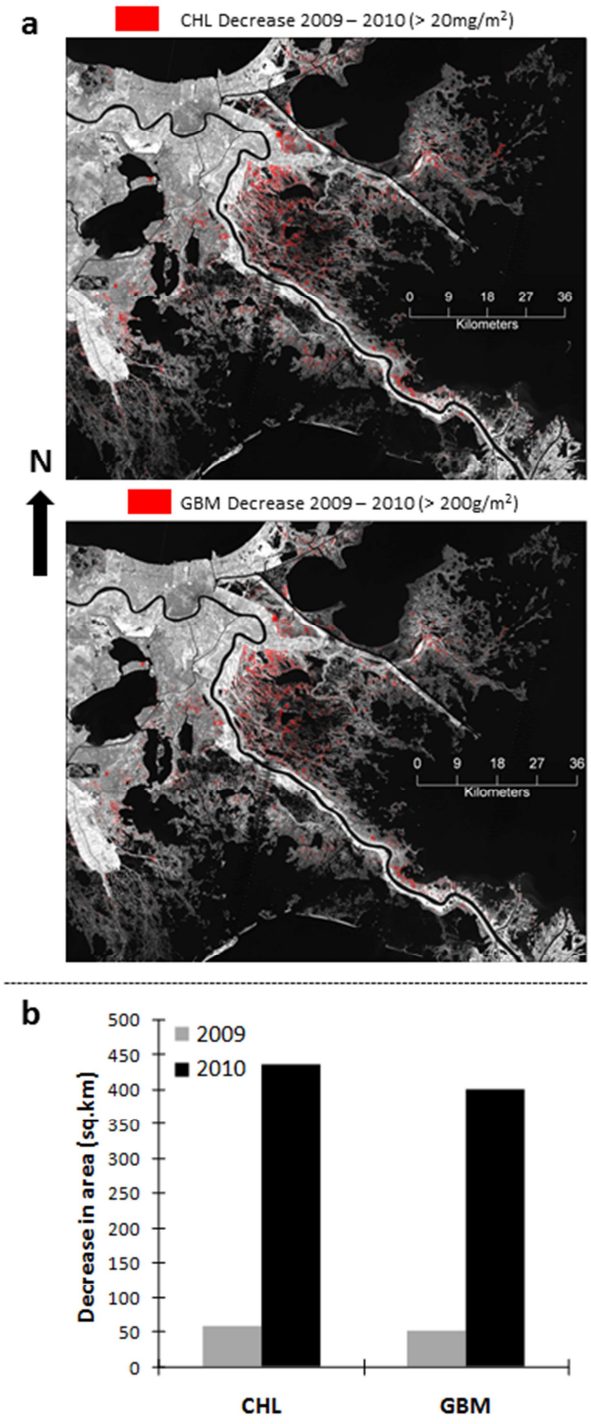

Figure 2.9. Biophysical Parameters Changes between 2009 and 2010: (a) Comparison of areas experiencing biomass and canopy chlorophyll amount in June ’09 and ’10; (b) Extent of salt marsh areas experiencing biomass and canopy chlorophyll reduction.

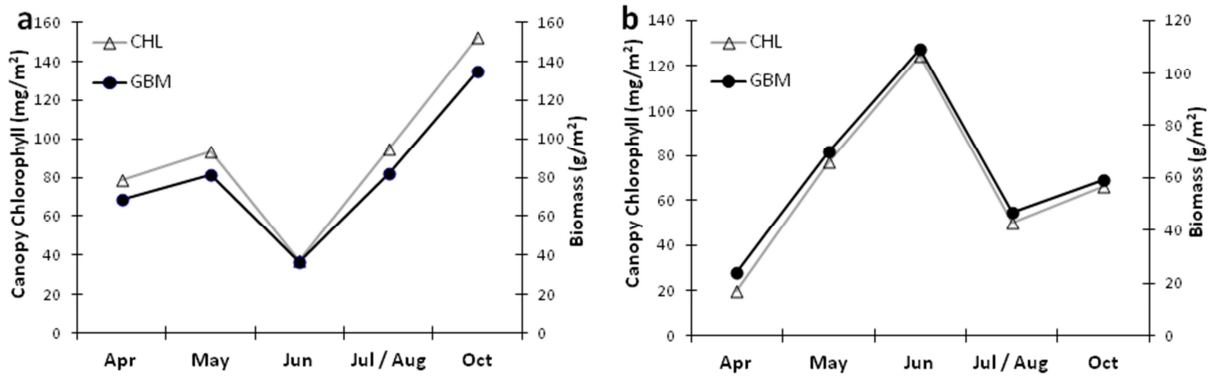

Figure 2.10. Variation of (a) GBM and (b) CHL in the growing season in the fringe and interior marshes post-spill growing season (2010).

CHAPTER 3

LONG–TERM MONITORING OF BIOPHYSICAL CHARACTERISTICS OF SALT MARSHES IN THE NORTHERN GULF OF MEXICO – A METHODOLOGICAL APPROACH USING MODIS[†]

[†]Ghosh, S., Mishra, D. R., and Gitelson, A. A. (2016). Long-term monitoring of biophysical characteristics of tidal wetlands in the northern Gulf of Mexico—A methodological approach using MODIS. *Remote Sensing of Environment*, 173, 39-58. Reprinted here with permission of Elsevier

Abstract:

Accurate and efficient monitoring is critically important for the effective restoration and conservation of threatened salt marshes in the Gulf Coast. The high carbon sequestration potential, habitat for important wildlife and fish, and numerous ecosystem services make these salt marshes highly valuable both ecologically and economically to Gulf Coast communities. Our study developed a new methodological approach for mapping biophysical health of coastal salt marsh habitats in terms of green leaf area index (GLAI), canopy level chlorophyll content (CHL), vegetation fraction (VF), and above ground green biomass (GBM). We measured these biophysical characteristics in salt marshes of the northern Gulf of Mexico using a combination of ground data collected from field surveys during the growing seasons of 2010 and 2011 and NASA's Moderate Resolution Imaging Spectroradiometer (MODIS) 250m and 500m images. Additionally, we compared and evaluated the performances of both *in situ* proximal and satellite remote sensing measurements in terms of their potential for mapping the marsh biophysical characteristics. MODIS–based models proved superior at the landscape level compared to models developed from *in situ* proximal sensing, as species level signals seemed to be diluted at coarser spatial scales. We selected Wide Dynamic Range Vegetation Index (WDRVI) for MODIS 250m and Visible Atmospheric Resistant Index (VARI) for MODIS 500m to map biophysical characteristics of salt marshes. Time–series composites and phenological information derived using the MODIS based models captured the impact of the selected disturbances in the last decade on the ecological and physiological status of the salt marsh habitats in the Gulf Coast. This is the first study to employ MODIS data to analyze the biophysical characteristics of salt marshes in the Gulf Coast, which, in turn, has the potential to improve our ability to predict their productivity and carbon sequestration potential. These

techniques could also be used to assess the success of previous and ongoing salt marsh restoration projects, and evaluate the productivity of marshes under threat from developmental activity, sea level rise, and industrial pollution.

Keywords: Gulf of Mexico; Salt marsh; Remote Sensing; Biophysical Characteristics; Green Leaf Area Index, Green Vegetation Fraction; Canopy Chlorophyll; Above Ground Biomass; Field Spectroscopy; MODIS

Introduction:

Salt marshes are one of the most ecologically and economically productive and vulnerable ecosystems in the world (Mitsch and Gosselink, 2007; Tiner, 2013). Thriving at the confluence of marine and terrestrial systems, they serve as critical habitats for fish and wildlife, as well as species, which are commercially valuable to the local community. These ecosystems also help buffer and maintain shorelines, clean natural waters, reduce siltation in navigable waters, and potentially help in storing floodwaters (Boesch and Turner, 1984; Deegan et al. 2002; Barbier et al. 2008; Morgan et al. 2009; Koch et al. 2009). Furthermore, in light of exponential increases in atmospheric CO_2 in recent decades, the high Carbon Sequestration Potential (CSP) of salt marshes makes them critical carbon sinks for atmospheric greenhouse gases (Gallagher et al. 1980; Connor et al. 2001; Chmura et al. 2003; Brevik and Homburg, 2004). The productive capacity of salt marshes has often been compared to that of tropical evergreen rain forests (Choi and Wang, 2004; Pidgeon, 2009). However, these critical habitats are highly threatened by natural and anthropogenic activities such as global warming induced sea–level rise (Fitzgerald et al. 2008; Nicholls et al. 1999), land use changes (Kennish, 2001; Silliman et al. 2009), soil erosion (Sugumaran et al. 2004; Ravens et al. 2009), natural and man–made disasters and associated clean–up efforts (Gilfillan et al. 1995; Hester and Mendelssohn, 2000; Mishra et al. 2012), and replacement by other species (Artigas and Pechmann, 2010).

A robust marsh monitoring program for sustainable management should be comprehensive in nature, covering various important indicators such as distribution, composition, characteristics, health, and productivity (Mishra et al. 2015; Adam et al. 2010). However, traditional monitoring efforts, which rely on field sampling to study such marsh properties, are often costly, time consuming, and inadequate for analyzing the broad regional trends and spatio–temporal

variability. Remote sensing using satellite and airborne sensors along with Geographic Information Systems (GIS) provides a cost–efficient alternative to intensive field surveys in monitoring and assessing coastal marsh ecosystems and their dynamics at different scales and resolutions (Tiner, 1996; Dahl, 2006).

In the last decade, advances in remote sensing technologies and increasing availability of high temporal and spectral resolution data, from both active and passive sensors, has significantly enhanced our ability to map marsh ecosystems (Jensen et al. 2007; Laba et al. 2008; Wang et al. 2010; Lefebvre et al. 2010; Zhang and Xie, 2012; Evans and Costa, 2013). Multi–temporal and multi–resolution imagery from sensors such as Landsat, Advanced Spaceborne Thermal Emission and Reflection Radiometer (ASTER), and Moderate Resolution Imaging Spectroradiometer (MODIS) are freely accessible to the general public and these sensors have been utilized in several studies for classification of marsh habitat (Jensen, 1996; Campbell, 2007; Lillesand et al. 2008). In addition, other moderate to high resolution satellite sensors such as SPOT, IKONOS, Quickbird, RapidEye, GeoEye, along with airborne hyperspectral imagers such as the Advanced Visible Infrared Imaging Spectrometer (AVIRIS) and Compact Airborne Spectrographic Imager (CASI), have been utilized by several researchers for classification of marsh cover and change detection analysis (Jensen, 1996; Rundquist et al. 2001; Schmidt and Skidmore, 2003; Rosso et al. 2005; Campbell, 2007; Lillesand, 2008; Gilmore et al, 2010; Klemas, 2011).

In general, wetland remote sensing is more challenging than remote sensing of terrestrial vegetation because the water or moist soil interface which reduces the intensity of the near–infrared (NIR) signal, shifts red–edge positions, and ultimately makes NDVI and red–edge–type indices less–sensitive to vegetation growth (Kearney et al. 2009; Turpie, 2013). These habitats

also exhibit high spectral and spatial variation due to the abrupt change of environmental conditions that produce narrow ecotones, causing difficulty in vegetation community boundary identification (Schmidt and Skidmore, 2003). The diversity of vegetation in the marsh habitats produce unique species assemblages with different phenological cycles, morphological structures, and bio–chemical compositions, which, in turn, produces diverse spectral behavior, making mapping of marshes difficult (Rosso et al. 2005, Zomer et al. 2009). A paucity of spectral library data is a challenge for marsh remote sensing because of species diversity (Zomer et al. 2009) and intraspecific morphologic differences. Further, the patchiness and fine scale heterogeneity of marsh vegetation are often not captured with medium resolution sensors such as Landsat and SPOT. High resolution aerial photography and imagery is expensive to acquire and labor intensive to process. On the other hand, classification using coarse resolution MODIS or Advanced Very High Resolution Radiometer (AVHRR) at 250–1,000m resolutions results in frequent misclassification of pixels (Loveland et al. 1999; Friedl et al. 2002).

The majority of research efforts for monitoring marshes using remote sensing have been focused on delineating the extent of marsh ecosystems, and classifying plant communities using both active and passive satellite sensors and numerous image processing techniques (Klemas et al. 1980; Filippi and Jensen, 2006; Adam et al. 2010; Gilmore et al. 2010; Simard et al. 2010; Wang, 2010; Jensen et al. 2007; Klemas, 2011; Artigas and Pechmann, 2010; Collin et al. 2010; Davranche et al. 2010; Goudie, 2013). This kind of mapping provides crucial information regarding the presence/absence of marsh patches, the previous and current spatial extent, and the dynamics of marsh cover change. However, it does not provide any information regarding the biophysical characteristics which are primary indicators of salt marshes' physiological status, photosynthetic capacity as well as, chlorophyll and nitrogen content (CHL, N). Remote

estimation of biophysical characteristics such as Leaf Area Index (LAI), Canopy Chlorophyll Content (CHL_c), Vegetation Fraction (VF), and Above Ground Green Biomass (GBM) should be performed regularly to assess the health of the marsh ecosystem.

Remote sensing has been extensively used to study biophysical characteristics of vegetation since late 1970's (Tucker, 1978; Tucker and Sellers, 1986; Tucker 1980). Over the past twenty years, studies have focused on protocols for mapping the biophysical characteristics of terrestrial vegetation, using *in situ* sensors along with satellite based surface reflectance. LAI mapping from spectral reflectance measurements has mainly focused on forests (e.g. Gong et al. 1995, 2003; Davi et al. 2006) and crops (Thenkabail et al. 2000; Hansen and Schjoerring, 2003; Pay et al. 2006). Developing regression based models with vegetation indices (VIs) such as NDVI and simple ratio, which are derived from visible and NIR wavelengths, has been the most widely used empirical model for estimating LAI (Thenkabail et al. 2000; Gong et al. 1995, 2003; Kovacs et al. 2005). Similar research studies have also been performed for estimating GBM using satellite derived VIs (Rendong and Jiyuan, 2004; Proisy et al. 2007). Apart from LAI and GBM, mapping CHL content through non–invasive techniques in terrestrial vegetation has been attempted often (Gitelson and Merzlyak, 1994; Markwell et al. 1995; Gamon and Surfus, 1999; Richardson et al. 2002; Gitelson et al. 2006). Finally, *in situ* reflectance and satellite derived VIs have been used for monitoring fractional cover of green vegetation, using different combinations of visible and NIR bands (Gitelson et al. 1996; Myneni et al, 1997a; Myneni et al, 1997b; Gitelson et al, 2002a; Gitelson et al, 2002b; Gitelson, 2004).

However, remote sensing studies focusing on monitoring and analyzing the biophysical properties of salt marsh ecosystems are very limited, and have only been attempted using satellite sensors with coarse temporal resolution. (e.g. Hardisky, 1980; Hardisky et al. 1984;

Jensen et al. 2002; Kearney et al. 2009; Mishra et al. 2012). These studies on salt marshes have mostly been conducted using traditional field sampling methods (Hopkinson et al. 1978; Stout, 1984; Darby and Turner, 2008). Although these studies provide in–depth site–specific information of biophysical characteristics, they often lack the ability to provide insight into the long–term spatio–temporal trends of the salt marshes at a landscape scale. Monitoring biophysical properties using remote sensing not only helps in assessing the overall dynamics of marshes but also facilitates prioritization of restoration efforts to areas that require immediate attention and allows conservation planning at a much broader spatial scale. A robust biophysical mapping protocol is also critical in assessing the success or failure of previous restoration efforts (Hinkle and Mitsch, 2005; Friess et al. 2012), as well as analysis of phenology and carbon budgets at regional and global scales across a wide range of ecosystem and climatic regimes (Baldocchi et al. 2001; Churkina et al. 2005; Richardson et al. 2009). For example, analysis of the biophysical characteristics based phenology can aid in isolating the natural variability in marshes from the variability introduced by environmental forcings such as such as localized drought, dieback events, or hurricanes. Furthermore, remote assessment of gross primary productivity (GPP) can be performed using these biophysical characteristics; and that is the long–term goal of our research.

The specific objectives of this research were to (1) calibrate and validate MODIS based VIs for estimating the salt marsh biophysical characteristics (GLAI, CHL_c, VF, GBM) in the northern Gulf of Mexico (GoM), (2) develop time–series composites of salt marsh biophysical characteristics for long–term productivity trend analysis, and (3) analyze broader phenological patterns of the biophysical characteristics to assess the impact of various natural and anthropogenic disasters. The novelty of this research is that it will allow researchers and coastal

managers to use high frequency MODIS data to study the biophysical characteristics of salt marsh habitats in the Gulf Coast, for the first time. This study has the potential of increasing our predictive capability with respect to carbon sequestration in these ecosystems. In addition, an efficient and non–destructive MODIS based biophysical mapping protocol for emergent marshes will be an invaluable tool for frequent monitoring as well as conservation and restoration decision making.

Study Area

Salt marshes cover more than 8500 sq. km of the coastal areas of the Northern GoM (Source: http://www.fws.gov/Marshs/) (Figure 3.1). The tidal marsh habitats are mostly dominated by smooth cord–grass (*Spartina alterniflora*), salt meadow cord–grass (*Spartina patens*), and black needle rush (*Juncus roemarianus*). Patchy distributions of American Glasswort (*Salicornia virginica*), saltwort (*Batis maritima*), and seashore saltgrass (*Distichlis spicata*) are also encountered. The highly saline and anoxic nature of the soil inhibits the growth of non–specialized plants; as such, floral diversity is remarkably low (Weis, 2010). Average annual temperature in this region varies between 15–25 degrees Celsius, while annual precipitation ranges from 80–100 cm (National Weather Service, http://www.weather.gov/).The region experiences tropical to sub–tropical climate characterized by hot and humid summers, with occasional tropical storms and moderately cold winters. In the last decade, the salt marsh habitats in the Gulf have experienced the landfall of major hurricanes, such as Lili (2002), Katrina and Rita (2005), Gustav (2008), Ida (2009), and Isaac (2012) in Louisiana (LA) and Gordon (2000), Gabrielle (2001), Ivan (2004), and Dennis (2005) in Florida (FL) (National Hurricane Centre, http://www.nhc.noaa.gov/). LA has the largest salt marsh extent among all the Gulf Coast states. However, the marshes here are also home to more than 160,000 oil and gas wells (Lyles and

Namwamba, 2005), accounting for 18% of oil and 24% of natural gas production in the U.S., valued at $6.3 billion, and $10.3 billion respectively (Tiner, 2013). As such, the marshes have been subjected to intense dredging and channelization for transportation as well as significant groundwater removal, which has led to soil and marsh erosion and localized subsidence. Further, the sediment flow from the Mississippi River, which typically provides nutrients and substrate for salt marshes, has been extensively trapped through excessive construction of levees across the LA coast. Hence, it is increasingly difficult for the salt marshes to sustain themselves. Disturbed salt marsh habitats in the region have been invaded by common reed (*Phragmites australis*) (Tiner, 2013). The marshes in FL have also been subjected to channelization, with excavated materials being dumped into the confined disposal areas within salt marshes (Tiner, 2013).

Over the past decade, there have been an increasing number of reports of salt marsh "dieback" in the U.S. In 2000 and 2007, LA experienced a sudden and acute dieback event (termed "brown marsh") that affected over 100,000 ha of *Spartina alterniflora* dominated Salt marsh throughout the Mississippi River deltaic plain (Siliman et al. 2005; Lindstedt and Swenson, 2006). In addition, although the long–term impact is still unknown, the Deepwater Horizon oil spill in 2010 had a severe short–term impact on the health of several fringe and interior salt marsh patches of LA, MS, and AL characterized by loss of chlorophyll, biomass, and subsequently a reduction in photosynthetic capacity (Biber et al. 2012; Mishra et al. 2012; Mishra et al. 2015). Therefore, this research is aimed at fulfilling the strong need to develop an accurate and non–destructive mapping protocol that uses high temporal resolution satellite data to frequently monitor the biophysical conditions of these vast patches of tidal emergent marshes of the Gulf Coast at a broad scale.

Material and Methods

a. Field Data Collection

The models developed for mapping salt marsh biophysical characteristics were based on establishing statistical relationships between MODIS 250m and 500m surface reflectance products and on–field estimates of these characteristics. Therefore, extensive fieldwork was conducted in four Gulf States (Louisiana (LA); Mississippi (MS); Alabama (AL); Florida (FL)) during the salt marsh growing season (May–October) of 2010 and 2011. The field data collection involved acquisition of top of canopy hyperspectral reflectance and biophysical characteristics *viz.* LAI, VF, CHL_l (Leaf Chlorophyll Content), and GBM, from numerous study plots. Field sites were selected in areas with extensive homogenous patches of marsh potentially covering multiple MODIS (250m and 500m) pixels. The site selection process involved analysis of high resolution satellite data (Landsat, QuickBird, and Google Earth), short field visits, aerial surveys, reconnaissance surveys, and in consultation with state and local officials. Multiple calibration and validation sites were selected across coastal counties covering the four Gulf States. Within each 250m or 500m MODIS pixel, multiple (~4–8) mono–specific sub–plots were selected for field data acquisition based on accessibility. Few pixels with single study plots were also incorporated in the analysis, after visual estimation of spatial homogeneity from aerial photographs and Google Earth images. Care was taken to make sure that the sub–plots were as homogenous as possible with similar health conditions and growth stages (Table 3.1). The data from all the sub–plots within a specific site were aggregated to represent a MODIS pixel during model calibration and validation. The detailed collection protocol for each field dataset is provided below.

1. Top of Canopy Reflectance (ρ)

A dual–fiber system, with two inter–calibrated Ocean Optics USB4000 hyperspectral radiometers (Ocean Optic Inc., Dunedin, FL, USA), mounted on an aluminum frame was used to acquire the top of canopy (TOC) spectral reflectance (R_{rs}, sr^{-1}) data in the range of 200–1100 nm with a sampling interval of 0.3 nm (Rundquist et al. 2004). The first radiometer with a field–of–view (FOV) of 25° pointed downwards to acquire upwelling radiance (L; Wm^2sr^{-1}), while the second radiometer equipped with a cosine corrector pointed upward to simultaneously acquire downwelling irradiance (E; Wm^{-2}). Based on the FOV and the height of the frame (5 m), the spatial resolution (IFOV) of the sensor was calculated to be 1.83 m (Figures 3.2a and 3.2b).

$$d = 2\{h \times (tan\frac{\propto}{2}) \quad (1)$$

where, d = diameter of the IFOV (m), h = height of the sensor from the target (m), α = FOV of the sensor (degree). Inter–calibration of the radiometers was accomplished by measuring the L and E of a 99% Spectralon white polytetrafluoroethylene (PTFE) reflectance panel (Labsphere, Inc., North Sutton, NH, USA) (Rundquist et al. 2004). To mitigate the impact of solar elevation on radiometer inter–calibration, the anisotropic reflectance from the calibration target was corrected in accordance with Jackson et al. (1992). Data were collected with the sensors configured to take 15 simultaneous L and E measurements, which were internally averaged and stored as a single data file. In case of changing sky conditions, the sensor was recalibrated at regular intervals (Figures 3.2c and 3.2d). The hyperspectral readings were smoothed using a moving window average of 7 nm to eliminate noise and then further interpolated at a 1 nm interval. The four scans of radiance and irradiance acquired per sub–plot were converted to four

R_{rs} readings by dividing L over E; percentage spectral reflectance (ρ) was estimated and then averaged out to obtain composite spectra of the sub–plot.

2. Above–ground Green Biomass (GBM)

GBM data were collected by destructive sampling from a 0.09 m^2 (1 ft^2) representative area within each sub–plot using a PVC frame and clippers (Figures 3.2e and f). Each biomass sample was sorted to separate the green from brown (standing dead), oven dried at 65°C overnight (~24 h) to get rid of any moisture, and then the dry weight was recorded using a standard measuring balance. Vegetation samples, mainly *Salicornia* and *Batis,* which showed presence of moisture, even after 24 hours of drying, were further dried for additional 24 hours, until all moisture was eliminated. Precautions were taken to avoid moisture absorption by the dried GBM during dry weight measurement. The dry GBM weights were then rescaled from gram dry weight per square feet (gft^{-2}) to gram dry weight per square meter (gm^{-2}).

3. Leaf Chlorophyll Content (CHL_l)

A Minolta 502 SPAD Chlorophyll meter (Spectrum Technologies Inc., East Plainfield, IL, USA) was used to measure the *in situ* CHL_l (Figure 3.2g). A total of twenty stratified random SPAD readings were acquired from each sub–plot across varying CHL levels inside the IFOV of the sensor. Conversion of SPAD readings to actual CHL_l was done by establishing a linear relationship between SPAD values and corresponding CHL estimated through chemical extraction and spectrophotometric measurements. The CHL extraction procedure used in this research has been described in details by Biber (2007). For this study, leaf samples of *Spartina, Juncus, and Distichlis,* showing varying degrees of greenness (from dark green to almost yellow/brown) were collected from the study plots. 5cm long sections from the basal portion of

the leaves were used for CHL extraction. Three SPAD readings were taken from selected sections on the leaves and averaged. These averaged SPAD values were then calibrated against chemically extracted CHL from those sections using the following equation:

$$CHL_l\ (mgm^{-2}) = SPAD \times 16.844 - 192.84 \quad (2)$$

Separate datasets were used for calibration and validation (14 readings for calibration and 18 for validation). The linear model between SPAD and analytically extracted chlorophyll content showed a percent normalized root mean square error (%NRMSE; described later in the article) of 9% (Figures 3.3a and 3.3b).

4. Vegetation Fraction (VF)

Percentage green VF was estimated from a circular crop of vertical digital photographs of the study plots acquired by OLYMPUS E–400 digital SLR camera (Olympus America Inc., Centre Valley, PA, USA). The camera was installed on the frame along with a laser pointer next to the hyperspectral radiometer. The laser pointer marked the center of the digital photograph and the IFOV of the hyperspectral radiometer. The digital photograph was cropped to match the IFOV of the hyperspectral radiometer and a simple pixel count code was implemented to count the total pixels and green pixels in the cropped photographs. VF (%) was estimated by the ratio of the number of green pixels to the total number of pixels in each photograph (Figure 3.2h) (White et al. 2000).

5. Leaf Area Index (LAI)

Leaf area index (LAI) was measured from each sub–plot using a LAI Plant Canopy Analyzer 2000 (LAI 2000; LICOR Biosciences Inc., Lincoln, NE, USA) (Gitelson et al. 2004) and AccuPAR LP–80 Ceptometer (Decagon Devices Inc., Pullman, WI, USA) (Delalieux et al. 2008,

Kovacs et al. 2009) (Figures 3.2i and j). The average value of four LAI readings taken within each sub–plot was used as the representative LAI. Each LAI measurement involved one above–canopy and four below canopy readings. Both LAI 2000 and AccuPAR measure canopy transmittance for estimating LAI and as such, do not differentiate between green and dead leaves. LAI 2000 has an optical filter, which rejects any radiation above 490m; the assumption behind this is that foliar transmission is minimal in the blue region of the electromagnetic spectrum (LAI Manual, 2000). AccuPAR on the other hand, measures radiation transmitted through the canopy and scattered by leaves within the canopy. It is also assumed that the leaf absorptivity is maximum in the visible region of the electromagnetic spectrum (approximately 90% in the blue and red and 75–80 % in the green region), thereby, assuming transmittance through leaves to be negligible (AccuPAR Manual, 2008). Based on these aforementioned assumptions, leaves are considered to be opaque, and as such, none of these instruments can differentiate between green and dead/yellow leaves.

Estimated LAI values, therefore, are a metric of total leaf area rather than green LAI. As the productive capacity of vegetation depends largely on the presence of green foliage containing CHL, Green Leaf Area Index (GLAI) serves as a better estimate of the vegetation health. Since VF is an estimate of the amount of greenness in the area of interest, we estimated Green LAI as the product of LAI and VF. Further, CHL_c (mgm^{-2}) was calculated as the product of LAI and CHL_l content (Gitelson et al. 2005).

$$GLAI = LAI \times VF \quad (3)$$

$$CHL_c\ (mgm^{-2}) = CHL_l\ (mgm^{-2}) \times LAI \quad (4)$$

b. Satellite Data

Multi–temporal 8–day Level 1B atmospherically corrected surface reflectance composites for the northern GoM (LA, MS, AL, and western FL coast) were acquired from National Aeronautics and Space Administration (NASA) website (http://modis–land.gsfc.nasa.gov) for the years 2000 through 2014. Both 250m and 500m scenes from MODIS sensor (MOD09Q1 and MOD09A1 respectively) were downloaded for the northern GoM and mosaicked. The mosaic scenes were cropped to isolate the salt marsh habitats by using the most recent vector boundaries obtained from NWI database (https://www.fws.gov/wetlands/). The aforementioned pre–processing of the MODIS images was performed using ERDAS Imagine 2013 (ERDAS Imagine, Intergraph Corporation Part of Hexagon, Norcross, GA). We used the MODIS Quality Assurance (QA) layer for both 250m and 500m data to select the highest quality pixels. The QA layers for 250m and 500m are 16–bit and 32–bit images, respectively, representing different permutations and combinations of MODIS land surface reflectance quality parameters. We chose the best combination of bits, e.g. 00 for both clouds and cloud shadows, 0000 for highest data quality for all the bands, 0 for both snow cover and fire, 0 for internal cloud, fire and snow algorithm, and 1 for atmospheric, adjacency and bi–directional reflectance function (BDRF) corrections to eliminate pixels affected by various natural and technical factors such as cloud cover, cloud shadows, atmospheric noise, snow cover, fire, sensor orbits, cloud adjacency, bi–directional reflection, sensor failure etc. (Vermote et al. 2011). Summary statistics for all the biophysical characteristics field data and coincident MODIS pixel data for 2010 and 2011 is provided in Table 3.2.

Analysis

a. Salt marsh Spectral Response: In situ and MODIS

In order to analyze the magnitude difference and the effect of species variability, MODIS and Ocean Optics derived *in situ* ρ data were compared. ρ values off both 250m and 500m MODIS surface reflectance products from *Spartina* and *Juncus* dominated pixels were extracted for all sites where Ocean Optics ρ data were acquired. *Salicornia* and *Distichlis* had patchy distributions; as such no homogenous MODIS pixels of these two species were found. Since plot level data for these two species were very limited (n<5), spectral response comparison between Ocean Optics and MODIS was limited to the dominant species (*Spartina* and *Juncus*) only. The Ocean Optics acquired data were further integrated to match the MODIS VNIR bandwidths. Ocean Optics spectra obtained for *Spartina* and *Juncus*, were averaged for the sites falling within one MODIS pixel (for both 250m and 500m), for accurate comparison between ground level and satellite level reflectance. As such, we used two visually mono–specific pixels (from both 250m and 500m images) for each species (*Spartina* and *Juncus*). Average hyperspectral ρ acquired using Ocean Optics data from mono–specific study plots within these MODIS pixels were compared with MODIS derived ρ.

b. Model Calibration and Validation

The main goal of model calibration was to establish relationships between several well established VIs and marsh biophysical characteristics. Then established models were validated using MODIS data. These VIs have been widely used at fine and coarse spatial resolutions to monitor terrestrial vegetation biophysical characteristics, both at site specific and broader ecosystem scales. However, these indices have not been used at the MODIS scale to map

biophysical characteristics such as GLAI, CHL, GBM, and VF of salt marshes so far. It has not been done because collecting accurate, long–term, and representative biophysical data for MODIS based VI calibration for marsh ecosystems is an extremely difficult task. Inaccessible areas in difficult terrain, unavailability of large visually homogenous patches of mono–specific marsh vegetation, and poor sampling design and improper *in situ* data collection procedure often limit large scale remote sensing studies on marsh biophysical characteristics. In this study, an extensive and comprehensive *in situ* data collection over a period of two years enabled us to perform a comparative assessment of the existing VIs which is crucial for providing insight into both selection of the best VI for mapping marsh biophysical characteristics, and the possible explanation for their respective performances.

1. Using In Situ Hyperspectral Data

In situ ρ spectra were collected for the growing season (April–October) of 2010, from 42 mono–specific and 22 multi–specific but visually homogenous study plots. Several well established VIs (Table 3.3) were derived from Ocean Optics *ρ*, and used for initial calibration against the biophysical characteristics using SPSS (SPSS IBM, New York, USA). Among these VIs, Normalized Difference Vegetation Index (NDVI), Enhanced Vegetation Index (EVI2), Chlorophyll Index (CI_{red}), Wide Dynamic Range Vegetation Index (WDRVI), and Soil Adjusted Vegetation Index (SAVI) were developed utilizing reflectance at red and NIR bands. CI_{red} is a modified (from Chlorophyll Index red edge or $CI_{red–edge}$) chlorophyll index, using the red band instead of the red edge band (Gitelson et al. 2006). Visible Atmospheric Resistant Index (VARI) was developed using the visible green and red bands (Gitelson et al. 2002).

Variability in spectral response is unavoidable in the salt marsh landscape because of marsh variability in terms of species composition, leaf and canopy structure, chlorophyll content, phenological stage, standing dead matter, and substrate nature. Therefore, species–specific models for biophysical mapping might account for this variability, and subsequently assist in the development of a robust method for mapping of biophysical characteristics. Therefore, both linear and non–linear (quadratic and exponential) biophysical models were calibrated for individual species using *in situ* Ocean Optics hyperspectral data. Coefficient of determination (R^2) was derived for species–specific biophysical models and also for a species–independent model combining all species data. However, since *Salicornia* and *Distichlis* had patchy occurrences, there were not enough mono–specific plots for these two species for reasonable calibration ($n<5$). Therefore, species–specific models were analyzed for only the two dominant species: *Spartina* and *Juncus.*

2. Using MODIS Data

Following the initial pre–processing of MODIS data, *in situ* sampling locations were used do extract pixel values from MODIS images. Scenes were chosen based on the proximity of the dates between the image acquisition and field data collection. The same set of VIs (Table 3.3) was derived using the extracted MODIS pixel values for individual biophysical characteristic model calibration. Since MODIS 250m has the red and NIR bands only, indices such as VARI and CI_{green} could not be derived at this resolution. For a pixel containing multiple sampling locations, the average value of the individual biophysical characteristic was calculated and used in model calibration. MODIS pixels corresponding to sampling locations which were too close to open water showed greater or similar observed NIR absorption compared to visible and had to be rejected from both the calibration and validation datasets. These pixels clearly contained a

greater signal from water than vegetation and were considered water dominated mixed pixels. Further, due to occasional equipment failure such as sensor saturation, internal errors, and battery drain–out during field sampling, biophysical data from few study plots were either unavailable, or not usable for analysis. Post elimination of unusable pixels and ground data, model calibration was performed using 2010 field data and validation using 2011 field data. During this process, roughly 69 sampling plots established in 2010 were reduced to 10–15 usable MODIS 250m and 7–10 usable MODIS 500m pixels. For model validation, data set acquired during the field campaigns in 2011 containing 91 sampling plots were reduced to 10–12 MODIS 250m pixels and 9–10 MODIS 500m pixels. These were the reasons for the observed range of usable MODIS pixels for calibration and validation. Performance uncertainties were analyzed based on percent normalized root mean squared error (percent NRMSE) (Mishra et al. 2012), and residuals (observed–predicted). Percent NRMSE is estimated as:

$$percent\ NRMSE = \frac{RMSE}{(MAX\ (VALIDATION\ data) - (MIN\ (VALIDATION\ data))} \times 100 \qquad (5)$$

c. Time–Series Composites and Phenology Characterization

Following successful calibration and validation, 8–day time–series composites were generated using ERDAS Imagine 2013 (ERDAS Imagine, Intergraph Corporation Part of Hexagon, Norcross, GA) for each biophysical characteristic (GLAI, VF, CHL, and GBM) from 2000–2014 using the best fit models. Map composites were generated for both 250m and 500m data. For each month, three to four composites per characteristic were created. Therefore, for an entire year, almost 46 composites were obtained for each biophysical characteristic. Composites were generated for all four characteristics, for the period 2000–2014. This amounted to more than 5500 8–day composites using both MODIS 250m and 500m data. These composites were then

used for qualitative assessments of northern GoM Salt marsh condition before and after significant natural and anthropogenic events such as hurricanes and droughts over the period of 2000–2014.

Phenology charts for site specific Salt marsh patches were derived from these time–series composites, using spatial analysis module in ArcGIS (ArcGIS 10, Environmental Systems Research Institute, Redlands, California) for the growing seasons over the course of fifteen years. The sites for phenology characterization were chosen based on records of natural/anthropogenic events that have occurred and affected salt marsh habitats in the Northern Gulf coast. Here, we show the phenology derived for Terrebonne parish and Plaquemines parish of Louisiana, using MODIS 250m and 500m data respectively. We sampled 40 pixels from Terrebonne parish and 16 pixels from Plaquemines parish in order to extract biophysical values for deriving phenology. Monthly biophysical values were estimated using the average of all available 8–day composites within the month. The averaging was done to avoid the noise related to tidal fluctuations or modelling error propagated through the numerous processing steps involved in the phenology extraction. The phenology charts were developed to examine the impact of discrete natural and anthropogenic events on the health of specific salt marsh areas, as well as the overall long term trends in the Salt marsh health in the Gulf Coast.

Results and Discussion

a. Salt marsh Reflectance Properties

In–situ spectral reflectance measured from most of the study plots of Salt marsh vegetation showed presence of reduced red–edge (Figure 3.4a). The spectral reflectance derived from MODIS 500m surface reflectance images showed a very similar overall trend (Figure 3.4b). A

reduced red–edge does not necessarily mean that the vegetation is unhealthy; rather, it may be influenced by canopy structure, vegetation density, and signals from targets other than the vegetation itself. In case of salt marshes this absence of red–edge is understandable since these habitats are perennially inundated by tidal waters; even when the tides are low, significant residual moisture saturates the soil. Water and vegetation have contrasting spectral response in the NIR region of the spectrum; while vegetation has a tendency to scatter, water absorbs radiation in NIR. Therefore, the contrasting responses result in the presence of a reduced red–edge unlike terrestrial vegetation.

Further, variations in the spectral characteristics are also notable at the species level. *Spartina* and *Distichlis* on one hand have similar foliar and canopy structures much like flat–leaved grasses. *Juncus* and *Salicornia*, on the other hand have very unique foliar and canopy characteristics usually characterized by low chlorophyll and denser canopy structures with an overall low reflectance in the visible–NIR region of the spectrum, as measured from *in situ* spectral acquisition (Figure 3.4c). Similar patterns were observed when the *in situ* ρ was averaged to MODIS visible and NIR bandwidths; the differences in the spectral response among different species were very much evident (Figure 3.4d). Studying species level spectral response is crucial before biophysical model construction as it provides some pre–insight into potential performances of species specific or species independent models. As the species level spectral response showed significant differences, constructing species specific biophysical models seemed logical.

b. In-situ Reflectance Based Biophysical Models

Three models were devise/developed using *in situ* hyperspectral spectra to estimate biophysical characteristics of (1) *Spartina*, (2) *Juncus*, and (3) Mixed/All species combined dataset. Coefficient of Determination (R^2) of the models of biophysical characteristics across species showed high variability and somewhat contrasting behavior (Figure 3.5). For GBM, both linear and nonlinear models performed poorly in terms of explaining the total variation in the data, not only at the individual species level but also when data for all species were combined. VF variation was explained in *Spartina* by both linear and non–linear models. The VIs based on red and NIR bands performed relatively better than the indices based only on the visible bands such as VARI. The opposite was true for VF models of *Juncus* and all species combined, where VARI performed better than the red–NIR based VIs. Variation was reasonably explained by some linear and non–linear models for CHL_c in *Juncus*, whereas, few non–linear quadratic models reasonably explained good variation in *Spartina*. The performances dropped considerably when all species were combined. Similar trends were observed for GLAI, which is expected since CHL_c is derived as a function of LAI. In general, the performances of VIs were not only inconsistent across species but also across different biophysical characteristics.

In addition, Pearson's rank correlation test showed significant correlations between almost all VIs and GBM (both in *Spartina* and *Juncus*) and VF (only in *Juncus*) at the 0.05 level of significance. CHL, VF, and GLAI did not bear significant correlations with VIs in *Spartina*. No significant correlation was observed between VIs and biophysical characteristics when all homogenous plots were combined (Table 3.4). The heterogeneous plots also did not exhibit strong relationships between *in situ* VIs and biophysical characteristics. The initial calibration attempted with Ocean Optics hyperspectral data was not encouraging enough to develop models

to be tested for validation with MODIS data. The lack of satisfactory performance in model calibration when using *in situ* hyperspectral data is attributed mainly to the strong influence of species variability. *In situ* reflectance spectra, particularly in NIR show significant variability across species because of the variations in cell structure and canopy architecture. That variability is somewhat lost in MODIS data because of the averaging effect over a broad area (Figures 3.4a–d).

c. MODIS Based Biophysical Models

After an extensive testing of numerous VIs retrieved from MODIS data using the aforementioned calibration and validation methods, the WDRVI ($\alpha = 0.1$) (Gitelson, 2004) was selected for estimating the biophysical characteristics (GLAI, CHL, VF, GBM) for the 250m data, whereas, VARI (Gitelson et al. 2002) was selected for estimating the biophysical characteristics for the 500m data (Tables 3.5–3.8; Figure 3.6–7). The performances of the non–linear models were similar to that of the linear ones in terms of R^2 and %NRMSE. Therefore, to avoid the saturation tendencies of non–linear models either at the very low or very high values, linear best fit models were used for both 250m and 500m data. Further, it was observed that the performances of several red–NIR based VIs on 250m data were similar to each other (Tables 3.5 and 3.6; Figure 3.6). This might be due to the fact that almost all of these VIs tend to normalize the differences between NIR and red bands, using different coefficients, to increase their sensitivity across a broad range of biophysical characteristics. Therefore, their overall performances in estimating biophysical characteristics will be very comparable, especially for a relatively low aboveground biomass ecosystem such as marshes. For 250m data, the few models that showed the highest R^2 such as NDVI, EVI2, and SAVI also showed high %NRMSE during validation. This may be due to some inherent bias in the models or a lack of uniform sensitivity

for the entire range of biophysical characteristics. To further investigate the overlapping performance of the VIs, we examined the residual (measured–predicted) and the slope ratio (M_v/M_c), ratio of the slopes of the validation (M_v) and calibration (M_c) trend–line, for all models. M_v/M_c should be close to 1 for models with minimum bias and maximum sensitivity across the entire range of biophysical characteristics. Selecting the best model for MODIS 250m data, therefore, was not straightforward. In order to choose the best model for all biophysical characteristics, we had to methodically eliminate all of the other models. This was done considering a combination of factors such as R^2, %NRMSE, M_v/M_c, and residual trends (Tables 3.5 and 3.6; Figure 3.8a–3.8e). First, we eliminated three models, NDVI, EVI2, and SAVI, which showed relatively high %NRMSE (Table 3.6) and highest deviation of M_v/M_c (Figure 3.8e). The highest deviation of M_v/M_c for the three VIs also explained their lack of uniform sensitivity across the entire range of biophysical characteristics and high RMSE in their predictions. This is further evident in residual trends which indicated that NDVI, EVI2, and SAVI produced some of the highest errors at the very low and very high magnitude of each biophysical characteristic (Figure 3.8a–3.8d). Next, we discarded CI_{red}, which showed an overall trend of under–estimation in residual plots (Figure 3.8a–3.8d). Finally, we eliminated WDRVI ($\alpha = 0.2$) which showed marginally higher deviation in slope ratio compared to ($\alpha = 0.1$). As such, WDRVI ($\alpha = 0.1$) was selected as the best fit model and was used to model and map the biophysical characteristics using MODIS 250m data. The WDRVI based linear models developed for mapping biophysical characteristics are as follows:

$$GLAI = 3.4886 \times WDRVI\ (\propto = 0.1) + 3.0865 \quad (6)$$

$$CHL = 1328.3 \times WDRVI\ (\propto = 0.1) + 1285.036 \quad (7)$$

$$VF = 172.74 \times WDRVI\ (\propto = 0.1) + 156.75 \quad (8)$$

$$GBM = 1757.423 \times WDRVI\ (\propto = 0.1) + 1654.197 \quad (9)$$

For 500m data, however, it was observed that VARI outperformed all other VIs by a large margin (Table 3.7 and 3.8; Figures 3.7 and 3.9). The overlapping performances of the VIs encountered in 250m data were not present in 500m data. This might be due to the enhanced water signal and increasingly fragmented patches of marshes, at the coarser 500m resolution making the NIR band unresponsive for vegetation specific analyses, particularly for the red–NIR based VIs. It is relatively difficult to find homogenous marsh pixels in 500m data compared to 250m data without having high influence of water background because salt marshes are by nature fragmented and heavily interspersed with creeks and channels, salt pans, muds and wracks. Therefore, despite careful study site and pixel selection before and during field visits, as well as in subsequent analysis, presence of enhanced water signal in the 500m data becomes unavoidable. This could be the reason why a green–red based VI such as VARI showed the highest sensitivity to the marsh biophysical characteristics. As evident for Table 3.7 and 3.8, VARI outperformed other VIs in terms of explaining the variance in the field data used in the model, as well as prediction errors. The linear models used for mapping biophysical characteristics for 500m are as follows:

$$GLAI = 7.8917 \times VARI + 0.5532 \quad (10)$$

$$CHL = 5041.7 \times VARI + 321.16 \quad (11)$$

$$VF = 409.42 \times VARI + 37.571 \quad (12)$$

$$GBM = 3617.104 \times VARI + 543.3514 \quad (13)$$

d. Performance Comparison: MODIS vs In situ

From the calibration results, it was clearly evident that MODIS based biophysical models outperformed models derived from Ocean Optics based *in situ* hyperspectral data integrated to represent MODIS bands. This was counterintuitive and interesting, because Ocean Optics data were acquired almost at a controlled setting over a homogenous sub–plot, in contrast to MODIS data where the degree of homogeneity was hard to maintain. Therefore, it was expected that the Ocean Optics data would be a better representative of the vegetation's biophysical characteristics. Our results indicated otherwise. In order to investigate the reason behind this, we compared spectral reflectance patterns of the dominant species *Spartina* and *Juncus* derived from both Ocean Optics and the MODIS sensor. Results demonstrate strong variability between *Spartina* and *Juncus* at the ground level (Schmidt and Skidmore, 2003), when spectral profiles are acquired by the Ocean Optics hyperspectral sensors. However, species level spectral variability seem to become diluted as the scale of the study site becomes coarser, as observed in the MODIS derived spectral response for both 250 and 500m data (Figure 3.10). This clarifies the contrasting performances between the MODIS derived and Ocean Optics derived Vis. Variation in the spectral response at the ground level can be explained by the foliar and canopy structures of *Spartina* and *Juncus*. Low average chlorophyll content and canopy structure of *Juncus* are also responsible for the absence of considerable scattering in the NIR band. *Spartina*, with relatively high chlorophyll content and canopy structure characterized by broader leaf area scatters more radiation in the NIR region. NIR reflectance is primarily controlled by leaf structure and canopy architecture; since *Spartina* and *Juncus* have very different leaf structure, the spectral variability for the two species in NIR is also the highest (Figure 3.10). However, as the scale becomes coarser, i.e. at the MODIS satellite level, the species specific spectral

variability is lost, and therefore, at the landscape level, species invariant models based on MODIS seem to perform better than models based on *in situ* ρ.

Further, as is evident from model performances, for both 250m and 500m resolutions, red–NIR band based VIs performed reasonably well; however, VIs based on only visible bands using MODIS 500m datasets had better correlations with the biophysical characteristics. This can also be explained by the loss of species specific signal in coarse resolution data, where a high degree of similarity is noticed in the spectral response of species in the visible and NIR region of the spectrum (Figure 3.10). This might also be attributed to the complex nature of salt marsh habitats, where homogenous patches are often interlaced by tidal creeks and channels, fed by the tidal waters. Water signals from those channels, as well as from the surrounding rivers/ocean, are highly influential in minimizing the reflectance in the NIR region, making it insensitive to species variability, with progressive coarseness in the spatial resolution. Tidal stage at the time of MODIS image acquisition also has a significant effect on the biophysical models, as images acquired during high tides considerably affect the sensitivity of the NIR, and subsequently reduce the sensitivity of red and NIR based vegetation indices. When using MODIS daily surface reflectance data, it is certainly possible to develop a filter to flag the tide dominated scenes by matching tide level from the nearby tide gauge(s) with the MODIS overpass time. However, since we are utilizing the MODIS 8-day surface reflectance products, which provide us with pre-calculated average reflectance over 8-day time period, it is not possible to determine the level of daily MODIS scene contribution to the 8-day surface reflectance imagery. In other words, it is not possible to determine for a particular pixel, whether it is an average of the complete 8 days of surface reflectance, or less than that. Therefore, tidal influence could be one source of variability in the biophysical models.

e. Time–Series Composites and Phenological Analysis

The time–series map composites that we generated for the 15 year time period using the best fit models for both 250m and 500m data provide relevant qualitative assessment of the biophysical status of the salt marshes (Figure 3.11 and 3.12). In particular, the models were able to illustrate the effects of large scale natural disasters affecting the region. For example, a comparison between the time–series composites pre and post hurricane Gustav, using MODIS 250m datasets, clearly illustrates the impact of the landfall, in southern LA. Gustav made landfall at Terrebonne Parish on September 1st, as a Category–2 hurricane, and downgraded to a tropical storm hours later causing heavy rainfall and flooding in Plaquemines, Jefferson, and St. Bernard Parish (~10–15 inches rainfall between August 29 and September 5; http://www.weather.gov). The 8-day composite derived from the MODIS image of August 5, 2008 showed high levels of CHL, GBM, GLAI and VF for those regions which is expected during the middle of the growing season. Post hurricane composites showed significant reduction in the levels of all biophysical characteristics, indicating severe short-term physical impact of the high energy phenomenon on the salt marsh habitats (Figure 3.11). Over the years hurricanes have severely impacted the Gulf coast marshes by causing substantial short-term damage due to a combination of wind, tide, and wave action. Most of the physical damage due to hurricane landfall includes (a) compressed marsh – a net decrease in surface area resulting from marsh being pushed together, (b) marsh balls – marsh being piled, rolled, and deformed to create large mounds, and (c) sediment deposition on marsh grass (Lovelace and McPherson, 1998). The biophysical map composites before and after Gustav demonstrated this immediate physical damage (Figure 3.11). Comparison between MODIS based GBM estimates from Terrebonne Parish with the monthly GBM estimates reported by Darby and Turner (2008) from a salt marsh patch in approximately the same geographic area (accurate GPS

location of their study area was unavailable) reveal some differences between GBM magnitude and phenology, particularly at the peak of the growing season. The peak biomass estimates from MODIS 250m data (634.7 gm^{-2}; October 2004) were less than their plot level estimates (877 gm^{-2}; September, 2004). Further, MODIS based model predicted the peak biomass level in October rather than in September as reported in their study. Similar differences were also noticed at the beginning of growing season. MODIS estimates of biomass from March 2004 (402.3 gm^{-2}) were being much higher than 114 gm^{-2} as observed by Darby and Turner (2008). Differences in the estimates could be due to the difference in location of the exact sites or due to mismatch between plot level estimates (their study) and coarse pixel level estimates (our study).

A similar comparison between pre and post Hurricane Katrina is shown using time-series composites generated from MODIS 500m datasets. Katrina made its second landfall in the Plaquemines parish as a Category 3 hurricane and maintained its intensity as it passed over St. Bernard parish towards New Orleans (Waple, 2005). The reduction in the levels of biophysical characteristics indicated severe stress in the salt marsh habitats in the Plaquemines, Jefferson and St. Bernard Parish near New Orleans (Figure 12). From these examples it is quite clear that such high frequency time-series map composites can not only help to identify extent and magnitude of physical damage to marsh patches after similar natural or anthropogenic disasters, but can also facilitate restoration and conservation measures. The high temporal resolution of the MODIS products allows for frequent monitoring, leading to rapid initiation of restoration efforts after disturbances and accurate monitoring of the restored habitats.

In addition, phenological charts derived from the time–series composites illustrate the trends in the biophysical values quantitatively (Figures 3.13 and 3.14). The MODIS based biophysical models enabled us to develop 15 years of high frequency phenology for any marsh site across the

four Gulf States. The site specific phenology shown in this study for selected locations in Terrebonne and Plaquemines parishes have been able to capture not only the natural seasonal variability, but also the effects of various natural and anthropogenic events that have occurred between 2000 and 2014 on the marsh biophysical status. These sites were carefully chosen for analysis, as they are not only diverse in terms of species composition, but also they have been subject to episodic tropical storms and severe drought, which have induced stress on the salt marsh habitats. Therefore, these sites can be considered as periodic critical hotspots of salt marsh stress and degradation.

The growing season of salt marshes along the Gulf Coast usually begins in March/April and reaches peak growth and photosynthetic activity in August/September, followed by period of senescence and dormancy from October until the beginning of the next growing season. Natural or anthropogenic disasters induce both short and long–term stress in these marsh habitats. Hurricanes and similar high energy phenomena such as tropical storms have been known to cause moderate to severe short-term physical damage to marshes. For example, the short-term effects of hurricanes Cindy and Katrina (2005), Gustav (2008) and Isaac (2012) on the marshes in Terrebonne parish are visible by the obvious reduction in the magnitudes of biophysical characteristics after each event shown in both the MODIS 250m composites and phenology plot (Figure 3.13). Further, stress induced by periodic drought are also visible in the growing seasons of 2000, 2006, and 2011, when marshes witnessed extreme (D3) to exceptional (D4) dry conditions in LA (US drought monitor archives; http://droughtmonitor.unl.edu/) (Figure 3.13a–d). A closer examination of the growing seasons of 2008 and 2009 clearly shows the stress induced by Hurricane Gustav in September 2008 similar to the effects seen in the map composites (Figure 3.11). However, the steady recovery from the stress is also visible in the

2009 phenology when the marsh habitats returned to the pre-hurricane biophysical levels by August 2009 (Figure 3.13e–h). It demonstrates the resiliency of these marshes even in the face of high intensity hurricanes. Möller et al. (2014) showed that up to 60% of observed wave attenuation can be attributed to marsh vegetation. They also found that although storm waves cause considerable physical damage to the stem and canopy of the vegetation, the marsh surface remains stable and resistant to surface erosion under all conditions. We found similar behavior in our phenology plots, which showed that Gulf marshes suffered severe short-term damage but bounced back after every hurricane because their surface and belowground architecture remained stable. Similarly, the 500m data derived phenology derived from marsh patches in Plaquemines parish, LA illustrates the impact of Hurricanes Cindy and Katrina in the growing seasons of 2005, and drought in 2000 and 2011. Comparative analysis between the growing seasons of 2005 and 2006 shows recovery of the marsh habitats from the stress induced by back-to-back landfall of Hurricanes Cindy and Katrina in the region (Figure 3.14 e–h). The effects of the stress seem directly proportional to the intensity and duration of a natural or anthropogenic event (such as Hurricane strength or length of drought period). Further, the magnitude of the impact also depends on the timing of an event. Stress induced during the middle of the growing season, when photosynthesis, growth and reproduction rates are high and susceptible to any environmental disturbances, is much more pronounced compared to disturbances during the non-growing season, when marsh plants are already in a stage of senescence.

In addition to events captured through phenology analysis, other fluctuations were also seen in the seasonal trends of the biophysical values; these may have been a result of natural variability, localized disturbances, or model uncertainties. Although detailed site-specific phenological analysis of salt marsh habitats is beyond the scope of this study, it is undeniable that such

phenological plots have the potential to provide both quantitative estimates of site specific characteristics, and the long–term trend of the Salt marsh health. MODIS is the only existing sensor that provides 8-day cloud free products which are necessary for high frequency regional phenological analysis. Such long–term trends can also be analyzed in conjunction with long–term climate data, such as temperature and sea level rise, to assess and predict response of Salt marshes climatic forcings.

MODIS derived time–series map composites and phenological charts provide coastal resource managers and policy makers with both qualitative and quantitative information of the status of salt marshes. The biophysical mapping methodology developed through this study can be used for identifying critical 'hotspots' of marsh degradation due to factors other than natural disasters such as developmental activities, oil and gas industry activities, urban runoff, sudden marsh die–off events, changes in soil biogeochemical properties, and herbivory. The models and products developed through this study have the potential to facilitate prioritization of restoration efforts through identification of areas in need of immediate attention; they can also be used to compare the biophysical status of marsh patches/habitats pre and post implementation of restoration.

Conclusion

This study provides novel methods for mapping salt marsh health and productivity, using fine temporal resolution MODIS data. For the first time statistical models were established for marsh biophysical characteristics by combining MODIS derived VIs and extensive ground data. This kind of regional marsh study has not been previously attempted at such a large scale because of the inherent difficulty in collecting ground data to represent coarse resolution satellite pixels. Furthermore, ground data collection can be expensive and time consuming. The MODIS based

models developed in this study have been able to map these biophysical characteristics effectively, and can serve as baseline for developing satellite based models of NPP/CSP potential of the salt marshes. Mapping NPP/CSP is crucial for detecting whether these ecosystems are functioning as sinks or sources of carbon in the environment. This is particularly important because these productive coastal ecosystems in the Gulf and elsewhere are vulnerable to climate change induced sea level rise and perpetual developmental pressures. Our approach to study salt marshes is different from conventional tidal remote sensing approaches which have concentrated on habitat delineation, species mapping and/or marsh gain/loss.

The biophysical characteristics, analyzed in this paper (GLAI, VF, CHL and GBM) are suitable proxies for photosynthetic capacity, nitrogen content, and the physiological status (Blackburn, 1998; Pierce et al. 1994; Pinar and Curran, 1996) of marsh vegetation since they are sensitive to natural processes and anthropogenic activities occurring across the region. These biophysical characteristics can be different between species of marsh vegetation due to their differences in foliar and canopy structures, distribution, and habitat preference, and inherent physiology. Species–dependent marsh biophysical models are generally more accurate and can be implemented only when marshes in the study area can be classified into individual plant communities. Classification of the marsh habitats into homogenous species communities is impractical as it requires significant ground data and tidal information; it is particularly difficult when using moderate and coarse spatial resolution sensors such as MODIS because of mixed pixel issues. Further, unavoidable classification errors can be introduced during mapping species composition prior to application of these biophysical models, which in turn have built–in uncertainties, which magnifies the error of the final output. As such, the information provided to the end user (restoration managers and conservationists) may be far from the reality. Therefore,

using species–independent biophysical models (not influenced by species diversity), is the best option to generate high frequency time–series composites. Moreover, our analysis and results clearly demonstrate the deterioration of the species level signal variation at the coarse spatial resolution of MODIS, which makes it suitable for broad scale regional mapping. This study has demonstrated the value of species–invariant biophysical models, which can be implemented for any marsh habitat regardless of its community composition. In addition, since these MODIS based models are species independent, they can be utilized for monitoring similar salt marsh habitats within United States such as coastal Georgia, Texas, California, and the Carolinas, as well as marshes in the temperate zones throughout the world. For other marsh habitats, such as the mangroves and freshwater marshes, these biophysical models may be applied after recalibration and optimization. This is due to the fact that mangroves and freshwater marshes have significantly different foliar and canopy architecture.

Although MODIS can be an excellent choice for broader landscape level biophysical mapping, certain site specific studies may require information at a much finer resolution. Mapping biophysical parameters using species specific models might be a better option than species invariant models if species classification map is available for a study site. Further, in order to implement these biophysical models using MODIS for a particular salt marsh habitat the extent of the habitat has to be completely covered by at least 8–10 pixels of MODIS 250m or 500m, which may be impossible in highly fragmented habitats. In essence, selection of the appropriate sensor for biophysical mapping should depend not only on the research questions and scale, but also on the nature of the marsh habitat. Since the models are somewhat influenced by tidal fluctuations, developing tide invariant models should be the next step which is certainly feasible on temporally dense MODIS daily surface reflectance data.

The high temporal resolution of MODIS 8–day surface reflectance products, coupled with the moderate spatial resolution, has immense potential in studying and monitoring both long and short–term salt marsh health and physiological status. Further studies can be performed both at site specific and landscape levels. The time–series maps and phenological charts derived from MODIS imagery provide the tools necessary for effective conservation and restoration of these fragile ecosystems. These products can be used in conjunction with different hydrological, meteorological, and land–use parameters to assess the influence of different factors on marsh health. Coastal resources managers and policy makers in the Gulf Coast will now have access to large–scale maps of the status of the marshes under their jurisdiction and can use these products to (a) identify problem areas that should be high priorities for restoration activities, (b) evaluate the relative success of prior restoration efforts, and (c) locate the vulnerable Marsh patches most likely to be affected by coastal developmental activities.

Acknowledgements

This study involved intense field data collection spanning over three years under harsh conditions and we would like to thank and acknowledge the large number of people involved in this effort, including Chris Downs, Mike Bryant, Calista Guthrie, Gary Alon Blakeney and Sachidananda Mishra (Mississippi State University), Paul Merani (University of Nebraska–Lincoln), Philemon Kirui (Jackson State University), Sarah Moore, Ross Del Rio, Lindsay Dunaj, Phil McCarty, Mike Brown (University of New Orleans), Christina Mohrman (Grand Bay National Estuarine Research Reserve), and Charles Jordan (University of Georgia). This research was partially funded by the National Aeronautics and Space Administration (NASA) Gulf of Mexico program (Grant # NNX10AE65G), National Science Foundation (NSF) Division of Environmental Biology (Grant # 1050500), and Gulf of Mexico Research Initiative (GoMRI)

(Grant # GRI–0012). Anatoly Gitelson is grateful to International Incoming Marie Curie Fellowship for supporting this work at Israel Institute of Technology.

References

Adam, E., Mutanga, O., and Rugege, D 2010. Multispectral and hyperspectral remote sensing for identification and mapping of wetland vegetation: a review, *Wetland Ecology and Management*, 18, 281–296.

Artigas, F. and Pechmann, I. C. 2010. Balloon imagery verification of remotely sensed *Phragmites australis* expansion in an urban estuary of New Jersey, USA, *Landscape and Urban Planning*, 95, 105–112.

Baldocchi, D. D. 2003): Assessing the eddy covariance technique for evaluating carbon dioxide exchange rates of ecosystems: past, present and future, *Global Change Biology*, 9, 479–492.

Barbier, E. B., Koch, E. W., Silliman, B. R., Hacker, S. D., Wolanski, E., Primavera, J., Granek, E.F., Polasky, S., Aswani, S., Cramer, L. A., Stoms, D. M., Kennedy, C., J., Bael, D., Kappel, C. V., Perillo, G. M. E., and Reed, D. J.2008. Coastal ecosystem–based management with nonlinear ecological functions and values, *Science*, 319, 321–323.

Biber, P. D. 2007. Evaluating a chlorophyll content meter on three coastal wetland plant species, *Journal of Agriculture, Food and Environmental Science*, 1, 1–11.

Biber, P. D., Wu, W., Peterson, M. S., Liu, Z. and Pham, L. 2012. Oil contamination in Mississippi saltmarsh habitats and the impacts to *Spartina alterniflora* photosynthesis, In: Alford, J. B., Peterson, M. S., and Green, C. G. (Eds.) *Impacts of Oil Spill Disasters on Marine Habitats and Fisheries in North America*, pp. 133 – 172, CRC Press, Boca Raton, Florida, USA.

Blackburn, G. A. 1998. Quantifying chlorophyll and carotenoids at leaf and canopy scales: an evaluation of some hyperspectral approaches, *Remote Sensing of Environment*, 66, 273–285

Boesch, D. F., and Turner, R. E. 1984. Dependence of fishery species on salt marshes: the role of food and refuge, *Estuaries and Coasts*, 7, 460–468.

Brevik, E. C., and Homburg, J. A. 2004. A 5000 year record of carbon sequestration from a coastal lagoon and wetland complex, Southern California, USA, *Catena*, 57, 221–232.

Campbell, J. B. (Ed.) 2007. Introduction to Remote Sensing, Guilford, New York, New York, USA.

Chmura, G. L., Anisfeld, S. C., Cahoon, D. R., and Lynch, J. C. 2003. Global carbon sequestration in tidal, saline wetland soils, *Global Biogeochemical Cycles*, 17, DOI: 10.1029/2002GB001917.

Choi, Y., and Wang, Y. 2004. Dynamics of carbon sequestration in a coastal wetland using radiocarbon measurements, *Global Biogeochemical Cycles*, 18, DOI: 10.1029/2004GB002261.

Churkina, G., Schimel, D., Braswell, B. H., and Xiao, X. M. 2005. Spatial analysis of growing season length control over net ecosystem exchange, *Global Change Biology*, 11, 1777–1787.

Collin, A., Long, B., and Archambault, P. 2010. Salt–marsh characterization, zonation assessment and mapping through a dual–wavelength LiDAR, *Remote Sensing of Environment*, 114, 520–530.

Connor, R. F., Chmura, G. L., and Beecher, C. B. 2001. Carbon accumulation in Bay of Fundy salt marshes: Implications for restoration of reclaimed marshes, *Global Biogeochemical Cycles*, 15, 943–954.

Dahl, T. E. 2006. Status and trends of wetlands in the conterminous United States 1998 to 2004, Fish and Wildlife Service, Fisheries and Habitat Conservation, Washington D. C., USA.

Darby, F. A., and Turner. R. E. 2008. Below-and Aboveground *Spartina alterniflora* Production in a Louisiana Salt Marsh, *Estuaries and Coasts*, 31, 223-231.

Davi, H., Soudani, K., Deckx, T., Dufrene, E., Le Dantec, V., and Francois, C. 2006. Estimation of forest leaf area index from SPOT imagery using NDVI distribution over forest stands, *International Journal of Remote Sensing*, 27, 885–902.

Davranche, A., Lefebvre, G., and Poulin, B. 2010. Wetland monitoring using classification trees and SPOT–5 seasonal time series, *Remote Sensing of Environment*, 114, 552–562.

Decagon Devices 2008. AccuPAR PAR/LAI ceptometer model LP–80: Operator's Manual, version 1.2., Decagon Devices, Pullman, WA.

Deegan, L. A., Hughes, J. E., and Rountree, R. A. 2002. Salt marsh ecosystem support of marine transient species, In: Kreeger, D. A. (Ed.) *Concepts and controversies in tidal marsh ecology*, 333–365, Springer Netherlands, Dordrecht, South Holland, The Netherlands.

Delalieux, S., Somers, B., Hereijgers, S., Verstraeten, W. W., Keulemans, W., and Coppin, P. 2008. A near–infrared narrow–waveband ratio to determine Leaf Area Index in orchards, *Remote Sensing of Environment*, 112, 3762–3772.

Evans, T. L., and Costa, M. 2013. Landcover classification of the Lower Nhecolândia subregion of the Brazilian Pantanal Wetlands using ALOS/PALSAR, RADARSAT–2 and ENVISAT/ASAR imagery, *Remote Sensing of Environment*, 128, 118–137.

Filippi, A. M., and Jensen, J. R. 2006. Fuzzy learning vector quantization for hyperspectral coastal vegetation classification, *Remote Sensing of Environment*, 100, 512–530.

Fitzgerald, D. M., Fenster, M. S., Argow, B. A., and Buynevich, I. V. 2008. Coastal impacts due to sea–level rise, *Annual Review of Earth and Planetary Science*, 36, 601–647.

Friedl, M. A., McIver, D. K., Hodges, J. C., Zhang, X. Y., Muchoney, D., Strahler, A. H., Woodcock, C. E., Gopal, S., Schneider, S., Cooper, A., Baccini, A., Gao, F., and Schaaf, C. 2002. Global land cover mapping from MODIS: algorithms and early results. *Remote Sensing of Environment*, 83, 287–302.

Friess, D. A., Spencer, T., Smith, G. M., Möller, I., Brooks, S. M., and Thomson, A. G. 2012. Remote sensing of geomorphological and ecological change in response to saltmarsh managed realignment, The Wash, UK, *International Journal of Applied Earth Observation and Geoinformation*, 18, 57–68.

Gallagher, J. L., Reimold, R. J., Linthurst, R. A., and Pfeiffer, W. J. 1980. Aerial production, mortality, and mineral accumulation–export dynamics in *Spartina alterniflora* and *Juncus roemerianus* plant stands in a Georgia salt marsh, *Ecology*, 6, 303–312.

Gamon, J. A. and Surfus, J. S. 1999. Assessing leaf pigment content and activity with a reflectometer, *New Phytologist*, 143, 105–117.

Gilfillan, E. S., Page, D. S., Bass, A. E., Foster, J. C., Fickett, P. M., Ellis, W. G. H., Rusk, S., and Brown, C. 1989. Use of Na/K ratios in leaf tissues to determine effects of petroleum on salt exclusion in marine halophytes, *Marine Pollution Bulletin*, 20; 272–276.

Gilmore, M. S., Civco, D. L., Wilson, E. H., Barrett, N., Prisloe, S., Hurd, J. D., and Chadwick, C. 2010. Remote sensing and in situ measurements for delineation and assessment of coastal

marshes and their constituent species, In: Wang, Y. (Ed.) *Remote Sensing of Coastal Environment*, CRC Press, Boca Raton, Florida, USA, 261–280.

Gitelson A. A., Kaufman Y. J., Stark, R., and Rundquist, D. 2002b. Novel algorithms for remote estimation of vegetation fraction, *Remote Sensing of Environment*, 80, 76–87.

Gitelson, A. A. 2004. Wide dynamic range vegetation index for remote quantification of crop biophysical characteristics, *Journal of Plant Physiology*, 161, 165–173, 2004.

Gitelson, A. A., Keydan, G. P., and Merzlyak, M. N. 2006. Three–band model for noninvasive estimation of chlorophyll, carotenoids, and anthocyanin contents in higher plant leaves, *Geophysical Research Letters*, 33, L11402.

Gitelson, A. A., Stark, R., Grits, U., Rundquist, D., Kaufman, Y. and Derry, D. 2002a. Vegetation and soil lines in visible spectral space: a concept and technique for remote estimation of vegetation fraction, *International Journal of Remote Sensing*, 23, 2537–2562.

Gitelson, A. A., Vina, A., Ciganda, V., Rundquist, D. C., and Arkebauer, T. J. 2005. Remote estimation of canopy chlorophyll content in crops, *Geophysical Research Letters*, 32.

Gitelson, A., and Merzlyak, M. 1994): Quantitative estimation of chlorophyll–a using reflectance spectra: experiments with autumn chestnut and maple leaves. *Journal of Photochemistry and Photobiology B: Biology*, 22, 247–252.

Gitelson, A., Kaufman, Y., and Merzlyak, M. 1996c. Use of a Green Channel in Remote Sensing of Global Vegetation from EOS–MODIS, *Remote Sensing of Environment*, 58, 289–298.

Gong, P., Pu, R., and Miller, J. R. 1995. Compact Airborne Spectrographic Imager Data, *Photogrammetric Engineering and Remote Sensing*, 61, 1107–1117.

Goudie, A. 2013. Characterising the distribution and morphology of creeks and pans on salt marshes in England and Wales using Google Earth, *Estuaries, Coastal and Shelf Science*, 129; 112–123.

Hansen, P. M., and Schjoerring, J. K. 2003. Reflectance measurement of canopy biomass and nitrogen status in wheat crops using normalized difference vegetation indices and partial least squares regression, *Remote Sensing of Environment*, 86, 542–553.

Hardisky, M. A. 1980. A comparison of *Spartina alterniflora* primary production estimated by destructive and nondestructive techniques. *Estuarine Perspectives: Proceedings of the 5th biennial international estuarine research conference*, Jekyll Island, Georgia, October 7 - 12, 1979, 223-234.

Hardisky, M. A., Daiber, F. C., Roman, C. T., and Klemas, V. 1984. Remote sensing of biomass and annual net aerial primary productivity of a salt marsh, *Remote Sensing of Environment*, 16, 91–106.

Hester, M. W., and Mendelssohn, I. A. 2000. Long–term recovery of a Louisiana brackish marsh plant community from oil–spill impact: vegetation response and mitigating effects of marsh surface elevation, *Marine Environmental Research*, 49, 233–254.

Hinkle, R. L., and Mitsch, W. J. 2005. Salt marsh vegetation recovery at salt hay farm wetland restoration sites on Delaware Bay, *Ecological Engineering*, 25, 240–251.

Hopkinson, C.S, Gosselink, J. G. and Parrando, R. T. 1978. Aboveground Production of Seven Marsh Plant Species in Coastal Louisiana, *Ecology*, 59, 760-769.

Huete, A. R. 1998. A soil–adjusted vegetation index (SAVI), *Remote Sensing of Environment*, 25, 295–309.

Huete, A., Didan, K., Miura, T., Rodriguez, E. P., Gao, X., and Ferreira, L. G. 2002) Overview of the radiometric and biophysical performance of the MODIS vegetation indices, *Remote Sensing of Environment*, 83, 195–213, 2002.

Jackson, T. J., Schmugge, T. J., Parry, R., Kustas, W. P. Ritchie, J. C., Shutko, A. M., Haldin, A., Reutov, E., Novichikhin, E., Liberman, B., Shiue, J. C., Davis, M. R., Goodrich, D. C., Amer, S. B., and Bach, L. B. 1992. Multifrequency passive microwave observations of soil moisture in an arid rangeland environment, *International Journal of Remote Sensing*, 13, 573–580.

Jensen, J. R. (Ed.) 1996. Introductory digital image processing, Prentice–Hall Inc., New York, New York, USA.

Jensen, J. R. (Ed.) 2007. Remote Sensing of the Environment: An Earth Resource Perspective, Prentice–Hall Inc., New York, New York, USA.

Jensen, J. R., Rutchey, K., Koch, M. S. and Narumalani, S. 2002. Inland wetland change detection in the Everglades water conservation area 2A using a time series of normalized remotely sensed data, *Photogrammetric Engineering and Remote Sensing*, 61, 199–209.

Jensen, R., Mausel, P., Dias, N., Gonser, R., Yang, C., Everitt, J., and Fletcher, R. 2007. Spectral analysis of coastal vegetation and land cover using AISA+ hyperspectral data, *Geocarto International*, 22, 17–28.

Kearney, M. S., Stutzer, D., Turpie, K., and Stevenson, J. C. 2009. The effects of tidal inundation on the reflectance characteristics of coastal marsh vegetation, *Journal of Coastal Research*, 25, 1177–1186.

Kennish, M. J. 2001. Coastal Salt Marsh Systems in the US: a Review of Anthropogenic Impacts: *Journal of Coastal Research*, 17, 731–748.

Klemas, V. 2011. Remote sensing of wetlands: case studies comparing practical techniques, *Journal of Coastal Research*, 27, 418–427.

Klemas, V., Bartlett, D. S., and Philpot, W. D. 1980. Remote sensing as a technique for synoptic inventories of fisheries related resources. *Estuarine Perspectives: Proceedings of the 5th biennial international estuarine research conference*, Jekyll Island, Georgia, October 7 - 12, 1979, 359-375.

Koch, E. W., Barbier, E. B., Silliman, B. R., Reed, D. J., Perillo, G. M., Hacker, S. D., Granek, E. F., Primavera, J. H., Muthiga, N., Polasky, S., Halpern, B. S., Kennedy, C. J., Kappel, C. V., and Wolanski, E. 2009. Non–linearity in ecosystem services: temporal and spatial variability in coastal protection, *Frontiers in Ecology and the Environment*, 7, 29–37.

Kovacs, J. M., King, J. M. L., de Santiago, F. F., and Flores–Verdugo, F. 2009. Evaluating the condition of a mangrove forest of the Mexican Pacific based on an estimated leaf area index mapping approach, *Environmental Monitoring and Assessment*, 157, 137–149.

Kovacs, J. M., Wang, J., and Flores–Verdugo, F. 2005. Mapping mangrove leaf area index at the species level using IKONOS and LAI–2000 sensors for the Agua Brava Lagoon, Mexican Pacific, *Estuaries, Coastal and Shelf Science*, 62, 377–384.

Laba, M., Downs, R., Smith, S., Welsh, S., Neider, C., White, S., Richmon, M., Philpot, W., and Baveye, P. 2008. Mapping invasive wetland plants in the Hudson River National Estuarine Research Reserve using Quickbird satellite imagery, *Remote Sensing of Environment*, 112, 286–300.

Lefebvre, A., Corpetti, T., Bonnardot, V., Quénol, H. and Hubert–Moy, L. 2010. Vineyard identification and characterization based on texture analysis in the Helderberg Basin (South Africa), *30th IEEE International Geoscience and Remote Sensing Symposium, Honolulu, Hawaii*, 25–30 July 2010, 2852–2855, 2010.

Li–COR Inc. 2000. LAI–2000 plant canopy analyzer: Instruction manual, Li–COR, Inc., Lincoln, Nebraska, USA.

Lillesand, T. M., Kiefer, R. W., and Chipman, J. W. (Eds.) 2008. Remote Sensing and Image Interpretation, John Wiley and Sons Ltd., Hoboken, New Jersey, USA.

Lindstedt, D.M., and Swenson, E.M. 2006. The case of the dying marsh grass, Louisiana Department of Natural Resources, Baton Rouge, LA.

Lovelace, J. K. and McPherson, B. F. 1995. Restoration, Creation, and Recovery: Effects of Hurricane Andrew (1992) on Wetlands in Southern Florida and Louisiana. National Water Summary on Wetland Resources, U. S. Geological Survey Water Supply Paper 2425, http://water.usgs.gov/nwsum/WSP2425/andrew.html

Loveland, T. R., Zhiliang, Z., Ohlen, D. O., Brown, J. F., Reed, B. C., and Limin, Y. 1999. An analysis of the IGBP global land-cover characterization process. *Photogrammetric Engineering and Remote Sensing*, 65, 1021–1032.

Lyles, L. D., Namwamba, F., and Campus, B. R. 2005. Louisiana coastal zone erosion: 100+ years of landuse and land loss using GIS and remote sensing. *5th Annual ESRI Education User Conference*, San Diego, California, 23–26 July.

Markwell, J., Osterman, J. C., and Mitchell, J. L. 1995. Calibration of the Minolta SPAD–502 leaf chlorophyll meter, *Photosynthesis Research*, 46, 467–472.

Mishra, D. R., Cho, H. J., Ghosh, S., Fox, A., Downs, C., Merani, P. B. T., Kirui, P., Jackson, N. and Mishra, S. 2012. Post–spill state of the marsh: Remote estimation of the ecological impact of the Gulf of Mexico oil spill on Louisiana Salt Marshes, *Remote Sensing of Environment*, 118; 176–185.

Mishra, D. R., Ghosh, S., Hladik, C., O'Connell, J. L., and Cho, H. J. 2015. Wetland mapping methods and techniques using multi–sensor, multi–resolution remote sensing: Successes and Challenges, In: Thenkabail, P. S. (Ed.) *Remote Sensing Handbook*, Vol. III, pp. 191 – 227, Taylor and Francis, New York, New York, USA.

Mitsch, W. J., and Gosselink, J. G. (Eds.) 2007. Wetlands, John Wiley and Sons, Hoboken, New Jersey, USA.

Möller, I., Spencer, T., French, J. R., Leggett, D. J., and Dixon, M. 1999. Wave transformation over salt marshes: a field and numerical modelling study from North Norfolk, England. Estuarine, *Coastal and Shelf Science*, 49, 411–426.

Morgan, P. A., Burdick, D. M., and Short, F. T. 2009. The functions and values of fringing salt marshes in northern New England, USA, *Estuaries and Coasts*, 32, 483–495.

Myneni, R. B., Keeling, C. D., Tucker, C. J., Asrar, G., and Nemani, R. R. 1997a. Increased plant growth in the northern high latitudes from 1981 to 1991, *Nature*, 386, 698–702.

Myneni, R. B., Nemani, R. R., Running, S. W. 1997b. Estimation of global LAI and FPAR from radiative transfer models, *IEEE Transactions in Geoscience and Remote Sensing*, 35, 1380–1393.

Nicholls, R. J., Hoozemans, F. M., and Marchand, M. 1999. Increasing flood risk and wetland losses due to global sea–level rise: regional and global analyses, *Global Enviromental Change*, 9, S69–S87.

Pay, S. S., Das, G., Singh, J. P., and Panigrahy, S. 2006. Evaluation of hyperspectral indices for LAI estimation and discrimination of potato crop under different irrigation treatments, *International Journal of Remote Sensing*, 27, 5373–5387.

Pidgeon, E. 2009. Carbon Sequestration by Coastal Marine Habitats: Important Missing Sinks, In: The Management of Natural Coastal Carbon Sinks, IUCN, Gland, Switzerland, 47–51.

Pierce, L. L., Running, S.W., and Walker, J. 1994. Regional-scale relationships of leaf area index to specific leaf area and leaf nitrogen, *Ecological Applications*, 4, 313–321

Pinar, A. and Curran, P. J. 1996. Grass chlorophyll and the reflectance red edge, *International Journal of Remote Sensing*, 17, 135–357

Proisy, C., Couteron, P., and Fromard, F. 2007. Predicting and mapping mangrove biomass from canopy grain analysis using Fourier–based textural ordination of IKONOS images, *Remote Sensing of Environment*, 109, 379–392.

Ravens, T. M., Thomas, R. C., Roberts, K. A., and Santschi, P. H. 2009. Causes of salt marsh erosion in Galveston Bay, Texas, *Journal of Coastal Research*, 25, 265–272.

Rendong L., and Jiyuan, L. 2004. Estimating wetland vegetation biomass in the Poyang Lake of central China from Landsat ETM data, *IEEE Transactions in Geoscience and Remote Sensing*, 4, 4590–4593.

Richardson, A. D., Braswell, B. H., Hollinger, D. Y., Jenkins, J. P., and Ollinger, S. V. 2009. Near–surface remote sensing of spatial and temporal variation in canopy phenology, *Ecological Applications*, 19, 1417–1428.

Richardson, A. D., Duigan, S. P., and Berlyn, G. P. 2002. An evaluation of noninvasive methods to estimate foliar chlorophyll content, *New Phytologist*, 153, 185–194.

Rosso, P. H., Ustin, S. L., and Hastings, A. 2005. Mapping marshland vegetation of San Francisco Bay, California, using hyperspectral data, *International Journal of Remote Sensing*, 26, 5169–5191.

Rouse, J. W., Haas Jr., R. H., Schell, J. A., and Deering, D. W. 1974. Monitoring vegetation systems in the Great Plains with ERTS, *Third ERTS–1 Symposium, NASA Special Publication*, NASA SP–351, 309–317.

Rundquist, D. C., Narumalani, S. and Narayanan. R. M. 2001. A review of wetlands remote sensing and defining new considerations, *Remote Sensing Reviews*, 20, 207–226.

Rundquist, D., Perk, R., Leavitt, B., Keydan, G. and Gitelson, A. 2004. Collecting spectral data over cropland vegetation using machine–positioning versus hand–positioning of the sensor, *Computers and Electronics in Agriculture*, 43; 173–178.

Schmidt, K. S., and Skidmore, A. K. 2003. Spectral discrimination of vegetation types in a coastal wetland, *Remote Sensing of Environment*, 85, 92–108.

Silliman, B. R., Grosholz, E. D., and Bertness, M. D. (Eds.) 2009. Human Impacts on Salt Marshes: A Global Perspective, University of California Press, Berkeley, California, USA.

Simard, M., Fatoyinbo, L. E., and Pinto, N. 2010. Mangrove canopy 3D structure and ecosystem productivity using active remote sensing, in: Remote Sensing of Coastal Environments, CRC Press, Boca Raton, Florida, USA, 61–78.

Stout, J. P. 1984. The Ecology of Irregularly Flooded Salt Marshes of the Northeastern Gulf of Mexico: A Community Profile, Biological Report 85 (7.1), U.S. Fish and Wildlife Service, Slidell, LA, 97 pp.

Sugumaran, R., Meyer, J. C., and Davis, J. 2004. A web–based environmental decision support system (WEDSS) for environmental planning and watershed management, *Journal of Geographical Systems*, 6, 307–322.

Thenkabail, P. S., Smith, R. B., and De Pauw, E. 2000. Hyperspectral vegetation indices and their relationships with agricultural crop characteristics, *Remote Sensing of Environment*, 71, 158–182.

Tiner, R. W. 1996. Wetland definitions and classifications in the United States, in: National Water Summary on Wetland Resources, US Geological Survey, Water–Supply Paper, 2425, 27–34.

Tiner, R.W. (Ed.) 2013. Tidal Wetlands Primer: An Introduction to their Ecology, Natural History, Status, and Conservation, The University of Massachusetts Press, Amherst, Massachusetts, USA.

Tucker, C. J. 1978. A comparison of satellite sensor bands for vegetation monitoring. *Photogrammetric Engineering and Remote Sensing*, 44, 1369-1380.

Tucker, C. J. 1980. Remote sensing of leaf water content in the near infrared. *Remote sensing of Environment*, 10, 23-32.

Tucker, C. J., and Sellers, P. 1986. Satellite Remote Sensing of Primary Production. *International Journal of Remote Sensing*, 7, 1395-1416.

Turpie, K. 2013. Explaining the spectral red–edge features of inundated marsh vegetation, *Journal of Coastal Research*, 29, 1111–1117.

Vermote, E. F., Kotchenova, S. Y., and Ray, J. P. 2011. MODIS surface reflectance user's guide. MODIS Land Surface Reflectance Science Computing Facility, version, 1 (http://modis-sr.ltdri.org/guide/MOD09_UserGuide_v1_3.pdf)

Wang, Y. 2010. Remote sensing of coastal environments: an overview, In: Wang, Y. (Ed.) Remote Sensing of Coastal Environments, CRC Press, Boca Raton, Florida, USA, 1–24.

Wang, Y., Christiano, M., and Traber, M. 2010. Mapping salt marshes in Jamaica Bay and terrestrial vegetation in Fire Island National Seashore using QuickBird satellite data, In: Wang, Y. (Ed.) Remote Sensing of Coastal Environments, CRC Press, Boca Raton, Florida, USA, 191–208.

Waple, A. 2005. Hurricane Katrina, National Climatic Data Center, NOAA, Asheville, NC.

Weis, J. S. 2010. Salt marsh, in: Encyclopedia of Earth, Environmental Information Coalition, National Council for Science and the Environment, Washington, D.C.

White, M. A., Asner, G. P., Nemani, R. R., Privette, J. L. and Running, S. W. 2000. Measuring Fractional Cover and Leaf Area Index in Arid Ecosystems: Digital Camera, Radiation Transmittance, and Laser Altimetry Methods, *Remote Sensing of Environment*, 74, 45–57.

Zhang, C., and Z. Xie. 2012. Combining object–based texture measures with a neural network for vegetation mapping in the Everglades from hyperspectral imagery, *Remote Sensing of Environment*, 124, 310–320.

Zomer, R. J., Trabucco, A., and Ustin, S. L. 2009. Building spectral libraries for wetlands land cover classification and hyperspectral remote sensing, *Journal of Environmental Management*, 90, 2170–2177.

Table 3.1: Detailed information on study sites used for MODIS model calibration and validation, with number of study plots in each site and number of corresponding usable MODIS 250m and 500m pixels.

Data	State	Site	Month	Year	No. of plots	Species	No. of usable MODIS pixels	
							250m	500m
Calibration	Louisiana	Bayou Savage	August	2010	7	*Spartina, Juncus*	7	7
	Mississippi	Marsh Point	September	2010	20	*Spartina, Juncus, Distichlis*	3	2
	Louisiana	Plaquemine/ Terreborne parish	September	2010	25	*Spartina, Salicornia, Distichlis*	3	1
	Mississippi	Marsh Point	September	2010	5	*Spartina*	1	1
	Mississippi/ Alabama	Grand Bay	October	2010	37	*Spartina, Salicornia, Distichlis, Juncus*	5	5
Validation	Mississippi/ Alabama	Grand Bay	May	2011	44	*Spartina, Salicornia, Distichlis, Juncus*	7	7
	Louisiana	Plaquemine/ Terreborne parish	June	2011	21	*Spartina, Salicornia, Distichlis*	4	3
	Mississippi	Marsh Point/ Cat Island	July	2011	10	*Spartina, Juncus*	5	2
	Florida	St Marks	August	2011	16	*Juncus*	4	2

Table 3.2: Summary statistics for the field data collected over growing seasons of 2010 and 2011, along with respective MODIS 250m and 500m pixel averages for each biophysical parameter.

Year		Raw Data				MODIS pixel average (250m)				MODIS pixel average (500m)			
		GBM	*VF*	*GLAI*	*CHL*	*GBM*	*VF*	*GLAI*	*CHL*	*GBM*	*VF*	*GLAI*	*CHL*
2010	*Max*	6094.53	98.75	1.87	1242.61	1091.77	97.46	1.79	842.71	1102.17	98.52	1.87	906.02
	Min	42.61	0.30	0.001	0.77	104.57	0.34	0.001	158.93	308.66	2.09	0.09	1.15
	Mean	858.42	44.78	0.53	321.10	714.68	55.33	0.81	522.27	694.74	53.14	0.81	278.67
	St. Dev	811.32	28.83	0.51	276.35	273.45	26.71	0.57	217.28	290.21	33.26	0.68	311.42
2011	*Max*	2422.20	95.01	3.54	1603.58	827.02	75.83	1.78	739.86	841.31	55.81	1.53	723.51
	Min	115.28	2.09	0.001	40.83	268.34	29.13	0.24	273.46	322.59	8.35	0.30	268.09
	Mean	579.04	32.27	1.05	521.94	584.04	51.17	0.89	473.25	582.73	37.56	0.92	457.14
	St. Dev	330.01	20.81	0.85	383.70	181.38	17.01	0.48	157.42	154.91	14.33	0.50	133.93

Table 3.3: List of satellite image derived VIs used for calibration and validation of the wetland biophysical characteristics. * R_{red} was used instead of $R_{red\text{-}edge}$ as described in Gitelson et al. (2006).

Vegetation Index	Formula	Reference
Normalized Difference Vegetation Index (*NDVI*)	$(R_{NIR} - R_{Red})/(R_{NIR} + R_{Red})$	Rouse et al. 1974
Enhanced Vegetation Index 2 (*EVI2*)	$\{2.5 \times (R_{NIR} - R_{Red})/(R_{NIR} + 2.4 \times R_{Red} + 1)\}$	Huete et al. 2002
Chlorophyll Index Red (*CI_{red}*)*	$(R_{NIR} - R_{Red})/R_{Red}$	Gitelson et al. 2006
Wide Dynamic Range Vegetation Index (*WDRVI*)	$(\alpha \times R_{NIR} - R_{Red})/(\alpha \times R_{NIR} + R_{Red})$	Gitelson, 2004
Soil Adjusted Vegetation Index (*SAVI*)	$(R_{NIR} - R_{Red}) \times (I + L)/(R_{NIR} + R_{Red} + L)$	Huete, 1988
Chlorophyll Index Green (*CI_{green}*)	$(R_{NIR} - R_{Green})/R_{Green}$	Gitelson et al. 2006
Green Normalized Difference Vegetation Index (*GNDVI*)	$(R_{NIR} - R_{Green})/(R_{NIR} + R_{Green})$	Gitelson et al. 1996c
Visible Atmospherically Resistant Index (*VARI*)	$(R_{Green} - R_{Red})/(R_{Green} + R_{Red})$	Gitelson et al. 2002a

Table 3.4: Pearson's rank correlation between biophysical characteristics and Ocean Optics derived VIs for Spartina, Juncus, all homogenous and heterogenous plots. Values in bold indicate significant correlation at 0.05 level.

Pearson's Rank Correlations		**NDVI**	**EVI2**	**WDRVI (α = 0.1)**	**WDRVI (α = 0.2)**	**CI_{Red}**	**SAVI**	**G NDVI**	**CI_{Green}**	**VARI**
Spartina (N=19)	*GBM*	**0.502**	**0.5**	**0.542**	**0.529**	**0.566**	**0.478**	**0.467**	**0.507**	.436
	VF	0.934	0.923	0.889	0.907	0.849	0.936	0.847	0.75	0.794
	CHL	0.611	0.603	0.622	0.62	0.621	0.594	0.613	0.616	.392
	GLAI	0.754	0.751	0.733	0.742	0.71	0.758	0.683	0.616	0.66
Juncus (N=13)	*GBM*	**0.573**	**0.573**	**0.62**	**0.606**	**0.642**	0.546	.532	**0.596**	**0.635**
	VF	**0.567**	**0.576**	**0.622**	**0.604**	**0.653**	**0.556**	.497	**0.578**	0.752
	CHL	**0.654**	**0.672**	0.75	0.721	0.798	**0.632**	**0.683**	0.799	.462
	GLAI	**0.619**	**0.632**	0.716	0.685	0.772	**0.591**	**0.568**	0.698	0.758
All Homogenous (N=42)	*GBM*	0.565	0.557	0.576	0.572	0.581	0.547	0.494	0.519	0.489
	VF	0.706	0.73	0.714	0.715	0.702	0.732	0.521	0.493	0.861
	CHL	0.544	0.562	0.574	0.568	0.578	0.552	0.418	0.433	0.599
	GLAI	0.678	0.703	0.703	0.699	0.702	0.698	0.524	0.516	0.788
Heterogenous (N=22)	*GBM*	0.053	0.057	0.053	0.054	0.051	0.058	-0.120	-0.084	**0.492**
	VF	0.218	0.217	0.178	0.194	0.138	0.230	0.009	-0.008	0.603
	CHL	0.292	0.278	0.265	0.275	0.240	0.278	0.151	0.135	**0.443**
	GLAI	0.326	0.317	0.281	0.299	0.238	0.325	0.049	0.050	0.798

Table 3.5: Linear R^2 for MODIS (250m) derived VIs calibrated against different biophysical characteristics. Because of the similarity in performance of all the red-NIR based VIs, it was not possible to determine the best model for the 250m data from the R^2 table alone. Best model selection was therefore dependent on the analysis of other parameters such as %NRMSE, slope ratio, and residual trends as explained in Section 5.3.

R^2	NDVI	EVI2	CI_{red}	WDRVI ($\alpha = 0.1$)	WDRVI ($\alpha = 0.2$)	SAVI
GLAI	0.867	0.865	0.770	0.821	0.846	0.867
VF (%)	0.864	0.868	0.811	0.845	0.859	0.864
GBM (g/m^2)	0.864	0.871	0.819	0.850	0.864	0.864
CHL (mg/m^2)	0.811	0.837	0.813	0.837	0.843	0.811

Table 3.6: Linear %NRMSE values for MODIS (250m) derived biophysical models for different biophysical characteristics. Relative high %NRMSE corresponding to high R^2 (NDVI, EVI2 and SAVI; from Table 4) signifies inherent bias in the model or non-uniform sensitivity of the indices to biophysical characteristics.

% NRMSE	NDVI	EVI2	CI_{red}	WDRVI ($\alpha = 0.1$)	WDRVI ($\alpha = 0.2$)	SAVI
GLAI	19.165	17.443	14.030	14.967	15.957	19.168
VF (%)	25.163	23.659	21.538	22.055	22.636	25.163
GBM (g/m^2)	19.504	19.355	20.151	19.616	19.425	19.505
CHL (mg/m^2)	26.297	25.913	26.052	25.817	25.789	26.292

Table 3.7: Linear R^2 for MODIS (500m) derived VIs calibrated against different biophysical characteristics. Most of the VIs (especially NIR based indices) show very poor/weak relationship with biophysical characteristics except for green-red based VARI. However, selection of best-fit model was done by examining the %NRMSE and residual trends.

R^2	NDVI	EVI2	CI_{red}	WDRVI (α=0.1)	WDRVI (α=0.2)	SAVI	GNDVI	CI_{Green}	VARI
GLAI	0.097	0.128	0.214	0.184	0.159	0.097	0.004	0.000	0.910
VF (%)	0.165	0.192	0.236	0.249	0.227	0.165	0.006	0.000	0.980
GBM (g/m^2)	0.477	0.548	0.658	0.632	0.615	0.478	0.212	0.206	0.938
CHL (mg/m^2)	0.000	0.000	0.000	0.446	0.482	0.000	0.718	0.000	0.864

Table 3.8: Linear %NRMSE values for MODIS (500m) derived biophysical models for different biophysical characteristics. %NRMSE of VARI was the lowest among the VIs tested; corroborating the failure of NIR based indices in terms of mapping biophysical characteristics coarser resolution.

%NRMSE	NDVI	EVI2	CI_{red}	WDRVI (α=0.1)	WDRVI (α=0.2)	SAVI	GNDVI	CI_{green}	VARI
GLAI	41.567	42.447	44.205	43.578	43.115	41.570	40.015	38.436	32.474
VF (%)	55.175	54.103	49.832	51.803	52.900	52.946	41.988	41.175	24.344
CHL (mg/m^2)	93.594	84.891	70.034	75.027	78.890	93.569	84.946	67.190	21.998
GBM (g/m^2)	84.850	75.253	59.066	64.532	68.718	84.818	68.707	49.218	17.340

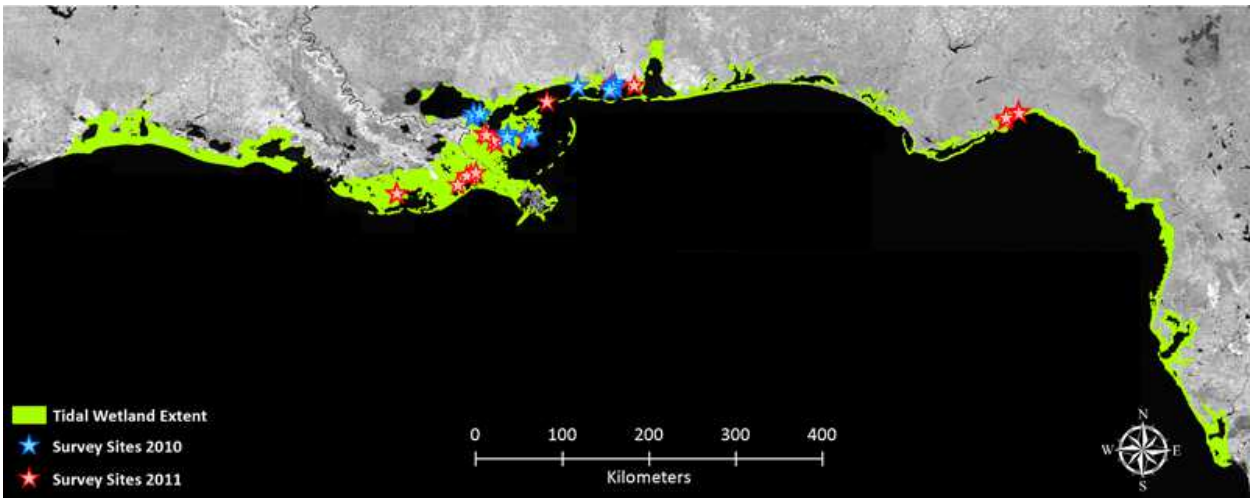

Figure 3.1. Map showing salt marsh extent in northern Gulf of Mexico, with survey sites for 2010 and 2011. Each of the survey sites contained numerous sub–plots from where the detailed field data were acquired.

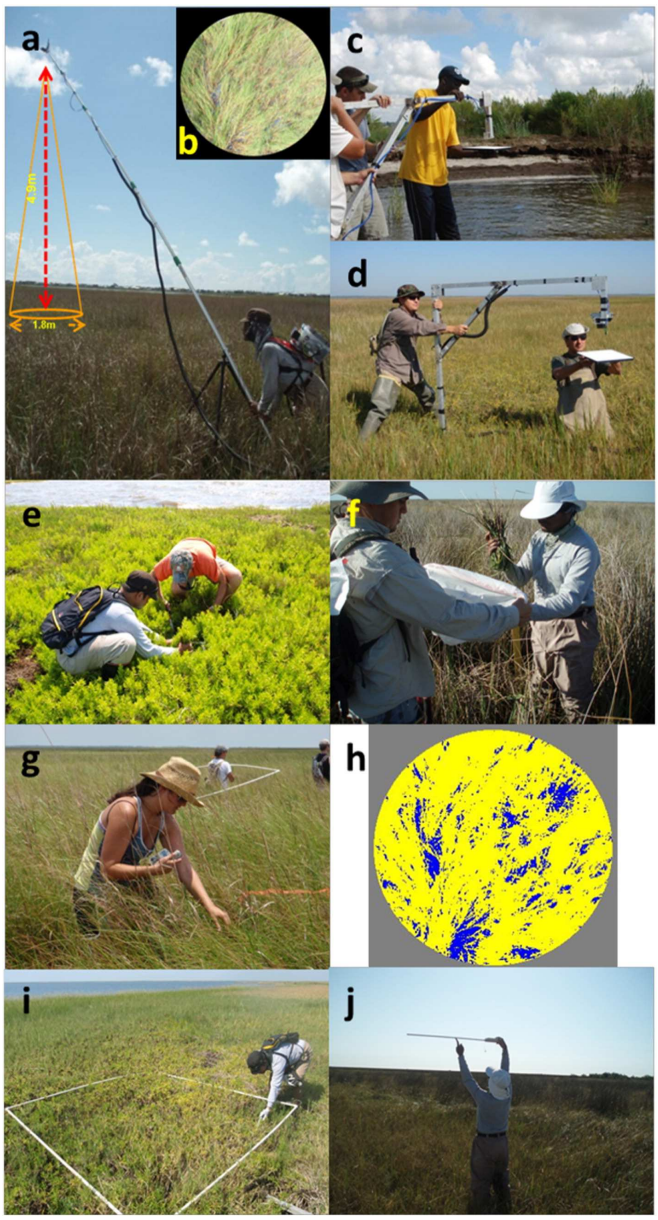

Figure 3.2. *In situ* data collection activities at each sub–plot; a: spectral reflectance acquisition using Ocean Optics sensor; b: sensor altitude (4.9m) and IFOV (1.8m); c and d: sensor calibration using a Labsphere 99% reflectance spectralon panel; e and f: biomass collection from sub–plot; g: leaf chlorophyll content (Chl) measurement using SPAD 502 chlorophyll meter; h: vegetation fraction binary mask measured from the IFOV of the sensor using a digital camera; i and j: LAI measurements using LICOR LAI Plant Canopy Analyzer 2000 and AccuPAR LP–80 Ceptometer.

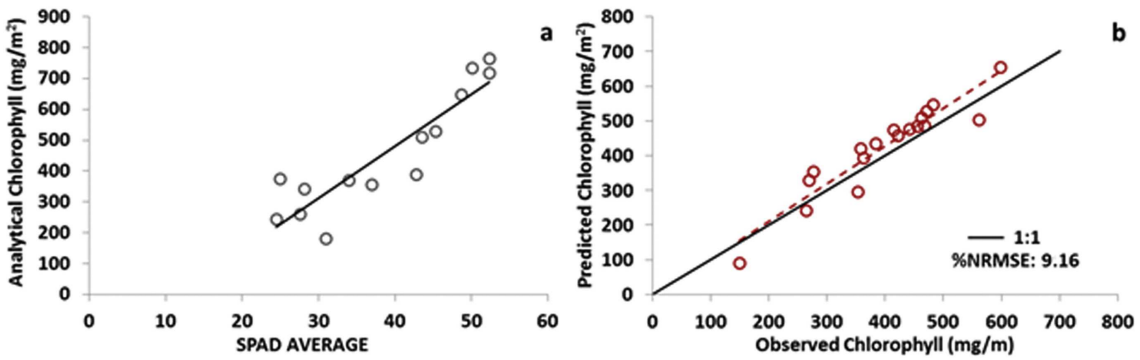

Figure 3.3. a. Relationship between SPAD readings acquired at each sub–plot calibrated against analytical chlorophyll content values from laboratory analysis; b. validation of the SPAD model showing % NRMSE and 1:1 line.

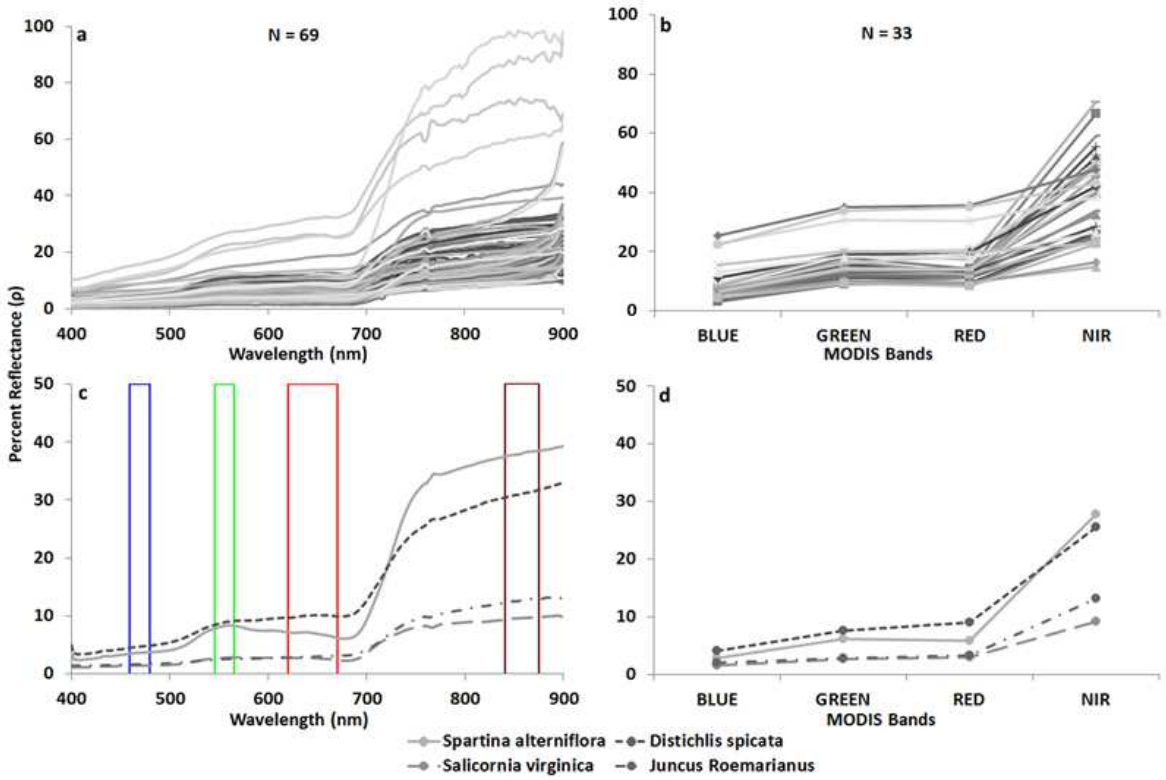

Figure 3.4. a. Reflectance (%) spectra of 69 sub–plots covering multiple species acquired using Ocean Optics sensor.; b. Reflectance (%) spectra derived from MODIS 8–day 500m surface reflectance images for 33 pixels containing the study plots from 2010–2011. c. Sample spectra for individual species as acquired by the *in situ* sensor with highlighted MODIS bandwidths. Differences in the species level spectral response pattern were mainly due to the variability in canopy structure and chlorophyll content; d. Sample spectra acquired using Ocean Optics sensor for individual species averaged to MODIS bandwidths. Differences in species specific spectral response were clearly visible similar to the *in situ* reflectance profile.

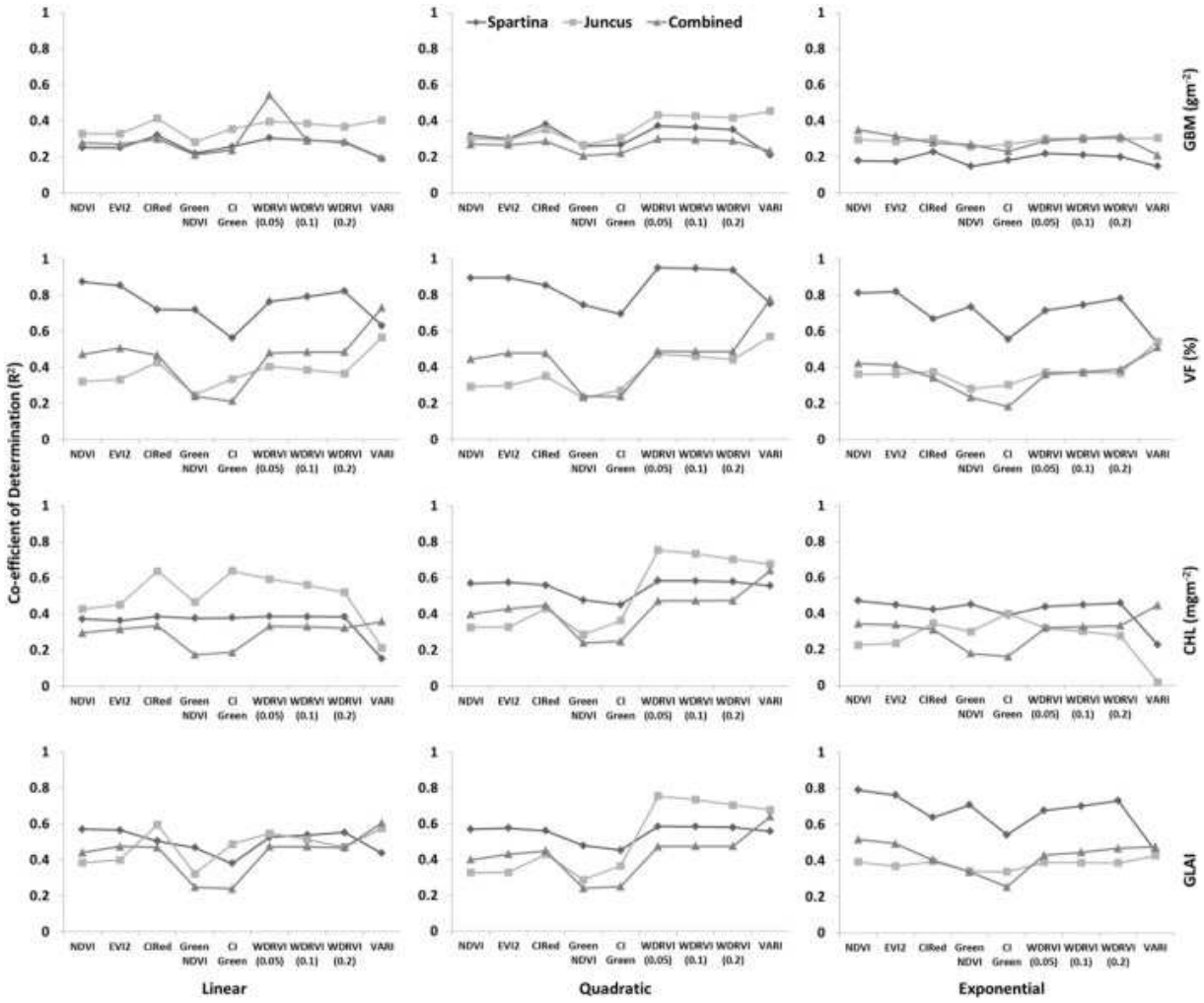

Figure 3.5. Coefficient of determination values of species specific and species invariant linear, quadratic, and exponential relationships between VIs and (a, e, i): GBM, (b, f, j): VF, (c, g, k): CHL and (d, h, i): GLAI, respectively developed from *in situ* sensor derived VIs.

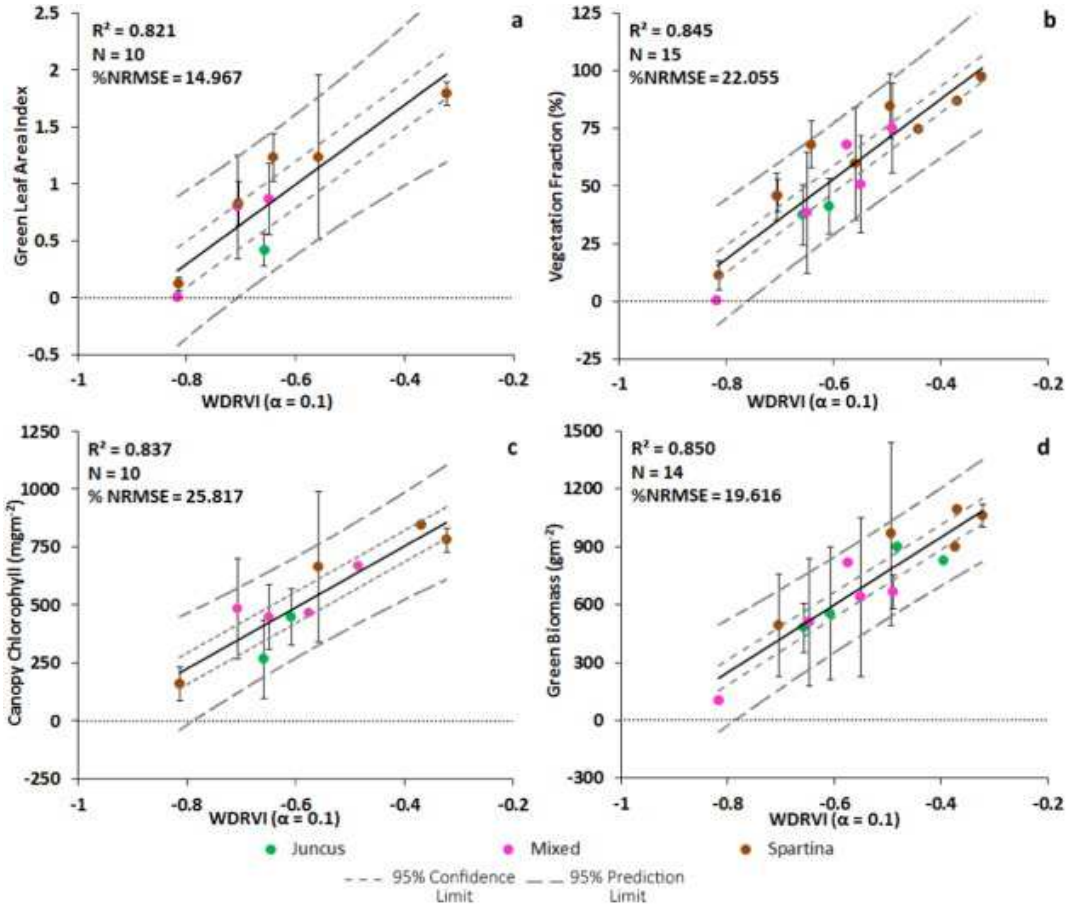

Figure 3.6. Calibration of MODIS (250m) derived WDRVI with a: GLAI, b: VF, c: CHL and d: GBM, with co–efficient of determination and 95% confidence intervals and limits. Error bars represent standard deviations. Coefficient of Determination (R), Sample size (N) and Percent Normalized Root Mean Square Error (%NRMSE) for respective models are also shown. Points with no error bars represent highly homogenous pixels with single study plots.

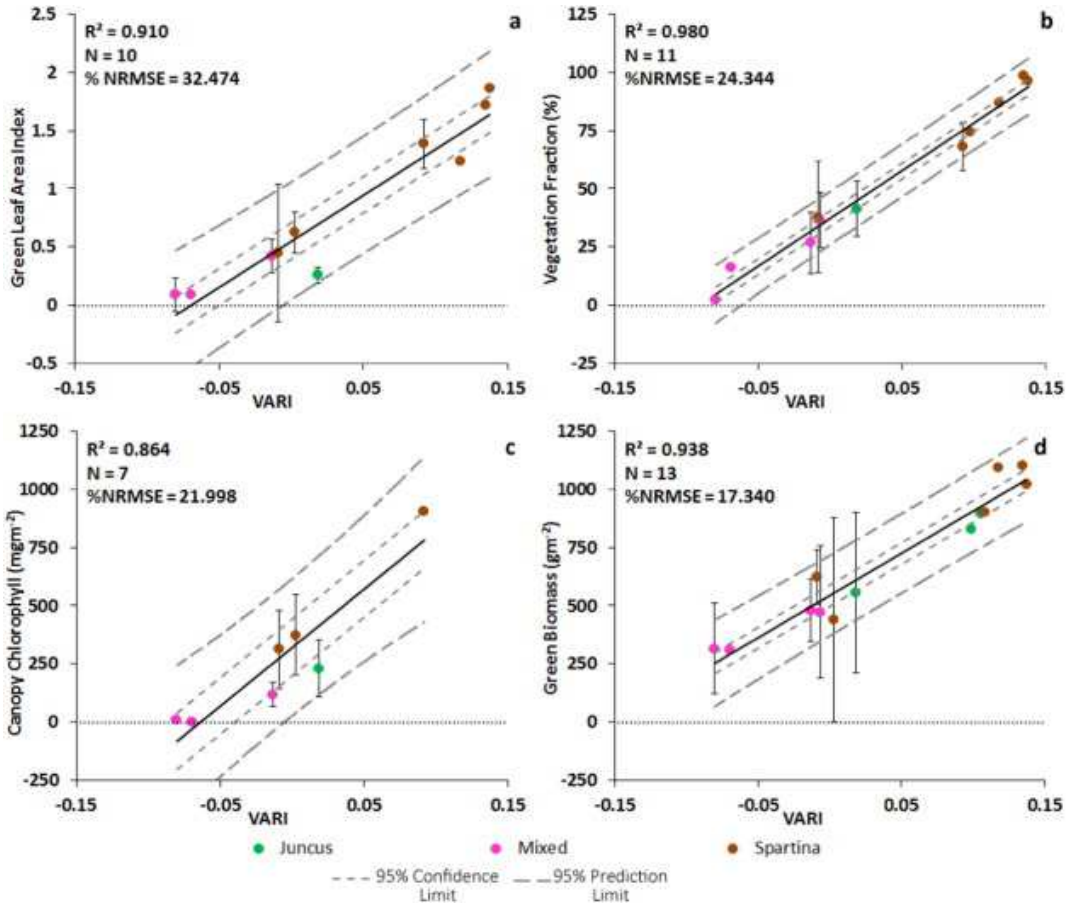

Figure 3.7. Calibration of MODIS (500m) derived VARI with a: GLAI, b: VF, c: CHL and d: GBM, with co–efficient of determination and 95% confidence intervals and limits. Error bars represent standard deviations. Coefficient of Determination (R), Sample size (N) and Percent Normalized Root Mean Square Error (%NRMSE) for respective models are also shown. Points with no error bars represent highly homogenous pixels with single study plots.

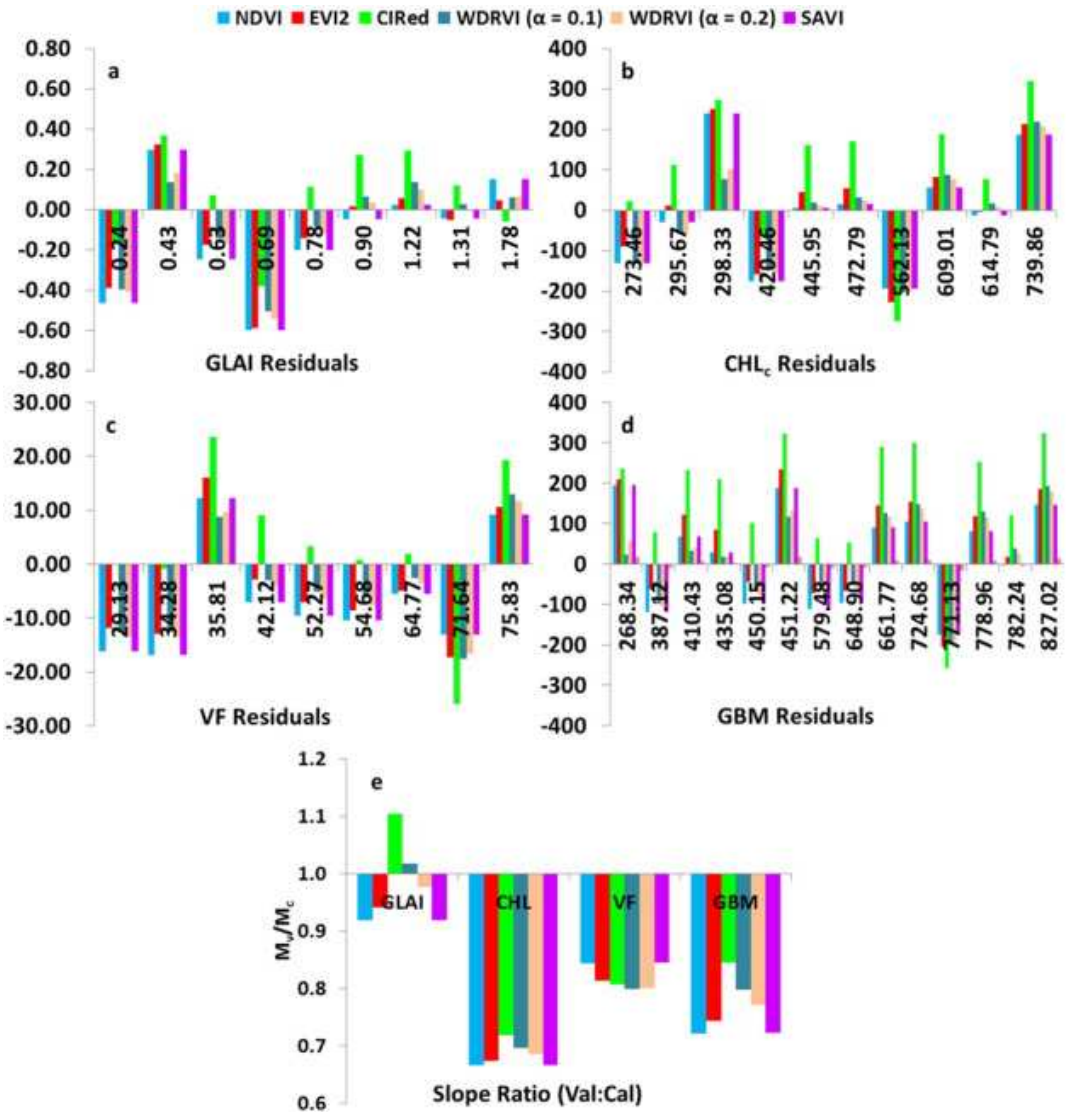

Figure 3.8. Residual plots for MODIS (250m) based biophysical models for a: GLAI, b: CHL, c: VF and d: GBM. WDRVI (α = 0.1) was chosen as the best–fit model. e: Slope ratio between linear trends of validation and calibration data. Models with minimum bias have ratios close to 1.

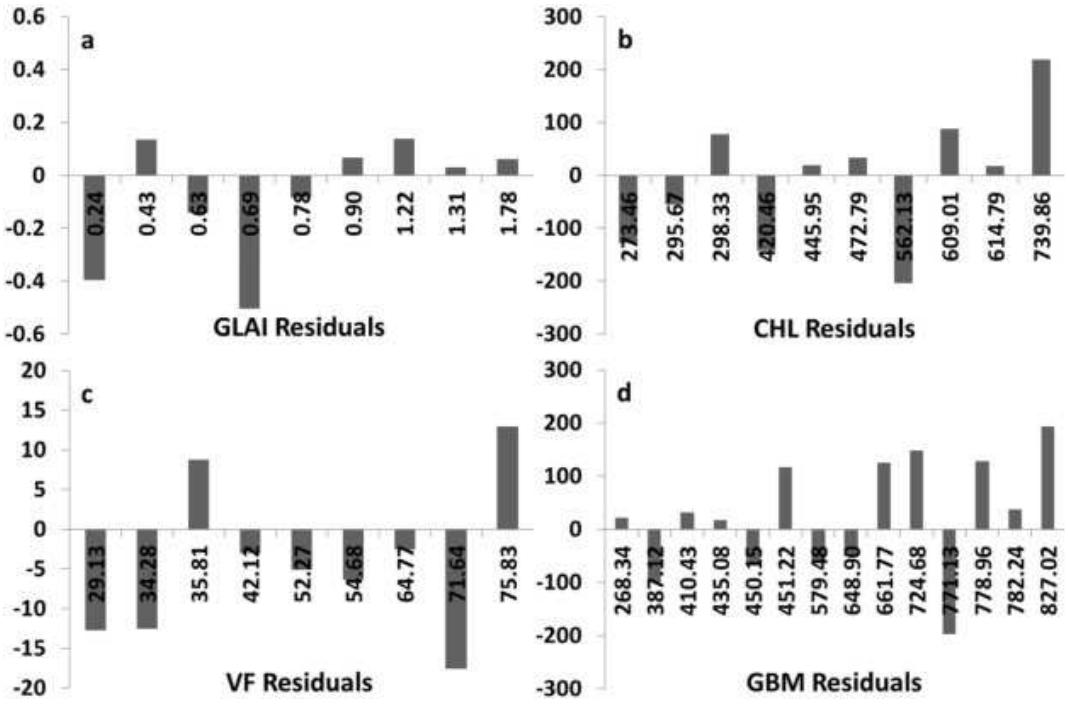

Figure 3.9. Residual plots for MODIS (500m) based best fit biophysical models (using VARI) for a: GLAI, b: CHL, c: VF and d: GBM.

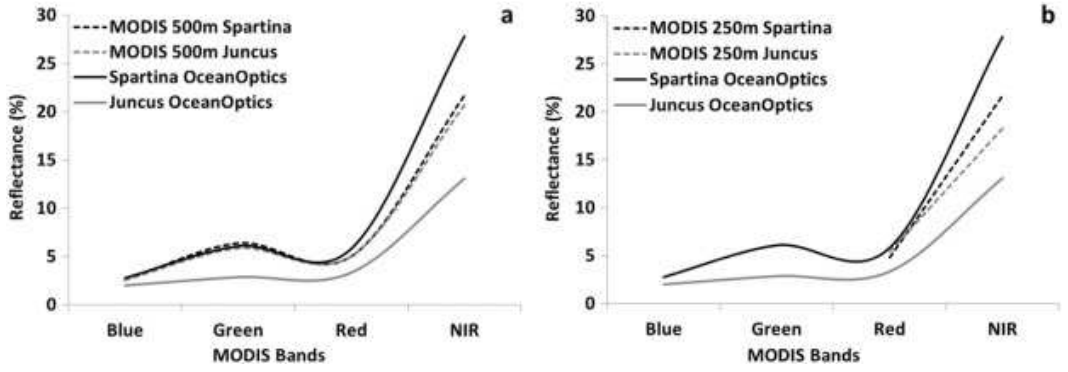

Figure 3.10. Comparison between reflectance (%) between Ocean Optics and MODIS derived spectral response for *Spartina* and *Juncus* from a: 250m and b: 500m spatial resolution. The plots show how species information is lost with progressive decrease in spatial resolution. MODIS 250m dataset does not have blue and green bands; as such spectral information for those bands are missing in Figure 10a.

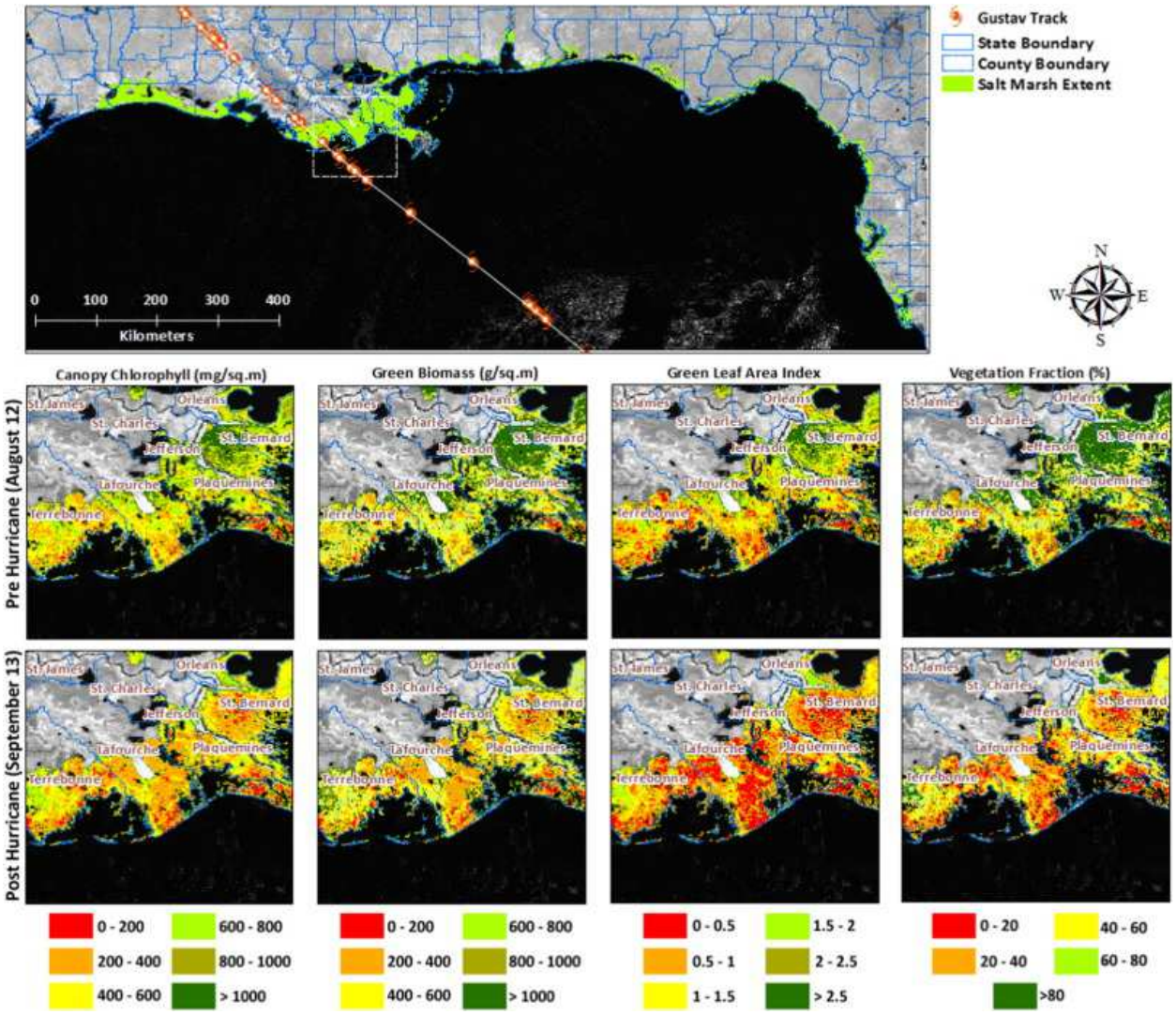

Figure 3.11. Sample composites (top image) showing spatial distribution of biophysical characteristics (in this case GBM) for four Gulf States using MODIS 250-m data. Expanded maps showing the magnitude and distribution of CHL, GBM, GLAI, and VF pre-and post-Hurricane Gustav.

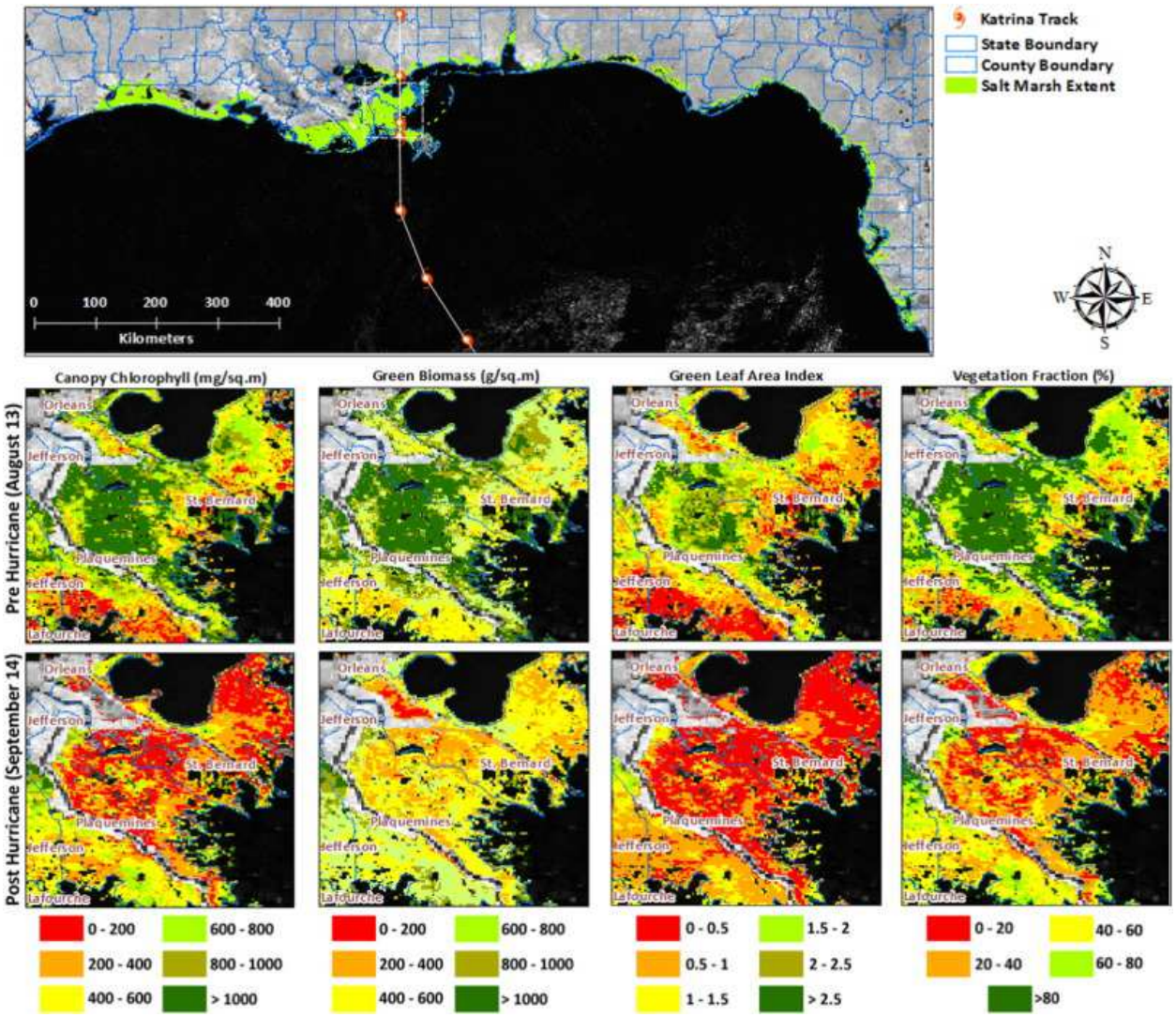

Figure 3.12. Sample composites (top image) showing spatial distribution of biophysical characteristics (in this case GBM) for four Gulf States using MODIS 500-m data. Expanded maps showing the magnitude and distribution of CHL, GBM, GLAI, and VF pre-and post-Hurricane Katrina.

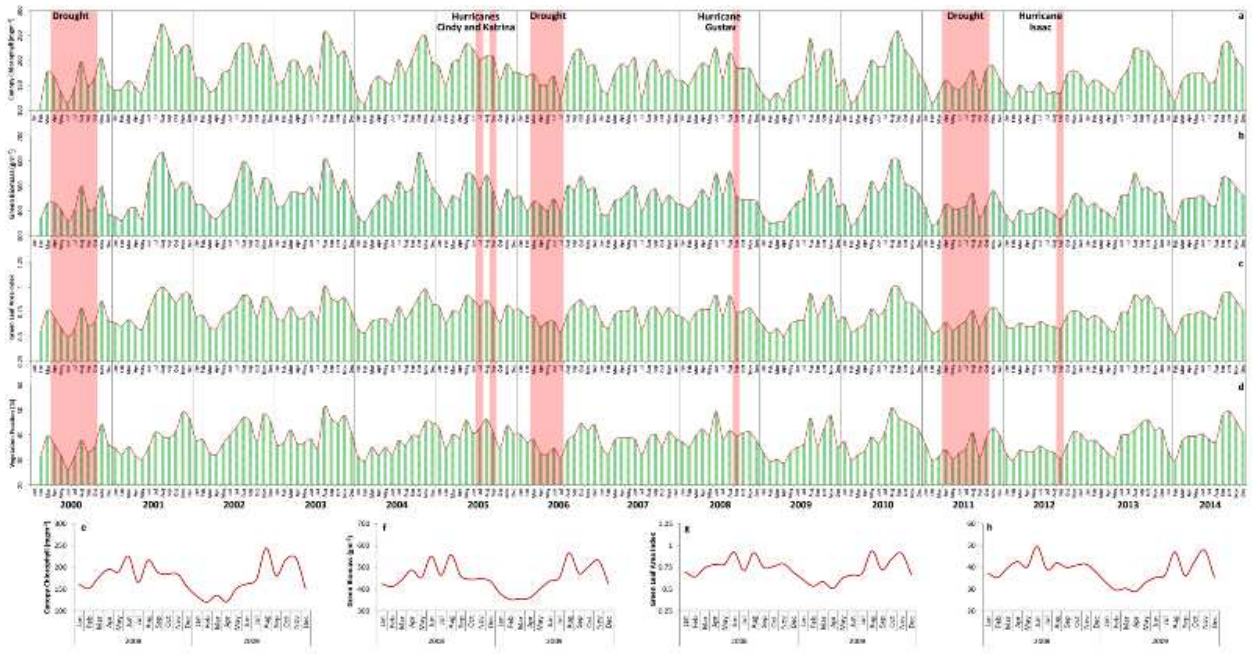

Figure 3.13. Phenological variations in a: CHL, b: GBM, c: GLAI, d: VF in tidal wetlands of Terrebonne Parish, LA, from 2000–2010 (250m MODIS data). The effects of Hurricanes Cindy, Katrina, Gustav, and Isaac and periodic Droughts have been highlighted. Comparisons between the levels of e: CHL, f: GBM, g: GLAI and h: VF in the growing seasons of 2008 and 2009 has been shown as specific example.

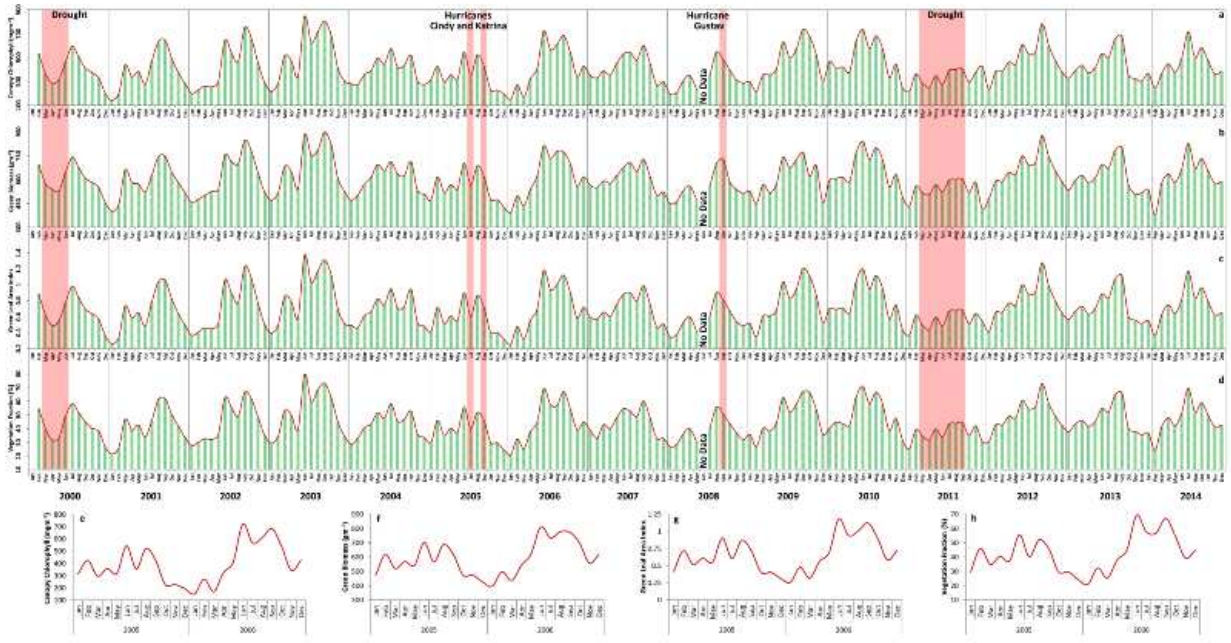

Figure 3.14. Phenological variations in a: CHL, b: GBM, c: GLAI, d: VF in tidal wetlands of Plaquemines Parish, LA, from 2000–2010 (500m MODIS data). The effects of Hurricanes Cindy and Katrina, and Gustav, and periodic Droughts have been highlighted. Comparisons between the levels of e: CHL, f: GBM, g: GLAI and h: VF in the growing seasons of 2005 and 2006 has been shown as specific example.

CHAPTER 4

ANALYZING THE LONG-TERM PHENOLOGICAL TRENDS OF SALT MARSH ECOSYSTEM ACROSS COASTAL LOUISIANA

Ghosh, S. and Mishra, D. R. Analyzing the long-term phenological trends of salt marsh ecosystem across coastal Louisiana, submitted to *Remote Sensing* for review

ABSTRACT

In this study, we examined the phenology of salt marsh ecosystem across coastal Louisiana (LA) for a sixteen-year time-period (2000-2015) using NASA's Moderate Resolution Imaging Spectroradiometer's (MODIS) 8-day average surface reflectance images (500m). We compared the performances of least squares fitted asymmetric Gaussian (AG) and double logistic (DL) smoothing functions in terms of increasing signal to noise ratio from the raw phenology derived from the time-series composites. We performed derivative analysis to determine the appropriate start of season (SOS) and end of season (EOS) thresholds. After that, we extracted seasonality parameters in TIMESAT, and studied the effect of environmental disturbances/anomalies on the seasonality parameters. Finally, we performed trend analysis using the derived seasonality parameters such as base Green Biomass (GBM) value, maximum GBM value, seasonal amplitude, and small seasonal integral. Based on root mean square error (RMSE) values and residual plots, we selected the best thresholds for SOS (5% of amplitude) and EOS (20% of amplitude), along with the best smoothing function. The selected SOS and EOS thresholds were able to capture the environmental disturbances that have affected the salt marsh ecosystem during the sixteen-year time-period. Our trend analysis results indicate positive trends in the base GBM values in salt marshes of LA. However, we did not notice as much positive trend in the maximum GBM levels. Hence, we observed mostly negative changes in the GBM amplitude and small seasonal integral, which indicate overall progressive decline in the rates of photosynthesis and biomass allocation in the LA salt marsh ecosystem; most likely due to elevated atmospheric carbon dioxide levels and sea level rise. The results illustrate both the relative efficiency of MODIS based biophysical models in analyzing salt marsh phenology and performances of the

smoothing techniques in terms of improving signal to noise ratio of the MODIS derived phenology.

Keywords: Salt Marsh; Phenology; MODIS; Louisiana; TIMESAT

Introduction

The global average atmospheric CO_2 concentration currently at 405 parts per million (ppm) has risen significantly almost by 45% since the pre-industrial revolution level of 280 ppm (NOAA ESRL, https://www.esrl.noaa.gov/gmd/ccgg/trends/). Such increasing levels of CO_2 will have wide-ranging consequences on ecosystem structure, function, and services; many natural systems have already started showing signs of being affected (Parmesan and Yohe, 2003; Menzel et al. 2006; Post et al. 2009). Conservation and restoration of natural ecosystems, especially those with high carbon sequestration capacity is crucial, in order to offset the rising levels of atmospheric carbon (Canadell and Raupach, 2008). Salt marshes are well recognized carbon sinks, and conservation of such a natural ecosystem is critical in maintaining carbon balance in the environment (Connor et al. 2001; Chmura et al. 2003). However, response of salt marshes to global fluctuations of atmospheric CO_2 may differ from the responses of terrestrial or aquatic ecosystems (Mayor and Hicks, 2009). Studies have demonstrated the differential response of salt marsh plant species to the increasing levels of CO_2, with C_3 plants (e.g. *Phragmites*) being more productive than C_4 plants (e.g. *Spartina*), an effect that has been found to be enhanced by sea-level rise as well (Erickson et al. 2007; White et al. 2012). This reduced productivity of C_4 plants puts them at an adaptive disadvantage, where they might be out-competed by C_3 species (Polley et al. 2007), causing massive shifts in biogeochemistry and ecosystem functioning. Continuous monitoring of phenology of salt marsh ecosystem for detection and analysis of any such trends is of utmost priority for successful implementation of conservation and restoration measures, both at the site-specific or at the landscape level (Ghosh et al. 2016).

One way to study and understand the productive health of any vegetation ecosystem is through analyzing the long–term spatio–temporal trends in phenology, with relation to their environment

(White et al. 1997). Phenological measurements such as the timing of budburst and flowering are now widely used to detect and study the effect of climate variability on vegetation health both at the site–specific or broader landscape scale (Kramer et al. 2000; Beaubien and Freeland, 2000; Primack et al. 2004). Further, phenology has been shown to be an effective indicator of forest and crop management practices (Keatinge et al. 1998; Hartkamp et al. 2002), urban heat islands (Roetzer et al. 2000; Zhang et al. 2004), the El–Nino Southern Oscillation (Keeling et al. 1996; Asner et al. 2000; Vicente-Serrano et al. 2006), and even the impact of allergies on human health (Van Vliet et al. 2002). Moreover, accurate monitoring of vegetation phenology is crucial for development of global surface energy and water flux models (Arora, 2002) and global carbon cycle (Running and Nemani, 1991; Wilson and Baldocchi, 2000). Therefore, phenological properties or seasonality parameters, such as the timing of the start and end of season, rate of green–up and brown–down, amplitude, and maximum growth level have become emerging indicators of global environmental changes (Kunkel et al. 2004; Scheifinger et al. 2002).

Satellite derived biophysical properties have been frequently utilized to understand vegetation phenology, the onset of leaf greenness in the spring and the onset of leaf coloring in the autumn (Soudani et al. 2008; Zhang and Goldberg, 2011). Remote sensing-based phenology began with the AVHRR (Reed et al. 1994) and has been significantly improved with the MODIS onboard Terra and Aqua satellites (Zhang et al. 2003). Both AVHRR and MODIS are operational right now, but MODIS provides images at a finer spatial resolution (250 m to 1 km vs. 1 km), spectral resolution (36 spectral bands vs. 6), and geolocation accuracy (Wolfe et al. 2002). Studies have utilized MODIS images for monitoring ecosystem phenology at both site-specific and landscape scales (Ahl et al. 2006; Fisher and Mustard, 2007; Zhang et al. 2006; de Beurs and Henebry, 2005; White et al. 1997).

Developing algorithms to automatically retrieve land surface phenology metrics from satellite data has been a popular research topic (de Beurs and Henebry, 2010; White et al. 2009; Walker et al. 2012). However, the nature of satellite data makes it difficult to extract phenological metrics from it directly (de Beurs and Henebry 2005; Verbesselt et al. 2010). Satellite derived time-series data inevitably contain disturbances caused by cloud presence (Gutman, 1991), atmospheric variability (Huete and Liu, 1994), and aerosol scattering (Xiao et al. 2003), that degrades the data quality and hinders analysis. Therefore, satellite derived time-series data are commonly quality-screened and/or smoothed to minimize noise and compensate for the absence of data before phenological metrics can be estimated (Atkinson et al. 2012). Several methods based on interpolation of time-series data have been proposed to remove such noise and to reconstruct high-quality time-series product (Viovy et al. 1992; Jonsson and Eklundh, 2002; Chen et al. 2005; Moody et al. 2005; Sellers et al. 1994; Roerink et al. 2000). The MATLAB based program TIMESAT (http://web.nateko.lu.se/timesat/timesat.asp) allows the user to test different smoothing techniques, along with various statistical filters for increasing signal to noise ratio and generating noise-free phenology that can be further utilized for generating seasonality parameters (Jonsson and Eklundh, 2002; 2004). such as derivative analysis of the smoothed time series, matching phenology dates derived from in-situ observations such as PhenoCam, or using known SOS/EOS thresholds on the smoothed time series (particularly for smoothed NDVI phenology) (Zhang et al. 2003; Heumann et al. 2007).

Phenology has been studied in details in a variety of different terrestrial such as tropical rainforests, deciduous habitats, grasslands, and aquatic ecosystems such as phytoplankton (Asner and Alencar, 2010; Hufkens et al. 2012; Shen et al. 2011; Palmer et al. 2015). However, very few studies have emphasized the need to analyze long-term phenology of salt marsh habitats

(Ghosh et al. 2016; Mishra and Ghosh, 2015; Mishra et al. 2015). In this study, we attempt to analyze long-term trends in the phenology and seasonality parameters of the salt marshes in LA using existing MODIS derived biophysical parameters , and analyze the broader implications of the trends observed. We first describe and test methods for deriving noise-free phenology and seasonality parameters for salt marshes in LA. After that, we try to validate our methods through analyzing the annual variations. Finally, we analyze the long-term change trends in the seasonality parameters using statistical trend analysis techniques.

Study Area

LA has the maximum acreage of salt marsh ecosystem (>6500 sq. km) in US (National Wetlands Inventory; http://www.fws.gov/wetlands/) (Figure 4.1). The ecosystem is mostly dominated by smooth cord-grass (*Spartina alterniflora*), and salt meadow cord-grass (*Spartina patens*). Apart from that, patchy distributions of American Glasswort (*Salicornia virginica*), saltwort (*Batis maritima*), and seashore saltgrass (*Distichlis spicata*) are also encountered. The distribution of black needle rush (*Juncus roemarianus*) is limited along the brackish regions. High salinity and anoxic soil does not allow growth or survival of nonspecialized plant species; floral diversity, hence, is remarkably low (Weis, 2010). The climate of the region is tropical to sub-tropical, characterized by hot and humid summers, with occasional tropical storms and moderately cold winters. The salt marshes stretch across four state climatic divisions, viz. southwest, southcentral, southeast and eastcentral. The majority of the salt marsh ecosystem falls within the southeast (~4000 km^2) and the southwest (~2000 km^2) climatic zones. Average annual temperature in this region varies between 15 and 25 ° Celsius, while annual precipitation ranges from 80 to 100 cm (National Weather Service, http://www.weather.gov/). Since 2000, the salt marsh ecosystem in LA have experienced the landfall of major hurricanes, such as Lili (2002, Category 1), Katrina

and Rita (2005, Category 4 and 3 respectively), Gustav (2008, Category 2), and Isaac (2012, Category 1) (National Hurricane Centre, http://www.nhc.noaa.gov/). The marsh ecosystem in LA are also home to more than 160,000 oil and gas wells (Lyles et al. 2005), that accounts for almost 18% of oil and 24% of natural gas production in the U.S., valued at $6.3 billion, and $10.3 billion respectively (Tiner, 2013). Hence, these ecosystems have been subjected to intense dredging and channelization for transportation as well as significant groundwater removal, which has led to soil and marsh erosion and localized subsidence. Further, the sediment flow from the Mississippi River, which typically provides nutrients and substrate for salt marshes, has been extensively trapped through excessive construction of levees across the LA coast. Therefore, it is increasingly difficult for the salt marshes to sustain themselves and fight against sea level rise. Disturbed salt marsh ecosystem in the region has been invaded by common reed (*Phragmites australis*) at certain places (Tiner, 2013).

Over the past decade, there have been an increasing number of reports of salt marsh "dieback" in the U.S. In 2000 and 2007, LA experienced a sudden and acute dieback event (termed "brown marsh") that affected over 100,000 ha of *Spartina alterniflora* dominated salt marsh throughout the Mississippi River deltaic plain (Bertness et al. 2009; Lindstedt and Swenson, 2006). In addition, although the long-term impact is still unknown, the Deepwater Horizon oil spill in 2010 had a severe short-term impact on the health of several fringe and interior salt marsh patches of LA, characterized by loss of chlorophyll, biomass, and subsequently a reduction in photosynthetic capacity (Mishra and Ghosh, 2015; Biber et al. 2012; Mishra et al. 2012).

Materials and Methods

a. *Time-series composites*

The MODIS Land Science Team provides several data products derived from MODIS observations to the public, including the 8-day composite Land Surface Reflectance (MOD09A1). The MOD09A1 datasets include seven spectral bands at a spatial resolution of 500m corrected for the effects of atmospheric gases, aerosols, and thin cirrus clouds (Vermote et al. 2011). We generated time-series composites for green biomass (GBM) for the salt marshes of LA, for a sixteen year period (2000 – 2015) using MODIS 8–day surface reflectance data (500m). We generated subsets of LA salt marshes using the most recent vector boundaries obtained from NWI database (https://www.fws.gov/wetlands/). We generated GBM composites using the relationship between GBM and Visible Atmospheric Resistant Index (VARI) (Gitelson et al. 2002) described in Ghosh et al. (2016) as follows:

$$GBM\ (grams\ per\ square\ meter) = 3617.104 * VARI + 543.3514 \quad (1)$$

The GBM biophysical model was developed using MODIS surface reflectance and in-situ estimates of GBM from 200 study plots across the northern Gulf of Mexico. The model produced an r^2 of 0.93 and an inherent percent normalized root mean square error of 17.34% in GBM estimation. Ghosh et al. (2016) had demonstrated the superior performance of VARI for mapping salt marsh GBM using the MODIS 500m images compared to the NIR based indices such as NDVI. The poor performance of the traditional NIR based indices was attributed to the severe interference of NIR wavelengths to the background moisture and tidal signals; whereas, the sensitivity of visible bands was argued to be less susceptible to background water signals. While generating GBM composites, we utilized MODIS quality assurance bands to retain only the best

quality pixels in the time-series composites (Vermote et al. 2011; Ghosh et al. 2016). This enabled us to assign equal weight to all the salt marsh pixels for extraction of phenology, rather than assigning weights based on quality pixels in TIMESAT. However, tidal correction was not performed, as it is not possible to determine the level of daily MODIS scene contribution to the 8-day surface reflectance imagery, which would otherwise, had helped correcting for tidal signals using daily tidal fluctuation data (Ghosh et al. 2016).

Since the MODIS surface reflectance products have a temporal resolution of 8 days, 46 GBM composites were generated per year for LA salt marshes; thus, for the sixteen year study period, 736 composites were generated in total. We analyzed the salt marshes of southeast and southwest climatic zone separately in order to avoid any discrepancy due to climate variability. We created subsets of salt marsh GBM composites for individual climatic zones, using the LA climate zone boundaries obtained from the NCDC archives (https://www.ncdc.noaa.gov/). Once subsets were generated for salt marshes for individual climatic zones, we converted the raw GBM composites to 16 bit signed generic binary format for running TIMESAT (http://web.natleko.lu.se/timesat/timesat.asp). We also compiled temperature, precipitation and PDSI (Palmer, 1965) data for the individual climatic zones from the NCDC archives, to investigate any significant temperature, precipitation and PDSI anomalies during the sixteen year period that might potentially contribute to salt marsh phenological trends.

b. TIMESAT

Although the pixels for time-series analysis were carefully screened using the MODIS quality assurance data, the raw time-series as derived from the GBM composites still showed presence of residual noise, possibly generated from short-term localized environmental disturbances, or

tides. However, since the GBM composites were generated using a visible band index (VARI), the tidal effect can be assumed to be minimal. We used the MATLAB based program TIMESAT to generate pixel-wise noise-free time-series of GBM. A number of methods have been developed to reduce noise prior to time-series such as Fourier Series (Andres et al. 1994; Olsson and Eklundh, 1994), Best Index Slope Extraction (Viovy et al. 1992), Logistic curve (Paruelo and Lauenroth, 1998), and Savitzky–Golay filtering (Chen et al. 2004; Jonsson and Eklundh, 2004). TIMESAT provides options to fit smooth continuous curve to raw time-series data using AG, DL and/or SG filters. In these methods local model functions are fitted to data in intervals around maxima and minima in the time-series (Jonsson and Eklundh, 2002, 2004).

For AG smoothing function, the basis function becomes:

$$g(t; x_1, x_2, \ldots, x_5) = \begin{cases} exp\left[-\left(\frac{t-x_1}{x_2}\right)^{x_3}\right], & if\ t > x_1 \\ exp\left[-\left(\frac{x_1-t}{x_4}\right)^{x_5}\right], & if\ t < x_1 \end{cases} \quad (1)$$

For this function x_1 defines the position of the maximum or minimum with respect to the independent time variable t; x_2 and x_3 determine the width and kurtosis of the right function half; while, x_4 and x_5 determines the same of the left function half.

The basis function for DL smoothing function is as follows:

$$g(t; x_1, \ldots, x_4) = \frac{1}{1+exp\left(\frac{x_1-t}{x_2}\right)} - \frac{1}{1+exp\left(\frac{x_3-t}{x_4}\right)} \quad (2)$$

where x_1 and x_3 defines the position of the left and right inflection point respectively, while x_2 and x_4 gives the rate of change at x_1 and x_3 respectively. Also for this function the parameters are restricted in range to ensure a smooth shape (Eklundh and Jonsson, 2012).

The AG and the DL filters have been found to produce similar results, with the AG filter being less sensitive to incomplete baseline time-series data (Gao et al. 2008). We tested both filters for generating noise-free time-series and then extracting seasonality parameters. The SG filter was not considered to be ideal for deriving smooth time-series as it is too much susceptible to localized noise in the raw phenology generated from the time-series images and hence might provide erroneous estimates of seasonality parameters (Tan et al. 2011). We used the STL method to remove spikes and outliers in the time-series. The STL method removes outliers by assigning weights to the values in time-series based on STL decomposition. This method does not depend on ancillary data, and is global in nature (Cleveland et al. 1990). Further, we also eliminated any negative or zero values observed in the raw phenology from our analysis. We specified an adaptive upper envelope assuming any noise to be negatively biased (Jonsson and Eklundh, 2002, 2004). We specified and adaptation strength of 2, as stronger adaptation strength is likely to put too much emphasis on single high data values leading to erroneous estimates of seasonality parameters (Jonsson and Eklundh, 2002, 2004).

c. *Start and End of Season determination*

TIMESAT allows the user to specify SOS and EOS dates as a user defined fraction of the seasonal amplitude. We derived SOS and EOS using different thresholds (fractions of seasonal amplitude), such as 5%, 10%, 15% and 20%. We tested thresholds below five percent, as it might be influenced by the noise from the non-growing season (Heumann et al. 2007). Phenology studies using TIMESAT have mostly preferred to use thresholds above 10% (usually 20%; sometimes 50%) for deriving SOS and EOS dates, using NIR wavelength based vegetation index time-series; most of these thresholds are usually determined based on expert opinions or on-field observations of SOS and EOS (Suepa et al. 2016; Zeng et al. 2011; Delbart et al. 2005).

However, phenology of salt marsh ecosystem have neither been studied in detail, nor did we have any on-field monitoring stations observing real-time SOS and EOS, based on which, appropriate thresholds of SOS and EOS could be chosen or validated for TIMESAT. Temperature variations at the start and end of the growing season may be used to determine SOS and EOS; however, plant phenology and seasonality parameters are not only influenced by temperature, but also by other environmental variables or local environmental disturbances and dynamics. Further, NDVI time-series or thresholds could not be utilized for deriving SOS and EOS, as NDVI or any NIR based indices are prone to insensitivity in salt marsh settings (Ghosh et al. 2016). GBM was derived from MODIS 500m 8-day surface reflectance composites for LA marshes using the VARI (VARI; Gitelson et al. 2002), which had been shown to be more sensitive than NIR based indices, especially for salt marshes with perpetually saturated soil (Ghosh et al. 2016). Therefore, we tested the performances of different thresholds by matching the SOS, and EOS dates derived using derivative analysis (Tan et al. 2011; discussed in the following analysis section) against dates derived using different thresholds in TIMESAT.

Analysis

a. Determination of start and end of season dates using derivative analysis

Unfortunately, there is no specific universal threshold, that can be applied to estimate SOS and EOS dates; and calibration is necessary before selection of any specific threshold. We investigated the derivatives of smoothed GBM time-series data, derived using both AG and DL methods from ~400 random pixels. We estimated the third order derivative from the smoothed time-series and derived local maxima and minima (Tan et al. 2011). The third order derivative has been demonstrated by Tan et al. as better indicator for identifying SOS and EOS than the

second order, as the latter represents the timing when the majority of vegetation within a pixel is turning green, rather than the timing when the change of green-up rate or brown-down rate is the greatest. For SOS and EOS, we matched the local maxima and local minima respectively, with the SOS and EOS dates derived using different thresholds in TIMESAT. We did this using smoothed time-series of both AG and DL method. We did not analyze derivatives for POS date estimations, as POS is a function of the maximum value encountered in the middle of the growing season; and it does not depend on the thresholds chosen for SOS and EOS. Once we matched SOS and EOS dates derived from derivative analysis against TIMESAT thresholds, we estimated the error between the observations using root mean square error (RMSE), and also analyzed residual plots for any specific trends. We selected TIMESAT SOS and EOS thresholds that illustrated the greatest agreement with the dates derived from derivative analysis. After that, we derived seasonality parameters using the best thresholds and the best smoothing technique in TIMESAT.

b. Seasonality Analysis

We extracted seasonality parameters (Table 4.1) for all the pixels covering salt marshes of LA, for the entire sixteen year period. Once extracted, they were analyzed for seasonal fluctuations. Seasonality parameters of salt marshes of different climate zones of LA were analyzed separately. In this study, we present the seasonal fluctuations in SOS and EOS for salt marshes in southeast and southwest LA, as these climatic zones contain the majority of the salt marsh extents in LA. Possible reasons behind the seasonal fluctuations were investigated, through careful study of environmental events such as temperature and precipitation anomalies, landfall of tropical storms, man-made hazards or other climatic hazards such as drought causing possible

localized dieback that might trigger an early end to a growing season, or a subsequent late/early start of growing season.

c. Trend Analysis

We extracted seasonality parameters, such as base value, max value, amplitude and small seasonal integral that are major indicators of seasonal photosynthesis and biomass production and accumulation, for all the salt marsh pixels covering coastal LA for sixteen year period. At first, we examined the overall trend in these seasonality parameters using simple linear regression. We examined the slope of the fitted trendline to determine any overall positive and negative trends over the sixteen year time period based on the positive or negative value of the slope magnitude. After that, in order to highlight the spatial distribution of the marsh pixels showing improvement (positive change) and stress/degradation (negative change), we employed the MK trend test (Kendall, 1970) to determine the phenological changes of salt marshes of southeast and southwest LA from 2000 – 2015, using R (R Core Team, http://www.R-project.org/). We calculated the MK trend test separately for every pixel for base value, amplitude, max value, and small seasonal integral composites for the southeast and southwest LA salt marshes. These parameters are crucial indicators of seasonal productivity. We classified changes based on the z-score distribution at 95% confidence interval. A positive or negative value of z represents an upward or downward trend, respectively. Changes beyond the lower critical limit ($z < -1.96$) were classified as strong negative change, while beyond higher critical limit ($z > 1.96$) were classified as strong positive change. Changes within the 95% confidence interval were classified as weak (negative or positive depending on negative or positive values of z).

Results and Discussion

a. Derivative Analysis

Results from the derivative analysis showed similar trends for both AG and DL methods of smoothing. This was not unexpected, since previous studies have shown similar behaviors of these two methods (Gao et al. 2008). For SOS (Figure 4.2a), the 5% threshold seemed to agree the most with the derivative analysis for both AG and DL smoothing functions, with the lowest RMSE. Higher thresholds showed greater RMSE. The SOS dates derived using AG method agreed marginally better with the derivative derived dates than the DL method; the AG method showing an error of ~25 days for the 5% threshold and ~28 days for the DL method. The residual plots for SOS showed no specific trends for the 5% threshold (Figure 4.3a). Higher thresholds predicted late SOS dates when compared to the derivative derived dates. For EOS, the 20% threshold showed the highest agreement with the derivative derived EOS dates (Figure 4.2b); with errors progressively increasing with lower thresholds. The residual plots also demonstrated late EOS predictions with progressive decreasing thresholds compared to the derivative derived EOS dates (Figure 4.3b). The AG method again agreed more closely with the derivative derived dates than the DL method in estimation of EOS. For the best threshold (20%), AG method showed an error of ~29 days, while the same for DL method was ~40 days. Although asymmetric thresholds may not be uncommon for AG or DL distribution (both smoothing function demonstrates skewness), seasonality parameters are usually derived using symmetric thresholds. However, as mentioned before, we did not have any in-situ observations of SOS and EOS to validate the dates derived using asymmetric thresholds in TIMESAT. Therefore, the only way to validate our thresholds for SOS and EOS was through analyzing the inter-annual variations of SOS and EOS, and investigating whether the major deviations from the normal

trends in SOS and EOS observed can be explained by occurrences of environmental disturbances/anomalies that might have influenced those deviations. The following section on seasonality analysis attempts to justify the validity of the thresholds used for SOS and EOS, through analyzing SOS and EOS variations in the sixteen year time period.

b. Seasonality Analysis

The median SOS date for salt marshes of southeast and south west Louisiana as derived from TIMESAT was ~60 Julian Days (Figs. 4.4a and 4.5a), which corresponds with the onset of spring at the end of February and beginning of March. However, in the years 2000, 2010 and 2013, the salt marshes of southeast LA displayed late SOS. The year 2000 had witnessed acute recurring dieback event that affected almost 100,000 ha of marshes in LA (Lindstetd and Swenson, 2006; Alber et al. 2008). This dieback might have been resulted from the extremely dry conditions for two consecutive years 1999 and 2000 (NCDC, https://www.ncdc.noaa.gov/). The acute dieback event had most likely delayed the normal SOS in 2000. The delayed start to the 2010 growing season was most likely due to late onset of spring owing to colder than normal temperatures at the beginning of the season (NCDC, https://www.ncdc.noaa.gov/); a phenomenon observed in the salt marshes of southwest LA as well.

Finally, a delayed SOS in 2013 might be attributed to the after-effects of Deepwater Horizon Oil-spill (2010) and Hurricane Isaac (2012). The residual oil and the clean-up efforts had negative effects in on the marsh patches in the southeast LA, and the restoration efforts may have been affected by the landfall of tropical storm Bonnie in 2010, which brought additional oil into the shoreline marsh. The short-term degradation due to oil-spill, clean-up efforts and stress induced by tropical storm Bonnie, delayed the peak growth of the marsh patches in the area in 2011

(Mishra and Ghosh, 2015). In spite of this, the marshes had started recovery from the oil-spill effects in 2011 (Khanna et al. 2013). However, recovery of the marsh patches, were further damaged by the landfall of Hurricane Isaac in 2012, during the peak of the growing season. Although Hurricane Isaac was a Category-1 hurricane, the timing of the landfall had an adverse effect, as the salt marshes were unable to achieve full recovery from the stress induced by the oil-spill. That could be the reason why we notice another delayed dormancy onset in 2013. Our observations are consistent with those made by Khanna et al. (2017). Any residual oil effects in 2011 or 2012 might have been much localized, as the marshes had started to recover or had already recovered from the oil-spill effects. Those localized effects were not severe enough to be manifested in the MODIS data. Further, the biomass model has a 17% error, so a minor localized disturbance producing localized effect in biomass level maybe below the error threshold and was not picked up by the model.

Salt marsh growing season in LA normally ends around mid-November (Figs. 4.4b and 4.5b), something that was observed in both southeast and southwest LA, with median EOS date being ~322 Julian days. However, salt marshes in both these regions experienced early end to the growing season in 2005 and 2008. In southeast LA, Hurricane Katrina had made landfall in September as a major Category 3 Hurricane, which had destroyed most of the salt marsh ecosystem (Costanza et al. 2006) that were unable to recover in the same year. Similar drastic EOS was observed in the year 2008, when Hurricane Gustav made landfall; however, the effects of the landfall were not as severe as Katrina. In southwest LA, landfalls and subsequent damages caused by Hurricane Rita (2005) and Hurricane Ike (2008) were the main reasons for early EOS in the respective years. These results provide justification to the SOS and EOS thresholds chosen for derivation of seasonality parameters, as they have been able to capture the environmental

events that have affected the SOS and EOS of salt marsh ecosystem during the sixteen year time period.

c. Trend Analysis

Simple linear trends in GBM base values, GBM max values, seasonal GBM amplitude and small GBM integral are shown in Figure 6. Overall, during the sixteen year study period, GBM base values showed positive trends during the sixteen year time period (Figure 4.6a), GBM max values remained stable, while the rest of the seasonality parameters showed negative trends (Figure 4.6b-d). The positive trend observed in the base GBM values is an indicator of the cumulative storage of carbon over time as aboveground biomass. However, max GBM values remained almost stable during the sixteen year time period; hence, negative changes were observed in seasonal amplitude and seasonal integral indicating long-term stress induced in the salt marsh vegetation, resulting in reduced photosynthesis and aboveground biomass accumulation. We observed severe short-term effects of the periodic dieback events occurring in the salt marsh habits in the years 2000, 2006and 2011, and landfalls of major hurricanes in 2005 (Katrina and Rita), 2008 (Gustav and Ike) and 2012 (Isaac), that affected the seasonal photosynthetic activity of the salt marsh habitats; which is evident in the relative lower magnitudes of seasonal amplitude, for those time-periods. However, we also observed the recovery of the marsh habitats from the stress induced by dieback events and hurricane landfalls, when the environmental conditions became normal and conducive for salt marsh vegetation growth.

Trend classes for the change in base values, max values, seasonal amplitude and small seasonal integral (refer to Table 4.1 for description and phenological significance) for southeast LA salt

marshes are shown in Figure 4.7. We observed positive changes in the GBM base values in almost 75.5% area of the salt marsh extent in southeast LA; with strong positive changes observed in 31.6% of the area. However, the max values did not show as much positive change; we observed strong positive changes in only 7.2% of the total salt marsh extent. On the other hand, we observed mostly negative changes in the seasonal amplitude and small seasonal integral, two parameters that are indicators of net seasonal photosynthesis rate and biomass production. 70.3% of the salt marsh ecosystem showed negative changes in seasonal amplitude (12.1% area showing strong negative change) while 67.9% showed negative changes in small seasonal integral (10.9% area showing strong negative change). Overall, the areas of positive changes in base value and negative changes in the seasonal amplitude and small seasonal integral matched well (Fig. 4.8).

Most of the salt marsh ecosystem showed a progressive increase in the base GBM value indicating that considerable amount of carbon has been accumulated overtime and stored as aboveground biomass in the salt marsh ecosystem. Interestingly, the maximum GBM value did not show as much progressive increase as the base GBM value; thus explaining the strong negative changes in seasonal amplitude and small seasonal integral. This indicates progressive decline in the levels of photosynthesis over the sixteen year time period. Normally, changes in the levels of photosynthesis are attributed to changes in the levels of temperature and precipitation, as they influence the photoperiod and salinity of the ecosystem (Song et al. 2013; Riddin and Adams, 2010). However, neither the temperature nor the precipitation anomalies for either southeast or southwest LA show any particular trend during the sixteen year time period (Figure 4.9). The salt marsh ecosystem of these regions have experience periodic diebacks,

however, salt marshes being resilient ecosystem, are capable of recovering from short term environmental stress if environmental conditions become normal again (Mishra et al. 2012).

Atmospheric CO_2 levels rose from 369ppm – 404ppm during the period 2000 – 2015, while sea-levels have been observed to rise at a rate of 9 – 12mm/year in coastal LA (NOAA Tides and Currents, https://www.tidesandcurrents.noaa.gov/sltrends/sltrends.html). Elevated CO_2 levels in the atmosphere have been known to induce photosynthetic saturation in C_4 plants; the saturation generally initiates at carbon dioxide concentrations beyond 350ppm (Taiz and Zeiger, 1991). In salt marsh habitats, elevated atmospheric CO_2 levels have been observed to reduce both above and below-ground biomass allocation in C_4 plant species (White et al. 2012, Erickson et al. 2007), as a result of reduction in stomatal conductance (Leakey et al. 2009), as well as rate of water usage (Ainsworth and Long, 2005; White et al. 2012, Erickson et al. 2007) ultimately reducing the rate of photosynthesis. . White et al. (2012) observed greater reduction in aboveground biomass allocation of C_4 plants than C_3 plants in response to elevated CO_2 and sea-level rise in a salt marsh habitat, even with altered nutrient levels in the environment. The salt marsh ecosystem in Louisiana is mostly dominated by the smooth cord-grass *(Spartina alterniflora*) and salt meadow cord–grass (*Spartina patens*), both of which C_4 species. Therefore, in light of observed rise in CO_2 levels and sea-level rise, this observed reduction in the level of net photosynthesis and biomass allocation in salt marshes of LA is not entirely unexpected. Although we haven't done any field experiments to test this, there are many studies, over the past decade, which have confirmed the phenomena using observed datasets.

If the progressive decline in the rates of photosynthesis and biomass allocation continues, the carbon sequestration rate of the LA salt marsh ecosystem might not be able to keep up with the rate of rising atmospheric CO_2; rather, with periodic disturbances such as hurricanes, dieback

and anthropogenic disasters, marsh loss will turn the ecosystem to carbon sources (DeLaune and White, 2012). On the other hand, such elevated levels of atmospheric CO_2 and sea levels will stimulate photosynthesis, water usage capacity and more efficient biomass allocation in C_3 plants compared to C_4 (White et al. 2012, Erickson et al. 2007). This might explain the invasion of *Phragmites australis* in the coastal salt marsh landscape of LA (Howard et al. 2008). *Phragmites* has a variable photosynthetic pathway, capable of exhibiting both C_3 and C_4 photosynthesis (Antonielli et al. 2002). Under elevated levels of CO_2, the C_3 pathway will probably become dominant in *Phragmites*, and this would allow the plant to dominate the coastal salt marsh ecosystem, especially if the ecosystem experiences nitrogen enrichment through run-off (Bertness et al. 2002). If *Phragmites* displaces *Spartina* as the dominant species in the coastal marsh landscape, there might be far-reaching ecological consequences such as changes in plant species abundance (Chambers et al. 2003) and trophic interactions (Minchinton and Bertness, 2003; Silliman and Bertness, 2004), herbivore population crashes (Pennings and Silliman, 2005) or changes in soil biogeochemistry (Windham and Ehrenfield, 2003). In this research, we don't claim that such a phenomenon is already underway as it is beyond the scope of this study, but supporting evidence from our analysis suggests that there is a risk of such a cascading effect in future.

Conclusion

The study provides a comprehensive analysis of the phenological trends of the salt marsh ecosystem of LA, showcasing the efficiency of the MODIS based biophysical model derived time-series composites of salt marsh GBM. We used TIMESAT to generate noise-free phenology from the GBM time–series composites after determining the SOS and EOS thresholds using derivative analysis. We justified our selection of the best smoothing algorithm (AG) and

SOS/EOS thresholds after matching the SOS and EOS dates derived using derivative analysis and TIMESAT thresholds. We analyzed the seasonality in the SOS and EOS dates over the sixteen year time period; the effects of the environmental events influencing the deviations from the normal SOS and EOS have been efficiently captured. Finally, the trend analysis demonstrated the reduction in the rates of seasonal amplitude and small seasonal integral, and improvement in the levels of GBM base value, indicating the progressive reduction in the levels of photosynthesis and biomass allocation in the salt marsh ecosystem, that might be attributed as a combination of environmental effects such as rising atmospheric CO_2 levels and sea–level rise.

Further, the trend analysis results have been able to capture areas that are demonstrating significant stress in terms of reduced photosynthetic activity and require immediate restoration and conservation efforts. The results of this study can be compared with GPP trends as observed from the MODIS 500m and 1-km GPP products; however, MODIS GPP products for coastal wetlands are derived using very generic grassland light use efficiency (LUE) estimates from Biome properties look-up table that do not incorporate tidal effects or other coastal marsh specific conditions. Therefore, conclusions from GPP trend matching should be derived exercising caution. Although trend analysis using MODIS derived images can provide a valuable insight into the phenological dynamics at the landscape level, site-specific trend analysis might require similar analysis using site specific records of sea–level changes, nitrogen enrichment and salinity, along with finer resolution images. In addition, with finer resolution images it will be possible to determine the distribution dynamics of the invasive *Phragmites australis* in an otherwise *Spartina* dominated landscape, and compare the progressive phenological trends of the two species, with respect to elevated CO_2 levels and sea–level rise. Such a future study will provide a clearer picture regarding possible ecological succession of *Spartina* by *Phragmites*.

In addition, due to coarse nature of the MODIS sensor, the possibility of encountering mixed pixels cannot be ruled out; but this problem persists even with fine resolution sensors. However, the advantages of the fine temporal resolution of MODIS (daily images combined to generate the 8 day surface reflectance product), as compared to other fine spatial resolution satellites cannot be ruled out, especially for analysis of long-term phenological trends. Finer spatial resolution satellites often present the problem of cloud cover that may render images completely unusable for analysis, resulting in frequent data gaps. This problem is particularly evident in coastal Gulf of Mexico, where cloud presence in images from fine resolution sensors especially during the peak growing season often hinders analysis. Further, their spatial coverage/swaths are much less than MODIS; hence combining scenes from multiple days may create biases in the analysis itself. Hence, for analysis at such broader landscape scale, MODIS is clearly a robust sensor.

This is for the first time that such a comprehensive analysis of the phenology of LA salt marsh ecosystem has been studied in terms of the seasonality parameters. Using the suggested methods in this study, monitoring of salt marsh ecosystem in LA, southeast US and elsewhere in the world with similar environmental settings will be possible, following necessary re–parameterization of the GBM model. Through continuous monitoring of the ecosystem, it will be possible to ascertain whether salt marshes will continue to be a major carbon sink in the environment, or changes in the environment will force them to become a net carbon source. As mentioned before, salt marshes are dynamic and critical ecosystems in terms of carbon sequestration. Therefore, continuous monitoring of these critical ecosystems is crucial for effective restoration and management practices and formulation of global change policies.

Acknowledgments

We would like to thank and acknowledge our project partners at Mississippi State University, University of Nebraska–Lincoln, and University of New Orleans. This research was partially funded by the National Aeronautics and Space Administration (NASA) Gulf of Mexico program (Grant # NNX10AE65G), National Science Foundation (NSF) Division of Environmental Biology (Grant # 1050500), and Gulf of Mexico Research Initiative (GoMRI) (Grant # GRI-0012). Shuvankar Ghosh is grateful to the University of Georgia Graduate School Dean's Award for Social Science for carrying out this research.

References

Ahl, D. E., Gower, S. T., Burrows, S. N., Shabanov, N. V., Myneni, R. B., and Knyazikhin, Y. 2006. Monitoring spring canopy phenology of a deciduous broadleaf forest using MODIS. *Remote Sensing of Environment*, 104, 88-95.

Ainsworth, E. A., and Long, S. P. 2005. What have we learned from 15 years of free-air CO2 enrichment (FACE)? A meta-analytic review of the responses of photosynthesis, canopy properties and plant production to rising CO_2. *New Phytologist*, 165, 351-372.

Andres, L., Salas, W. A., and Skole, D. 1994. Fourier analysis of multi-temporal AVHRR data applied to a land cover classification. *Remote Sensing*, 15, 1115-1121.

Antonielli, M., Pasqualini, S., Batini, P., Ederli, L., Massacci, A., and Loreto, F. 2002. Physiological and anatomical characterization of *Phragmites australis* leaves. *Aquatic Botany*, 72, 55-66.

Arora, V. K. 2002. The use of the aridity index to assess climate change effect on annual runoff. *Journal of Hydrology*, 265, 164–177.

Asner, G. P., and Alencar, A. 2010. Drought impacts on the Amazon forest, the remote sensing perspective. *New Phytologist*, 187, 569–578.

Asner, G. P., Townsend, A. R., and Braswell, B. H. 2000. Satellite observation of El Nino effects on Amazon forest phenology and productivity. Geophysical Research Letters, 27, 981–984.

Atkinson, P. M., Jeganathan, C., Dash, J., and Atzberger, C. 2012. Inter–comparison of four models for smoothing satellite sensor time–series data to estimate vegetation phenology. *Remote Sensing of Environment*, 123, 400–417.

Beaubien, E. G., and Freeland, H. J. 2000. Spring phenology trends in Alberta, Canada, links to ocean temperature. *International Journal of Biometeorology*, 44, 53–59.

Bertness, M. D., Ewanchuk, P. J., and Silliman, B. R. 2002. Anthropogenic modification of New England salt marsh landscapes. *Proceedings of the National Academy of Sciences*, 99, 1395–1398.

Bertness, M. D., Silliman, B. R., and Holdredge, C. 2009. Shoreline development and the future of New England salt marsh landscapes. In: Silliman, B. R., Grosholz, E. D. and Bertness, M. D. (Eds.), *Human Impacts on Salt Marshes, A global perspective*, pp. 137–148, University of California Press, Berkeley, California, USA.

Biber, P. D., Wu, W., Peterson, M. S., Liu, Z., and Pham, L. 2012. Oil contamination in Mississippi salt marsh habitats and the impacts to *Spartina alterniflora* photosynthesis. In: Alford, J. B., Peterson, M. S., and Green, C. G. (Eds.), *Impacts of oil spill disasters on marine habitats and fisheries in North America*, pp. 133 – 172, CRC Press, Boca Raton, Florida, USA.

Canadell, J. G., and Raupach, M. R. 2008. Managing forests for climate change mitigation. *Science*, 320, 1456–1457.

Chambers, R. M., Osgood, D. T., Bart, D. J., and Montalto, F. 2003. Phragmites australis invasion and expansion in tidal wetlands, interactions among salinity, sulfide, and hydrology. *Estuaries and Coasts*, 26, 398–406.

Chen, X., Hu, B., and Yu, R. 2005. Spatial and temporal variation of phenological growing season and climate change impacts in temperate eastern China. *Global Change Biology*, 11, 1118–1130.

Chmura, G. L., Anisfeld, S. C., Cahoon, D. R., and Lynch, J. C. 2003. Global carbon sequestration in tidal, saline wetland soils. *Global Biogeochemical Cycles,* 17, DOI: 10.1029/2002GB001917

Cleveland, R. B., Cleveland, W. S., and Terpenning, I. 1990. STL, A seasonal–trend decomposition procedure based on loess. *Journal of Official Statistics,* 6, 3.

Connor, R. F., Chmura, G. L., and Beecher, C. B. 2001. Carbon accumulation in Bay of Fundy salt marshes, Implications for restoration of reclaimed marshes. *Global Biogeochemical Cycles,* 15, 943–954.

Costanza, R., Mitsch, W. J., and Day, J. W. 2006. A new vision for New Orleans and the Mississippi delta, applying ecological economics and ecological engineering. *Frontiers in Ecology and the Environment,* 4, 465-472.

De Beurs, K. M., and Henebry, G. M. 2005. A statistical framework for the analysis of long image time series. *International Journal of Remote Sensing*, 26, 1551–1573.

DeLaune, R. D., and White, J. R. 2012. Will coastal wetlands continue to sequester carbon in response to an increase in global sea level?, a case study of the rapidly subsiding Mississippi river deltaic plain. *Climatic Change,* 110, 297–314.

Delbart, N., Kergoat, L., Le Toan, T., Lhermitte, J., and Picard, G. 2005. Determination of phenological dates in boreal regions using normalized difference water index. *Remote Sensing of Environment*, 97, 26–38.

Eklundh, L., and Jönsson, P. 2012. TIMESAT 3.2 with parallel processing–Software Manual. Lund University.

Erickson, J. E., Megonigal, J. P., Peresta, G., and Drake, B. G. 2007. Salinity and sea level mediate elevated CO_2 effects on C_3–C_4 plant interactions and tissue nitrogen in a Chesapeake Bay tidal wetland. *Global Change Biology*, 13, 202–215.

Fisher, J. I., and Mustard, J. F. 2007. Cross–scalar satellite phenology from ground, Landsat, and MODIS data. *Remote Sensing of Environment*, 109, 261–273.

Gao, F., Morisette, J. T., Wolfe, R. E., Ederer, G., Pedelty, J., Masuoka, E., Myneni. R., Tan. B. and Nightingale, J. 2008. An algorithm to produce temporally and spatially continuous MODIS–LAI time series. *IEEE Geoscience and Remote Sensing Letters*, 5, 60–64.

Ghosh, S., Mishra, D. R., and Gitelson, A. A. 2016. Long–term monitoring of biophysical characteristics of tidal wetlands in the northern Gulf of Mexico – A methodological approach using MODIS. *Remote Sensing of Environment*, 173, 39–58.

Gitelson, A. A., Stark, R., Grits, U., Rundquist, D., Kaufman, Y., and Derry, D. 2002. Vegetation and soil lines in visible spectral space, a concept and technique for remote estimation of vegetation fraction. *International Journal of Remote Sensing*, 23, 2537–2562.

Gutman, G. G. 1991. Vegetation indices from AVHRR, An update and future prospects. *Remote Sensing of Environment*, 35, 121–136.

Hartkamp, A. D., Hoogenboom, G., and White, J. W. 2002. Adaptation of the CROPGRO growth model to velvet bean (Mucuna pruriens), II. Cultivar evaluation and model development. *Field Crops Research*, 78, 9–25.

Heumann, B. W., Seaquist, J. W., Eklundh, L., and Jönsson, P. 2007. AVHRR derived phenological change in the Sahel and Soudan, Africa, 1982–2005. *Remote Sensing of Environment*, 108, 385–392.

Howard, R. J., Travis, S. E., and Sikes, B. A. 2008. Rapid growth of a Eurasian haplotype of Phragmites australis in a restored brackish marsh in Louisiana, USA. *Biological Invasions*, 10, 369–379.

Huete, A. R., and Liu, H. Q. 1994. An error and sensitivity analysis of the atmospheric–and soil–correcting variants of the NDVI for the MODIS–EOS. *IEEE Transactions on Geoscience and Remote Sensing*, 32, 897–905.

Hufkens, K., Friedl, M., Sonnentag, O., Braswell, B. H., Milliman, T., and Richardson, A. D. 2012. Linking near–surface and satellite remote sensing measurements of deciduous broadleaf forest phenology. *Remote Sensing of Environment*, 117, 307–321.

TIMESAT [Software], Lund University, http,//web.nateko.lu.se/timesat/timesat.asp

Jonsson, P., and Eklundh, L. 2002. Seasonality extraction by function fitting to time–series of satellite sensor data. *IEEE transactions on Geoscience and Remote Sensing*, 40, 1824–1832.

Jonsson, P., and Eklundh, L. 2004. TIMESAT—a program for analyzing time–series of satellite sensor data. *Computers and Geosciences*, 30, 833–845.

Keatinge, J. D. H., Qi, A., Wheeler, T. R., Ellis, R. H., and Summerfield, R. J. 1998. Effects of temperature and photoperiod on phenology as a guide to the selection of annual legume cover and green manure crops for hillside farming systems. *Field Crops Research*, 57, 139–152.

Keeling, C. D., Chin, F. J. S. and Whorf, T. P. 1996. Increased activity of northern vegetation inferred from atmospheric CO_2 measurements. *Nature*, 382, 146–149.

Kendall, M.G. (Ed.) 1970. Rank Correlation Methods, 4th ed., Griffin, London, UK.

Khanna, S., Santos, M. J., Koltunov, A., Shapiro, K. D., Lay, M., and Ustin, S. L. 2017. Marsh Loss due to cumulative impacts of Hurricane Isaac and the Deepwater Horizon Oil Spill in Louisiana. *Remote Sensing*, 9, 169.

Khanna, S., Santos, M. J., Ustin, D. S. L., Koltunov, A., Kokaly, R. F., and Roberts, D. A. 2013. Detection of salt marsh vegetation stress after the Deepwater Horizon BP oil spill along the shoreline of Gulf of Mexico using AVIRIS data. *PloS ONE*, 8, e78989

Kramer, K., Leinonen, I., and Loustau, D. 2000. The importance of phenology for the evaluation of impact of climate change on growth of boreal, temperate and Mediterranean forests ecosystems, an overview. *International Journal of Biometeorology*, 44, 67–75.

Kunkel, K. E., Easterling, D. R., Hubbard, K., and Redmond, K. 2004. Temporal variations in frost-free season in the United States, 1895–2000. *Geophysical Research Letters*, 31, DOI: 10.1029/2003GL018624

Leakey, A. D. 2009. Rising atmospheric carbon dioxide concentration and the future of C4 crops for food and fuel. *Proceedings of the Royal Society of London B, Biological Sciences*, 276, 2333–2343.

Lyles, L. D., Namwamba, F., and Campus, B. R. 2005. Louisiana coastal zone erosion, 100+ years of land use and land loss using GIS and remote sensing. *5th Annual ESRI Education User Conference*, San Diego, California, 23–26.

Mayor, J. R., and Hicks, C. E. 2009. Potential impacts of elevated CO_2 on plant interactions, sustained growth, and carbon cycling in salt marsh ecosystems. In: Silliman, B. R., Grosholz, E. D. and Bertness, M. D. (Eds.), *Human Impacts on Salt Marshes: A global perspective*, pp. 207–230. University of California Press, Berkeley, California, USA.

Menzel, A., Sparks, T. H., Estrella, N., Koch, E., Aasa, A., Ahas, R., Alm–Kubler, K., Bissolli, P., Braslavska, O., Briede, A., Chmielewski, F. M., Crepinsek, Z., Curnel, Y., Dahl, A., Defila, C., Donnelly, A., Filella, Y., Jatczak, K., Mage, F., Mestre, A., Nordli, O., Penuelas, J., Pirinen, P., Remisova, V., Scheifinger, H., Striz, M., Susnik, A., Van Vliet, A. J. H., Wielgolaski, F. E., Zach, S. and Chmielewski, F. M. 2006. European phenological response to climate change matches the warming pattern. *Global Change Biology*, 12, 1969–1976.

Minchinton, T. E., and Bertness, M. D. 2003. Disturbance-mediated competition and the spread of *Phragmites australis* in a coastal marsh. *Ecological Applications*, 13, 1400–1416.

Mishra, D. R. and Ghosh, S. 2015. Using moderate resolution satellite sensors for monitoring the biophysical parameters and phenology of tidal wetlands. In: Tiner, R., Land, M. and Klemas, V. (Eds.) *Remote Sensing of Wetlands, Applications and Advances*, pp. 283 – 314, CRC Press, Boca Raton, Florida, USA.

Mishra, D. R., Cho, H. J., Ghosh, S., Fox, A., Downs, C., Merani, P. B. T., Kirui, P., Jackson, N., and Mishra, S. 2012. Post–spill state of the marsh, Remote estimation of the ecological impact of the Gulf of Mexico oil spill on Louisiana Salt Marshes. *Remote Sensing of Environment*, 118, 176–185.

Mishra, D. R., Ghosh, S., Hladik, C., O'Connell, J. L., and Cho, H. J. 2015. Wetland mapping methods and techniques using multi–sensor, multi–resolution remote sensing, Successes and

Challenges. In: Thenkabail, P. S. (Ed.) *Remote Sensing Handbook*, Vol. III, pp. 191 – 227, CRC Press, Boca Raton, Florida, USA.

Moody, E. G., King, M. D., Platnick, S., Schaaf, C. B., and Gao, F. 2005. Spatially complete global spectral surface albedos, Value–added datasets derived from Terra MODIS land products. *IEEE Transactions on Geoscience and Remote Sensing*, 43, 144–158.

NOAA Earth System Research Laboratory, Global Monitoring Division, *Trends in Atmospheric Carbon Dioxide*, retrieved December 25, 2016, https,//www.esrl.noaa.gov/gmd/ccgg/trends/graph.html

NOAA Center for Operational Oceanographic Products and Services, NOAA Tides and Currents, *Sea Level Trends*, Retrieved on January 21, 2017, https,//tidesandcurrents.noaa.gov/sltrends/sltrends.html

NOAA National Centers for Environmental information, Climate at a Glance, U.S. Time Series, published December 2016, retrieved on December 1, 2016, http,//www.ncdc.noaa.gov/cag/

NOAA National Hurricane Centre, NHC Data Archive, retrieved on June 2016, http,//www.nhc.noaa.gov/data/

NOAA National Weather Service, retrieved on September 21, http,//www.weather.gov/

Olsson, L., and Eklundh, L. 1994. Fourier series for analysis of temporal sequences of satellite sensor imagery. *International Journal of Remote Sensing*, 15, 3735–3741.

Palmer, S. C., Odermatt, D., Hunter, P. D., Brockmann, C., Presing, M., Balzter, H., and Tóth, V. R. 2015. Satellite remote sensing of phytoplankton phenology in Lake Balaton using 10years of MERIS observations. *Remote Sensing of Environment*, 158, 441–452.

Palmer, W. C. 1965. Meteorological drought. U. S. Dept. of Commerce, Weather Bureau Research Paper No. 45, Washington, DC, USA.

Parmesan, C. and Yohe, G. 2003. A globally coherent fingerprint of climate change impacts across natural systems. Nature, 421, 37–42.

Paruelo, J. M., and Lauenroth, W. K. 1998. Interannual variability of NDVI and its relationship to climate for North American shrublands and grasslands. Journal of Biogeography 25, 721–733.

Pennings, S. C., and Silliman, B. R. 2005. Linking biogeography and community ecology, latitudinal variation in plant–herbivore interaction strength. *Ecology*, 86, 2310–2319.

Polley, H. W., Dugas, W. A., Mielnick, P. C., and Johnson, H. B. 2007. C_3–C_4 composition and prior carbon dioxide treatment regulate the response of grassland carbon and water fluxes to carbon dioxide. *Functional Ecology*, 21, 11–18.

Post, E., Forchhammer, M. C., Bret–Harte, M. S., Callaghan, T. V., Christensen, T. R., Elberling, B., Fox, A. D., Gilg, O., Hik, D. S., Høye, T. T. and Ims, R. A. 2009. Ecological dynamics across the Arctic associated with recent climate change. *Science*, 325, 1355–1358.

Primack, D., Imbres, C., Primack, R. B., Miller–Rushing, A. J., and Del Tredici, P. 2004. Herbarium specimens demonstrate earlier flowering times in response to warming in Boston. *American Journal of Botany*, 91, 1260–1264.

R Core Team 2013. R, A language and environment for statistical computing. R Foundation for Statistical Computing, Vienna, Austria. ISBN 3-900051-07-0, http,//www.R-project.org/

Reed, B. C., Brown, J. F., VanderZee, D., Loveland, T. R., Merchant, J. W., and Ohlen, D. O. 1994. Measuring phenological variability from satellite imagery. *Journal of Vegetation Science*, 5, 703–714.

Riddin, T., and Adams, J. B. 2010. The effect of a storm surge event on the macrophytes of a temporarily open/closed estuary, South Africa. *Estuarine, Coastal and Shelf Science*, 89, 119–123.

Roerink, G. J., Menenti, M., and Verhoef, W. 2000. Reconstructing cloudfree NDVI composites using Fourier analysis of time series. *International Journal of Remote Sensing*, 21, 1911–1917.

Roetzer, T., Wittenzeller, M., Haeckel, H., and Nekovar, J. 2000. Phenology in central Europe–differences and trends of spring phenophases in urban and rural areas. *International Journal of Biometeorology*, 44, 60–66.

Running, S. W., and Nemani, R. R. 1991. Regional hydrologic and carbon balance responses of forests resulting from potential climate change. *Climatic Change*, 19, 349–368.

Scheifinger, H., Menzel, A., Koch, E., Peter, C., and Ahas, R. 2002. Atmospheric mechanisms governing the spatial and temporal variability of phenological phases in central Europe. *International Journal of Climatology*, 22, 1739–1755.

Sellers, P. J., Tucker, C. J., Collatz, G. J., Los, S. O., Justice, C. O., Dazlich, D. A., and Randall, D. A. 1994. A global 1° by 1° NDVI data set for climate studies, Part II. The generation of global fields of terrestrial biophysical parameters from the NDVI. *International Journal of Remote Sensing*, 15, 3519 – 3545.

Shen, M., Tang, Y., Chen, J., Zhu, X., and Zheng, Y. 2011. Influences of temperature and precipitation before the growing season on spring phenology in grasslands of the central and eastern Qinghai–Tibetan Plateau. *Agricultural and Forest Meteorology*, 151, 1711–1722.

Silliman, B. R., and Bertness, M. D. 2004. Shoreline development drives invasion of *Phragmites australis* and the loss of plant diversity on New England salt marshes. *Conservation Biology*, 18, 1424–1434.

Song, Q., Zhang, G., and Zhu, X. G. 2013. Optimal crop canopy architecture to maximize canopy photosynthetic CO_2 uptake under elevated CO_2 – a theoretical study using a mechanistic model of canopy photosynthesis. *Functional Plant Biology*, 40, 108–124.

Soudani, K., Le Maire, G., Dufrêne, E., François, C., Delpierre, N., Ulrich, E., and Cecchini, S. 2008. Evaluation of the onset of green–up in temperate deciduous broadleaf forests derived from Moderate Resolution Imaging Spectroradiometer (MODIS) data. *Remote Sensing of Environment*, 112, 2643–2655.

Suepa, T., Qi, J., Lawawirojwong, S., and Messina, J. P. 2016. Understanding spatio–temporal variation of vegetation phenology and rainfall seasonality in the monsoon Southeast Asia. *Environmental Research*, 147, 621–629.

Tan, B., Morisette, J. T., Wolfe, R. E., Gao, F., Ederer, G. A., Nightingale, J., and Pedelty, J. A. 2011. An enhanced TIMESAT algorithm for estimating vegetation phenology metrics from MODIS data. *IEEE Journal of Selected Topics in Applied Earth Observations and Remote Sensing*, 4, 361–371.

Taiz, L., and Zeiger, E. (Eds.) 1991. Plant physiology, Sinauer Associates Inc., Sunderland, MA, USA

US Fish and Wildlife Service, National Wetlands Inventory, Retrieved on December 1, 2016 https,//www.fws.gov/wetlands/Data/Data-Download.html

Van Vliet, A. J., Overeem, A., De Groot, R. S., Jacobs, A. F., and Spieksma, F. 2002. The influence of temperature and climate change on the timing of pollen release in the Netherlands. *International Journal of Climatology*, 22, 1757–1767.

Verbesselt, J., Hyndman, R., Zeileis, A., and Culvenor, D. 2010. Phenological change detection while accounting for abrupt and gradual trends in satellite image time series. *Remote Sensing of Environment*, 114, 2970–2980.

Vermote, E. F., Kotchenova, S. Y., and Ray, J. P. 2011. MODIS surface reflectance user's guide. MODIS land surface reflectance science computing facility, version 1.

Vicente–Serrano, S. M. 2006. Spatial and temporal analysis of droughts in the Iberian Peninsula (1910–2000), *Hydrological Sciences*, Journal 51, 83–97.

Viovy, N., Arino, O., and Belward, A. S. 1992. The Best Index Slope Extraction (BISE), A method for reducing noise in NDVI time–series. *International Journal of Remote Sensing*, 13, 1585–1590.

Weis, J. S. 2010. Salt marsh, In: Cleveland, C. J. (Eds.) *Encyclopedia of Earth*, Washington, D.C., Environmental Information Coalition, National Council for Science and the Environment.

White, K. P., Langley, J. A., Cahoon, D. R., and Megonigal, J. P. 2012. C_3 and C_4 biomass allocation responses to elevated CO_2 and nitrogen, contrasting resource capture strategies. *Estuaries and Coasts*, 35, 1028–1035.

White, M. A., Thornton, P. E., and Running, S. W. 1997. A continental phenology model for monitoring vegetation responses to interannual climatic variability. *Global Biogeochemical Cycles*, 11, 217–234.

Wilson, K. B., and Baldocchi, D. D. 2000. Seasonal and inter–annual variability of energy fluxes over a broadleaved temperate deciduous forest in North America. *Agricultural and Forest Meteorology*, 100, 1–18.

Windham, L., and Ehrenfeld, J. G. 2003. Net impact of a plant invasion on nitrogen-cycling processes within a brackish tidal marsh. *Ecological Applications*, 13, 883–896.

Wolfe, R. E., Nishihama, M., Fleig, A. J., Kuyper, J. A., Roy, D. P., Storey, J. C., and Patt, F. S. 2002. Achieving sub–pixel geolocation accuracy in support of MODIS land science. *Remote Sensing of Environment*, 83, 31–49.

Xiao, X., Braswell, B., Zhang, Q., Boles, S., Frolking, S., and Moore, B. 2003. Sensitivity of vegetation indices to atmospheric aerosols, continental–scale observations in Northern Asia. *Remote Sensing of Environment*, 84, 385–392.

Zeng, H., Jia, G., and Epstein, H. 2011. Recent changes in phenology over the northern high latitudes detected from multi–satellite data. *Environmental Research Letters*, 6, 045508.

Zhang, X. and Goldberg, M. D. 2011. Monitoring fall foliage coloration dynamics using time–series satellite data. *Remote Sensing of Environment*, 115, 382–391.

Zhang, X., Friedl, M. A., and Schaaf, C. B. 2006. Global vegetation phenology from Moderate Resolution Imaging Spectroradiometer (MODIS), Evaluation of global patterns and comparison with *in situ* measurements. Journal of Geophysical Research, *Biogeosciences*, 111, DOI: 10.1029/2006JG000217

Zhang, X., Friedl, M. A., Schaaf, C. B., and Strahler, A. H. 2004. Climate controls on vegetation phenological patterns in northern mid-and high latitudes inferred from MODIS data. *Global Change Biology*, 10, 1133–1145.

Zhang, X., Friedl, M. A., Schaaf, C. B., Strahler, A. H., Hodges, J. C., Gao, F., Reed, B. and Huete, A. 2003. Monitoring vegetation phenology using MODIS. *Remote Sensing of Environment*, 84, 471–475.

Zhang, X., Wang, J., Gao, F., Liu, Y., Schaaf, C., Friedl, M., Yu, Y., Jayavelu, S., Gray, J., Liu, L. and Yan, D. 2017. Exploration of scaling effects on coarse resolution land surface phenology. *Remote Sensing of Environment*, 190, 318–330.

Table 4.1. Seasonality Parameters estimated by TIMESAT

Seasonality Parameters	Description/ Phenological Interpretation	Unit
Start of Season (SOS)	Time at the beginning of growing season, when GBM begins to increase and photosynthesis starts	Julian Days from Jan 1
End of Season (EOS)	Time at the end of growing season, when GBM ends to decrease and photosynthesis stops completely	Julian Days from Jan 1
Peak of Season (POS)	Computed as the mean of the time-period for which the green-up process stops and brown-down starts; time when the GBM and photosynthesis reaches its maximum level	Julian Days from Jan 1
Length of Season (LOS)	Time from start to end of growing season	Days
Base Value	Mean of the minimum GBM values at the start (initial GBM) and end (final GBM) of growing season	GBM unit
Max Value	Maximum GBM value for the fitted function during the growing season/ GBM value during the peak of the growing season	GBM unit
Amplitude	Difference between base and max value; Maximum increase in canopy photosynthetic activity above the baseline	GBM unit
Left Derivative	Rate of Green-up; rate of increase of GBM value from the beginning till the peak of growing season	GBM unit/ 8 days
Right Derivative	Rate of Brown-down; rate of decrease of GBM value from the peak to the end of the growing season	GBM unit/ 8 days
Small Seasonal Integral	Integral of the function describing the season from start to end of season, above the base level; indicator of net canopy photosynthetic rate across the entire growing season	GBM unit
Large Seasonal Integral	Integral of the function describing the season from start to end of season; indicator of gross canopy photosynthetic rate across the entire growing season along with the base GBM	GBM unit

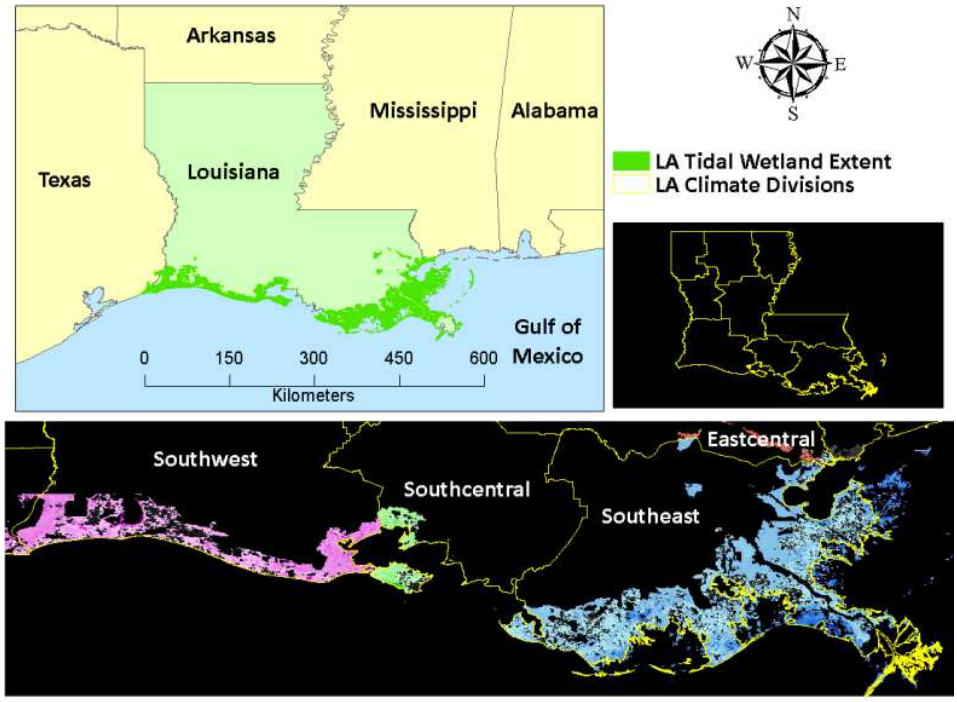

Figure 4.1: Salt marsh extent in coastal Louisiana spread across four climatic zones.

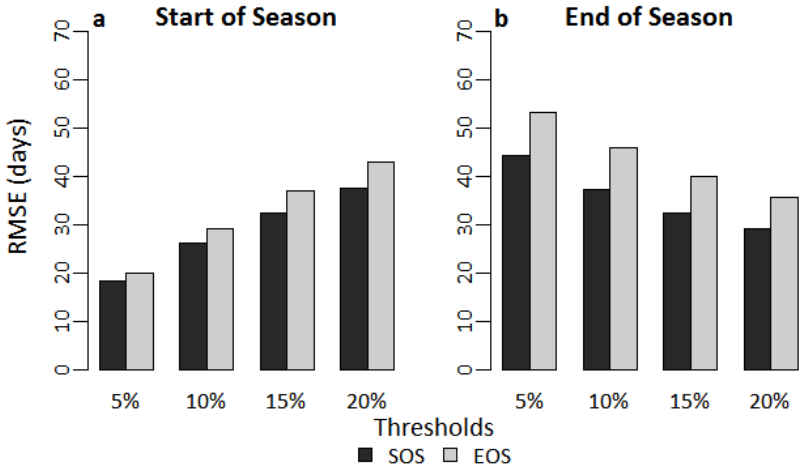

Figure 4.2: Root mean square error estimates for (a) start of season and (b) end of season dates between derivative analysis and TIMESAT thresholds for both asymmetric Gaussian and double logistic smoothing functions.

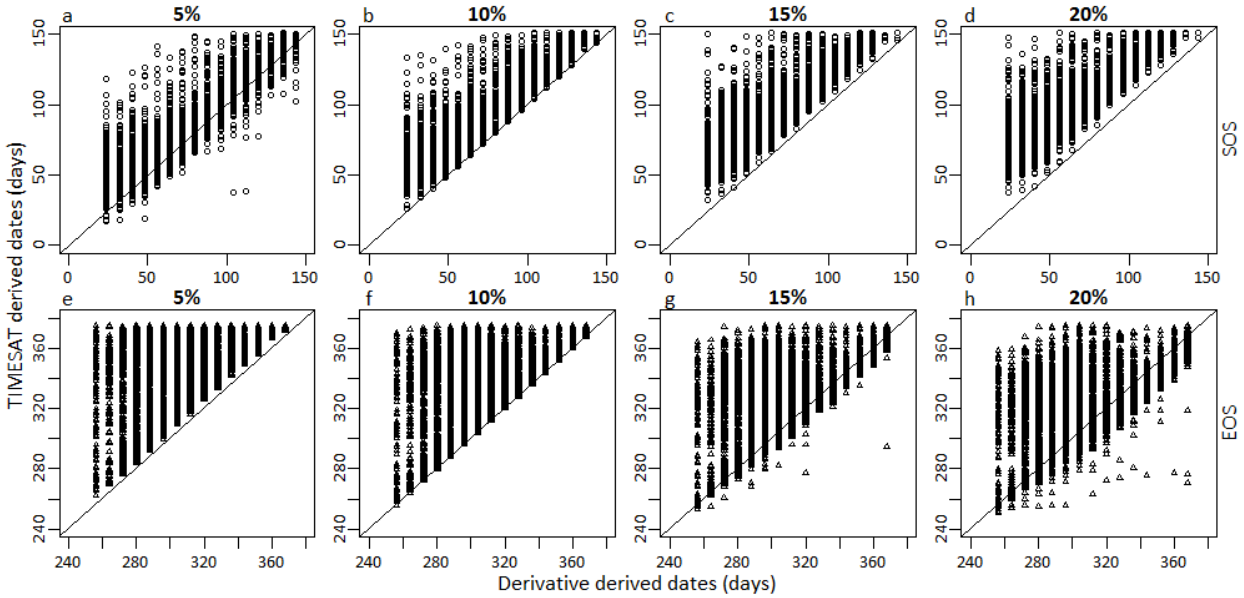

Figure 4.3: Residual plots matching dates between derivative analysis and TIMESAT thresholds for start of season (a-d) and end of season (e-h)

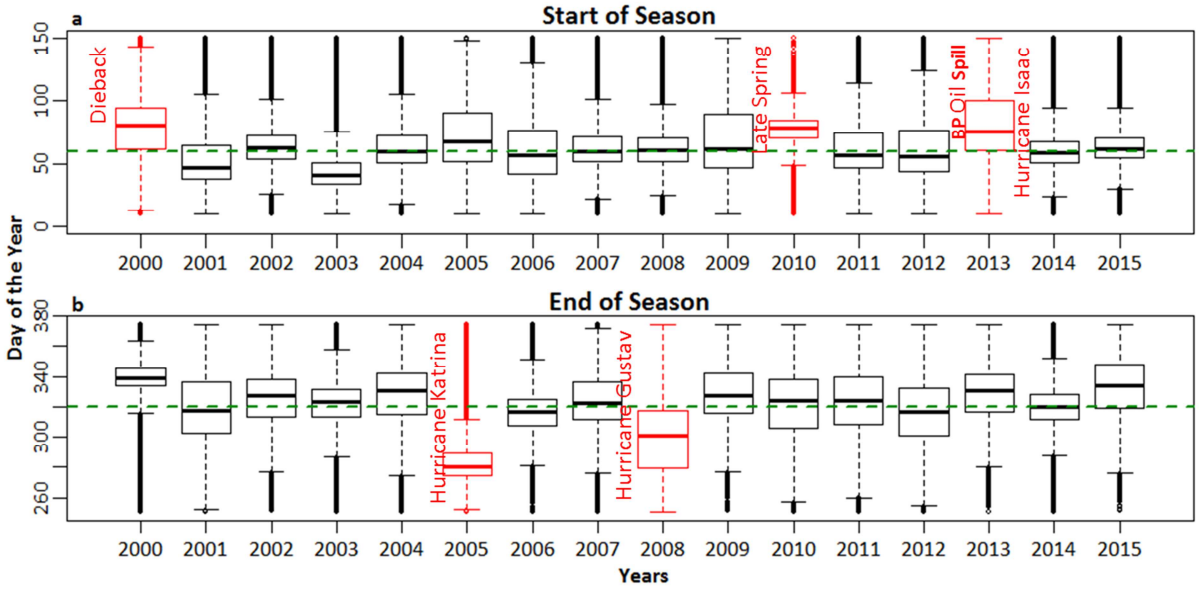

Figure 4.4: (a) SOS and (b) EOS dates for salt marshes of southeast LA. Dotted line represents median SOS and EOS dates. Late SOS and early EOS are highlighted along with environmental factors possibly influencing such events.

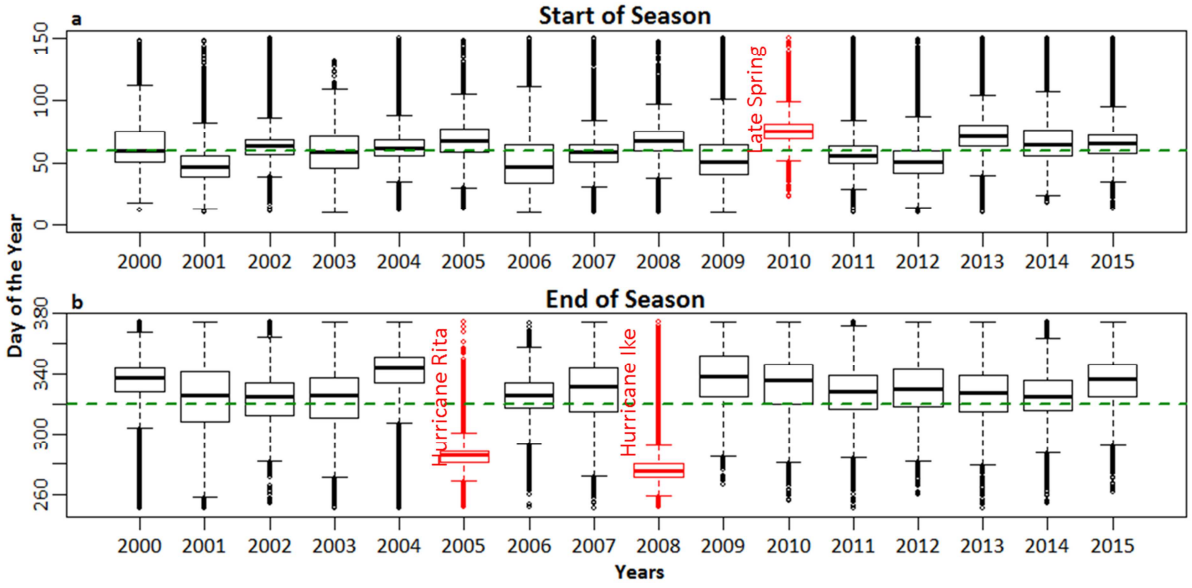

Figure 4.5: (a) SOS and (b) EOS dates for salt marshes of southwest LA. Dotted line represents median SOS and EOS dates. Late SOS and early EOS are highlighted along with environmental factors possibly influencing such events.

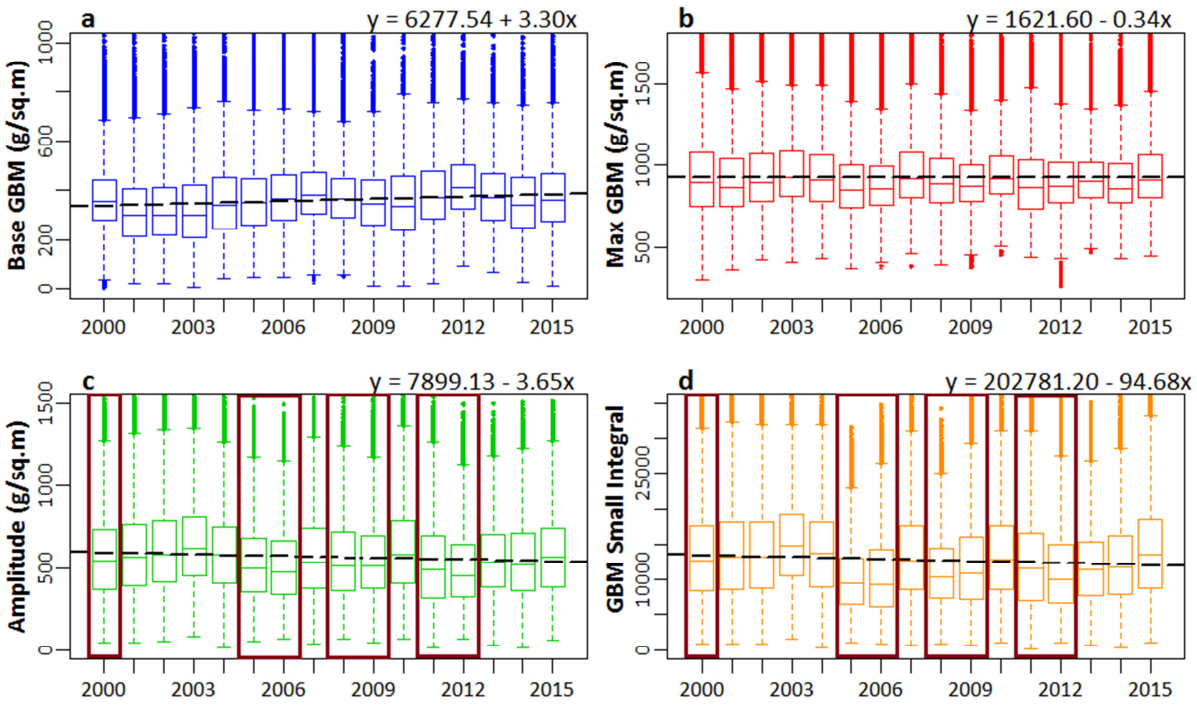

Figure 4.6: Linear trends in the seasonality parameters during the sixteen year time period (2000 – 2015): (a) Base GBM value, (b) Max GBM value, (c) seasonal amplitude and (d) small seasonal integral. Dotted line represents linear trend. Highlighted years in (c) and (d) indicate severe short term effects of dieback events and hurricane landfalls on seasonal amplitude and small seasonal integral.

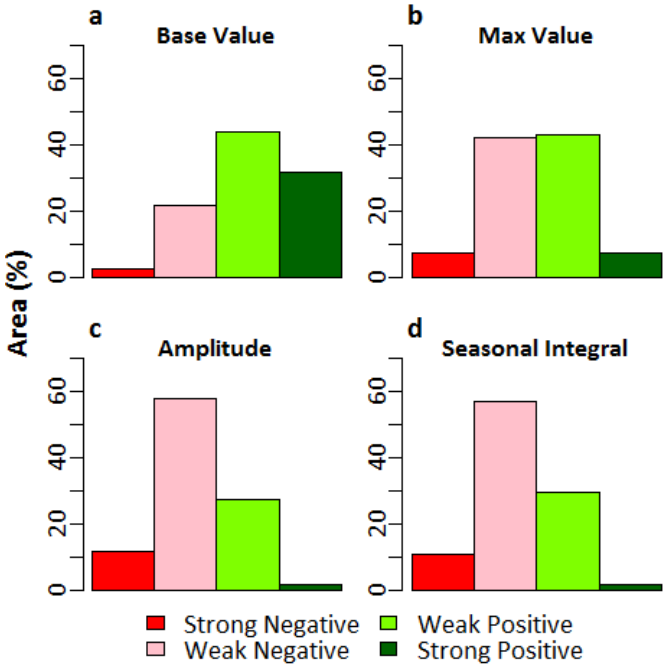

Figure 4.7**:** Percentage area coverage with different trends for (a) GBM base value, (b) GBM max value, (c) GBM amplitude and (d) GBM small seasonal integral for salt marshes in Louisiana.

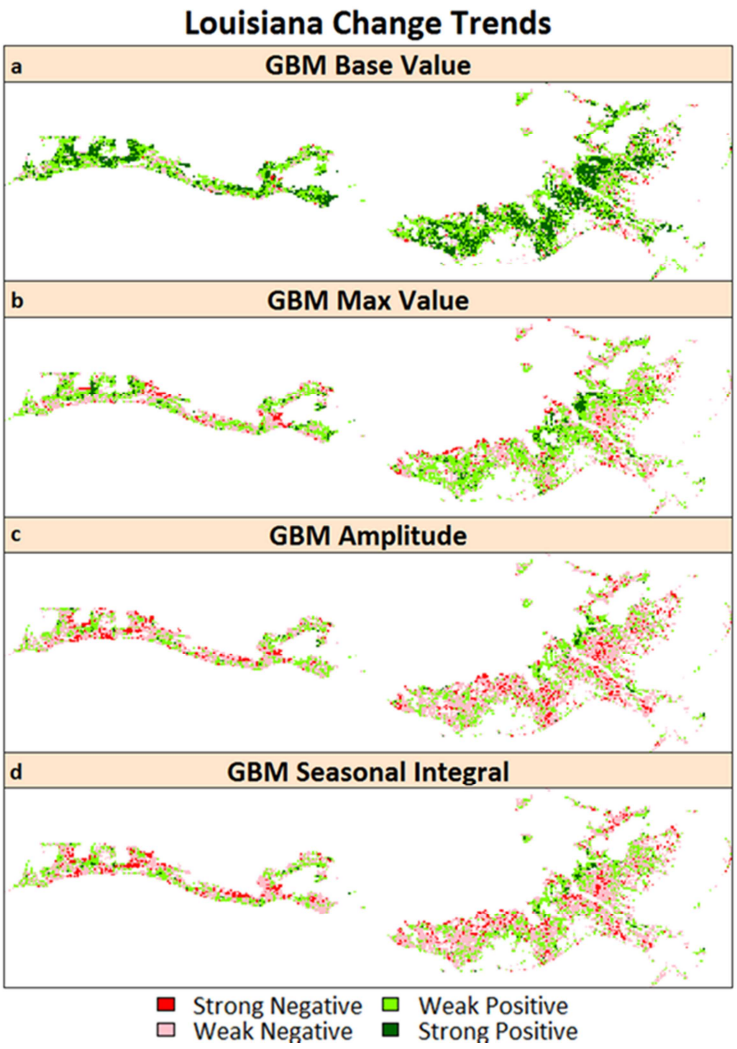

Figure 4.8: Spatial distribution of the areas showing different trends for (a) GBM base value, (b) GBM max value, (c) GBM amplitude and (d) GBM small seasonal integral for salt marshes in Louisiana.

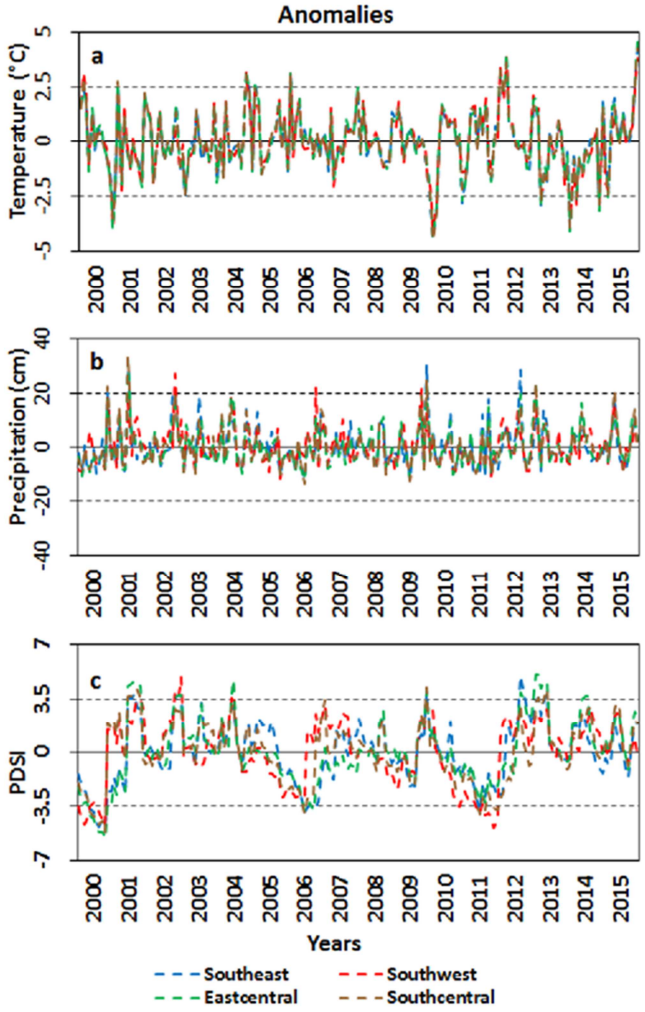

Figure 4.9: (a) Temperature (b) Precipitation anomalies for southeast LA, (c) Temperature and (d) Precipitation anomalies for LA.

CHAPTER 5

LONG-TERM TRENDS IN PHENOLOGY OF SALT MARSH ECOSYSTEM IN GEORGIA USING MODIS[†]

[†]Ghosh, S., O'Connell, J. R., and Mishra, D. R. Long-term trends in phenology of salt marsh ecosystem in Georgia using MODIS, to be submitted to IEEE Transactions on Geoscience and Remote Sensing

ABSTRACT

Study of saltmarsh phenology is imperative to understand its response to environmental change. In this study, we examined the phenology of salt marsh ecosystem across coastal Georgia for a sixteen-year time-period (2000-2015) using NASA's Moderate Resolution Imaging Spectroradiometer's (MODIS) 8-day average surface reflectance images (500m). We utilized the least squares fitted asymmetric Gaussian (AG) smoothing function to increase signal to noise ratio from the raw phenology derived from the time-series composites. We performed derivative analysis to determine the appropriate start of season (SOS) and end of season (EOS) thresholds. We validated the derived SOS and EOS using *in-situ* observations of SOS and EOS acquired using PhenoCam. We extracted seasonality parameters in TIMESAT, and studied the effect of environmental disturbances/anomalies on the seasonality parameters. Finally, we performed trend analysis using the derived seasonality parameters such as base Green Biomass (GBM) value, maximum GBM value, seasonal amplitude, and small seasonal integral. Based on root mean square error (RMSE) values and residual plots, we selected the best thresholds for SOS (5% of amplitude) and EOS (20% of amplitude). The selected SOS and EOS thresholds were able to capture the environmental disturbances that have affected the salt marsh ecosystem during the last sixteen-year time period. Our trend analysis results indicate positive trends in the base GBM values in salt marshes of GA. However, we observed mostly negative changes in the max GBM values, GBM amplitude and small seasonal integral, which indicate overall progressive decline in the rates of photosynthesis and biomass allocation in the GA salt marsh ecosystem. This observed decline in photosynthesis and biomass allocation is most likely due to elevated atmospheric carbon dioxide (CO_2) levels and sea level rise. The results illustrate both the relative efficiency of MODIS based biophysical models in analyzing salt marsh phenology

and performances of the smoothing technique in terms of improving signal to noise ratio of the MODIS derived phenology.

Keywords: Salt Marsh; Phenology; MODIS; Georgia; TIMESAT

Introduction:

Salt marshes are one of the extremely valuable components of the coastal landscape because they provide many critical ecosystem services, such as nutrient cycling, storm surge protection, carbon sequestration, and organic material production (Valiela et al. 2000). These ecosystems are well recognized carbon sinks, and conservation of such a natural ecosystem is critical in maintaining carbon balance in the environment (Connor et al. 2001; Chmura et al. 2003). However, coastal marsh habitats are particularly vulnerable to periodic and slow moving environmental events, such as sea–level rise (Craft et al. 2009, Stralberg et al. 2011), rising atmospheric CO_2 (McLeod et al. 2011), changes in salinity (Callaway et al. 2007), dieback (Ogburn and Alber, 2006) and ecological succession (Artigas and Pechmann, 2010). These environmental factors can significantly affect the small term and long term phenology of salt marsh habitats both at site–specific and landscape levels, which in turn, may have serious implications on carbon cycle and primary productivity (Xiao et al. 2009). One way to study and understand the response of any vegetation ecosystem to environmental changes is through analyzing the long–term spatio–temporal trends in phenology (White et al. 1997). Phenological measurements such as the timing of budburst and flowering are now widely used to detect and study the effect of climate variability on vegetation health both at the site–specific or broader landscape scale (Kramer et al. 2000; Beaubien and Freeland, 2000; Primack et al. 2004). Moreover, accurate monitoring of vegetation phenology is crucial for development of global surface energy and water flux models (Arora, 2002) and global carbon cycle (Running and Nemani, 1991; Wilson and Baldocchi, 2000). Therefore, phenological properties or seasonality parameters, such as the timing of the start and end of season, rate of green–up and brown–down,

amplitude, and maximum growth level have become emerging indicators of global environmental changes (Kunkel et al. 2004; Scheifinger et al. 2002).

Substantial effort has recently been devoted to expanding networks that track seasonal vegetation dynamics (Morisette et al. 2009). With decades of remote sensing imagery in freely available public archives, it is possible to quantify phenological changes through time and space, thus enabling phenological monitoring at local, regional and global scales (e.g. Myneni et al. 1997; Zhang et al. 2006). The Moderate Resolution Imaging Spectroradiometer (MODIS) provides valuable data for monitoring ecosystem dynamics with appropriate temporal resolutions and substantially improved geometric and radiometric properties (Zhang et al. 2006), and has been utilized for mapping and studying long-term salt marsh biophysical characteristics (Mishra and Ghosh, 2015; Mishra et al, 2015; Ghosh et al, 2016; O'Donnell and Schalles, 2016). Studies have utilized MODIS images for monitoring ecosystem phenology at both site-specific and landscape scales (Ahl et al. 2006; Fisher and Mustard, 2007; Zhang et al. 2006; de Beurs and Henebry, 2005; White et al. 1997). Studies have also developed algorithms to automatically retrieve land surface phenology metrics from satellite data (de Beurs and Henebry, 2010; White et al. 2009; Walker et al. 2012). However, the nature of satellite data makes it difficult to extract phenological metrics from it directly (de Beurs and Henebry 2005; Verbesselt et al. 2010). Time-series data derived from satellite images inevitably contain disturbances caused by cloud presence (Gutman, 1991), atmospheric variability (Huete and Liu, 1994), and aerosol scattering (Xiao et al. 2003), that degrades the data quality and hampers analysis. Therefore, satellite derived time-series data needs to be quality-screened and/or smoothed to increase signal-noise ratio before phenological parameters can be estimated (Atkinson et al. 2012). Several methods have been proposed to remove such noise and to reconstruct high-quality time-series products,

based on interpolation of time-series data (Viovy et al. 1992; Jonsson and Eklundh, 2002; Chen et al. 2005; Moody et al. 2005; Sellers et al. 1994; Roerink et al. 2000). The MATLAB based program TIMESAT (http://web.nateko.lu.se/timesat/timesat.asp), allows users to test different smoothing techniques, along with various statistical filters for increasing signal-noise ratio and generating noise-free phenology that can be further utilized for generating seasonality parameters (Jonsson and Eklundh, 2002; 2004). After smoothing the raw phenology, various statistical methods are used to determine the start and end of the seasons, such as analysis of derivatives of the smoothed phenology, using known thresholds (particularly for smoothed NDVI phenology), or matching with phenology dates observed *in-situ*, usually from continuously archived digital photographs (Zhang et al. 2003; Heumann et al. 2007).

While numerous studies have explored the use of satellite remote sensing data for monitoring terrestrial phenology at landscape to regional scales (Fisher et al. 2007; Myneni et al. 1997; Soudani et al. 2008; White et al. 2009), assessing the relationship between satellite-based measurements of phenology, and *in-situ* phenological observations remains a challenge. Imagery from remote sensing platforms such as MODIS is often collected at coarse spatial resolutions that encompass considerable landscape heterogeneity within each pixel. Therefore, comparison of phenological dates derived from satellite images with *in-situ* observations is necessary for evaluation of uncertainties in phenological measurements (Graham et al. 2010, Hufkens et al. 2012, Elmore et al. 2012, Klosterman et al. 2014). *In-situ* observations provide the oldest and longest running phenology records in existence (e.g., Aono and Kazui 2008); although visual observations are labor intensive to collect and the spatial extent of observations collected by an individual is inherently limited. Digital repeat photography, a form of near-surface remote sensing, provides data at higher spatial and temporal resolution than satellite remote sensing

(Richardson et al. 2009). Specifically, digital repeat photography can provide imagery that is nearly continuous in time, rarely affected by atmospheric noise, and robust to variation in illumination conditions (Sonnentag et al. 2012). Exploiting these advantages, color indices derived from digital repeat photography have been used to characterize the phenology of diverse plant communities and functional types (PFT) such as deciduous broadleaf forest (Richardson et al. 2007: Ahrends et al. 2008: Sonnentag et al. 2012: Hufkens et al. 2012: Dragoni et al. 2011), evergreen broadleaf forest (Zhao et al. 2012), evergreen needleleaf forest (Ide and Oguma 2010: Bater et al. 2011), desert shrublands (Kurc and Benton 2010), bryophyte communities (Graham et al. 2006) and invasive plants (Sonnentag et al. 2011). However, phenology characterization of salt marsh ecosystems using *in-situ* digital repeat photography have hardly gained importance; the first PhenoCam for monitoring salt marsh ecosystem was set up in 2013 (Georgia Coastal Ecosystem LTER; https://gce-lter.marsci.uga.edu/). In addition, processing of images for phenology characterization of salt marsh ecosystem is challenging (O'Connell and Alber, 2016).

Phenology has been studied in details in a variety of different terrestrial ecosystems such as tropical rainforests, deciduous habitats, grasslands, and aquatic ecosystems such as phytoplankton (Asner and Alencar, 2010; Hufkens et al. 2012; Shen et al. 2011; Palmer et al. 2015). However, analyzing long-term phenology of salt marshes using remote sensing is challenging due to the inherent nature of salt marsh; high degree of fragmentation and background water/tidal signal renders most of the traditional vegetation indices insensitive towards plant growth stage (Ghosh et al. 2016). Hence, very few studies have emphasized the need to analyze long-term phenology of salt marsh habitats (Ghosh et al. 2016; O'Connell and Schalles, 2016; Mishra and Ghosh, 2015; Mishra et al. 2015). In this paper, we analyze the long-term trends in the phenology and seasonality parameters of the salt marshes in GA using a

combination of MODIS and *in-situ* derived phenological dates. We also discuss the broader implications of the observed trends. We first test the performance of an existing MODIS based GBM mapping algorithm, for mapping GBM of salt marshes across coastal Georgia (GA). Next, we describe and test methods for deriving noise-free phenology and seasonality parameters for salt marshes in GA, using time-series GBM composites generated using MODIS and *in-situ* phenological observations. Finally, we analyze the long-term change trends in the seasonality parameters using statistical trend analysis techniques.

Study Area

Georgia's coast has approximately one-half million acres of tidal wetland habitats, with marsh habitats extending from 4 to 8 miles into the mainland from the sea-coast (Figure 5.1). Georgia contains almost one third of the total salt marsh extent in the eastern seacoast of US (Reimold, 1977). The most dominant macrophyte in these marsh habitats is *Spartina alterniflora*; covering more than 80% of the total marsh area (Hladik et al. 2013). *Spartina alterniflora* can grow up to 2m tall along the regularly-flooded creek banks in the low marsh, while medium (approximately 0.5–1.0 m) and short (< 0.5m) *Spartina* is observed in the mid-marsh and irregularly flooded high marsh respectively. In the high marshes, occasional presence of other marsh species such as *Salicornia virginica*, *Batis maritima*, *Distichlis spicata* is also observed. At the highest elevations, *Juncus roemerianus* and *Borrichia frutescens* becomes the dominant species. The salt marshes in GA fall completely within the southeast climatic division; the coastal climate is characterized by warm and wet summers and moderately cold winters (National Climatic Data Centre, https://www.ncdc.noaa.gov/). The temperatures range between 12.5 and 25.5 degree Celsius, with an average annual rainfall of 125 cm (National Weather Service; http://www.weather.gov/). Tides are semi-diurnal with a mean tide range of 2.5 m.

Since the late 1990s, severe dieback events have periodically affected Georgia (GA) coast (Ogburn and Alber, 2006). Marsh dieback interrupts ecosystem functions by limiting above ground biomass production and increasing erosion (Ogburn and Alber, 2006). These dieback events could be related to a combination of stressors such as hydrological alteration, pollution, sea level rise, severe drought events, changes in soil chemistry, wrack accumulation, fungal pathogens, and herbivory, although precise reasons for the occurrence of marsh diebacks have been disputed (Goodman and Williams, 1961; Ogburn and Alber, 2006; Brown and Pezeshki, 2007).

Materials and Methods

a. Time-series composites and climate data:

The MODIS Land Science Team provides several data products derived from MODIS observations to the public, including the 8-day composite Land Surface Reflectance (MOD09A1). The MOD09A1 dataset includes seven spectral bands at a spatial resolution of 500m corrected for the effects of atmospheric gases, aerosols, and thin cirrus clouds (Vermote et al. 2011). We generated time-series composites of GBM for the salt marshes of GA, for a sixteen year period (2000 – 2015) using MOD09A1 based on biophysical models which are described in Ghosh et al. (2016). The GBM biophysical model is primarily a linear relationship between Visible Atmospheric Resistant Index (VARI) derived from MODIS surface reflectance images and *in-situ* estimates of GBM from 200 study plots across the northern Gulf of Mexico (GoM) as follows:

$$GBM\ (grams\ per\ square\ meter) = 3617.104 * VARI + 543.3514 \quad (1)$$

The model produced a co-efficient of determination (r^2) of 0.93 and has an inherent percent normalized RMSE of 17.34% in GBM estimation. Ghosh et al. (2016) had justified the use of VARI for mapping salt marsh biophysical characteristics such as GBM, based on the superior performance of VARI compared to other traditional NIR wavelength based indices such as NDVI. The poor performance of the NIR based indices was attributed to the severe interference of the NIR wavelengths to the background soil moisture or tidal signals; sensitivity of visible bands to water signals was argued to be much less susceptible. We validated the GBM model using *in-situ* GBM measurements from Georgia Coastal Ecosystem Long-Term Ecological Research's (GCE-LTER) permanent marsh monitoring plots (Georgia Coastal Ecosystem Long-Term Ecological Research Network; http://gce-lter.marsci.uga.edu) (described in the following section). GBM composites were generated post model validation and error estimation.

While generating GBM composites, we utilized MODIS quality assurance bands to retain only the pixels that have been corrected for atmospheric noise, sensor level errors, and bidirectional reflectance in the time-series composites (Vermote et al. 2011; Ghosh et al. 2016). This enabled us to assign equal weightage to all salt marsh pixels for extraction of phenology, rather than assigning weights based on quality pixels for time-series analysis. However, tidal correction was not performed, as it is not possible to determine the level of daily MODIS scene contribution to the 8-day surface reflectance imagery, which would otherwise, have helped correcting for tidal signals using daily tidal fluctuation data (Ghosh et al. 2016). Since the MODIS surface reflectance products have a temporal resolution of 8 days, 46 GBM composites were generated per year for GA salt marshes; thus, for the sixteen year study period, 736 composites were generated in total. Once subsets were generated, we converted the raw GBM composites to 16 bit signed generic binary format for running TIMESAT. We also compiled temperature,

precipitation and Palmer Drought Severity Index (PDSI) (Palmer, 1965) data for the GA southeast climatic zone from the National Climate Data Centre (NCDC) (National Climate Data Centre, https://www.ncdc.noaa.gov) archives, to investigate any significant temperature, precipitation and PDSI anomalies during the sixteen-year period that might potentially contribute to the variability in salt marsh GBM phenological trends.

b. In-situ GBM observations:

The GCE-LTER permanent marsh monitoring plots were established in 2000 for long-term monitoring of plant parameters such as stem count, height and flowering status of every plant in each plot (Pennings, 2016). Stem clipping samples were collected adjacent to plots in 2002 and 2007, then measured, dried, weighed and statistically analyzed in order to generate allometric regression relationships between height and mass for estimation of plant biomass in corresponding plots. This data set includes cumulative long-term observations of plant stem count, height and biomass per marsh zone, plot and species at 10 GCE-LTER sampling sites from 2000 to 2015. We used the rescaled GBM value (plot level observations rescaled to gm per square meter) derived using the allometric regression relationship (Li and Pennings, 2016), to validate the MODIS based GBM model.

c. Phenology smoothing using TIMESAT:

As mentioned before, the MODIS pixels for time-series analysis were carefully screened using the MODIS quality assurance data. In spite of such quality control measures, the raw time-series derived from the GBM composites still showed presence of residual noise, which can possibly be attributed to localized environmental disturbances, or tidal water induced background soil moisture. However, since the GBM composites were generated using a visible band index

(VARI), the tidal effect can be assumed to be minimal. We used TIMESAT to generate smooth time-series of GBM and to estimate the seasonality parameters for our study area. TIMESAT fits smooth continuous curve to time-series data using Asymmetric Gaussian (AG), Double Logistic (DL) and Savitzky–Golay filters (SG). In these methods local model functions are fit to data in intervals around maxima and minima in the time-series. The AG and the DL smoothing functions have been found to produce similar results, with the AG filter being less sensitive to incomplete baseline time-series data (Gao et al. 2008). Since MODIS started acquiring images from late February/early March in the year 2000, images from the beginning of our study period were missing. Therefore, we considered to utilize the AG filter for constructing noise-free phenology and derivation of seasonality parameters. The SG filter was not considered to be ideal for deriving smooth time-series as it is susceptible to localized noise in the original raw phenology generated from the time-series images and hence might provide erroneous estimates of seasonality parameters (Tan et al. 2011).

The base function of asymmetric Gaussian is:

$$g(t; x_1, x_2, \ldots, x_5) = \begin{cases} exp\left[-\left(\frac{t-x_1}{x_2}\right)^{x_3}\right], \ if\ and t > x_1 \\ exp\left[-\left(\frac{x_1-t}{x_4}\right)^{x_5}\right], \ if\ t < x_1 \end{cases} \quad (2)$$

For this function, x_1 determines the position of the maximum or minimum with respect to the independent time variable *t*, while x_2 and x_3 determine the width and flatness (kurtosis) of the right function half. Similarly, x_4 and x_5 determine the width and flatness of the left half.

We used the Seasonal and Trend decomposition using Loess (STL) method to remove spikes and outliers in the time-series; the STL method removes outliers by assigning weights to the values in time-series based on STL decomposition. This method does not depend on ancillary data, and

is global in nature (Cleveland et al. 1990). Further, we also eliminated any negative or zero values observed in the raw phenology, from our analysis. The upper limit of GBM was set to 2000 g/m^2, marginally higher than the upper limit of the predictive range of the GBM models described in Ghosh et al. (2016). We specified an adaptive upper envelope assuming any noise to be negatively biased (Jönsson and Eklundh, 2002, 2004), with an adaptive strength of 2; as stronger adaptation strength is likely to put too much emphasis on single high data values leading to erroneous estimates of seasonality parameters (Jönsson and Eklundh, 2002, 2004).

d. Start and End of Season determination:

We derived SOS and EOS using different thresholds (fractions of seasonal amplitude), such as 5%, 10%, 15% and 20%. Thresholds below 5% were not tested, as they might be influenced by the noise from the non-growing season (Heumann et al. 2007). Phenology studies using TIMESAT have mostly preferred to use thresholds above 10% (usually 20%; sometimes 50%) for deriving SOS and EOS dates, using NIR wavelength based vegetation index time-series; most of these thresholds were determined based on expert opinions or on-field observations of SOS and EOS (Suepa et al. 2016; Zeng et al. 2016; Delbart et al. 2005). We did not test any NDVI thresholds for SOS and EOS estimation, as NDVI or any NIR based indices are prone to insensitivity in salt marsh settings (Ghosh et al. 2016). For this study, we utilized a modified approach; we tested the performances of different thresholds by matching the SOS, and EOS dates derived using derivative analysis (Tan et al. 2011; see analysis section) against dates derived using the aforementioned thresholds in TIMESAT. Once we selected the best thresholds for SOS and EOS, we matched the TIMESAT derived dates with SOS and EOS dates derived from continuous images of a salt marsh patch acquired by a digital camera (PhenoCam; see

following section), set up in Sapelo Island, GA. Once we validated the best SOS and EOS thresholds, we derived seasonality parameters using TIMESAT, for further analysis.

e. PhenoCam Data:

PhenoCam images are digital images of vegetated landscapes acquired by cameras mounted on towers or platforms to create almost continuous photo-record of seasonal changes occurring within the landscapes (http://budburst.org/what-is-PhenoCam). GCE-LTER became an active participator in the PhenoCam network in September 2013. A StarDot Netcam was installed in the GCE-LTER eddy covariance flux tower deployed in a marsh off the Duplin River at Sapelo Island. The IFOV of the PhenoCam digital camera is pointed in the north-east direction, covering a marsh patch almost the size of a MODIS 500m pixel (Figure 5.1). Images are being retrieved every 30 minutes by a waterproof computer installed at Marsh Landing, then relayed hourly to servers at the University of Georgia. Tides are semi-diurnal with a range of ~1.2 m on the marsh platform. We analyzed images from January 1, 2014 through December 1, 2015 except when the camera was not functional between July 16, 2014 and September 2, 2014. To reduce solar illumination variation, analyses were limited to images collected between 10:00 and 14:30. PhenoCam images were corrected for tides, haze, clouds and cloud shadows using a smart classifier (O'Connell and Alber, 2016). We used a color index that tracked temporal change while still allowing for year to year variation, the Green Chromatic Coordinate (GCC; Richardson et al. 2007). GCC is calculated as follows

$$G_a = G_a/(R_a + G_a + B_a) \quad (3)$$

where R_a, G_a and B_a represent the average value of *R*, *G*, and *B* within the marsh ROI. GCC, a color-based phenology index, tracks the seasonal progress of vegetation green-up. Green

Chromatic Coordinate (GCC) was estimated for the salt marsh region of interest. A sequential logarithmic curve was fitted to the extracted time-series GCC, as follows:

$$g(t) = \frac{c}{a+e^{bt}} + d \quad (4)$$

where *t* is time (day of year, DOY), *a* and *b* are empirical coefficients associated with the rate of change in *g*, *c* is the potential maximum g for a given vegetation type, and *d* represents the background *g* value. The dates of tidal wetland green-up or start of season (SOS), peak greenness/peak of season (POS) and complete brown down/end of season (EOS) were derived from the corrected images using derivative analysis (Zhang et al. 2004). These dates were used for validation of the phenological dates, derived using the best selected thresholds for AG smoothing function in TIMESAT.

Analysis:

a. Validation of MODIS GBM model using in-situ GBM observation:

We used the GBM value derived using the aforementioned allometric regression relationship to validate the MODIS based GBM model developed initially for the salt marshes of the GoM. Since the salt marshes of Georgia are inhabited by the same halophytic macrophytes as observed in northern GoM, we tested the performance of the model in GA coast. GBM values within particular pixel were aggregated to match the MODIS derived GBM value for that particular pixel. Percent normalized root mean square error (%NRMSE, see Ghosh et al. 2016) was estimated and residual plots were analyzed for detection of possible model saturation. GBM composites were generated post error estimation and model validation.

b. Determination of SOS and EOS:

There is no specific universal method that can be used to determine TIMESAT thresholds to estimate SOS and EOS dates; calibration is necessary before selection of any specific threshold. Therefore, we investigated the derivatives of smoothed GBM time-series data, derived using AG smoothing function from ~100 random pixels. We estimated the third order derivative from the smoothed time-series and derived local maxima and minima (Tan et al. 2011). The third order derivative has been demonstrated by Tan et al. as better indicator for identifying SOS and EOS than the second order; the former representing the timing when the change of green-up rate or brown-down rate is the greatest, rather than the timing when the majority of vegetation within a pixel is turning green. For SOS and EOS, we matched the local maxima and local minima respectively, with the SOS and EOS dates derived using different thresholds in TIMESAT. We did not analyze derivatives for POS date estimations, as POS is a function of the maximum value encountered in the middle of the growing season; and it does not depend on the thresholds chosen for SOS and EOS. Once we matched SOS and EOS dates derived from derivative analysis against TIMESAT thresholds, we estimated the error between the observations using RMSE, and also analyzed residual plots for any specific trends.

We selected TIMESAT SOS and EOS thresholds that illustrated the greatest agreement with the dates derived from derivative analysis to match with dates derived from PhenoCam digital images. The PhenoCam tower is located near the northwest corner of the MODIS pixel, and the IFOV of the camera is pointed towards the northeast direction. The IFOV of the PhenoCam, hence, covers salt marsh extent of approximately two MODIS pixels. Therefore, we matched PhenoCam derived phenological dates with the average of the SOS, EOS and POS dates derived for the two pixels, using the best thresholds in TIMESAT. We estimated RMSE and examined

residual plots in order to detect any observable bias in the dates derived using TIMESAT thresholds in comparison to the PhenoCam dates. Thereafter, we extracted statistics for seasonality parameters and also generated their time-series composites for trend analysis, using the appropriate thresholds in TIMESAT.

c. Trend Analysis

We extracted seasonality parameters, such as base value, max value, amplitude and small seasonal integral that are major indicators of seasonal photosynthesis and biomass production, for all the salt marsh pixels covering coastal GA for sixteen year period. At first, we examined the overall trend in these seasonality parameters using simple linear regression. We examined the slope of the fitted trendline to determine any positive and negative trends over the sixteen year time period based on the positive or negative value of the slope magnitude. After that, in order to highlight the marsh areas showing improvement (positive change) and degradation (negative change) in the aforementioned seasonality parameters, we employed the Mann Kendall (MK) trend test (Kendall, 1970) using time-series composites of these seasonality parameters from 2000 – 2015, using R (R Core Team, http://www.R-project.org/). We conducted the MK trend test separately for every pixel of the GA salt marsh habitat using time-series composites of aforementioned seasonality parameters. These parameters are crucial indicators of seasonal productivity. We classified changes based on the z-score distribution at 95% confidence interval. A positive or negative value of z represents an upward or downward trend, respectively. Changes below the lower critical limit ($z < -1.96$) were classified as strong negative change, while above higher critical limit ($z > 1.96$) were classified as strong positive change. Changes within the 95% confidence interval were classified as weak negative or weak positive depending on negative or positive values of z.

Results and Discussion:

a. GBM validation:

The %NRMSE between GBM values derived using the MODIS based model and the averaged *in-situ* observation was observed to be 24.97%, slightly higher than the inherent error in the model (17.34%). The increase in the error magnitudes might be attributed to the local geomorphological and environmental conditions, such as degree of fragmentation of the salt marsh habitats, and the range of local tidal fluctuations. GA salt marshes are inundated by the semi-diurnal Atlantic tides in comparison to diurnal tides, as observed in the coastal GoM. Further, GA tides average approximately 6.5ft, but exceed 10ft during the highest spring tides, as compared to 3ft in northern GoM (NOAA Tides and Currents, https://tidesandcurrents.noaa.gov). In addition, since the *in-situ* observations of GBM were derived using the allometric relationship between plant height and GBM unlike the northern GoM model which used destructive sampling data, some level of error might have propagated from the conversion relationship. However, the residual analysis did not show any significant bias in GBM prediction by the MODIS GBM model for GA.

b. Derivative Analysis and PhenoCam validation:

For SOS (Figure 5.2), the 5% threshold seemed to agree the most with the derivative analysis for AG smoothing function, with the lowest RMSE. Higher thresholds showed greater RMSE. The AG method showed an error of ~22 days for the 5% threshold. The residual plots for SOS showed no specific trends for the 5% threshold (Figure 5.3a). Higher thresholds predicted late SOS dates when compared to the derivative derived dates (Figure 5.3a-d). For EOS, the 20% threshold showed the highest agreement with the derivative derived EOS dates (Figure 5.3h). We

observed an error of ~29 days (Figure 5.2), with no significant bias observed in the residual plots. Error levels progressively increased with lower thresholds; the residual plots demonstrated late EOS predictions with progressive decreasing thresholds compared to the derivative derived EOS dates (Figure 5.4e-g). Although asymmetric thresholds may not be uncommon for AG distribution due to its inherent skewness, seasonality parameters are usually derived using symmetric thresholds.

When we matched the SOS and EOS dates derived using derivative analysis and TIMESAT thresholds with the *in-situ* observed SOS and EOS dates derived from PhenoCam, we observed that the 5% threshold in TIMESAT seemed to agree with the PhenoCam derived SOS dates (Figure 5.4). For the 5% threshold, the RMSE observed was ~27 days. The residual plots for SOS showed no specific trends for the 5% threshold. For EOS, the 20% threshold showed good agreement with the PhenoCam derived EOS dates with the observed RMSE being ~29 days (Figure 5.4). The magnitude of error may be due to the differences in the IFOV of the camera and the MODIS sensor, the viewing angle, pixel heterogeneity, local geomorphology or the influence of tidal signal on MODIS 8 day surface reflectance images that could not be accounted for in TIMESAT. Further, our observations may have been influenced by the differences in the temporal resolution of MODIS images and PhenoCam. Since we are utilizing the MODIS 8-day surface reflectance products, which provide us with pre-calculated average reflectance over 8-day time period, it is not possible to determine the level of daily MODIS scene contribution to the 8-day surface reflectance imagery; on the other hand PhenoCam images used in this study were acquired at an interval of 30 mins. In addition, the error magnitudes may have been influenced by the inherent bias in the GBM model as well as the allometric relationship used to derive biomass from plant height. However, our observations were similar to those observed by

Ghosh and Mishra (in review), for the salt marsh habitats of Louisiana, where SOS and EOS dates derived using derivative analysis showed the highest agreement with 5% and 20% thresholds respectively. POS dates matched best between AG and PhenoCam, with AG smoothing function predicting late POS with a margin of error of 12 days. Based on our observations, we analyzed the seasonality parameters using the best thresholds (5% for SOS and 20% for SOS).

c. Trend Analysis:

Simple linear trends in salt marsh seasonality parameters (Table 5.1) GBM base values, GBM max values, seasonal GBM amplitude and small GBM integral are shown in Figure 5.5. Overall, during the sixteen year study period, GBM base values showed positive trends during the sixteen year time period (Figure 5.5a), while the rest of the seasonality parameters showed negative trends (Figure 5.5b-d). The positive trend observed in the base GBM values is an indicator of the cumulative storage of carbon over time as aboveground biomass. However, negative trends observed in the max values, and subsequently the seasonal amplitude and integral indicate long-term stress induced in the salt marsh vegetation, resulting in reduced photosynthesis and aboveground biomass accumulation. We observed severe short-term effects of the periodic dieback events occurring in the salt marsh habits in the years 2000-02, 2006-07 and 2011-2012, that affected the seasonal photosynthetic activity of the salt marsh habitats; which is evident in the relative lower magnitudes of seasonal amplitude, for those time-periods. However, the marsh habitats recovered from these dieback events when the environmental conditions became normal and conducive for salt marsh vegetation growth.

Trend classes for the change in base values, max values, seasonal amplitude and small seasonal integral for GA salt marshes and are shown in Figure 5.6. We observed positive changes in the GBM base values in almost 74% area of the salt marsh extent in GA; with strong positive changes observed in 28.5% of the area. On the other hand, the max values did not show as much positive change as the base values; rather, the extent of marsh areas with negative changes was much higher than those with positive change. We observed strong positive changes in only 2.7% of the total salt marsh extent; while strong negative changes were observed in almost 10% area. Therefore, we observed mostly negative changes in the seasonal amplitude and small seasonal integral. 76% of the salt marsh habitat showed negative changes in seasonal amplitude (14.89% area showing strong negative change) while 69.5% showed negative changes in small seasonal integral (14.8% area showing strong negative change). Overall, we observed good match in the areas showing strong positive change in base value, and strong negative changes in seasonal amplitude and small seasonal integral (Figure 5.7).

A progressive increase in base GBM value was observed in most of the salt marsh habitat indicating that considerable amount of carbon has been accumulated over time and stored as aboveground biomass in the salt marsh habitat. However, no similar progressive increase was not observed in the maximum GBM values; rather, it showed progressive decline in most of the marsh areas, thus explaining the strong negative changes in seasonal amplitude and small seasonal integral. This indicates progressive decline in the levels of photosynthesis over the sixteen year time period. Variations in the levels of photosynthesis are generally attributed to variations in the levels of temperature and precipitation, as these environmental factors influence the photoperiod and salinity of the salt marsh ecosystem (Song et al, 2013; Riddin and Adams, 2010). However, the temperature and the precipitation anomalies for GA did not show any

particular trend during the sixteen year time period (Figure 5.8a-b). The salt marsh habitats of these regions have experienced strong periodic drought conditions (Figure 5.8c) that have caused massive marsh dieback. However, salt marshes have been known to be resilient ecosystem, capable of recovering from short term environmental stress if environmental conditions become normal again; both *Spartina* and *Juncus* are resilient enough to recover from dieback with improvement in environmental conditions (McFarlin 2012).

The major driver of marsh GBM decline may have been increasing levels of CO_2 in the atmosphere, as well as sea level rise. Atmospheric CO_2 levels rose from 369ppm – 404ppm during the period 2000 – 2015 (NOAA ESRL, https://www.esrl.noaa.gov/gmd/ccgg/trends/), while sea-levels have been observed to rise at a rate of 3 – 6 mm/year in coastal GA (NOAA Tides and Currents, https://www.tidesandcurrents.noaa.gov/sltrends/sltrends.html). Increased CO_2 levels in the atmosphere, along with steady sea-level rise have been observed to reduce the rate of both above and below ground biomass accumulation in C_4 plants, through reduction in stomatal conductance (Leakey, 2009), rate of photosynthesis and water usage (Ainsworth and Long 2005; Erickson et al, 2007; White et al. 2012). The salt marsh habitat in GA is mostly dominated by the smooth cord-grass (*Spartina alterniflora*) and salt meadow cord-grass (*Spartina patens*), both of which C_4 species. Therefore, this observed reduction in the level of photosynthesis and biomass allocation is not entirely unexpected. However, if the progressive decline in the rates of photosynthesis and biomass allocation continues, the salt marsh ecosystem might not be able to sequester any more atmospheric carbon; rather, with periodic natural disasters such as hurricanes, diebacks or any anthropogenic disasters, marsh loss will turn the ecosystem to carbon sources (Delaune and White, 2012). Such an event might assist not only facilitate spread of invasive species, such as *Phragmites* (Howard et al. 2008), but may also

assist succession of salt marsh habitats by mangroves, especially with rising global temperatures and sea-levels (Saintilan et al. 2014; Krauss et al. 2011). Either of the two scenarios will, in turn, have far reaching ecological implications (Minchinton and Bertness, 2003; Silliman and Bertness, 2004; Chambers et al. 2003; Pennings and Silliman, 2005; Windham and Ehrenfield, 2003; Howe et al. 2009; Bianchi et al. 2013; Hopkinson et al. 2012). Although we do not claim that such an event is already underway in Georgia; however, our findings indicate that there is a risk of such cascading effects in future.

Conclusion

The study provides a comprehensive analysis of the phenological trends of the salt marsh habitats of GA, showcasing the efficiency of the MODIS derived time-series composites of salt marsh GBM. We have utilized the MATLAB based program TIMESAT to generate noise-free phenology from the GBM time-series composites after determining the SOS and EOS thresholds using derivative analysis. We justified our selection of the best SOS/EOS thresholds after matching the SOS and EOS dates derived using TIMESAT thresholds and derivative analysis. We further justified the thresholds by matching them with *in-situ* observations of SOS and EOS using PhenoCam. Finally, the trend analysis demonstrated the reduction in the rates of maximum GBM values, seasonal amplitude and small seasonal integral, and increment in the levels of GBM base value, indicating the progressive reduction in the levels of photosynthesis and biomass accumulation in the salt marsh habitat, that might be attributed as a combination of environmental effects such as stress induced by rising atmospheric CO_2 levels, and sea-level rise.

Further, the trend analysis results have been able to capture areas that are demonstrating significant stress in terms of reduced photosynthetic activity and require immediate restoration

and conservation efforts. The results of this study can potentially be compared with GPP trends as derived from MODIS 500m and 1-km GPP images; however, the MODIS GPP algorithm uses very generic grassland light use efficiency (LUE) values from Biome properties look-up table to estimate GPP for salt marshes. The algorithm does not take into account any LUE variability that might result from tidal effects or any other salt marsh specific conditions. Therefore, conclusions from GPP trend matching should be drawn carefully. Although trend analysis using MODIS derived images can provide a valuable insight into the phenological dynamics at the landscape level, site-specific trend analysis might require similar analysis using site specific records of sea-level changes, freshwater discharge, nitrogen enrichment and salinity, along with finer resolution images. With finer resolution images and time-series analysis, it will also be possible to estimate the marsh habitats lost due to localized dieback events, and the extent of marsh area that needs to be restored.

Due to coarse pixel footprint of the MODIS sensor, the possibility of encountering mixed pixels cannot be ruled out in this study; however, this problem persists to some extent even with fine resolution sensors. In spite of coarse spatial resolution, the advantages MODIS as a fine temporal resolution sensor (daily images combined to generate the 8 day surface reflectance product) cannot be overlooked, especially in terms of analyzing long-term phenological trends of critical ecosystems such as salt marshes, as compared to other fine spatial resolution satellites. Finer spatial resolution sensors often present the problem of cloud cover that render images completely unusable for analysis, resulting in frequent data gaps; a problem particularly evident in coastal ecosystems, where cloud presence in images from fine resolution sensors are very common especially during the peak growing. Further, their spatial coverages are inadequate when compared to MODIS, especially for analyzing regional phenology trends; combining scenes

from multiple days to study phenology trends at broader landscape, creates biases in the analysis itself. Therefore, MODIS is clearly a robust sensor for studying long-term phenological trends of ecosystems at a broader regional scale.

This is for the first time that such a comprehensive analysis of the phenology of salt marsh habitat in the Atlantic sea-board has been studied in terms of the seasonality parameters. Using the suggested methods in this study, monitoring of salt marsh habitats in GA and elsewhere with similar environmental settings will be feasible. Through continuous monitoring of the ecosystem, both at the landscape and site-specific scale, it will be possible to ascertain whether salt marshes will continue to be a major carbon sink in the environment, or changes in the environment will force it to become a carbon source or at the best carbon neutral. As mentioned before, salt marshes are dynamic and critical ecosystems in terms of carbon sequestration. Therefore, continuous monitoring of these critical ecosystems is crucial for effective restoration and management practices and formulation of global change policies.

Acknowledgements

This project was funded by Deepak Mishra's NASA grant#NNX14AR30G and the Georgia Coastal Ecosystems LTER, which is supported by the National Science Foundation (OCE12-37140).We are thankful to the NASA Develop Georgia Ecological Forecasting team members Steve Padgett-Vasquez, Joe White, Ning Chen, Jiaying He, Pradeep Kumar and Auryn Baruch, for helping us with the data processing. We thank Jessica O'Donnell for providing us the R code for processing PhenoCam images. Shuvankar Ghosh is grateful to the University of Georgia Graduate School Dean's Award and the Summer Doctoral Research Fellowship for Social Science for carrying out this research.

References

Ahl, D. E., Gower, S. T., Burrows, S. N., Shabanov, N. V., Myneni, R. B., and Knyazikhin, Y. 2006. Monitoring spring canopy phenology of a deciduous broadleaf forest using MODIS. *Remote Sensing of Environment*, 104, 88-95.

Ahrends, H. E., Brügger, R., Stöckli, R., Schenk, J., Michna, P., Jeanneret, F., Wanner, H. and Eugster, W. 2008. Quantitative phenological observations of a mixed beech forest in northern Switzerland with digital photography. *Journal of Geophysical Research: Biogeosciences*, 113, DOI: 10.1029/2007JG000650.

Ainsworth, E. A., and Long, S. P. 2005. What have we learned from 15 years of free-air CO2 enrichment (FACE)? A meta-analytic review of the responses of photosynthesis, canopy properties and plant production to rising CO_2. *New Phytologist*, 165, 351-372.

Aono, Y., and Kazui, K. 2008. Phenological data series of cherry tree flowering in Kyoto, Japan, and its application to reconstruction of springtime temperatures since the 9th century. *International Journal of Climatology*, 28, 905-914.

Arora, V. K. 2002. The use of the aridity index to assess climate change effect on annual runoff. *Journal of Hydrology*, 265, 164–177.

Artigas, F., and Pechmann, I. C. 2010. Balloon imagery verification of remotely sensed Phragmites australis expansion in an urban estuary of New Jersey, USA. *Landscape Urban Plan.*, 95, 105-112.

Asner, G. P., and Alencar, A. 2010. Drought impacts on the Amazon forest: the remote sensing perspective. *New Phytologist*, 187, 569-578.

Atkinson, P. M., Jeganathan, C., Dash, J., and Atzberger, C. 2012. Inter–comparison of four models for smoothing satellite sensor time–series data to estimate vegetation phenology. *Remote Sensing of Environment*, 123, 400–417.

Bater, C. W., Coops, N. C., Wulder, M. A., Hilker, T., Nielsen, S. E., McDermid, G., and Stenhouse, G. B. 2011. Using digital time-lapse cameras to monitor species-specific understorey and overstorey phenology in support of wildlife habitat assessment. *Environmental Monitoring and Assessment*, 180, 1-13.

Beaubien, E. G., Freeland, H. J. 2000. Spring phenology trends in Alberta, Canada, links to ocean temperature. *International Journal of Biometeorology*,, 44, 53–59.

Bianchi T. S., Allison M. A., Zhao, .J, Li, X., Comeaux, R. S., Feagin, R. A., Kulawardhana, R. W. 2013. Historical reconstruction of mangrove expansion in the Gulf of Mexico: Linking climate change with carbon sequestration in coastal wetlands. *Estuarine, Coastal and Shelf Science*, 119, 7-16.

Brown, C. E., and Pezeshki, S. R. 2007. Threshhold for recovery in the marsh halophyte Spartina alterniflora grown under the combined effects of salinity and soil drying. *Journal of Plant Physiology*, 164, 274-282.

Callaway, J. C., Parker, V. T., Vasey, M. C., and Schile, L. M. 2007. Emerging issues for the restoration of tidal marsh ecosystems in the context of predicted climate change. *Madroño*, 54, 234-248.

Chambers, R. M., Osgood, D. T., Bart, D. J., and Montalto, F. 2003. *Phragmites australis* invasion and expansion in tidal wetlands: interactions among salinity, sulfide, and hydrology. *Estuaries and Coasts,* 26, 398–406.

Chen, X., Hu, B., and Yu, R. 2005. Spatial and temporal variation of phenological growing season and climate change impacts in temperate eastern China. *Global Change Biology*, 11, 1118–1130.

Chmura, G. L., Anisfeld, S. C., Cahoon, D. R., and Lynch, J. C. 2003. Global carbon sequestration in tidal, saline wetland soils. *Global Biogeochemical Cycles*, 17, DOI: 10.1029/2002GB001917

Cleveland, R. B., Cleveland, W. S., and Terpenning, I. 1990. STL, A seasonal–trend decomposition procedure based on loess. *Journal of Official Statistics,* 6, 3.

Connor, R. F., Chmura, G. L., and Beecher, C. B. 2001. Carbon accumulation in Bay of Fundy salt marshes, Implications for restoration of reclaimed marshes. *Global Biogeochemical Cycles*, 15, 943–954.

Craft, C., Clough, J., Ehman, J., Joye, S., Park, R., Pennings, S., Guo, H. and Machmuller, M. 2009. Forecasting the effects of accelerated sea-level rise on tidal marsh ecosystem services. *Frontiers in Ecology and the Environment*, 7, 73-78.

De Beurs, K. M., and Henebry, G. M. 2010. Spatio-temporal statistical methods for modelling land surface phenology. In: Hudson , I . L. and Keatley, M. R. (Eds.) *Phenological research* (pp. 177-208. Springer, Netherlands.

De Beurs, K. M., and Henebry, G. M. 2005. A statistical framework for the analysis of long image time series. *International Journal of Remote Sensing*, 26, 1551–1573.

DeLaune, R. D., and White, J. R. 2012. Will coastal wetlands continue to sequester carbon in response to an increase in global sea level?, a case study of the rapidly subsiding Mississippi river deltaic plain. *Climate Change*, 110, 297–314.

Delbart, N., Kergoat, L., Le Toan, T., Lhermitte, J., and Picard, G. 2005. Determination of phenological dates in boreal regions using normalized difference water index. *Remote Sensing of Environment*, 97, 26–38.

Dragoni, D., Schmid, H. P., Wayson, C. A., Potter, H., Grimmond, C. S. B., and Randolph, J. C. 2011. Evidence of increased net ecosystem productivity associated with a longer vegetated season in a deciduous forest in south-central Indiana, USA. *Global Change Biology*, 17, 886-897.

Elmore, A. J., Guinn, S. M., Minsley, B. J., and Richardson, A. D. 2012. Landscape controls on the timing of spring, autumn, and growing season length in mid-Atlantic forests. *Global Change Biology*, 18, 656-674.

Erickson, J. E., Megonigal, J. P., Peresta, G., and Drake, B. G. 2007. Salinity and sea level mediate elevated CO_2 effects on C_3–C_4 plant interactions and tissue nitrogen in a Chesapeake Bay tidal wetland. *Global Change Biology*, 13, 202–215.

Fisher, J. I., and Mustard, J. F. 2007. Cross–scalar satellite phenology from ground, Landsat, and MODIS data. *Remote Sensing of Environment*, 109, 261–273.

Gao, F., Morisette, J. T., Wolfe, R. E., Ederer, G., Pedelty, J., Masuoka, E., Myneni. R., Tan. B., and Nightingale, J. 2008. An algorithm to produce temporally and spatially continuous MODIS–LAI time series. *IEEE Geoscience and Remote Sensing Letters*, 5, 60–64.

Ghosh, S. and Mishra, D. R. (in review) Analyzing the long-term phenological trends of salt marsh ecosystem across coastal Louisiana, *Remote Sensing*.

Ghosh, S., Mishra, D. R., and Gitelson, A. A. 2016. Long–term monitoring of biophysical characteristics of tidal wetlands in the northern Gulf of Mexico – A methodological approach using MODIS. *Remote Sensing of Environment*, 173, 39–58.

Goodman, P. J., and Williams, W. T. 1961. Investigations into Die-back in *Spartina townsendii* Agg.: III. Physiological Correlates of Die-Back. *Journal of Ecology*, 391-398.

Graham, E. A., Hamilton, M. P., Mishler, B. D., Rundel, P. W., and Hansen, M. H. 2006. Use of a networked digital camera to estimate net CO_2 uptake of a desiccation-tolerant moss. *International Journal of Plant Science*, 167, 751-758.

Graham, E. A., Riordan, E. C., Yuen, E. M., Estrin, D., and Rundel, P. W. 2010. Public internet-connected cameras used as a cross-continental ground-based plant phenology monitoring system. *Global Change Biology*, 16, 3014-3023.

Gutman, G. G. 1991. Vegetation indices from AVHRR, An update and future prospects. *Remote Sensing of Environment*, 35, 121–136.

Heumann, B. W., Seaquist, J. W., Eklundh, L., Jönsson, P. 2007. AVHRR derived phenological change in the Sahel and Soudan, Africa, 1982–2005. *Remote Sensing of Environment*, 108, 385–392.

Hladik, C., Schalles, J., and Alber, M. 2013. Salt marsh elevation and habitat mapping using hyperspectral and LIDAR data. *Remote Sensing of Environment*, 139, 318-330.

Hopkinson, C. S., Cai, W. J., and Hu, X. 2012. Carbon sequestration in wetland dominated coastal systems—a global sink of rapidly diminishing magnitude. *Current Opinion in Environmental Sustainability*, 4, 186-194.

Howard, R. J., Travis, S. E., and Sikes, B. A. 2008. Rapid growth of a Eurasian haplotype of *Phragmites australis* in a restored brackish marsh in Louisiana, USA. *Biological Invasions*, 10, 369–379.

Howe A. J., Rodríguez, J. F., and Saco, P. M. 2009. Surface evolution and carbon sequestration in disturbed and undisturbed wetland soils of the Hunter estuary, southeast Australia. *Estuarine, Coastal and Shelf Science*, 84, 75-83

Huete, A. R., and Liu, H. Q. 1994. An error and sensitivity analysis of the atmospheric–and soil–correcting variants of the NDVI for the MODIS–EOS. *IEEE Transactions in Geoscience and Remote Sensing*, 32, 897–905.

Hufkens, K., Friedl, M., Sonnentag, O., Braswell, B. H., Milliman, T., and Richardson, A. D. 2012. Linking near-surface and satellite remote sensing measurements of deciduous broadleaf forest phenology. *Remote Sensing of Environment*, 117, 307-321.

Ide, R., and Oguma, H. 2010. Use of digital cameras for phenological observations. *Ecological Informatics*, 5, 339-347.

Jonsson, P., Eklundh, L. 2002. Seasonality extraction by function fitting to time–series of satellite sensor data. *IEEE Transactions in Geoscience and Remote Sensing*, 40, 1824–1832.

Jonsson, P., Eklundh, L. 2004. TIMESAT—a program for analyzing time–series of satellite sensor data. *Comput. Geosci.* 30, 833–845.

Kendall, M.G. (Ed.) 1970, Rank Correlation Methods, 4th ed., Griffin, London, UK

Klosterman, S. T., Hufkens, K., Gray, J. M., Melaas, E., Sonnentag, O., Lavine, I., Mitchell, L., Norman, R., Friedl, M.A. and Richardson, A. D. 2014. Evaluating remote sensing of deciduous forest phenology at multiple spatial scales using PhenoCam imagery. *Biogeosciences,* 4305 - 4320.

Kramer, K., Leinonen, I., Loustau, D. 2000. The importance of phenology for the evaluation of impact of climate change on growth of boreal, temperate and Mediterranean forests ecosystems, an overview. *International Journal of Biometeorology*, 44, 67–75.

Kunkel, K. E., Easterling, D. R., Hubbard, K., Redmond, K. 2004. Temporal variations in frost-free season in the United States, 1895–2000. *Geophysical Research Letters,* 31, DOI: 10.1029/2003GL018624

Kurc, S. A., and Benton, L. M. 2010. Digital image-derived greenness links deep soil moisture to carbon uptake in a creosote bush-dominated shrubland. *Journal of Arid Environment*, 74, 585-594.

Leakey, A. D. 2009. Rising atmospheric carbon dioxide concentration and the future of C_4 crops for food and fuel. *Proceedings of the Royal Society B: Biological Sciences,* 276, 2333–2343.

Li, S. and Pennings, S.C. 2016. Disturbance in Georgia salt marshes: variation across space and time. *Ecosphere*, 7, DOI: 10.1002/ecs2.1487.

McFarlin, C. 2012. Salt Marsh Dieback: The Response of *Spartina alterniflora* to Disturbances and the Consequences for Marsh Invertebrates, retrieved from University of Georgia Theses and Dissertations, url: http://purl.galileo.usg.edu/uga_etd/mcfarlin_caroline_r_201205_phd

Mcleod, E., Chmura, G. L., Bouillon, S., Salm, R., Björk, M., Duarte, C. M., Lovelock, C.E., Schlesinger, W.H. and Silliman, B. R. 2011. A blueprint for blue carbon: toward an improved understanding of the role of vegetated coastal habitats in sequestering CO_2. *Frontiers in Ecology and the Environment*, 9, 552-560.

Minchinton, T. E., and Bertness, M. D. 2003. Disturbance-mediated competition and the spread of Phragmites australis in a coastal marsh. *Ecological Applications*, 13, 1400–1416.

Mishra, D. R. and Ghosh, S. 2015. Using moderate resolution satellite sensors for monitoring the biophysical parameters and phenology of tidal wetlands. In: Tiner, R., Land, M. and Klemas, V. (Eds.) *Remote Sensing of Wetlands, Applications and Advances*, pp. 283 – 314, CRC Press, Boca Raton, Florida, USA.

Mishra, D. R., Ghosh, S., Hladik, C., O'Connell, J. L., and Cho, H. J. 2015. Wetland mapping methods and techniques using multi–sensor, multi–resolution Remote Sensing, Successes and Challenges. In: Thenkabail, P. S. (Ed.) *Remote. Sensing Handbook*, Vol. III, pp. 191 – 227, CRC Press, Boca Raton, Florida, USA.

Moody, E. G., King, M. D., Platnick, S., Schaaf, C. B., Gao, F. 2005. Spatially complete global spectral surface albedos, Value–added datasets derived from Terra MODIS land products. *IEEE Transactions in Geoscience and Remote Sensing*, 43, 144–158.

Morisette, J. T., Richardson, A. D., Knapp, A. K., Fisher, J. I., Graham, E. A., Abatzoglou, J., Wilson, B.E., Breshears, D.D., Henebry, G.M., Hanes, J.M. and Liang, L. 2009. Tracking the rhythm of the seasons in the face of global change: phenological research in the 21st century. *Frontiers in Ecology and the Environment*, 7, 253-260.

Myneni, R. B., Keeling, C. D., Tucker, C. J., Asrar, G., and Nemani, R. R. 1997. Increased plant growth in the northern high latitudes from 1981 to 1991. *Nature*, 386, 698.

NOAA Center for Operational Oceanographic Products and Services, NOAA Tides and Currents, Sea Level Trends, Retrieved on March, 2017, https,//tidesandcurrents.noaa.gov/sltrends/sltrends.html

NOAA Earth System Research Laboratory, Global Monitoring Division, Trends in Atmospheric Carbon Dioxide, retrieved February 14, 2016, https,//www.esrl.noaa.gov/gmd/ccgg/trends/graph.html

NOAA National Centers for Environmental information, Climate at a Glance, U.S. Time Series, published December 2016, retrieved on May 1, 2016, http://www.ncdc.noaa.gov/cag/

NOAA National Weather Service, retrieved on April 21, http://www.weather.gov/

O'Donnell, J. P., and Schalles, J. F. 2016. Examination of abiotic drivers and their influence on Spartina alterniflora biomass over a twenty-eight year period using Landsat 5 TM satellite imagery of the Central Georgia Coast. *Remote Sensing*, 8, 477.

O'Connell, J. L., and Alber, M. 2016. A smart classifier for extracting environmental data from digital image time-series: Applications for PhenoCam data in a tidal salt marsh. *Environmental Modelling and Software*, 84, 134-139.

Ogburn, M. B., and Alber, M. 2006. An investigation of salt marsh dieback in Georgia using field transplants. *Estuaries and Coasts*, 29, 54-62.

Palmer, S. C., Odermatt, D., Hunter, P. D., Brockmann, C., Presing, M., Balzter, H., Tóth, V. R. 2015. Satellite Rem. Sens of phytoplankton phenology in Lake Balaton using 10years of MERIS observations. *Remote Sensing of Environment*, 158, 441–452.

Palmer, W. C. 1965 *Meteorological drought*. U. S. Dept. of Commerce (Weather Bureau Research Paper No. 45), Washington, DC, USA.

Pennings, S. C., and Silliman, B. R. 2005. Linking biogeography and community ecology: latitudinal variation in plant–herbivore interaction strength. *Ecology*, 86: 2310–2319.

Pennings, Steven C. 2016): Long-term Plant Biomass Monitoring Data from the Georgia Coastal Ecosystems LTER Project on Sapelo Island, Georgia. Georgia Coastal Ecosystems LTER Project; University of Georgia; Long Term Ecological Research Network. (http://dx.doi.org/10.6073/pasta/20f7a203bcf5812c89e560184a93f0f7)

Primack, D., Imbres, C., Primack, R. B., Miller–Rushing, A. J., Del Tredici, P. 2004. Herbarium specimens demonstrate earlier flowering times in response to warming in Boston. *American Journal of Botany*, 91, 1260–1264.

R Core Team 2013. R, A language and environment for statistical computing. R Foundation for Statistical Computing, Vienna, Austria. ISBN 3-900051-07-0, http://www.R-project.org/

Reimold, R. J. 1977. Mangals and salt marshes of eastern United States. In: Chapman, V. J. (Ed.) *Wet coastal ecosystems of the world*, pp. 157-164. Elsevier Science, New York, USA.

Richardson, A. D., Braswell, B. H., Hollinger, D. Y., Jenkins, J. P., and Ollinger, S. V. 2009. Near-surface remote sensing of spatial and temporal variation in canopy phenology. *Ecological Applications*, 19, 1417-1428.

Richardson, A. D., Jenkins, J. P., Braswell, B. H., Hollinger, D. Y., Ollinger, S. V., and Smith, M. L. 2007. Use of digital webcam images to track spring green-up in a deciduous broadleaf forest. *Oecologia*, 152, 323-334.

Riddin, T., Adams, J. B. 2010. The effect of a storm surge event on the macrophytes of a temporarily open/closed estuary, South Africa. *Estuarine, Coastal and Shelf Science*, 89, 119–123.

Roerink, G. J., Menenti, M., Verhoef, W. 2000. Reconstructing cloudfree NDVI composites using Fourier analysis of time series. *International Journal of Remote Sensing*, 21, 1911–1917.

Running, S. W., Nemani, R. R. 1991. Regional hydrologic and carbon balance responses of forests resulting from potential climate change. *Climate Change*, 19, 349–368.

Scheifinger, H., Menzel, A., Koch, E., Peter, C., Ahas, R. 2002. Atmospheric mechanisms governing the spatial and temporal variability of phenological phases in central Europe. *International Journal of Climatology*, 22, 1739–1755.

Sellers, P. J., Tucker, C. J., Collatz, G. J., Los, S. O., Justice, C. O., Dazlich, D. A., Randall, D. A. 1994. A global 1° by 1° NDVI data set for climate studies, Part II. The generation of global fields of terrestrial biophysical parameters from the NDVI. *International Journal of Remote Sensing*, 15, 3519 – 3545.

Shen, M., Tang, Y., Chen, J., Zhu, X., and Zheng, Y. 2011. Influences of temperature and precipitation before the growing season on spring phenology in grasslands of the central and eastern Qinghai-Tibetan Plateau. *Agriculture and Forest Meteorology*, 151, 1711-1722.

Silliman, B. R., and Bertness, M. D. 2002. A trophic cascade regulates salt marsh primary production. *Proceedings of the National Academy of Sciences, USA*, 99, 10500-10505.

Silliman, B. R., and Bertness, M. D. 2004. Shoreline development drives invasion of *Phragmites australis* and the loss of plant diversity on New England salt marshes. *Conservation Biology*, 18, 1424–1434.

Song, Q., Zhang, G., and Zhu, X. G. 2013. Optimal crop canopy architecture to maximise canopy photosynthetic CO_2 uptake under elevated CO_2–a theoretical study using a mechanistic model of canopy photosynthesis. *Funct. Plant Biol.*, 40, 108-124.

Sonnentag, O., Detto, M., Vargas, R., Ryu, Y., Runkle, B. R. K., Kelly, M., and Baldocchi, D. D. 2011. Tracking the structural and functional development of a perennial pepperweed (*Lepidium latifolium* L.) infestation using a multi-year archive of webcam imagery and eddy covariance measurements. *Agriculture and Forest Meteorology*, 151, 916-926.

Sonnentag, O., Hufkens, K., Teshera-Sterne, C., Young, A. M., Friedl, M., Braswell, B. H., Milliman, T., O'Keefe, J. and Richardson, A. D. 2012. Digital repeat photography for phenological research in forest ecosystems. *Agriculture and Forest Meteorology*, 152, 159-177.

Stralberg, D., Brennan, M., Callaway, J. C., Wood, J. K., Schile, L. M., Jongsomjit, D., Kelly, M., Parker, V.T. and Crooks, S. 2011. Evaluating tidal marsh sustainability in the face of sea-level rise: a hybrid modeling approach applied to San Francisco Bay. *PloS One*, 6, e27388.

Suepa, T., Qi, J., Lawawirojwong, S., Messina, J. P. 2016. Understanding spatio–temporal variation of vegetation phenology and rainfall seasonality in the monsoon Southeast Asia. *Environmental Research*, 147, 621–629.

Tan, B., Morisette, J. T., Wolfe, R. E., Gao, F., Ederer, G. A., Nightingale, J., Pedelty, J. A. 2011. An enhanced TIMESAT algorithm for estimating vegetation phenology metrics from MODIS data. *IEEE Journal of Selected Topics in Applied Earth Observation and Remote Sensing*, 4, 361–371.

US Fish and Wildlife Service, National Wetlands Inventory, Retrieved on April 1, 2016 https,//www.fws.gov/wetlands/Data/Data-Download.html

Valiela, I., Cole, M. L., Mcclelland, J., Hauxwell, J., Cebrian, J., and Joye, S. B. 2002. Role of salt marshes as part of coastal landscapes. pp. 23-36, In: Winston, M. P. and Kreeger, D. A. (Ed.) *Concepts and controversies in tidal marsh ecology*, Springer Netherlands, Dordrecht, South Holland, The Netherlands.

Verbesselt, J., Hyndman, R., Zeileis, A., Culvenor, D. 2010. Phenological change detection while accounting for abrupt and gradual trends in satellite image time series. *Remote Sensing of Environment*, 114, 2970–2980.

Vermote, E. F., Kotchenova, S. Y., Ray, J. P. 2011. *MODIS surface reflectance user's guide*. MODIS land surface reflectance science computing facility, version 1.

Viovy, N., Arino, O., Belward, A. S. 1992. The Best Index Slope Extraction (BISE), A method for reducing noise in NDVI time–series. *International Journal of Remote Sensing*, 13, 1585–1590.

Walker, J. J., De Beurs, K. M., Wynne, R. H., and Gao, F. 2012. Evaluation of Landsat and MODIS data fusion products for analysis of dryland forest phenology. *Remote Sensing of Environment*, 117, 381-393.

White, K. P., Langley, J. A., Cahoon, D. R., Megonigal, J. P. 2012. C_3 and C_4 biomass allocation responses to elevated CO_2 and nitrogen, contrasting resource capture strategies. *Estuaries and Coasts*, 35, 1028–1035.

White, M. A., Beurs, D., Kirsten, M., Didan, K., Inouye, D. W., Richardson, A. D., Jensen, O.P., O'keefe, J., Zhang, G., Nemani, R.R.and Leeuwen, V. 2009. Intercomparison, interpretation, and assessment of spring phenology in North America estimated from remote sensing for 1982–2006. *Global Change Biology*, 15, 2335-2359.

White, M. A., Thornton, P. E., Running, S. W. 1997. A continental phenology model for monitoring vegetation responses to interannual climatic variability. *Global Biogeochemical Cycles*, 11, 217–234.

Wilson, K. B., Baldocchi, D. D. 2000. Seasonal and inter–annual variability of energy fluxes over a broadleaved temperate deciduous forest in North America. *Agriculture and Forest Meteorology*, 100, 1–18.

Windham, L., and Ehrenfeld, J. G. 2003. Net impact of a plant invasion on nitrogen-cycling processes within a brackish tidal marsh. *Ecological Applications*, 13, 883–896.

Xiao, X., Braswell, B., Zhang, Q., Boles, S., Frolking, S., Moore, B. 2003. Sensitivity of vegetation indices to atmospheric aerosols, continental–scale observations in Northern Asia. *Remote Sensing of Environment*, 84, 385–392.

Zeng, H., Jia, G., Epstein, H. 2011. Recent changes in phenology over the northern high latitudes detected from multi–satellite data. *Environmental Research Letters*, 6, 045508.

Zhang, X., Friedl, M. A., Schaaf, C. B. 2006. Global vegetation phenology from Moderate Resolution Imaging Spectroradiometer (MODIS), Evaluation of global patterns and comparison with in situ measurements. *Journal of Geophysical Research: Biogeosciences*, 111, DOI: 10.1029/2006JG000217

Zhang, X., Friedl, M. A., Schaaf, C. B., Strahler, A. H. 2004. Climate controls on vegetation phenological patterns in northern mid-and high latitudes inferred from MODIS data. *Global Change Biology*, 10, 1133–1145.

Zhang, X., Friedl, M. A., Schaaf, C. B., Strahler, A. H., Hodges, J. C., Gao, F., Reed, B. Huete, A. 2003. Monitoring vegetation phenology using MODIS. *Remote Sensing of Environment*, 84, 471–475.

Zhao, J., Zhang, Y., Tan, Z., Song, Q., Liang, N., Yu, L., and Zhao, J. 2012. Using digital cameras for comparative phenological monitoring in an evergreen broad-leaved forest and a seasonal rain forest. *Ecological Informatics*, 10, 65-72.

Table 5.1. Seasonality Parameters estimated by TIMESAT

Seasonality Parameters	Description/ Phenological Interpretation	Unit
Start of Season (SOS)	Time at the beginning of growing season, when GBM begins to increase and photosynthesis starts	Julian Days from Jan 1
End of Season (EOS)	Time at the end of growing season, when GBM ends to decrease and photosynthesis stops completely	Julian Days from Jan 1
Peak of Season (POS)	Computed as the mean of the time-period for which the green-up process stops and brown-down starts; time when the GBM and photosynthesis reaches its maximum level	Julian Days from Jan 1
Length of Season (LOS)	Time from start to end of growing season	Days
Base Value	Mean of the minimum GBM values at the start (initial GBM) and end (final GBM) of growing season	GBM unit
Max Value	Maximum GBM value for the fitted function during the growing season/ GBM value during the peak of the growing season	GBM unit
Amplitude	Difference between base and max value; Maximum increase in canopy photosynthetic activity above the baseline	GBM unit
Left Derivative	Rate of Green-up; rate of increase of GBM value from the beginning till the peak of growing season	GBM unit/ 8 days
Right Derivative	Rate of Brown-down; rate of decrease of GBM value from the peak to the end of the growing season	GBM unit/ 8 days
Small Seasonal Integral	Integral of the function describing the season from start to end of season, above the base level; indicator of net canopy photosynthetic rate across the entire growing season	GBM unit
Large Seasonal Integral	Integral of the function describing the season from start to end of season; indicator of gross canopy photosynthetic rate across the entire growing season along with the base GBM	GBM unit

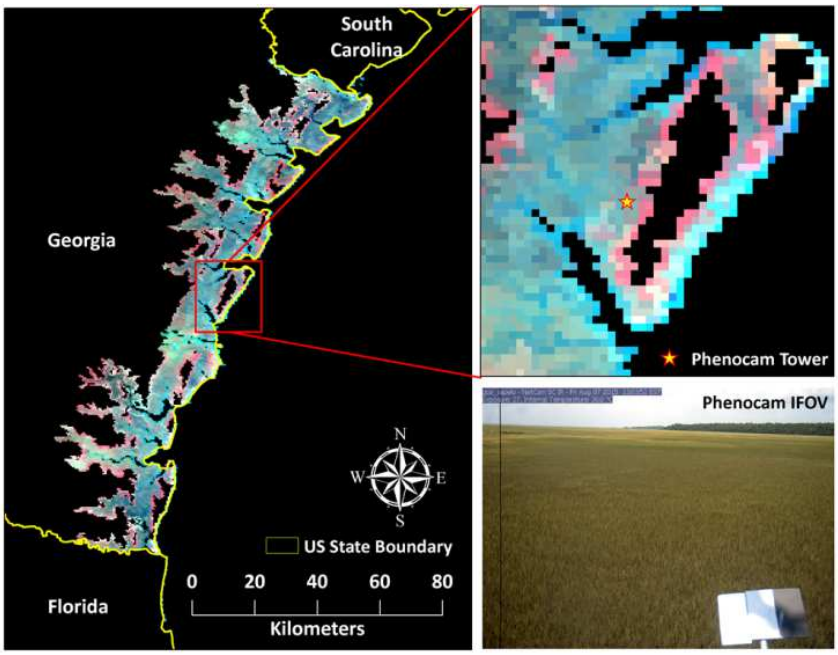

Figure 5.1: Salt Marsh extent in coastal Georgia, with location and IFOV of the PhenoCam tower (PhenoCam IFOV photo credit: Georgia Coastal Ecosystem LTER).

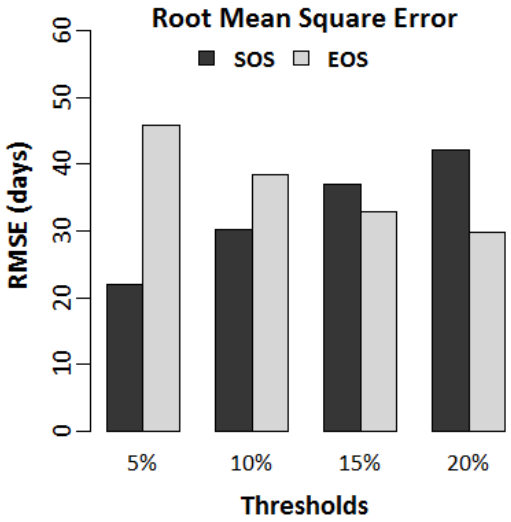

Figure 5.2: Root mean square error estimates for (a) start of season and (b) end of season dates between derivative analysis and TIMESAT thresholds for asymmetric Gaussian smoothing functions.

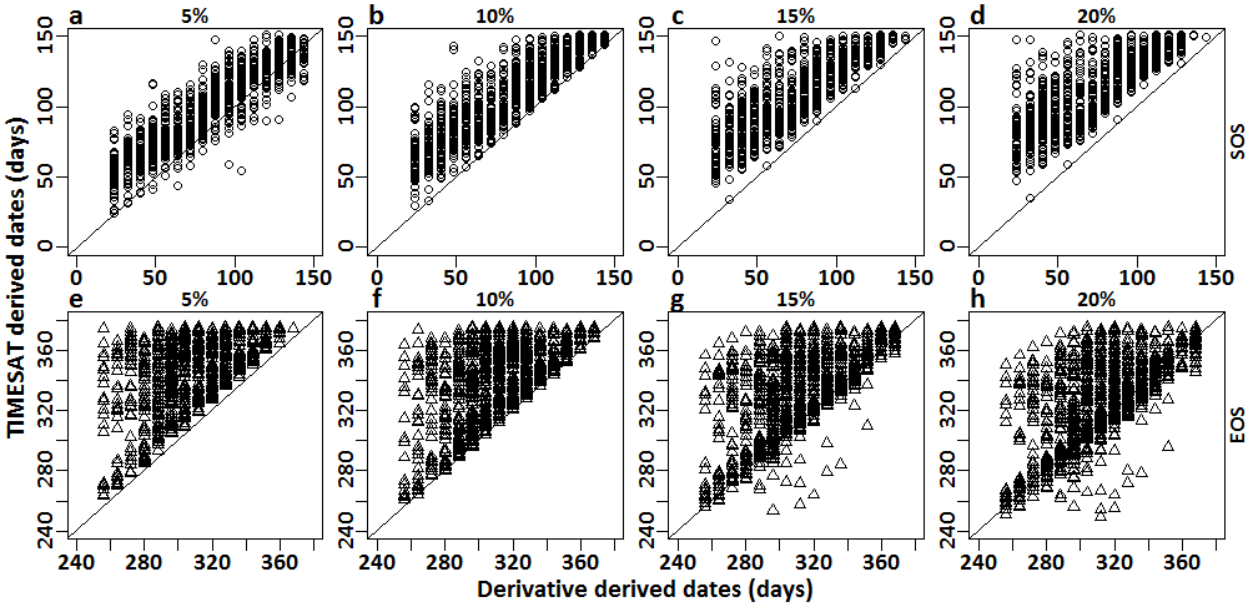

Figure 5.3: Residual plots matching Julian dates derived from derivative analysis (x-axis) and TIMESAT thresholds (y-axis) for start of season (a-d) and end of season (e-h) from randomly selected 400 pixels.

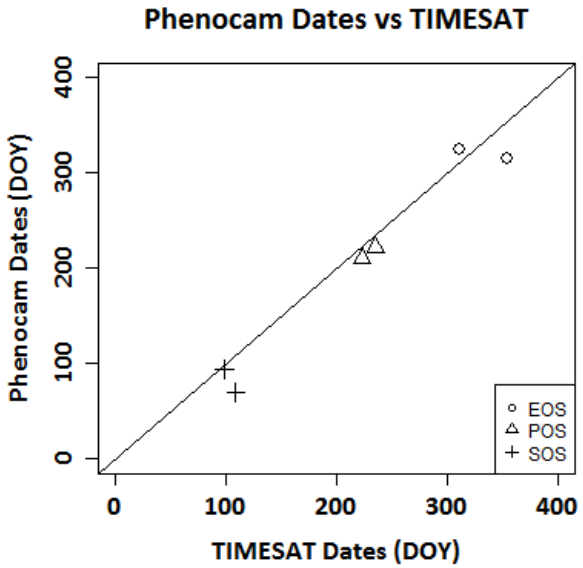

Figure 5.4: Residual plots matching phenological dates derived using the best TIMESAT thresholds (x-axis) and PhenoCam observed dates (y-axis).

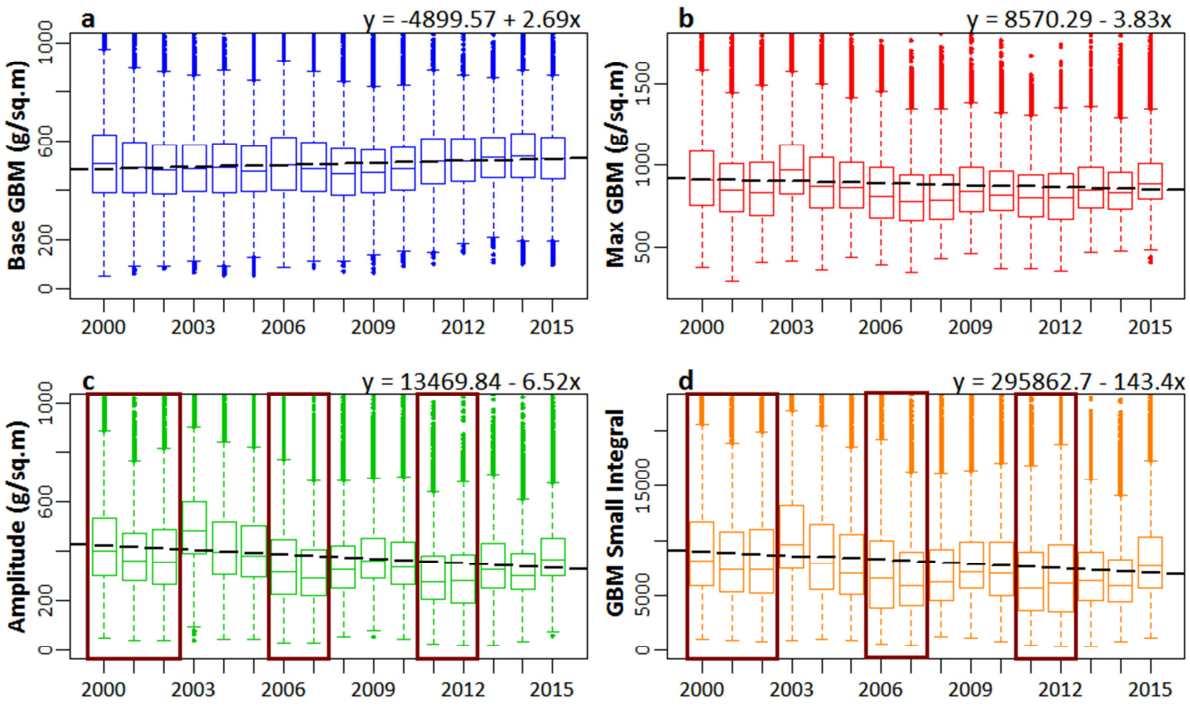

Figure 5.5: Linear trends in the seasonality parameters during the sixteen year time period (2000 – 2015): (a) Base GBM value, (b) Max GBM value, (c) seasonal amplitude and (d) small seasonal integral. Dotted line represents linear trend. Highlighted years in (c) and (d) indicate severe short term effects of dieback events and hurricane landfalls on seasonal amplitude and small seasonal integral.

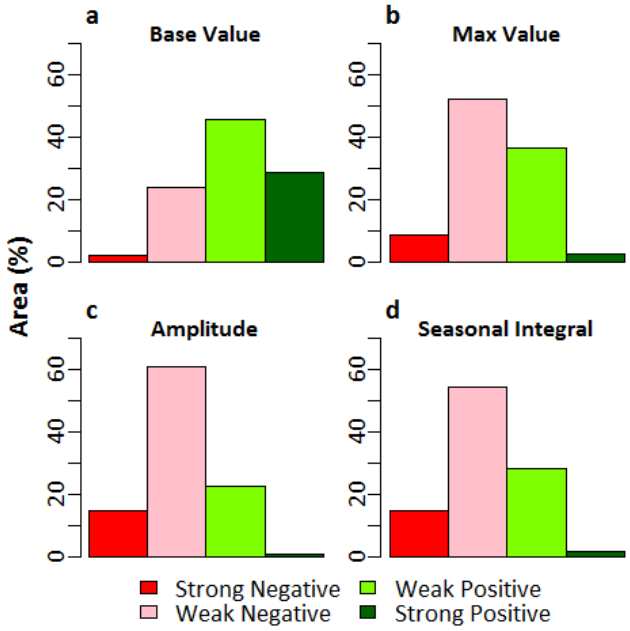

Figure 5.6: Percentage area coverage with different trends for (a) GBM base value, (b) GBM max value, (c) GBM amplitude and (d) GBM small seasonal integral for salt marshes in Georgia.

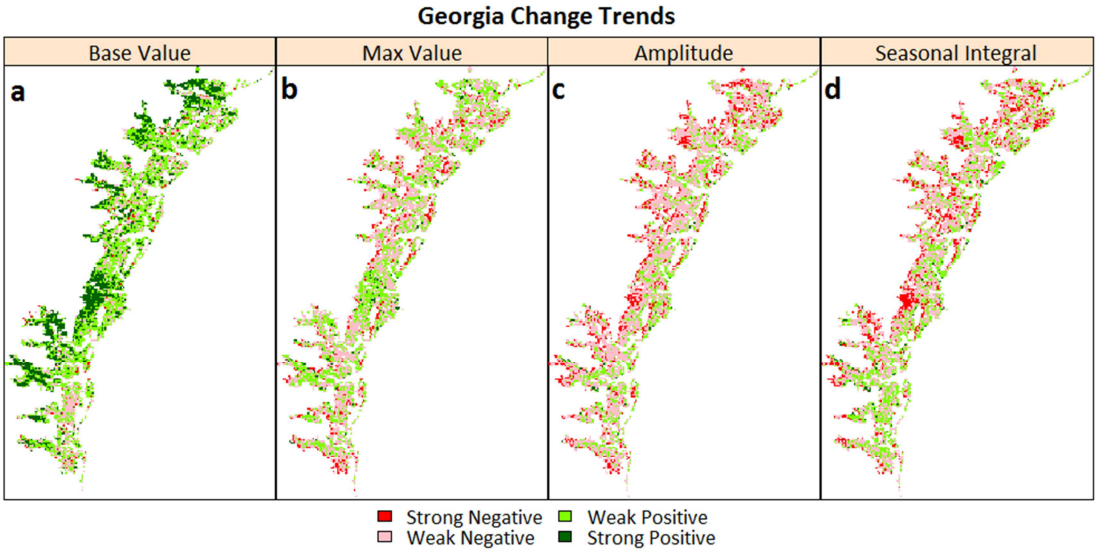

Figure 5.7: Spatial distribution of the areas showing different trends for (a) GBM base value, (b) GBM max value, (c) GBM amplitude and (d) GBM small seasonal integral for salt marshes in Georgia.

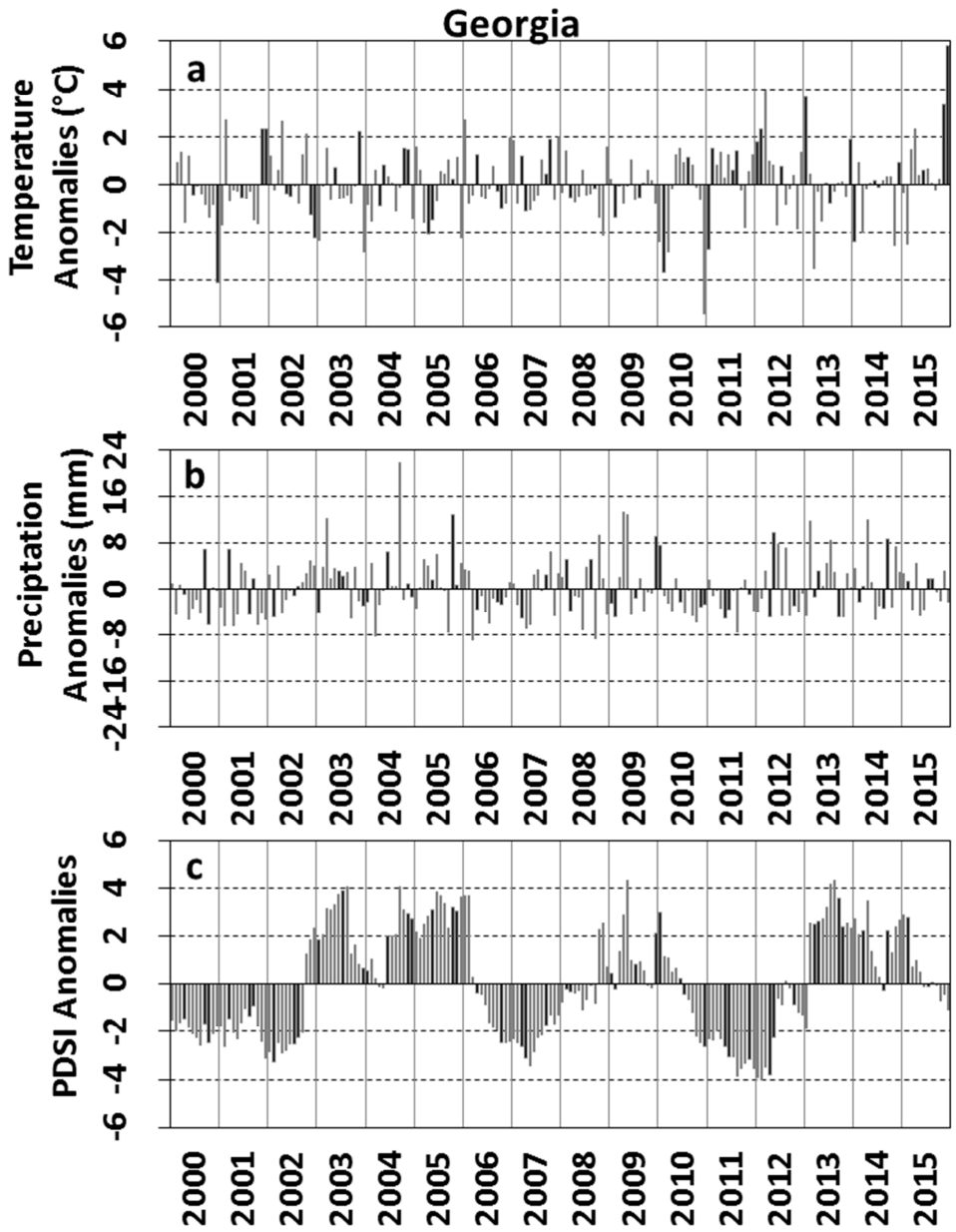

(a) Temperature, (b) Precipitation and (c) PDSI anomalies for southeast climatic zone of Georgia.

CHAPTER 6

DEVELOPING A MODIS BASED BIOPHYSICAL MODEL TO ESTIMATE AND ANALYZE LONG-TERM VARIATIONS IN GPP OF A SALT MARSH HABITAT IN NORTHERN GULF OF MEXICO[†]

[†]Ghosh, S., Cotten, D., and Mishra, D. R. Long-term trends in phenology of salt marsh ecosystem in Georgia using MODIS, to be submitted to *Biogeosciences*

Abstract:

We developed a protocol for mapping Gross Primary Productivity (GPP) for salt marshes using *in-situ* estimates of GPP from the eddy covariance CO_2 flux tower measurements and MODIS 8-day 500m surface reflectance derived Green Biomass (GBM) composites. Eddy Covariance flux tower was set in a salt marsh habitat within Grand Bay National Estuarine Research Reserve (GBNERR), in coastal Mississippi. Flux readings were acquired for two successive growing seasons (2015 – 2016). GPP was estimated from the flux towers and interpolated at 8 day intervals to match with MODIS derived GBM time-series. GPP was calibrated with both raw time-series GBM values derived from the MODIS composites as well as smoothed time-series GBM data values from 2015. Post calibration, the GPP model was validated using data and MODIS images acquired in 2016. Performance of the individual models was evaluated using combination of statistical parameters, such as co-efficient of determination (R^2), percent normalized root mean square error (%NRMSE), and residual analysis. Strong relationship was observed between smoothed GBM values and GPP ($p < 0.05$), while the relationship between the raw GBM values and GPP was insignificant ($p > 0.05$). %NRMSE was comparable; therefore GPP time-series products were generated using the statistical relationship established between smoothed GBM and GPP. The time-series GPP composites and the phenology derived from the composites were able to capture both intra-seasonal variability of GPP of the GBNERR salt marshes. They were also able to capture the inter-seasonal variability of GPP caused due to environmental events such as drought events or hurricane landfall. The study highlights the efficiency of MODIS images as well as GPP models in mapping GPP for salt marsh habitats. This is the first study attempting to develop models for mapping GPP for salt marsh habitats in the Gulf Coast, using MODIS images. The study has the potential to improve our understanding

long-term carbon sequestration potential of salt marsh habitats within the Gulf Coast, and similar salt marsh settings. These techniques could also be used to assess the success of previous and ongoing salt marsh restoration projects, and evaluate the long-term productivity trends of salt marshes under threat from natural and anthropogenic disasters.

Keywords: Salt Marsh; MODIS; Gross Primary Productivity; Eddy Covariance; CO_2 Flux; TIMESAT

Introduction

The potential of salt marshes as significant carbon sinks is well recognized (Connor et al. 2001; Chmura et al. 2003; McLeod et al. 2011). Rates of carbon dioxide sequestration in salt marshes have been reported to be higher than that of terrestrial forests, but uncertainties exist in the global area of salt marsh and the rates of carbon dioxide sequestration throughout each marsh (McLeod et al. 2011). The carbon burial rates reported for tidal salt marshes range from 18 to 1713 g C m^{-2} yr^{-1}; and considering the global extent of salt marshes between 22,000 to 400,000 km^2, these habitats could be storing 4.8 - 87.2 Tg C yr^{-1} (Mcleod et al. 2011). Furthermore, salt marshes can store carbon for millennia (Macreadie et al. 2013); the carbon stock often termed as 'blue carbon' (Nelleman and Corcoran, 2009). However, despite their value as carbon sinks, salt marsh habitats have experienced significant global reduction (~25% since the 1800s; Bridgham et al. 2006; Duarte et al. 2008), mostly due to developmental activities, conversion of marsh habitats to agriculture, sea-level rise and environmental hazards (Coverdale et al. 2013; Kennish, 2001; Mishra et al. 2012). Due to such natural and anthropogenic drivers, the environment is gradually losing a crucial carbon sink; significant amounts of carbon is being released in the form of carbon dioxide (CO_2) to the atmosphere due to disturbances, which, in turn, is accelerating global warming (Macreadie et al. 2013). In order to protect such invaluable resources, implementation of effective conservation and restoration of such habitats is crucial (Friess et al. 2012; Hinkle and Mitsch, 2005).

Long-term monitoring of biophysical properties of salt marsh habitats helps to understand current and future trends in both physiological health and productive status of marsh habitat (Ghosh et al. 2016; O'Donnell and Schalles, 2016). Gross Primary Productivity (GPP), defined as the total amount of energy produced by vegetation as biomass and a key component of

ecosystem carbon fluxes, is one of the most important biophysical characteristics and a key indicator of vegetation productivity and carbon sequestration capacity (Monteith 1972: Beer et al. 2010). GPP can be calculated as the sum of vegetation assimilated carbon flux, partitioned from net carbon exchange measured at eddy covariance (EC) tower sites (Baldocchi et al. 2001; Reichstein et al. 2007); although such observations are limited both temporally and spatially. Furthermore, the EC towers only provide integrated CO_2 flux measurements over the tower footprint ranging from a hundred meters to several kilometers at the ecosystem level (Gockede et al. 2008; Osmond et al. 2004). Satellite remote sensing can provide consistent observation of vegetation over large areas, and has been reported to be widely used for characterization of canopy structure and GPP estimation that can overcome the lack of extensive EC flux tower measurements (Running et al. 2000; Wu et al. 2010). Various diagnostic models taking advantage of spatially extensive remote sensing and meteorological data have been developed to estimate GPP across stand-to-global scales for a relatively long period (Jung et al.2008; Running et al. 2004; Sims et al. 2008; Xiao et al. 2005a, 2005b). These models can be generally categorized into three categories: light-use-efficiency (LUE) models, machine learning algorithms and canopy photosynthesis models (Verma et al. 2014).

The LUE theory was first proposed by Monteith (1972), in which GPP is generally represented as the product of LUE, photosynthetically active radiation (PAR), the fraction of PAR absorbed by vegetation (f_{APAR}),and environmental scalars. f_{APAR} is a strong function of vegetation greenness, as measured by vegetation indices (VIs), such as the normalized difference vegetation index (NDVI; Goward and Huemmrich, 1992) and the enhanced vegetation index (EVI; Xiao et al. 2004a,b). However, this approach is often limited by the difficulty of measuring LUE, and coarse resolution of climate data inputs (Xiao et al. 2005) which introduce significant errors in

GPP estimation models (Heinsch et al. 2006; Zhao et al. 2005). Machine learning algorithms, such as artificial neural networks (Papale and Valentini, 2003), support vector machines (Yang et al. 2007), and model tree ensembles (Jung et al. 2009), predict GPP based on the non-functional patterns extracted from training data set. Again, the accuracy of machine learning algorithms relies on the abundance and representativeness of input information including remote sensed vegetation properties, meteorological, and land cover data (Jung et al. 2011). Consequently, Canopy Photosynthesis Models (also called Vegetation Photosynthesis Models) have successfully demonstrated their great potential for scaling-up GPP from flux tower sites to the regional scale by integrating remote sensing proxies of vegetation health and flux measurements. These models have gained interest in the past decade among researchers for measuring GPP (e.g., Li et al. 2007; Xiao et al. 2004a, 2004b; Xiao et al. 2005a, 2005b; Wu et al.2009; Jung et al. 2008; Rahman et al. 2005; Sims et al. 2006).

Research efforts have focused on estimating GPP for terrestrial and aquatic vegetation using satellite imageries and flux tower observations such as boreal forest (Goulden et al. 1998; Baldocchi 2003), peatlands (Lafleur et al. 2005; Wille et al. 2008), grasslands (Ponton et al. 2006), and crops (Baker and Griffis 2005). However, similar methods for studying GPP of salt marsh ecosystem have been lacking. In the last century, field based harvesting methods proposed and used for GPP estimation in salt marshes have yielded discrepant results, with estimates of GPP ranging from 750 – 2600 $g/m^2/yr$, depending on the methods adopted and integration of measurements (Kaswadji et al. 1990). Effective conservation and restoration of salt marsh ecosystem requires precise information regarding their actual productivity, especially rising atmospheric carbon dioxide and sea-levels pose a significant threat to the long-term health and productivity of these habitats. Gitelson et al. (2006) suggested estimating GPP remotely by

exploiting the consistent and not species-specific relationship between total crop chlorophyll (CHL) content and the low frequency variation of GPP. Results showed that the product of total CHL and PAR explained more than 98% of GPP variation in both irrigated and rain-fed maize and soybean crops. Therefore, a procedure for remotely assessing GPP of crops and other vegetation types may be implemented through the estimation of total CHL content. Changes in CHL content induce large differences in canopy reflectance. Several algorithms and indices have been proposed for CHL estimation, most notably by Gitelson et al. (2003), using R_{green}, R_{NIR}, and $R_{red\text{-}edge}$, and finally estimation of GPP using statistical relationships between CHL and GPP. Similar relationships can also be established between GPP and other plant biophysical parameters such as Green Leaf Area Index (GLAI), Vegetation Fraction (VF), and Green Biomass (GBM).

In this study, we developed a GPP estimation algorithm combining *in-situ* estimations of GPP from flux towers and MODIS derived GBM (Ghosh et al. 2016) for the long-term monitoring of salt marsh habitats at the Grand Bay National Estuarine Research Reserve (GBNERR), Mississippi. At first, we established a statistical relationship between MODIS derived GBM and *in-situ* observations of GPP, after which we generated time-series GPP composites and derived phenology to study the spatio-temporal trends in GPP of GBNERR salt marshes for a seventeen-year time period (2000 – 2016). Remote estimation of GPP has not been attempted before for salt marsh habitats in the Gulf coast. The models and products developed through this study will potentially improve our understanding long-term carbon sequestration potential of salt marsh habitats within the Gulf Coast.

Study Area

The GBNERR, located in southeastern Jackson County, Mississippi spanning over 75 km^2, is one of the largest estuarine systems in the state (Figure 6.1). The salt marshes in the southern part of the refuge are dominated by *Spartina alterniflora*, *Juncus roemerianus*, and *Spartina patens*. These salt marsh plants are distributed over most of the salinity range from brackish to saline marshes (Mississippi Department of Marine Resources 1998). The estuarine areas are composed of low, mid, and high marsh zones. The regularly flooded low marsh area consists of *Spartina alterniflora*. The irregularly flooded mid-marsh zone is dominated by *Juncus roemerianus*, typically occupying most of the zone in pure stands or intermixed with *Distichlis spicata* in some areas. *Distichlis spicata* occurs as pure stands or with *Scirpus robustus* and *Scirpus americanus*. The high marshes are typically dominated by *Spartina patens*, with occasional associations with *Distichlis spicata* and *Salicornia virginica* and short *Juncus roemerianus*. Other high marsh inhabitants are *Limonium carolinianum*, *Agalinis maritima*, *Fimbristylis caroliniana*, and *Borrichia frutescens*. Scattered across the reserve are small but distinct, sparsely vegetated zones with pore salinities ≥ 30 psu, called salt pans or flats, which are usually associated with the high marsh, but also occur along mid and low-marshes. The hypersaline areas are typically inhabited by *Salicornia virginica* and *Salicornia bigelovii*, with B*atis maritima* and *Suaeda linearis* found at the fringes.

Mean maximum summer air temperatures vary between 20 – 32° C (mean of 27.6° C), with mean monthly precipitation ranging between 10.7 to 12.7 cm. July and August are the wettest, with a mean of 83.8 cm of precipitation. Precipitation in the dry, early fall months is usually reduced, with a maximum mean total during October and November of 30.5 cm and a minimum of 12.7 cm. Between December and March, mean precipitation ranges from 20.3 –22.9 cm per

month. The mean temperature in October and November ranges between 16 – 20° C with winter (December through February) temperatures ranging between 5 – 17° C and a mean of 11° C. Late summer and early fall is characterized by cyclonic activities in the Gulf of Mexico. Hurricane Katrina (2005), by far the most extensive and catastrophic storm ever recorded in the Gulf, inundated a large portion of the Mississippi coast, including the entire GBNERR. Storm surge elevation at Bay St. Louis, Mississippi reached 8.2 m above sea level (National Weather Service, 2006).

Material and Methods

a. Flux tower measurement:

We measured carbon dioxide (CO_2) fluxes using the eddy covariance technique during the period of January – December of 2015–2016. An open path CO_2/H_2O infrared gas analyzer (model LI-7500A, https://www.licor.com/env/products/gas_analysis/LI-7500RS/) was deployed at a salt marsh location at GBNERR dominated by *Juncus roemarianus* (Figure 6.1). Photosynthetically Active Radiation (PAR) was measured using LI-190R Quantum Sensor (model LI - 190, https://www.licor.com/env/products/light/quantum.html). Wind velocity and sonic temperature were measured by a WindMaster Pro 3–D sonic anemometer (model: WindMaster Pro, http://gillinstruments.com/products/anemometer/windmaster.htm#sonicanemometer) mounted along with the CO_2/H_2O infrared gas analyzer 3.05 m aboveground with the micrometeorological measurements recorded at a frequency of 10 Hz. The average canopy height of the vegetation near the tower was 1.2 – 1.3m. We assumed the fetch to be almost 100 times the magnitude of the flux measurement height. The data were stored as GHG files on a USB memory drive via analyzer interface unit (model LI-7550, LI-COR Biosciences, Inc.)

b. Data processing and Quality control:

Raw data were processed to fluxes with an averaging interval of 30 minutes using the EddyPro software (Version 6.0; https://www.licor.com/env/products/eddy_covariance/eddypro.html). Since we used the Gill Anemometer, we used the field calibration method from Nakai and Shimoyama (2012) to correct for the angle of attack. A planar fit method was applied for tilt correction (Wilczak et al. 2001) and turbulent fluxes were calculated using linear de-trending. Time lags between the sonic anemometer and the gas analyzer were compensated for by using the covariance maximization with default method. This method determines the time lag between the two high frequency sensors by maximizing their covariance within a plausible window, using the methods described by Fan et al. (1990). To incorporate effects on traces gas measurements specifically water vapor, the air density fluctuations based on air temperature and pressure fluctuations were compensated using the WPL method Webb et al. (1980).

Quality assurance was determined by using the methods of Mauder and Foken (2004). This method consists of a 0-1-2 system that flags time stamps based on the quality of fluxes for that time period. For this study anything with a 2, poor quality fluxes, was excluded while anything intermediate, 1, or lower, 0, was used for final analysis. The flux footprint was determined using a one dimensional estimation described by Kljun et al. (2004). However, the friction velocity cut off we used ensured we never had fetches outside of the study area. EddyPro 6.0 default statistical analysis methods were used to get rid of any outlier information. Co-spectra were filtered according to Vickers and Mahrt (1997). Low frequency spectral correction was used as well as high frequency corrections using the fully analytic methods of Moncrieff et al. (1997).

c. Gap-filling and flux partitioning

We created a modeled respiration (R) data set based on the relationship between air temperature and nighttime efflux (Reichstein et al. 2005). Gaps at night were filled with the modeled respiration data set. Gaps during the day were filled using modeled daytime net uptake calculated from a three parameter hyperbolic fit between CO_2 uptake and incoming Photosynthetic Photon Flux Density (PPFD) (Falge et al. 2001). Threshold in friction velocity (u^*) for nighttime fluxes was set to 0.2 m/s for the two seasons of data (Papale et al. 2006). After applying the friction velocity cutoff, removing missing data, and removing poor quality data 57% of the observations were removed (72% of the nighttime fluxes and 50% of the daytime fluxes). Finally, GPP was estimated as the difference between Net Ecosystem Exchange (NEE) and Respiration (R) as follows:

$$GPP = NEE - R \quad (1)$$

The GPP data integrated over 30 min interval were further integrated to estimate daily, and finally averaged over 8 day time period to estimate 8 day average GPP, to match with MODIS derived 8 day average GBM.

d. MODIS data:

The MODIS Land Science Team provides several data products derived from MODIS observations to the public, including the 8-day composite Land Surface Reflectance (MOD09A1). The MOD09A1 datasets include seven spectral bands at a spatial resolution of 500m corrected for the effects of atmospheric gases, aerosols, and thin cirrus clouds (Vermote et al. 2011). We generated time-series composites for GBM for the salt marshes of GBNERR, for a sixteen year period (2000 – 2016) using MODIS 8–day surface reflectance data (500m) and

biophysical models which are described in Ghosh et al. (2016). The GBM biophysical model, as described in Ghosh et al. (2016) was developed using MODIS surface reflectance and *in-situ* estimates of GBM from 200 study plots across the northern Gulf of Mexico. The model has an inherent percent normalized root mean square error of 17.34% in GBM estimation. While generating GBM composites, we utilized MODIS quality assurance bands to retain only the best quality pixels in the time-series composites (Vermote et al. 2011; Ghosh et al. 2016). However, tidal correction was not performed, as it is not possible to determine the level of daily MODIS scene contribution to the 8-day surface reflectance imagery, which would otherwise, had helped correcting for tidal signals using daily tidal fluctuation data (Ghosh et al. 2016). Since the MODIS surface reflectance products have a temporal resolution of 8 days, 46 GBM composites were generated per year for GBNERR; thus, for the seventeen year study period, 782 composites were generated in total. These images were utilized for derivation of phenology from the flux tower location. Since we set the cut-off of the footprint of the flux tower to 100m, and the footprint extended over two pixels, we estimated the average of the GBM phenology from the two pixels. Once subsets were generated for salt marshes of GBNERR, we derived both raw and smoothed (using TIMESAT; discussed in the following section) GBM phenology from the times-series composites for the tower and adjacent pixels to match with the flux tower derived GPP (Figure 6.2).

e. Climate data

We compiled temperature, precipitation and Palmer Drought Severity Index (PDSI) (Palmer, 1965) data for the MS Coastal climatic zone from the National Climate Data Centre (NCDC) (National Climate Data Centre, https://www.ncdc.noaa.gov) archives, to investigate any

significant temperature, precipitation and PDSI anomalies during the sixteen-year period that might potentially contribute to the variability in salt marsh GPP phenological trends.

f. TIMESAT

In addition to investigating the relationship between MODIS derived raw GBM and GPP observations, we also derived noise-free GBM time-series to match with the flux tower derived GPP. Therefore, we converted the raw GBM composites to 16 bit signed generic binary format for running the MATLAB based program TIMESAT, to generate pixel-wise noise-free time-series of GBM. TIMESAT (http://web.natleko.lu.se/timesat/timesat.asp) provides options to fit smooth continuous curve to raw time-series data using Asymmetric Gaussian (AG), Double Logistic (DL) and/or Savitzky Golay (SG) filters. In these methods local model functions are fitted to data in intervals around maxima and minima in the time-series (Jonsson and Eklundh, 2002, 2004).

For AG smoothing function, the basis function becomes:

$$g(t; x_1, x_2, \ldots, x_5) = \begin{cases} exp\left[-\left(\frac{t-x_1}{x_2}\right)^{x_3}\right], & if\ t > x_1 \\ exp\left[-\left(\frac{x_1-t}{x_4}\right)^{x_5}\right], & if\ t < x_1 \end{cases} \quad (2)$$

For this function x_1 defines the position of the maximum or minimum with respect to the independent time variable t; x_2 and x_3 determine the width and kurtosis of the right function half; while, x_4 and x_5 determines the same of the left function half.

The AG and the DL filters have been found to produce similar results, with the AG filter being less sensitive to incomplete baseline time-series data (Gao et al. 2008). We tested both filters for generating noise-free time-series and then extracting seasonality parameters. The SG filter was

not considered to be ideal for deriving smooth time-series as it is too much susceptible to localized noise in the raw phenology generated from the time-series images and hence might provide erroneous estimates of seasonality parameters (Tan et al. 2011). We used the STL method to remove spikes and outliers in the time-series. The STL method removes outliers by assigning weights to the values in time-series based on STL decomposition. This method does not depend on ancillary data, and is global in nature (Cleveland et al. 1990). Further, we also eliminated any negative or zero values observed in the raw phenology from our analysis. We specified an adaptive middle envelope (Jonsson and Eklundh, 2002, 2004). We specified and adaptation strength of 2, as stronger adaptation strength is likely to put too much emphasis on single high data values leading to erroneous estimates of phenology (Jonsson and Eklundh, 2002, 2004).

Analysis

a. Model calibration and validation:

The main goal of model calibration was to establish relationships between MODIS derived GBM time series and flux tower based GPP estimates. Model calibration and validation was performed using 2015 and 2016 flux tower measurements respectively. We performed calibrations using GPP and both raw and smoothed GBM phenology, using simple linear regression. Since the footprint of the flux tower extended over two adjacent marsh pixels, both the raw and the smoothed phenology were averaged for the two pixels for matching with the GPP estimates from the flux tower. Once a statistical relationship was established between MODIS GBM and GPP, the models were validated using MODIS GBM and GPP data from 2016. Performance uncertainties were analyzed based on percent normalized root mean squared error (percent

NRMSE) (Mishra et al. 2012; Ghosh et al. 2016), and residuals (observed–predicted). Percent NRMSE is estimated as:

$$percent\ NRMSE = \frac{RMSE}{MAX(Validation\ Data) - MIN(Validation\ Data)} \times 100 \quad (3)$$

b. Time-series composites and phenology/seasonality characterization

Following successful calibration and validation, 8-day time-series composites of GPP were generated using TIMESAT and ERDAS Imagine (ERDAS Imagine, Hexagon Geospatial, Norcross, GA) from 2000 to 2016 using the best GPP model. For an entire year, 46 GPP composites were obtained; therefore, for the seventeen year study period, a total of 782 GPP composites were generated. These composites were then used for qualitative assessments of GBNERR salt marsh condition in response to significant environmental events, such as hurricanes and droughts over the period of 2000–2014. In addition, phenology charts for GBNERR were derived from these time-series composites, for the growing seasons over the course of seventeen years. The phenology charts were matched with the climatic data acquired from NOAA NCDC archives, to examine the effects of the climatic parameters on both inter and intra-annual variability in GPP of GBNERR salt marshes. Further, we also investigated the possible impacts of discrete natural and anthropogenic events, such as tropical storm landfalls and drought induced dieback events on the short-term and long-term health of GBNERR salt marsh habitats.

Results and Discussion

a. Calibration and Validation:

We observed a no significant relationship ($r^2 = 0.01$; $p > 0.05$) between raw GBM values and GPP (Figure 6.3a). On the other hand, the relationship between smoothed GBM and GPP was significantly stronger ($r^2 = 0.84$; $p < 0.05$) (Figure 6.3b), with %NRMSE value of 37.59%. One of the reasons for observation of no significant relationship between raw GBM values and GPP may be due to the footprint of the flux tower extending over two adjacent MODIS pixels. Although, MODIS QA/QC data were utilized to minimize the effect of any atmospheric noise, localized noise generated beyond the footprint of the flux tower, as well as pixel heterogeneity, manifested itself in the MODIS surface reflectance; thus weakening the relationship between GBM and GPP. This limitation was overcome using smoothed GBM values using the AG smoothing function, which minimized the effects of those noises, thus increasing the signal to noise ratio in the MODIS derived GBM. Therefore, we selected the linear relationship between the GPP and smoothed GBM values for generating time-series GPP composites for the GBNERR salt marshes.

b. Time-series composites

The time-series map composites that we generated for the seventeen years using the best GPP model for 500 m data provided relevant qualitative assessment of the GPP status of the GBNERR salt marshes (Figure 6.4). The GPP model was able to illustrate the effects of the large scale natural disasters affecting the region. For example, monthly GPP composites of 2000 shows GPP levels consistently low throughout the entire growing season (Figure 6.4a), which might be due to the effect of the prevailing drought conditions during the growing season of

2000. The year 2000 was characterized by severe drought that affected the growth and productivity of salt marsh habitats at GBNERR; monthly PDSI values of the Mississippi Coastal Climatic division, for the year 2000 corroborates severe drought conditions with PDSI values ranging between -2 to -6. It is evident from these examples that the GPP model developed in this study has been able to capture the effects of the environmental events that have affected the salt marsh growth and productivity.

In addition, monthly GPP composites from the year 2005 clearly shows the stress induced on the salt marsh habitats by Hurricane Katrina (Figure 6.4b), Hurricane Katrina hit the Mississippi Gulf Coast as a Category 3 storm on August 29 at the Mississippi/Louisiana border, with an estimated wind speed of 190 km/h (118 mph), that generated storm surges of almost 8m above sea level, as measured in Grand Isle, Mississippi (National Weather Service; http://www.weather.gov/); and caused massive destruction to the salt marshes, with most of the marsh habitats being converted to open water (Evans et al. 2012). As evident from the GPP time-series composites of 2005, GPP was clearly reduced in the month of September. The effect of the landfall of the hurricane and the associated storm surge actually caused an early end of the growing season of salt marsh habitats of GBNERR. Salt marshes of the Gulf coast usually attain peak growth and photosynthetic activity between July-September, before entering the period of senescence from October till the beginning of the subsequent growing season. An example would be the GPP composited of GBNERR from the year 2009 (Figure 6.4c).

The results demonstrated the utility of such high frequency GPP time-series composites, not only in terms of identifying the extent and magnitude of physical damage to marsh patches after environmental disasters, but also aiding restoration and conservation activities. The high temporal resolution of the MODIS products allows for frequent monitoring, leading to rapid

initiation of restoration efforts after disturbances and targeted monitoring of the restored habitats. Further, these time-series composited can be utilized from long-term GPP phenological trend analysis to analyze long-term carbon sequestration potential of the marsh habitats and identifying potential sources and sinks within marsh habitats.

c. Phenology Charts

In addition, phenological charts derived from the time-series composites illustrate the trends in the biophysical values quantitatively. The GPP model enabled us to develop seventeen years of high frequency GPP phenology for the GBNERR salt marshes (Figure 6.5). The GPP levels as predicted by the GPP model developed in this study range between ~0.2 $kgCm^{-2}y^{-1}$ at the beginning of the growing season to ~1.1 $kgCm^{-2}yr^{-1}$ at the peak of the growing season. Although, salt marsh GPP using a biophysical approach has not been attempted before, the predicted values are within the range of GPP values observed by Kaswadji et al. (1990).

A closer investigation of GPP phenology from specific years such as 2000, 2006, and 2011 reveals reduced GPP levels in the peak of the growing season, with median GPP levels of the peak growing season months (median of GPP for July, August and September) below the seventeen year median values (median of GPP of July – September for 2000 – 2016) (Figure 6.6a – c). Compared to these, 2009 was a better growing season (Figure 6.6d), when median GPP levels during the peak of the growing season were above the seventeen year median level. Since temperature during the peak of the growing season remained almost similar during these years, the reduced GPP levels during 2000, 2006 and 2011, can probably be attributed to the drought conditions; PDSI values during the growing seasons of these years indicate severe drought (PDSI < -2) (Figure 6.6e – g), compared to 2009 (PDSI > -2) (Figure 6.6h). The reduction in GPP in

2006 may also have been enhanced by the damage caused by the storm surges during the landfall of Hurricane Katrina, at peak of the 2005 growing season. The dominant species in salt marsh ecosystem respond differently to drought conditions; while massive dieback has been frequently reported in *Spartina* during drought conditions, *Juncus* has been found to be more tolerant (McKee et al. 2004; Alber et al. 2008). Since the MODIS based biophysical model for mapping GBM and GPP is species invariant, and species signals get diluted at the spatial resolution of MODIS (Ghosh et al. 2016), it is difficult to separate the responses of the two species from the GPP phenology.

The GPP for the 2005 growing season reveals the stress induced by the storm surge generated due to the landfall of Hurricane Katrina (Figure 6.7a-b). The stress induced by the storm surge is evident from the sudden reduction in the levels of GPP in the month of September. Salt marshes usually achieve their peak productive levels between the months of July – September, following which they enter the period of senescence from the month of October. The landfall of the Hurricane actually brought an advanced end to the season in 2005. The extent of stress is also visible from the comparison of the time-series composites pre and post-landfall of Hurricane Katrina.

In addition to environmental events captured through the GPP phenology analysis, other fluctuations were also seen in the seasonal trends of the GPP values; these may have been a result of natural variability, localized disturbances, or model uncertainty. It cannot be denied that such phenological analysis not only provide both qualitative and quantitative estimates of site specific salt marsh productivity along with their seasonal variability, but also helps analyzing long-term trend of the salt marsh health. Currently, MODIS is the only operational sensor that provides atmospherically corrected fine temporal cloud free products which are necessary for

high frequency regional phenological analysis. Such phenological trends can also be analyzed in conjunction with long-term environmental data, such as temperature, rising atmospheric carbon dioxide and sea level rise, to assess and predict response of salt marshes towards environmental changes. The GPP mapping methodology developed through this study can be used for identifying salt marsh habitats that require immediate restoration and conservation. The GPP time-series composites can be utilized for further statistical trend analysis that can not only identify marsh areas displaying progressive stress, but also help determine whether salt marsh habitats are likely to become potential sources or sinks with changes in environmental conditions. Salt marsh productivity is likely to be greatly affected by rising atmospheric CO_2 and sea-levels rise (McLeod et al. 2011; White et al. 2012; Erickson et al. 2007). Therefore high frequency periodic monitoring of salt marsh productivity, both at site-specific and at landscape level is necessary for both identification of salt marsh habitats under physiological stress as well as prioritization of restoration and conservation efforts.

Conclusions

This study provides novel methods for mapping salt marsh GPP using fine temporal resolution MODIS image based biophysical models. For the first time statistical relationship has been established between salt marsh GPP by combining MODIS derived GBM composites and *in-situ* observations of GPP estimated from CO_2 eddy covariance flux data. This kind of salt marsh study has not been previously attempted because of the inherent difficulty in collecting and analyzing ground data from such a complex ecosystem. Field based harvesting methods had been attempted to estimate salt marsh GPP in the last century (Kaswadji et al. 1990), however, such methods are time and labor intensive. The MODIS based model developed in this study has been able to map GPP, although optimization of the model using additional data for calibration and

validation may be necessary, prior to expanding the model for GPP estimation at a broader landscape level. Optimization of the GPP model may even improve its performance by reducing its predictive error levels. is a crucial indicator of carbon sequestration potential, and long-term trend analysis is crucial for detecting whether these ecosystems are likely to function as sinks or sources of carbon in the environment in future. This is particularly important because these productive coastal ecosystems in the Gulf and elsewhere are vulnerable to climate change induced sea level rise, rising atmospheric CO_2 and perpetual developmental pressures.

Although MODIS can be an excellent choice for broader landscape level GPP mapping, certain site specific studies may require information at a much finer resolution. The MODIS based GPP model described in this study is inherently species invariant. However, at the site-specific level, mapping GPP using species specific models might be a better option than species invariant models. In addition, finer resolution images might yield more accurate estimates of the spatio-temporal variation of GPP at the site-specific level. In addition, since both the GPP and MODIS 8-day images are vulnerable to tidal effect, the GPP model described here might have been affected by the tidal conditions. Therefore, developing methods and techniques to account for the error induced by the tidal effect on the GPP model is the next target.

The high temporal resolution of MODIS 8-day surface reflectance products, coupled with the moderate spatial resolution, has immense potential in studying and monitoring both long and short-term salt marsh productive status. The time-series maps and phenological charts derived from MODIS imagery provide the tools necessary for effective conservation and restoration of these vulnerable ecosystems. These products can be used in conjunction with different hydrological, climatological, and land-use parameters to assess the influence of different environmental factors on salt marsh health and productivity. Coastal resource managers and

policy makers in the Gulf and elsewhere can utilize these large-scale map composites to identify marsh areas that should be prioritized for restoration activities. Further, through continuous monitoring of the inter and intra-annual variations in salt marsh GPP, both at the landscape and site-specific scale, it will be possible to ascertain whether salt marshes will continue to be a major carbon sink in the environment, or environmental changes will force it to become a carbon source or at the best carbon neutral. Even if salt marshes become carbon neutral, periodic natural hazards might destroy salt marsh habitats, thus releasing carbon into the atmosphere, further enhancing global warming. Salt marshes are dynamic and critical ecosystems in terms of carbon sequestration; continuous monitoring of these critical ecosystems is therefore, crucial for effective restoration and management practices and formulation of global change policies.

Acknowledgements

Shuvankar Ghosh is grateful to the University of Georgia Graduate School Dean's Award and the Summer Doctoral Research Fellowship for Social Science for carrying out this research.

References

Alber, M., Swenson, E. M., Adamowicz, S. C., and Mendelssohn, I. A. 2008. Salt marsh dieback: an overview of recent events in the US. *Estuarine, Coastal and Shelf Science*, 80, 1-11.

Baker, J. M., and Griffis, T. J. 2005. Examining strategies to improve the carbon balance of corn/soybean agriculture using eddy covariance and mass balance techniques. *Agricultural and Forest Meteorology*, 128, 163-177.

Baldocchi, D. D. 2003. Assessing the eddy covariance technique for evaluating carbon dioxide exchange rates of ecosystems: past, present and future. *Global Change Biology*, 9, 479-492.

Baldocchi, D., Falge, E., Gu, L., Olson, R., Hollinger, D., Running, S., Anthoni, P., Bernhofer, C., Davis, K., Evans, R., and Fuentes, J. 2001. FLUXNET: A new tool to study the temporal and spatial variability of ecosystem–scale carbon dioxide, water vapor, and energy flux densities. *Bulletin of the American Meteorological Society*, 82, 2415-2434.

Beer, C., Reichstein, M., Tomelleri, E., Ciais, P., Jung, M., Carvalhais, N., Rödenbeck, C., Arain, M.A., Baldocchi, D., Bonan, G.B., and Bondeau, A. 2010. Terrestrial gross carbon dioxide uptake: global distribution and covariation with climate. *Science*, 329, 834-838.

Bridgham, S. D., Patrick Megonigal, J., Keller, J. K., Bliss, N. B., and Trettin, C. 2006. The carbon balance of North American wetlands. *Wetlands*, 26, 889-916.

Chmura, G. L., Anisfeld, S. C., Cahoon, D. R., and Lynch, J. C. 2003. Global carbon sequestration in tidal, saline wetland soils. *Global Biogeochemical Cycles*, 17, DOI: 10.1029/2002GB001917

Connor, R. F., Chmura, G. L., and Beecher, C. B. 2001. Carbon accumulation in Bay of Fundy salt marshes: Implications for restoration of reclaimed marshes. *Global Biogeochemical Cycles*, 15, 943-954.

Coverdale, T. C., Herrmann, N. C., Altieri, A. H., and Bertness, M. D. 2013. Latent impacts: the role of historical human activity in coastal habitat loss. *Frontiers in Ecology and the Environment*, 11, 69-74.

Duarte, C. M., Dennison, W. C., Orth, R. J., and Carruthers, T. J. 2008. The charisma of coastal ecosystems: addressing the imbalance. *Estuaries and Coasts*, 31, 233-238.

EddyPro (software, version 6.0), LiCOR Biosciences, https://www.licor.com/env/products/eddy_covariance/eddypro.html

Erickson, J. E., Megonigal, J. P., Peresta, G., and Drake, B. G. (2007). Salinity and sea level mediate elevated CO2 effects on C_3–C_4 plant interactions and tissue nitrogen in a Chesapeake Bay tidal wetland. *Global Change Biology*, 13, 202–215.

Evans, E. D., Anjaneyulu, Y., and Tchnouwou, P. B. 2012. Effects of Hurricane Katrina on land cover within the Grand Bay National Estuarine research reserve in Mississippi, USA. In: Ksenija, V. (Ed.) Environmental and Food Safety and Security for South-East Europe and Ukraine, pp. 173-188, Springer, Dordrecht, The Netherlands.

Falge, E., Baldocchi, D., Olson, R., Anthoni, P., Aubinet, M., Bernhofer, C., Burba, G., Ceulemans, R., Clement, R., Dolman, H. and Granier, A. 2001. Gap filling strategies for defensible annual sums of net ecosystem exchange. *Agricultural and Forest Meteorology*, 107, 43-69.

Friess, D. A., Spencer, T., Smith, G. M., Möller, I., Brooks, S. M., and Thomson, A. G. 2012. Remote sensing of geomorphological and ecological change in response to saltmarsh managed realignment, The Wash, UK, *International Journal of Applied Earth Observation and Geoinformation*, 18, 57–68.

Gao, F., Morisette, J. T., Wolfe, R. E., Ederer, G., Pedelty, J., Masuoka, E., Myneni. R., Tan. B. and Nightingale, J. 2008. An algorithm to produce temporally and spatially continuous MODIS–LAI time series. *IEEE Geoscience and Remote Sensing Letters*, 5, 60–64.

Ghosh, S., Mishra, D. R., and Gitelson, A. A. 2016. Long-term monitoring of biophysical characteristics of tidal wetlands in the northern Gulf of Mexico – A methodological approach using MODIS. Remote Sensing of Environment, 173, 39-58.

Gitelson, A. A., Verma, S. B., Vina, A., Rundquist, D. C., Keydan, G., Leavitt, B., Arkebauer, T. J., Burba, G. G., and Suyker, A. E. 2003. Novel technique for remote estimation of CO_2 flux in maize. *Geophysical Research Letters*, 30, DOI: 10.1029/2002GL016543

Gitelson, A. A., Viña, A., Verma, S. B., Rundquist, D. C., Arkebauer, T. J., Keydan, G., Leavitt, B., Ciganda, V., Burba, G. G., and Suyker, A. E. 2006. Relationship between gross primary production and chlorophyll content in crops: Implications for the synoptic monitoring of vegetation productivity. *Journal of Geophysical Research: Atmospheres*, 111, DOI: 10.1029/2005JD006017

Göckede, M., Foken, T., Aubinet, M., Aurela, M., Banza, J., Bernhofer, C., Bonnefond, J. M., Brunet, Y., Carrara, A., Clement, R., and Dellwik, E. 2008. Quality control of CarboEurope flux data–Part 1: Coupling footprint analyses with flux data quality assessment to evaluate sites in forest ecosystems. *Biogeosciences*, 5, 433-450.

Goulden, M. L., Wofsy, S. C., Harden, J. W., Trumbore, S. E., Crill, P. M., Gower, S. T., Fries, T., Daube, B. C., Fan, S. M., Sutton, D. J. and Bazzaz, A. (1998). Sensitivity of boreal forest carbon balance to soil thaw. *Science*, 279, 214-217.

Goward, S. N., and Huemmrich, K. F. 1992. Vegetation canopy PAR absorptance and the normalized difference vegetation index: an assessment using the SAIL model. *Remote Sensing of Environment*, 39, 119-140.

Heinsch, F. A., Zhao, M., Running, S. W., Kimball, J. S., Nemani, R. R., Davis, K. J., Bolstad, P. V., Cook, B. D., Desai, A. R., Ricciuto, D. M., and Law, B. E. 2006. Evaluation of remote sensing based terrestrial productivity from MODIS using regional tower eddy flux network observations. *IEEE Transactions on Geoscience and Remote Sensing*, 44, 1908-1925.

Hinkle, R. L., and Mitsch, W. J. 2005 Salt marsh vegetation recovery at salt hay farm wetland restoration sites on Delaware Bay, *Ecological Engineering*, 25, 240–251.

TIMESAT [Software], Lund University, http://web.nateko.lu.se/timesat/timesat.asp

Jonsson, P., Eklundh, L. 2002. Seasonality extraction by function fitting to time–series of satellite sensor data. *IEEE Transactions on Geoscience and Remote Sensing*, 40, 1824–1832.

Jonsson, P., Eklundh, L. 2004. TIMESAT—a program for analyzing time–series of satellite sensor data. *Computers and Geosciences*, 30, 833–845.

Jung, M., Reichstein, M., and Bondeau, A. 2009. Towards global empirical upscaling of FLUXNET eddy covariance observations: validation of a model tree ensemble approach using a biosphere model. *Biogeosciences*, 6, 2001-2013.

Jung, M., Reichstein, M., Margolis, H. A., Cescatti, A., Richardson, A. D., Arain, M. A., Arneth, A., Bernhofer, C., Bonal, D., Chen, J. and Gianelle, D. 2011. Global patterns of land-atmosphere fluxes of carbon dioxide, latent heat, and sensible heat derived from eddy covariance, satellite, and meteorological observations. *Journal of Geophysical Research: Biogeosciences*, 116, DOI:10.1029/2010JG001566.

Jung, M., Verstraete, M., Gobron, N., Reichstein, M., Papale, D., Bondeau, A., Robustelli, M., and Pinty, B. 2008. Diagnostic assessment of European gross primary production. *Global Change Biology*, 14, 2349-2364.

Kaswadji, R. F., Gosselink, J. G., and Turner, R. E. 1990. Estimation of primary production using five different methods in a *Spartina alterniflora* salt marsh. *Wetlands Ecology and Management*, 1, 57-64.

Kennish, M. J. 2001. Coastal Salt Marsh Systems in the US: a Review of Anthropogenic Impacts, *Journal of Coastal Research*, 17, 731–748.

Kljun, N., Calanca, P., Rotach, M. W., and Schmid, H. P. 2004. A simple parameterisation for flux footprint predictions. *Boundary-Layer Meteorology*, 112, 503-523.

Lafleur, P. M., Moore, T. R., Roulet, N. T., and Frolking, S. 2005. Ecosystem respiration in a cool temperate bog depends on peat temperature but not water table. *Ecosystems*, 8, 619-629.

Li, Z., Yu, G., Xiao, X., Li, Y., Zhao, X., Ren, C., Ren, C., Zhang, L., and Fu, Y. 2007. Modeling gross primary production of alpine ecosystems in the Tibetan Plateau using MODIS images and climate data. *Remote Sensing of Environment*, 107, 510-519.

LI-190R Quantum Sensor, LiCOR Biosciences, https://www.licor.com/env/products/gas_analysis/LI-7500RS/

Li-7500A Open Path CO2/H2O Gas Analyzer, Licor Biosciences, https://www.licor.com/env/products/gas_analysis/LI-7500RS/

Macreadie, P. I., Hughes, A. R., and Kimbro, D. L. 2013. Loss of 'blue carbon'from coastal salt marshes following habitat disturbance. *PloS one*, 8, e69244.

Mauder, M., and Foken, T. 2004. Quality control of eddy covariance measurements (c: 0, 1, 2). CarboEurope-IP Task, 1.2.2

McKee, K. L., Mendelssohn, I. A., and D Materne, M. 2004. Acute salt marsh dieback in the Mississippi River deltaic plain: a drought-induced phenomenon? *Global Ecology and Biogeography*, 13, 65-73.

Mcleod, E., Chmura, G. L., Bouillon, S., Salm, R., Björk, M., Duarte, C. M., Lovelock, C.E., Schlesinger, W.H. and Silliman, B. R. 2011. A blueprint for blue carbon: toward an improved understanding of the role of vegetated coastal habitats in sequestering CO_2. *Frontiers in Ecology and the Environment*, 9, 552-560.

Mishra, D. R., Cho, H. J., Ghosh, S., Fox, A., Downs, C., Merani, P. B. T., Kirui, P., Jackson, N. and Mishra, S. 2012. Post–spill state of the marsh: Remote estimation of the ecological impact of the Gulf of Mexico oil spill on Louisiana Salt Marshes, *Remote Sensing of Environment*, 118, 176–185.

Mississippi Department of Marine Resources, 1998. Grand Bay National Estuarine Research Reserve Final Environmental Impact Statement/Reserve Management Plan, Submitted to: National Oceanic and Atmospheric Administration.

Moncrieff, J. B., Massheder, J. M., De Bruin, H., Elbers, J., Friborg, T., Heusinkveld, B., Kabat, P., Scott, S., Soegaard, H. and Verhoef, A. 1997. A system to measure surface fluxes of momentum, sensible heat, water vapour and carbon dioxide. *Journal of Hydrology*, 188, 589-611.

Monteith, J. L. 1972. Solar radiation and productivity in tropical ecosystems. *Journal of Applied Ecology*, 9, 747-766.

Nakai, T., and Shimoyama, K. 2012. Ultrasonic anemometer angle of attack errors under turbulent conditions. *Agricultural and Forest Meteorology*, 162, 14-26.

Nellemann, C., and Corcoran, E. (Eds.) 2009. Blue carbon: the role of healthy oceans in binding carbon: a rapid response assessment, UNEP/Earthprint.

NOAA National Centers for Environmental information, Climate at a Glance: U.S. Time Series, published December 2016, retrieved on December 1, 2016, http://www.ncdc.noaa.gov/cag/

NOAA National Weather Service, retrieved on September 21, 2016, http://www.weather.gov/

O'Donnell, J. P., and Schalles, J. F. 2016. Examination of abiotic drivers and their influence on *Spartina alterniflora* biomass over a twenty-eight year period using Landsat 5 TM satellite imagery of the Central Georgia Coast. *Remote Sensing*, 8, 477.

Osmond, B., Ananyev, G., Berry, J., Langdon, C., Kolber, Z., Lin, G., Monson, R., Nichol, C., Rascher, U., Schurr, U. and Smith, S. 2004. Changing the way we think about global change research: scaling up in experimental ecosystem science. *Global Change Biology*, 10, 393-407.

Palmer, W. C. 1965. Meteorological drought, Vol. 30. Washington, DC: US Department of Commerce, Weather Bureau.

Papale, D., and Valentini, R. 2003. A new assessment of European forests carbon exchanges by eddy fluxes and artificial neural network spatialization. *Global Change Biology*, 9, 525-535.

Papale, D., Reichstein, M., Aubinet, M., Canfora, E., Bernhofer, C., Kutsch, W., Longdoz, B., Rambal, S., Valentini, R., Vesala, T., and Yakir, D. (2006). Towards a standardized processing of Net Ecosystem Exchange measured with eddy covariance technique: algorithms and uncertainty estimation. *Biogeosciences,* 3, 571-583.

Ponton, S., Flanagan, L. B., Alstad, K. P., Johnson, B. G., Morgenstern, K. A. I., Kljun, N., Black, T. A. and Barr, A. G. 2006. Comparison of ecosystem water-use efficiency among Douglas-fir forest, aspen forest and grassland using eddy covariance and carbon isotope techniques. *Global Change Biology*, 12, 294-310.

Rahman, A. F., Sims, D. A., Cordova, V. D., and El-Masri, B. Z. 2005. Potential of MODIS EVI and surface temperature for directly estimating per-pixel ecosystem C fluxes. *Geophysical Research Letters*, 32, DOI: 10.1029/2005GL024127

Reichstein, M., Ciais, P., Papale, D., Valentini, R., Running, S., Viovy, N., Cramer, W., Granier, A., Ogee, J., Allard, V. and Aubinet, M. 2007. Reduction of ecosystem productivity and

respiration during the European summer 2003 climate anomaly: a joint flux tower, remote sensing and modelling analysis. *Global Change Biology*, 13, 634-651.

Running, S. W., Nemani, R. R., Heinsch, F. A., Zhao, M., Reeves, M., and Hashimoto, H. 2004. A continuous satellite-derived measure of global terrestrial primary production. *American Institute of Biological Science Bulletin*, 54, 547-560.

Running, S. W., Thornton, P. E., Nemani, R., and Glassy, J. M. 2000. Global terrestrial gross and net primary productivity from the Earth Observing System. *Methods in Ecosystem Science*, 3, 44-45.

Sims, D. A., Rahman, A. F., Cordova, V. D., El-Masri, B. Z., Baldocchi, D. D., Bolstad, P. V., Flanagan, L. B., Goldstein, A. H., Hollinger, D. Y., Misson, L., and Monson, R. K. 2008. A new model of gross primary productivity for North American ecosystems based solely on the enhanced vegetation index and land surface temperature from MODIS. *Remote Sensing of Environment*, 112, 1633-1646.

Sims, D. A., Rahman, A. F., Cordova, V. D., El-Masri, B. Z., Baldocchi, D. D., Flanagan, L. B., Goldstein, A.H., Hollinger, D. Y., Misson, L., Monson, R. K. and Oechel, W. C. 2006. On the use of MODIS EVI to assess gross primary productivity of North American ecosystems. *Journal of Geophysical Research: Biogeosciences*, 111, DOI: 10.1029/2006JG000162.

Tan, B., Morisette, J. T., Wolfe, R. E., Gao, F., Ederer, G. A., Nightingale, J., and Pedelty, J. A. 2011. An enhanced TIMESAT algorithm for estimating vegetation phenology metrics from MODIS data. *IEEE Journal of Selected Topics in Applied Earth Observations and Remote Sensing*, 4, 361–371.

Verma, M., Friedl, M. A., Richardson, A. D., Kiely, G., Cescatti, A., Law, B. E., Wohlfahrt, G., Gielen, B., Roupsard, O., Moors, E. J., and Toscano, P. 2014. Remote sensing of annual terrestrial gross primary productivity from MODIS: an assessment using the FLUXNET, La Thuile data set.

Vermote, E. F., Kotchenova, S. Y., and Ray, J. P. 2011. MODIS surface reflectance user's guide. MODIS Land Surface Reflectance Science Computing Facility, version, 1 (http://modis-sr.ltdri.org/guide/MOD09_UserGuide_v1_3.pdf)

Vickers, D., and Mahrt, L. 1997. Quality control and flux sampling problems for tower and aircraft data. *Journal of Atmospheric and Oceanic Technology*, 14, 512-526.

Webb, E. K., Pearman, G. I., and Leuning, R. 1980. Correction of flux measurements for density effects due to heat and water vapor transfer. *Quarterly Journal of the Royal Meteorological Society*, 106, 85-100.

White, K. P., Langley, J. A., Cahoon, D. R., and Megonigal, J. P. 2012. C_3 and C_4 biomass allocation responses to elevated CO_2 and nitrogen: contrasting resource capture strategies. *Estuaries and Coasts*, 35, 1028–1035.

Wilczak, J. M., Oncley, S. P., and Stage, S. A. 2001. Sonic anemometer tilt correction algorithms. *Boundary-Layer Meteorology*, 99, 127-150.

Wille, C., Kutzbach, L., Sachs, T., Wagner, D., and Pfeiffer, E. V. A. 2008. Methane emission from Siberian arctic polygonal tundra: eddy covariance measurements and modeling. *Global Change Biology*, 14, 1395-1408.

WindMaster Pro 3-Axis Anemometer, Gill Instruments, http://gillinstruments.com/products/anemometer/windmaster.htm#sonicanemometer

Wu, C., Munger, J. W., Niu, Z., and Kuang, D. 2010. Comparison of multiple models for estimating gross primary production using MODIS and eddy covariance data in Harvard Forest. *Remote Sensing of Environment*, 114, 2925-2939.

Wu, C., Niu, Z., Tang, Q., Huang, W., Rivard, B., and Feng, J. 2009. Remote estimation of gross primary production in wheat using chlorophyll-related vegetation indices. *Agricultural and Forest Meteorology*, 149, 1015-1021.

Xiao, X., Hollinger, D., Aber, J., Goltz, M., Davidson, E. A., Zhang, Q., and Moore, B. 2004b. Satellite-based modeling of gross primary production in an evergreen needleleaf forest. *Remote Sensing of Environment*, 89, 519-534.

Xiao, X., Zhang, Q., Braswell, B., Urbanski, S., Boles, S., Wofsy, S., Moore, B., and Ojima, D. 2004a. Modeling gross primary production of temperate deciduous broadleaf forest using satellite images and climate data. *Remote Sensing of Environment*, 91, 256-270.

Xiao, X., Zhang, Q., Hollinger, D., Aber, J., and Moore, B. 2005b. Modeling gross primary production of an evergreen needleleaf forest using MODIS and climate data. *Ecological Applications*, 15, 954-969.

Xiao, X., Zhang, Q., Saleska, S., Hutyra, L., De Camargo, P., Wofsy, S., Frolking, S., Boles, S., Keller, M., and Moore, B. 2005a. Satellite-based modeling of gross primary production in a seasonally moist tropical evergreen forest. *Remote Sensing of Environment*, 94, 105-122.

Yang, F., Ichii, K., White, M. A., Hashimoto, H., Michaelis, A. R., Votava, P., Zhu, A. X., Huete, A., Running, S. W., and Nemani, R. R. 2007. Developing a continental-scale measure of gross primary production by combining MODIS and AmeriFlux data through Support Vector Machine approach. *Remote Sensing of Environment*, 110, 109-122.

Zhao, M., Heinsch, F. A., Nemani, R. R., and Running, S. W. 2005. Improvements of the MODIS terrestrial gross and net primary production global data set. *Remote Sensing of Environment*, 95, 164-176.

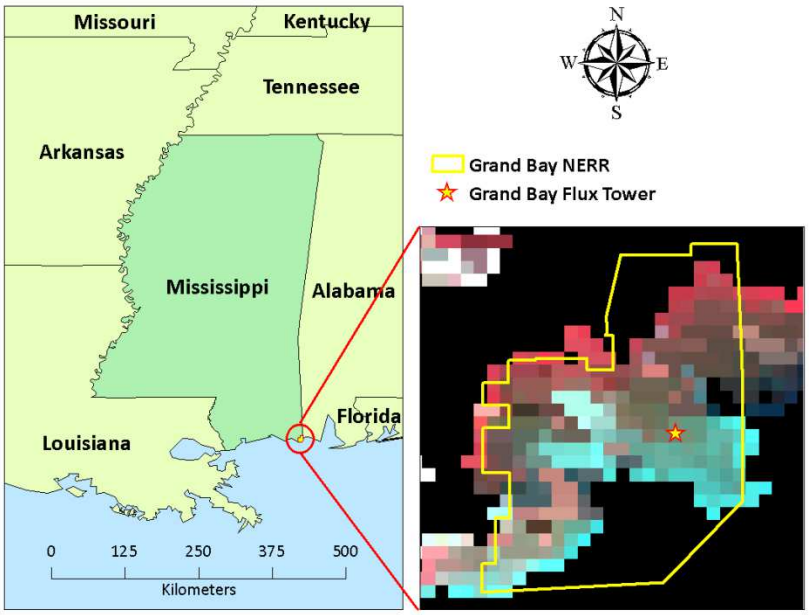

Figure 6.1: Map showing study area of Grand Bay National Estuarine Research Reserve (GBNERR), with the Eddy Covariance flux tower location.

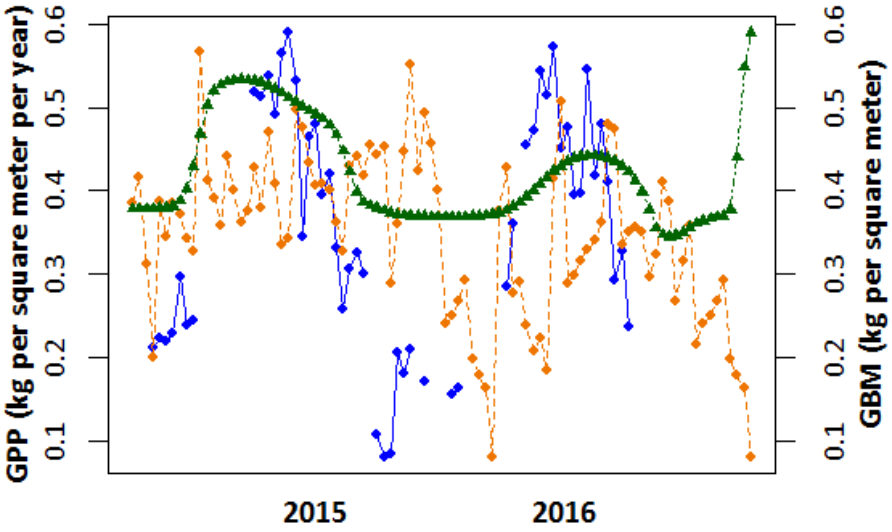

Figure 6.2: GPP measured from Eddy Covariance flux tower (blue line), along with MODIS derived raw GBM (orange line) and TIMESAT derived smoothed GBM (green line).

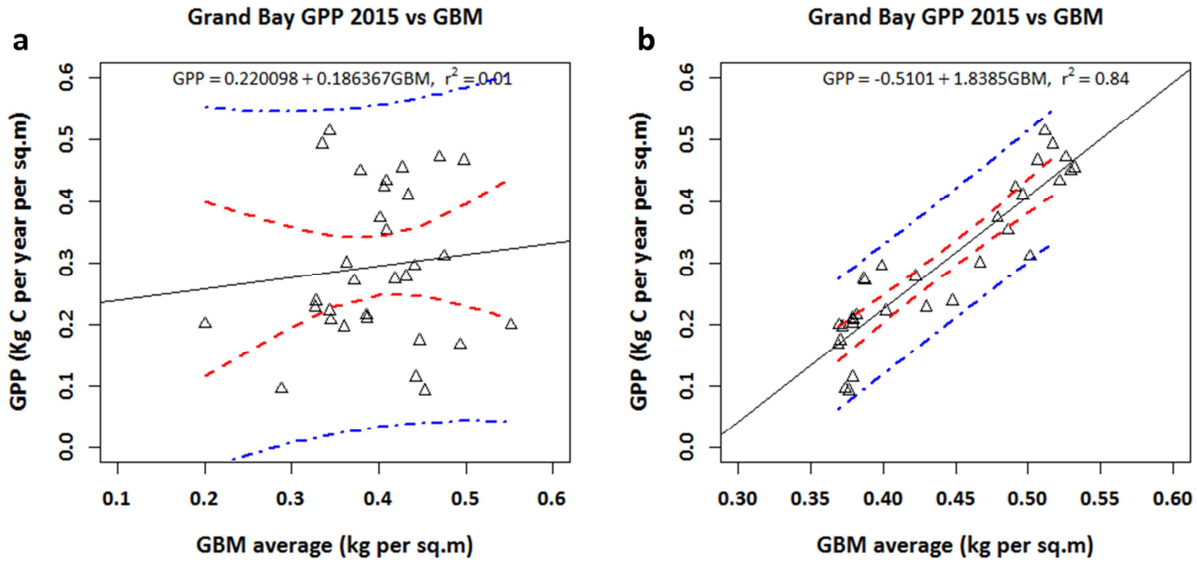

Figure 6.3: Linear relationship between GPP and (a) raw GBM values and (b) smoothed GBM values. The red and the blue lines represent 95% confidence and prediction interval.

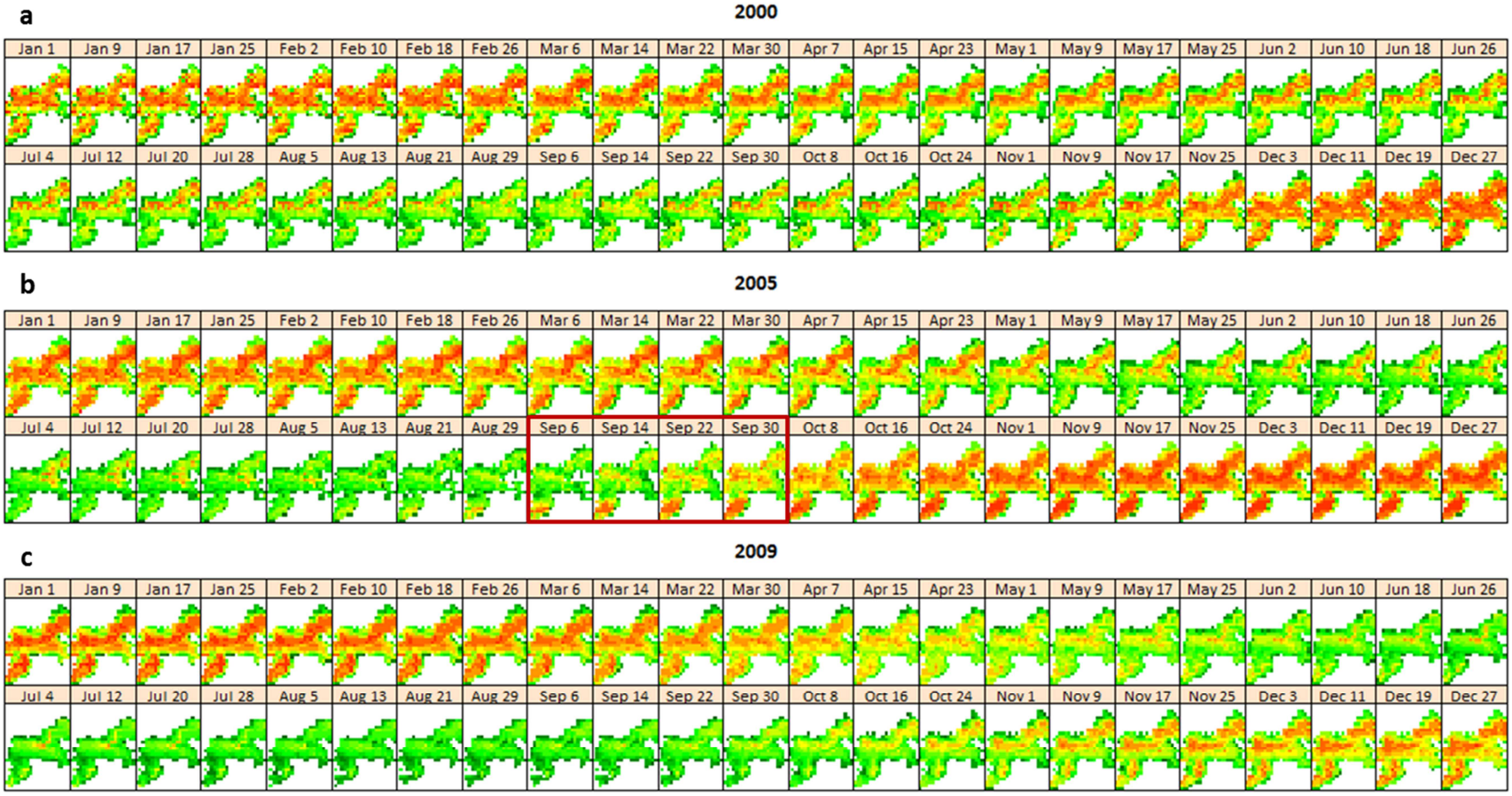

Figure 6.4: Sample time-series GPP composites from the growing season of (a) 2000, (b) 2005 and (c) 2009. The highlighted composites of 2005 show the effect of the storm surge generated by Hurricane Katrina on the GBNERR salt marshes.

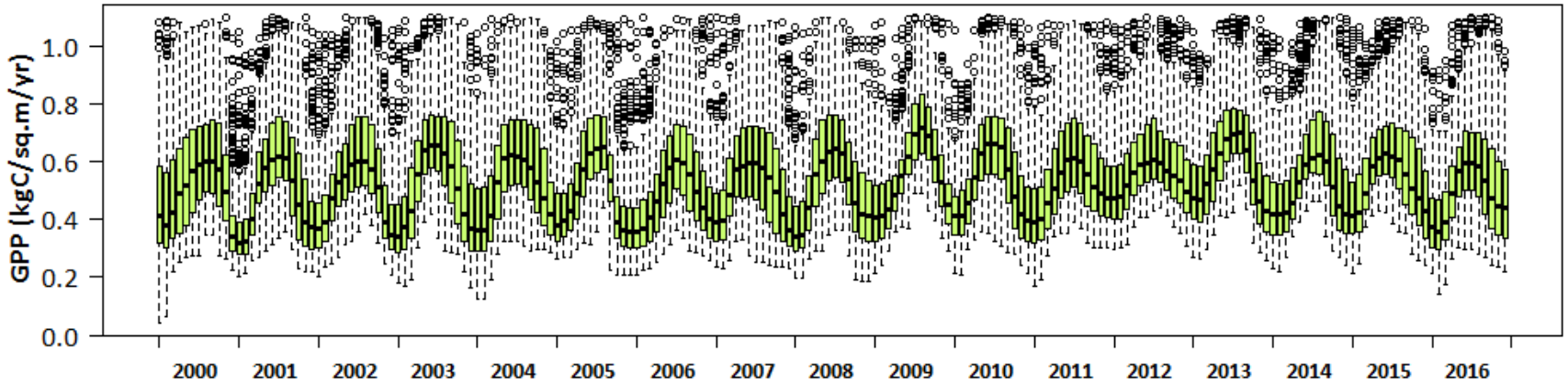

Figure 6.5: Boxplots (green) showing GPP phenology generated for GBNERR salt marsh for the seventeen year time period (2000 – 2016)

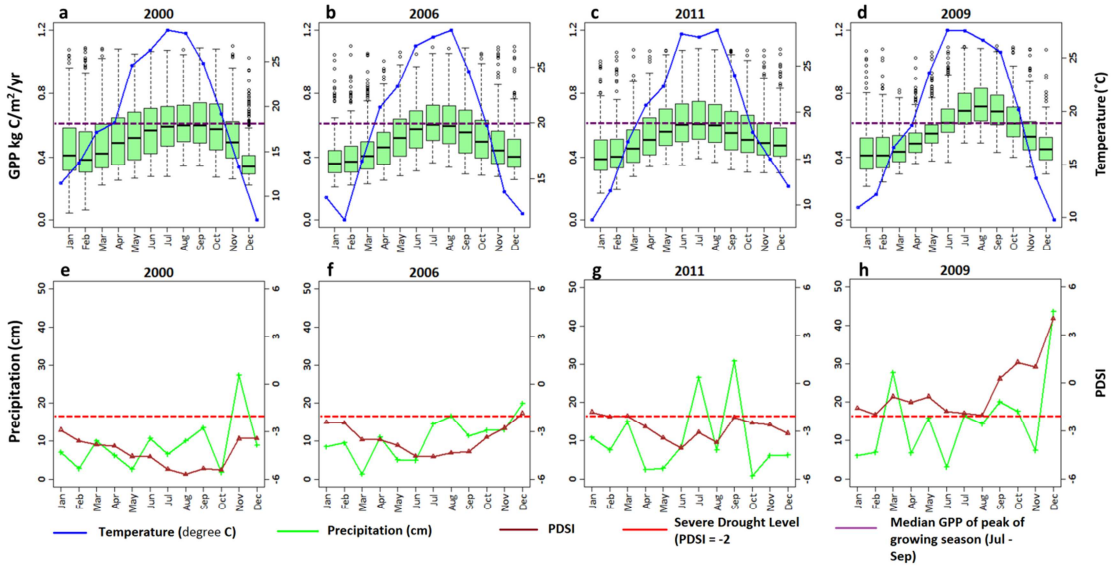

Figure 6.6a-d: GPP Phenology of the 2000, 2006, 2011 and 2009 (normal) growing season, along with monthly average temperature levels; purple dotted line indicates median GPP of peak of growing season highlighted in purple, 6e-h: Monthly precipitation and PDSI levels of 2000, 2006, 2011 and 2009; severe drought threshold indicated by red dotted line.

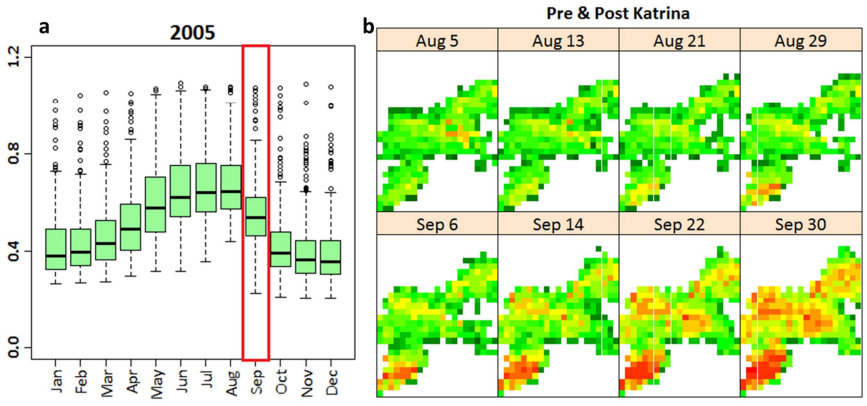

Figure 6.7a: GPP Phenology of 2005 showing effect of Hurricane Katrina on GBNERR salt marshes; highlighted month (September) shows sudden reduction in GPP levels; 6.7b: Time-series GPP composites comparing pre-landfall (August 5 – 29) and post-landfall (Sep 6 – 30) GPP of GBNERR.

CHAPTER 7

CONCLUSIONS

Salt marshes are one of the extremely valuable components of the coastal landscape due to their critical ecosystem services; however, these habitats are extremely vulnerable to global environmental change. For effective conservation and restoration of these critically threatened habitats, continuous monitoring of their biophysical properties is necessary. Biophysical properties such as GLAI, VF, CHL_c, GBM and GPP are primary indicators of the physiological and productive health of any vegetation including salt marsh vegetation. Monitoring of these properties using remote sensing not only helps in assessing the overall dynamics of salt marshes but also facilitates prioritization of restoration efforts to areas that require immediate attention and allows conservation planning at a much broader spatial scale. Unfortunately remote monitoring of salt marsh biophysical properties using remote sensing has been rarely attempted. This study attempted to develop mapping protocols for salt marsh biophysical properties using remote sensing methods, and studied the long-term spatio-temporal trends of the biophysical properties for the salt marshes in south-east United States.

The first study presented the first quantitative assessment on the ecological impact of the BP oil-spill and the subsequent clean-up efforts on the salt marsh habitats along the southeastern Louisiana (LA) coast, using combination of Landsat images and *in*-situ estimations of CHL_c, and GBM. We observed significant post-spill increase in areas with reduced biomass and canopy chlorophyll (>400 km^2) during the 2010 growing season compared to 50–65 km^2 during the 2009

growing season. Phenological analysis of the post oil-spill data revealed a significant decrease in the magnitude of CHL_c, and GBM during the peak of the 2010 growing season. June was consistently found to be the worst month in terms of salt marsh health across LA over the 2010 phenological cycle followed by the initial signs of recovery along the fringing marsh areas proximal to the shoreline that were first impacted by oil. Interior marsh patches exhibited persistent signs of stress towards the end of the growing season. The study highlighted the potential of the scientific approach and the products generated in successfully delineating the critical hotspots of marsh stress which is crucial for prioritization of areas needing immediate restoration efforts. The time-series products can be used in conjunction with biogeochemical data to analyze the changes in one of the most important wetland functions i.e. carbon sequestration reduction related to the oil spill effects. Further the study also provided the encouragement to expand the approach to study salt marshes at a broader landscape scale.

The second study developed a novel methodological approach for mapping biophysical health of coastal tidal wetland habitats in terms of GLAI, CHL_c, VF, and GBM. We measured these biophysical characteristics in salt marshes of the northern Gulf of Mexico using similar approach of combining remotely sensed images (MODIS for this study) and *in-situ* estimates of these biophysical properties, from growing seasons of 2010 and 2011. We found MODIS-based models performing better than proximal sensing based methods at the landscape level; as species level signals seemed to get diluted at coarser spatial scales. In addition, visible wavelength based vegetation indices performed better than near infra-red (NIR) based indices, as background moisture made NIR based indices insensitive to marsh biophysical properties at coarser spatial resolution. The study once again substantiated the methods and time-series products in studying salt marsh biophysical properties. Time-series composites and phenological information derived

using the MODIS based models were able to capture the impact of the selected disturbances on the physiology of the salt marsh habitats in the Gulf Coast. This is the first study to employ MODIS data to analyze the biophysical characteristics of salt marshes in the Gulf Coast, which, in turn, has the potential to improve our ability to predict their productivity and carbon sequestration potential. These techniques could also be used to assess the success of previous and ongoing tidal wetland restoration projects, and evaluate the productivity of marshes under threat from developmental activity, sea level rise, and industrial pollution.

The biophysical properties analyzed in this are different between species of marsh vegetation due to their differences in foliar and canopy structures, distribution, and habitat preference, and inherent physiology. Species-dependent marsh biophysical models are generally more accurate and can be implemented only when marshes in the study area can be classified into individual plant communities. Classification of the marsh habitats into homogenous species communities using MODIS is particularly difficult because of mixed pixel issues. Further, unavoidable classification errors can be introduced during mapping species composition prior to application of these biophysical models, which in turn have built-in uncertainties, which magnifies the error of the final output. Therefore, using species-independent biophysical models (not influenced by species diversity), is the best option to generate high frequency time-series composites. Moreover, our analysis and results clearly demonstrate the deterioration of the species level signal variation at the coarse spatial resolution of MODIS, which makes it suitable for broad scale regional mapping.

Although MODIS can be an excellent choice for broader landscape level biophysical mapping, finer resolution images such as Landsat may be more effective for site-specific studies of marsh biophysical parameters, which can capture species level signals. Mapping biophysical parameters

using species specific models might be a better option than species invariant models if species classification map is available for a study site. Further, in order to implement these biophysical models using MODIS for a particular tidal wetland habitat the extent of the habitat has to be completely covered by at least 8–10 pixels of MODIS 250 m or 500 m, which may be impossible in highly fragmented habitats. In essence, selection of the appropriate sensor for biophysical mapping should depend not only on the research questions and scale, but also on the nature of the marsh habitat.

The third study examines the phenology of salt marsh ecosystem across coastal Louisiana (LA) for a sixteen-year time-period (2000-2015), using MODIS 500m images, along with a pre-developed biophysical model to generate time-series composites of above-ground green biomass (GBM). We selected the best thresholds for SOS (5% of amplitude) and EOS (20% of amplitude), along with the best smoothing function (Asymmetric Gaussian) for deriving seasonality parameters. We analyzed the seasonality in the SOS and EOS dates over the sixteen year time period; the effects of the environmental events influencing the deviations from the normal SOS and EOS have been efficiently captured. Finally, the trend analysis demonstrated the reduction in the rates of seasonal amplitude and small seasonal integral, and improvement in the levels of GBM base value, indicating the progressive reduction in the levels of photosynthesis and biomass allocation in the salt marsh ecosystem, that might be attributed as a combination of environmental effects such as rising atmospheric CO_2 levels and sea–level rise. Further, the trend analysis results have been able to capture areas that are demonstrating significant stress in terms of reduced photosynthetic activity and require immediate restoration and conservation efforts. Through continuous monitoring of the ecosystem, it will be possible to

ascertain whether certain salt marsh habitats will continue to be a major carbon sink in the environment, or changes in the environment will force them to become a net carbon source.

Although trend analysis using MODIS derived images can provide a valuable insight into the phenological dynamics at the landscape level, site-specific trend analysis might require similar analysis using site specific records of sea–level changes, nitrogen enrichment and salinity, along with finer resolution images. In addition, with finer resolution images it will be possible to determine the distribution dynamics of the invasive *Phragmites australis* in an otherwise *Spartina* dominated landscape, and compare the progressive phenological trends of the two species, with respect to elevated CO_2 levels and sea–level rise. Such a future study will provide a clearer picture regarding possible ecological succession of *Spartina* by *Phragmites*. The study also illustrate both the relative efficiency of MODIS based biophysical models in analyzing salt marsh phenology and performances of the smoothing techniques in terms of improving signal to noise ratio of the MODIS derived phenology.

Using the methods described in the third chapter, the phenology of salt marsh ecosystem across coastal Georgia was examined for a sixteen-year time-period (2000-2015) in the fourth chapter. We validated the GBM mapping algorithm developed for the Gulf Coast marshes on the salt marshes of GA coast. We further justified the selection of SOS/EOS thresholds by matching them with *in-situ* observations of SOS and EOS using PhenoCam. The trend analysis demonstrated similar reduction in the rates seasonal amplitude and small seasonal integral, and increment in the levels of GBM base value, indicating the progressive reduction in the levels of photosynthesis and biomass accumulation in the salt marsh habitat, that might be attributed as a combination of environmental effects such as stress induced by rising atmospheric CO_2 levels, and sea-level rise. This is for the first time that such a comprehensive analysis of the phenology

of salt marsh habitat in the Atlantic sea-board has been studied in terms of the seasonality parameters. Using the suggested methods in the previous two studies, monitoring of salt marsh habitats will be possible elsewhere with similar environmental settings.

The final study develops methods for mapping salt marsh GPP by integrating *in-situ* observations of GPP from eddy covariance flux towers and MODIS derived GBM values, for the salt marshes of Grand Bay National Estuarine Research Reserve (GBNERR). This kind of study salt marsh study has not been previously attempted because of the inherent difficulty in collecting and analyzing ground data from such a complex ecosystem. The MODIS based model developed in this study has been able to map GPP, although optimization of the model using additional data for calibration and validation may be necessary, prior to expanding the model for GPP estimation at a broader landscape level. Optimization of the GPP model may even improve its performance by reducing its predictive error levels. GPP is a crucial indicator of marsh carbon sequestration potential, and long-term trend analysis is crucial for detecting whether these ecosystems are likely to function as sinks or sources of carbon in the environment in future. This is particularly important because these productive coastal ecosystems in the Gulf and elsewhere are vulnerable to climate change induced sea level rise, rising atmospheric CO_2 and perpetual developmental pressures.

Although, MODIS can be an excellent choice for broader landscape level GPP mapping, certain site specific studies may require information at a much finer resolution. The MODIS based GPP model described in this study is inherently species invariant. However, at the site-specific level, mapping GPP using species specific models might be a better option than species invariant models. In addition, finer resolution images might yield more accurate estimates of the spatio-temporal variation of GPP at the site-specific level. GPP varies across different salt marsh

species, particularly between *Spartina* (C_4 plant) and *Juncus* (C_3 plant); hence the two species are likely to respond differently to the changing global environment. With rising atmospheric carbon dioxide and sea-levels, C_4 plant species will be at a competitive disadvantage compared to C_3 plant species, with the possibility of C_4 species being replaced by C_3 plant species (in case of salt marshes *Spartina* being possibly replaced by *Phragmites*). Unfortunately, species level signals get diluted at the coarser spatial resolution of MODIS. Therefore, sensors which retain species level signals, such as Landsat might be more useful for studying such species level dynamics. In addition, since both the GPP and MODIS 8-day images are vulnerable to tidal effect, the GPP model described here might have been affected by the tidal conditions. Therefore, developing methods and techniques to account for the error induced by the tidal effect on the GPP model is the next target. Further, comparison between different approaches of estimating GPP can be made and validated using MODIS GPP product, to determine the uncertainties. Finally, long-term trend analysis of GPP in salt marsh habitats may be studied and predicted using simulation models incorporating environmental factors, such as atmospheric CO_2, sea-level rise, temperature and other climatic variables. Since salt marshes play a crucial role in carbon sequestration, understanding its environmental response is crucial for formulation and implementation of both site specific and global policies for salt marsh conservation.